CASE NO.

7459

APPlicaTION,
TranscripTS,
Small ExhibiTS,

ETC.

ERNEST L. PADILLA
ATTORNEY AND COUNSELOR AT LAW

P.O. Box 2523
Santa Fe, New Mexico 87501
(505) 988-7577

May 21, 1982

MAY 21 1982

Mr. Richard Stamets
Oil Conservation Division
Post Office Box 2088
Santa Fe, New Mexico

Dear Mr. Stamets:

Enclosed is a copy of another water analysis, made by Core Laboratories in Albuquerque, of a water sample from the fresh water well in Section 28.

Please let me know if you have any questions.

Very truly yours,

Ernest L. Padilla

ELP:PM
Enclosure
cc: Red Mountain Associates

CORE LABORATORIES, INC.
3428 Stanford Dr., N.E.
Albuquerque, New Mexico 87107
Phone: 505-344-0274

Client: Red Mountain Associates
Address: 1517 Reisterstown Rd.
Pikesville, Md. 21208
Authorized By: Steve Meszaros

Date Received: 5/14/82
Analyzed By: JFA
Date: 5/18/82
Job Number: W82138

Sample Identification: Sample Received 5/14/82

Resistivity 472 ohm-cm @ 25°C pH 8.7 Specific Gravity -

Hydrogen Sulfide Negative Calculated Total Dissolved Solids 1580

CATIONS	Mg/L	Meq/L	ANIONS	Mg/L	Meq/L
Sodium	480	20.87	Sulfate	460	9.58
Potassium	1.60	.04	Chloride	92	2.59
Calcium	4.40	.22	Carbonate	14.7	.49
Magnesium	0.67	.06	Bicarbonate	530.0	8.69
Iron	0.06	.003			
	Total Cations	21.19		Total Anions	21.36

ERNEST L. PADILLA
ATTORNEY AND COUNSELOR AT LAW

P.O. Box 2523
Santa Fe, New Mexico 87501
(505) 988-7577

May 17, 1982

Oil Conservation Division
Post Office Box 2088
Santa Fe, New Mexico 87501

Attn: Mr. Richard L. Stamets
Hearing Examiner

Re: Red Mountain Associates
Case No. 7459

Dear Mr. Stamets:

Enclosed you will find the following:

(1) Copy of water analysis
(2) Map of water flood area
(3) Speed letter from Cementers, Inc. to Red Mountain Associates

The water analysis is an analysis of a water sample taken from the "fresh" water well in the SE¼NW¼ of Section 28 as shown in the map which is enclosed as item (2) above. I believe that the analysis speaks for itself, however, I should explain that the water sample was submitted for analysis by Mr. Lloyd Temple of Temple Securities Corporation which is affiliated with Red Mountain Associates to Penniman & Browne, Inc., the firm who made the analysis.

The third item is a speed letter from Cementers, Inc. in Farmington, to Mohamed Zenati which briefly states that the breakdown pressure on the State Well No. 7 was 600 psi. This well is located in the NE¼NE¼ of Section 28, Township 20 North, Range 9 West and the breakdown pressure is of the Menafee formation the same zone involved in the application of Red Mountain Associates. In fact, this well was included in Red Mountain's original water flood plans.

Additionally, I have inspected the file of the original application of Red Mountain Associates for a water floor project and it contains water analyses for injected water and for produced water. These analyses were submitted after the original hearing, presumably requested from Mr. Zenati during the course of the original hearing on the application.

TO
Red Mountain Associates
ATTN: Mohamed Zenati
2626 Holly
Denver, CO 80207

FROM
CEMENTERS INC.
~~DUGAN PRODUCTION CORP.~~
P. O. BOX ~~200~~ 302
FARMINGTON, N. M. 87401
(505) 325-1821

SUBJECT	DATE
Acid job 10-11-80 State Well #7	3-23-82

MESSAGE

Breakdown Pressure 600 PSI.

After breakdown - started taking fluid - 1/2 Bbl. per min. @ 150 PSI.

Boyce Ulrich

Boyce Ulrich

Cementers Inc.

SIGNED

SEND WHITE COPY   RETAIN YELLOW COPY

Finally, Red Mountain Associates is informed that the fresh water well is about 300 feet deep operated by a windmill-type pumping device.

I believe that the foregoing information completes the additional information which you have requested. In this regard, please let me know if you have any questions.

Very truly yours,

Ernest L. Padilla

ELP:PFM
Enclosures

cc: Mr. Mohamed Zenati
Mr. Lloyd Temple

DR. WM. B. D. PENNIMAN
1866-1938
DR. ARTHUR LEE BROWNE
1867-1933

EXECUTIVE STAFF

PHILIP M. AIDT
ALLEN W. THOMPSON
DANTE G. BERETTA
J. ADRIAN BUTT
DONALD W. SMITH

PENNIMAN & BROWNE, INC.

CHEMISTS-ENGINEERS-INSPECTORS
6252 FALLS ROAD
BALTIMORE, MARYLAND 21209

ESTABLISHED
1896

CABLE ADDRESS
"BALTEST"

TELEPHONE
825-4131
AREA CODE 301

ANALYTICAL DIVISION

REPORT OF ANALYSIS

Attn: Lloyd L. Temple, Jr. May 4, 1982

No. 820893

Sample of One Water

From Temple Securities Corporation

Marked For Analysis

Sodium, mg/l	326.78
Chloride, mg/l	148.
Oil & Grease, mg/l	0.1
Total Coliform, MPN/100 cc	400,000

Notebook J8, p.117
EPA Methods of Chemical Analysis for Water & Wastes, 1979.

spl

Philip M. Aidt

Philip M. Aidt

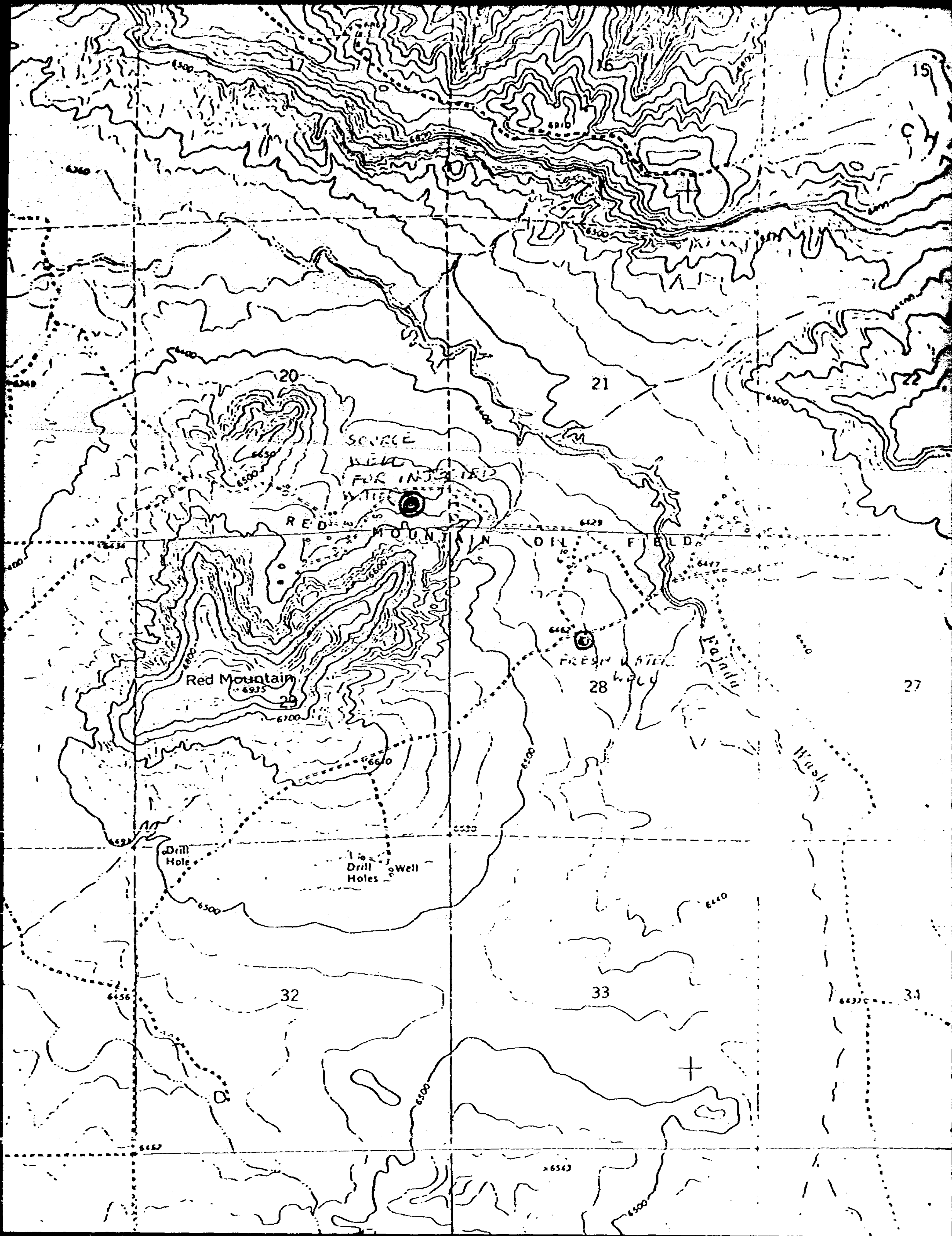

17
16
15
20
21
22
RED MOUNTAIN OIL FIELD
Red Mountain
6935
29
28
27
32
33
Fajada
Wash
Drill Hole
Drill Holes
Well
6500
6600
6700
6800
6650
6610

RECEIVED
OCT 17 1980
OIL CONSERVATION
SANTA FE

KEPLINGER and Associates, Inc.
INTERNATIONAL ENERGY CONSULTANTS

2200 SECURITY LIFE BUILDING
16TH AND GLENARM STREET
DENVER, COLORADO 80202
AREA 303 / 825-7722
CABLE: KEPPET TELEX: 762-324

October 10, 1980

Mr. Dan Nutter
Energy & Minerals Department
Oil Conservation Division
State Land Office Building
P.O. Box 2088
Santa Fe, New Mexico 87501

Re: Waterflood Application
Case No. 7039

Dear Mr. Nutter:

Enclosed are the Produced Water Analysis report for State #1, Injection Water Analysis report for Chaco 20-1, and Chaco Wash Pool existing and proposed well locations.

Sincerely yours,

Mohamed Zenati

Mohamed Zenati
Project Engineer

MZ:nlb

Enclosures (3)

RECEIVED
OCT 17 1980
OIL CONSERVATION DIVISION
SANTA FE

PRODUCED WATER ANALYSIS

Well Name:	State #1
Location:	970/FNL 970/FEL 28-20N-9W
Formation:	Menefee
Resistivity:	1.03 ohm.m @ 69.1°F
Density:	1.0 gm/cc
pH:	7.45
Solid Content (ppm):	less than 2,900
Calcium (ppm):	less than 50
Magnesium (ppm):	Absent
Chloride (ppm):	118
Bicarbonates (ppm):	1,552
Sulfides (ppm):	Absent
Iron (ppm):	Absent
Potassium (ppm):	Absent

RECEIVED
OCT 17 1980
OIL CONSERVATION DIVISION
SANTA FE

INJECTION WATER ANALYSIS

Well Name:	CHACO 20-1
Location:	660/FSL 660/FEL 20-20N-9W
Formation:	Hopash-Gallup
Resistivity:	70 ohm.m @ 69.2^{o}F
Density:	1.0 gm/cc
pH:	7.763
Solid Content (ppm):	less than 2,900
Calcium (ppm):	less than 50
Magnesium (ppm):	Absent
Chloride (ppm):	472
Bicarbonates (ppm):	420
Sulfides (ppm):	750
Iron (ppm):	Absent
Potassium (ppm):	Absent

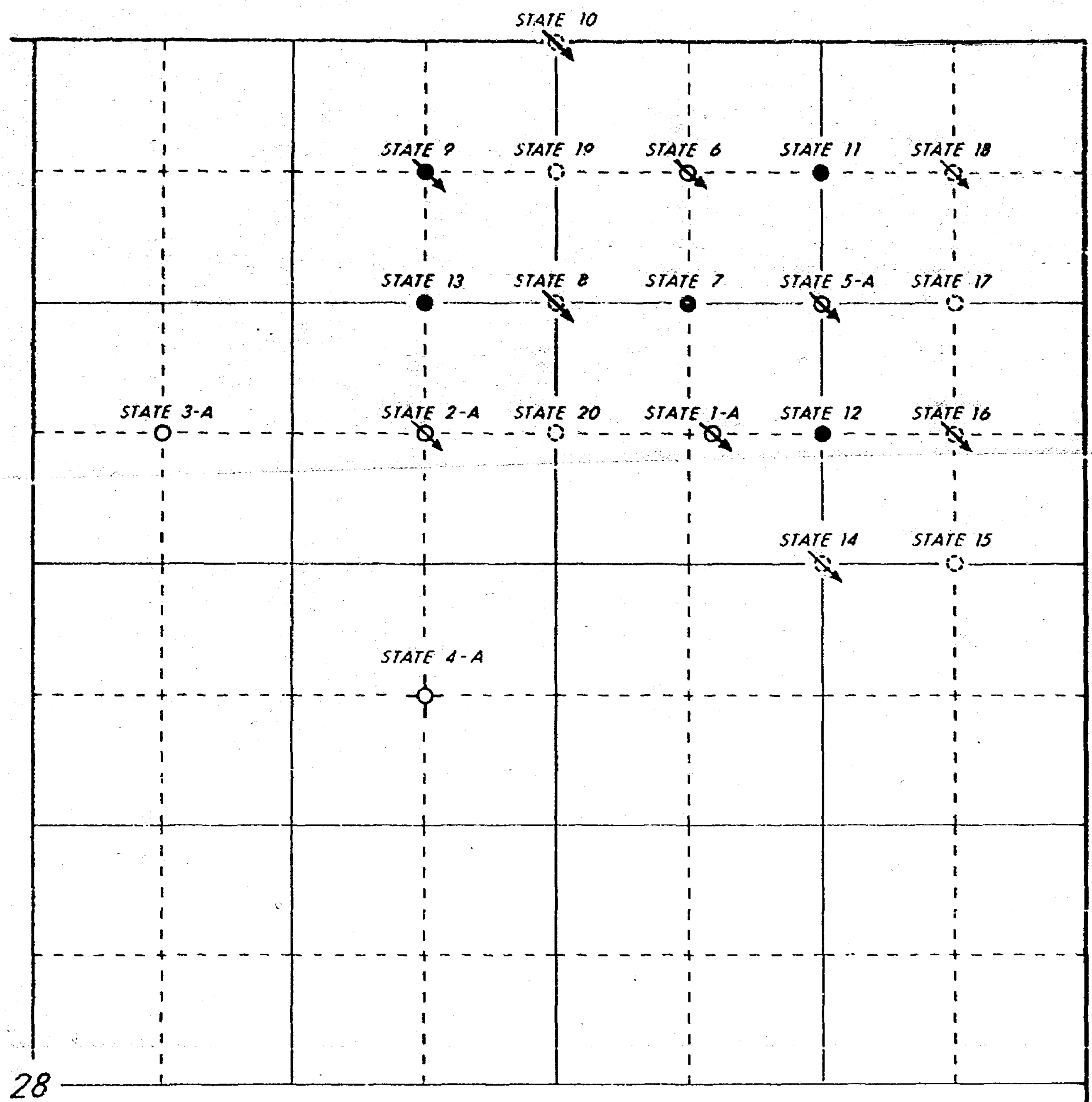

CHACO WASH POOL

28 - 20 N - 9 W

O LOCATION OF EXISTING WELL
○ LOCATION OF PROPOSED WELL

STATE OF NEW MEXICO
ENERGY AND MINERALS DEPARTMENT
OIL CONSERVATION DIVISION
STATE LAND OFFICE BLDG.
SANTA FE, NEW MEXICO
16 March 1982

EXAMINER HEARING

IN THE MATTER OF:

Application of Red Mountain Associates for the amendment of Order No. R-6538, McKinley County, New Mexico.

CASE 7459

BEFORE: RICHARD L. STAMETS

TRANSCRIPT OF HEARING

A P P E A R A N C E S

For the Oil Conservation Division:

W. Perry Pearce, Esq.
Legal Counsel to the Division
State Land Office Bldg.
Santa Fe, New Mexico 87501

For the Applicant:

Ernest L. Padilla, Esq.
P. O. Box 2523
Santa Fe, New Mexico 87501

INDEX

EXHIBITS

MR. STAMETS: We'll call next Case 7459.

MR. PEARCE: Application of Red Mountain Associates for the amendment of Order No. R-6538, McKinley County, New Mexico.

MR. PADILLA: Mr. Examiner, Ernest L. Padilla, Santa Fe, New Mexico, on behalf of the applicant in this case.

I have one witness to be sworn.

(Witness sworn.)

MOHAMED ZENATI

being called as a witness and being duly sworn upon his oath, testified as follows, to-wit:

DIRECT EXAMINATION

BY MR. PADILLA:

MR. STAMETS: Mr. Padilla, I'm not certain it would be necessary to requalify the witness since he has been previously qualified, but I think in view of the extended time since the first case it might be well today.

MR. PADILLA: Okay.

Q Mr. Zenati, for the record would you please state your name and where you reside?

A. My name is Mohamed Zenati. I reside in Denver, Colorado.

Q. Mr. Zenati, what's your connection with the applicant, Red Mountain Associates, in this case?

A. I'm the consulting engineer.

Q. Mr. Zenati, have you previously testified before the Oil Conservation Division and had your credneitals accepted as a matter of record?

A. Yes, I have.

Q. Are you familiar with the purpose of today's case?

A. Yes.

MR. PADILLA: Mr. Examiner, we tender Mr. Zenati as an expert petroleum engineer.

MR. STAMETS: The witness is considered qualified.

MR. PADILLA: Also, Mr. Examiner, I believe that at the conclusion of the last hearing that Red Mountain Associates had on January 16th, they were to bring additional data or evidence in support of their application, as requested at that time.

We believe at this point that Mr. Zenati has brought that evidence, especially evidence concerning the fracture point of the formation where they are injecting water.

In that connection, with your permission, now we will proceed.

Q Mr. Zenati, turning to what has been marked as Exhibit Number One, would you please identify what that is and explain what it contains?

A. I've written down the formulas to calculate the horizontal fracture initiation pressure and the vertical fracture intitiation pressure.

Q Mr. Zenati, would you go through the explanation of that formula and how it applies to the lands wherein the injection is taking place?

A. Presented in Exhibit One, three papers that explain how these formulas were derived.

Q Mr. Zenati, are these labeled as Exhibits One-A and One-B?

A. That's correct.

Q And are these the source documents for your formula?

A. That's correct.

Q Would you then explain in more detail what the -- how you arrived at the figures that you -- or your conclusion and also the pertinent data in the source papers?

A. We considered that because of the very shallow depth of these -- of the formation, that it would probably be horizontal fracture. We came out to using some investigation that the average overburden pressure gradient would be one psi per foot, which would result in an initiation pressure of at least 300 pounds for that particular formation.

Q. Mr. Zenati, did you make certain assumptions in plugging in certain figures into your formula?

A. Yeah. In trying to calculate if there was no tensile strength to the material, that the fracture could be vertical, calculated the pressures that it would require to get a vertical fracture. For that I have made some assumptions, since we have not run any tests on the -- on either the sands or the shales as to the value of the pore sands ratio, and they are documented also in, I believe, Exhibit Two.

Q. Is that Exhibit Two-A and Two-B, is that, would you explain what sources --

A. These are the result of investigation made by several people that present the ranges of -- of these parameters that I'm going -- that I've been using in the ensuing calculations.

Q. Now, those papers, Mr. Zenati, are they recent -- do they present reasonable assumptions or that you have obtained from the papers?

A. I believe so.

Q In your opinion. And in your opinion the factors that you have used and you have derived from those papers, are they applicable to the formation in which the injection is taking place?

A. I believe they are.

Q Before we proceed, would you explain also, I don't think that I -- that I asked you what these papers are as far as Exhibits One-A and One-B and Two-A and Two-B. What are those papers and where did you -- where did you obtain them?

A. Okay, these papers were presented at the Society of Petroleum Engineer annual meetings, and the first exhibit is titled, Comprehensive Design Formula for Hydraulic Fracturing. This is where I got the theoretical relation that I'm using to calculate the different pressures.

Q Mr. Zenati, how do you or how does the formula presented in Exhibit One relate to the waterflood project? You arrived at a determination that the formation could withstand 300 psi. How does that relate to that waterflood?

A. We've been authorized to inject at a surface pressure of 68 pounds. At 68 pounds it is not enough pressure to be able to move any fluid into the formation, and by there, we are in fact withdrawing more fluids than we are injecting, and we're asking to increase our injection pressure in order to be able to inject more fluid and at least maintain the pressure in the reservoir.

Q Mr. Zenati, could you derive your figures through other kind of testing that would probably be expensive?

A. It is possible to obtain -- to measure some of these parameters. Because of the low production of these wells, I do not feel it would be economical, and we went the other way by making a literature survey and obtaining average values and looking at the range and applying theoretical formulas.

Q To what pressure do you want to increase the waterflood at the surface now?

A. I believe that if the pressure is increased to 207 pounds enough water would be injected to maintain the pressure of the reservoir.

Q Mr. Zenati, I believe that at the last hearing, and I'm not too -- since I didn't represent Red Mountain in that case or that hearing, I'm not -- it's my understanding that there was some concern by the Division as to vertical fracturing.

Would you now turn to Exhibit Number Three and Three-A and describe what that is and what it contains, and also indicate how those affect vertical fracturing and how it relates to the formation which is under consideration here today.

A. Since we haven't measured the -- the vertical tensile strength of the different rocks, it is possible, although unlikely, that a vertical fracture would result.

The concern that the Commission voiced in the last hearing was the possible contamination of water sands.

In Exhibit Two and Three I present some theoretical investigation as to determining how a fracture can be contained on a vertical plane, and what would be the extent of this vertical fracture into the bordering layers, the upper and the lower layers. These are recent papers that were also presented at the Society of Petroleum Engineer 19 -- in the annual meeting, 1981.

In Exhibit Two I show that if we use average parameters, we are way below -- we are below the critical factors that would make the fracture propogate from the sand into the -- into the shale above and below the reservoir.

Q. It's your conclusion, then, that vertical fracturing, given the overburden pressure, would be minimal or at least not occur in such a fashion as to contaminate any potential fresh water aquifers in the area?

A. Yeah, it is my belief. We have cored or have examined the core of the sand. The description given by the geologist is a well consolidated sand which would indicate that the vertical tensile strength is not nil, but we did not run a test for that. The calculation on the containment of fracture was in the unlikely case that a fracture was vertical that it would not spread very far into the underlying and overlying shale and therefor would not contaminate any sand above that shale, above and below these shales.

Q. Mr. Zenati, what is the of the reservoir?

A. There are several studies that have been published by Dr. Black where he indicates that the Menefee formation in that area is composed of sands that are very lenticular and I've presented that.

Q. Is that in the form of Exhibits Four-A, B, and C?

A. That is correct.

Q. Do you have any logs that would also demonstrate that the sands are lenticular in nature?

A. We do.

Q. Would you --

MR. PADILLA: Mr. Examiner, we have only set of these logs and we can provide copies or leave these logs with you, but to finish the testimony he will have to refer to them.

MR. STAMETS: I think at this stage one set of logs would be sufficient. If it develops we need another one, we will ask for it.

Q Okay. Mr. Zenati, would you go through those and explain how the sands are lenticular in nature?

A Okay, these sands -- these several logs are from wells that were drilled in the formation of interest. Although we haven't drilled any well yet outside the particular formation, you can see that there are other sands lying over and below the particular sand, and in fact they are lenticular. They disappear from the logs. You see that their areal disposition is rather random and of very limited nature.

Q Could some of those sands be water-bearing sands?

A It is possible. These sands have not been tested for quality of the water.

Q Assuming that there are water-bearing sands, would that mean that should contamination occur, that contamination would be confined just to those particular sands and it would not migrate throughout the reservoir?

A. According to the previous calculation on the containment pressure of a fracture, it would be very unlikely that these sands would be contaminated.

Q Assuming that some of these sands are water-bearing sands, would -- what is the size of the -- or the areal extent of the sands? How big are they, in other words?

A. They would be, the order of magnitude would be only 20 acres.

Q In your opinion would exploitation of the water resources, should there be any there, occur in the foreseeable future?

A. I do not believe so. There are not any population center of any size within, I believe, 30 to 40 miles radius.

Q Mr. Zenati, do you have anything further to add to your testimony concerning, well, concerning your testimony here today?

A. The only thing that I'd like to add is to restate the last point that we tried to make, that the Menefee formation is a series of shale and sand stringers of very areal extent. We do not have, we do not know if some of the overlying sands contain fresh water, but if they did, the very limited extent of these sands doesn't seem to make them usable in the foreseeable future.

Q Mr. Zenati, another issue involved in this case is injecting or deletion of the requirement in the original order authorizing the waterflood to allow or to delete the requirement that injection be through tubing and a packer.

In that connection would it make any difference, given your testimony here today, whether you were injecting through a packer or -- and tubing as opposed to the -- through a casing?

A. We do not believe so for similar reasons as were stated in trying to receive an increase of the injection pressure.

Injecting through casing instead of tubing would not, because of the low pressures involved, would not damage any of the -- of the sands overlying and underlying the formation, whether they contain fresh water or brackish water.

Q Mr. Zenati, does it make any difference that the casing is cemented from total depth to the surface in all the injection wells?

A. We believe we have had a very good casing and cementing program and there again, the level of the injection pressure is so low that we do not see any damage occurring.

Q Even if you increase the pressure to, say, did you say 150 psi?

A. 170.

Q 170, even if you increase the pressure to that point?

A. That's correct.

MR. PADILLA: Mr. Examiner, I believe that's all we have. We'd pass the witness for cross examination. At this time we'd also tender Exhibits One through Four, and these logs as well.

MR. STAMETS: These exhibits will be admitted.

CROSS EXAMINATION

BY MR. STAMETS:

Q Mr. Zenati, just to confirm if I got the right figure written down, I thought at one stage you said you wanted 270 and the second time you said 170 and it says 170 in the original transcript, so 170 is the correct figure?

A. That is the pressure.

Q And that is a surface injection pressure.

A. Surface injection pressure.

Q Okay. Now in the first case you also

mentioned -- the first day of this hearing, you also mentioned that you had a number of acidizing operations, I believe, which had a breakdown pressure of 350 pounds. Did you bring any copies of those records with you?

A. We did not acidize in any other formation. What I did was found out records of previous operators who did acidize. I contacted the companies that did the acidizing job and I had at least a verbal confirmation of one of these service companies. I have not received their charts or a notarized statement indicating that the breakdown pressures were above 350 pounds.

Q. Are you saying that you or your company do not have copies of any treatment records on these wells, is that correct?

A. Yeah, on the wells that were drilled and operated by the previous owners.

Q. Do you have any copies of treatment records that were written out?

A. No, we haven't acidized any of these formations.

Q. Have you fractured any of the formations?

A. We have not. As of Friday, I'm supposed to receive a chart and a statement from Cementers, Inc., that did acidizing of a few wells two or three years ago.

Q Will you forward copies of those to the Division when and if you receive them?

A I will.

Q What's the depth of the injection interval?

A 300, 290 to 300 feet, 305 feet.

Q And is the -- are you saying that there may be water, fresh water, above that interval but it's going to be isolated, discontinuous sandstones?

To your knowledge are there -- are there any shallow fresh water wells in the area of this project?

A. There is a fresh water well a mile and a half, I believe, or a mile away from the -- from the lease, but I do not know, there are no records on the -- on the depth of the zone that is producing.

Q How long do you believe it will be, assuming that you get an injection pressure increase, how long will it be before you will be able to evaluate the project, whether or not it's going to be a success?

A. With continuous injection, provided that we do increase the pressure and inject enough fluids, I believe in a month to a month and a half would be enough. These wells are drilled on a very close spacing.

Q Is the injection equipment available to you at the lease to provide you with the ability to alter your pressure and injection rates?

A. Yes, it does.

Q. Could you run your own step rate test?

A. I could.

Q. Is there any significant expense involved in that?

A. No.

Q. If the order came out granting you your relief you seek here but requiring step rate tests within six months, is that the sort of thing that could be done?

A. Yes.

MR. STAMETS: Any other questions of the witness?

MR. CHAVEZ: Yes.

QUESTIONS BY MR. CHAVEZ:

Q. Mr. Zenati, the sandstones which exist at shallow intervals, are they the same geologic age and character as the oil producing sandstones?

A. Yes, they are.

Q. Would you presume that the water quality would probably be the same, being out of the same geologic age?

A. It is possible.

Q. What is the source of water for injection?

A. The source water is the supply well is perforated to the Gallup formation.

Q. And that's the Gallup?

A. Yeah.

Q. Is the water quality in the massive Gallup formation, how does that compare with the water that you produce naturally out of the Menefee?

A. Well, it's slightly more brackish. But in terms of injection it is compatible.

MR. CHAVEZ: I have no more questions.

MR. STAMETS: Any other questions of this witness?

MR. HALL: Mr. Examiner, my name is Scott Hall, representing the Commissioner of Public Lands, for the purposes of entering an appearance. I have no questions.

MR. STAMETS: The witness may be excused.

Is there anything further in this case?

The case will be taken under advisement.

(Hearing concluded.)

CERTIFICATE

I, SALLY W. BOYD, C.S.R., DO HEREBY CERTIFY that the foregoing Transcript of Hearing before the Oil Conservation Division was reported by me; that the said transcript is a full, true, and correct record of the hearing, prepared by me to the best of my ability.

Sally W. Boyd CSR

I do hereby [illegible] that the foregoing is
a [illegible]
the [illegible] in
heard [illegible] 3-16 [illegible] 7459,
19 82.
Richard L. Stamets, Examiner
Oil Conservation Division

SALLY W. BOYD, C.S.R.
Rt. 1 Box 193-B
Santa Fe, New Mexico 87501
Phone (505) 455-7409

CERTIFICATE

I, SALLY W. BOYD, C.S.R., DO HEREBY CERTIFY that the foregoing Transcript of Hearing before the Oil Conservation Division was reported by me; that the said transcript is a full, true, and correct record of the hearing, prepared by me to the best of my ability.

Sally W. Boyd CSR

I do hereby certify that the foregoing is
7459
3-16 82
Richard L. Stamets, Examiner
Oil Conservation Division

SALLY W. BOYD, C.S.R.
Rt. 1 Box 193-B
Santa Fe, New Mexico 87501
Phone (505) 455-7409

STATE OF NEW MEXICO
ENERGY AND MINERALS DEPARTMENT
OIL CONSERVATION DIVISION
STATE LAND OFFICE BLDG.
SANTA FE, NEW MEXICO
17 February 1982

EXAMINER HEARING

IN THE MATTER OF:

Application of Red Mountain Associates for the amendment of Order No. R-6538, McKinley County, New Mexico. CASE 7459

BEFORE: Richard L. Stamets

TRANSCRIPT OF HEARING

A P P E A R A N C E S

For the Oil Conservation Division: W. Perry Pearce, Esq.
Legal Counsel to the Division
State Land Office Bldg.
Santa Fe, New Mexico 87501

For the Applicant:

MR. STAMETS: We'll call Case 7459.

MR. PEARCE: Application of Red Mountain Associates for the amendment of Order No. R-6538, McKinley County, New Mexico.

MR. STAMETS: At the request of the applicant this case will be continued to the March 16th Examiner Hearing.

(Hearing concluded.)

CERTIFICATE

I, SALLY W. BOYD, C.S.R., DO HEREBY CERTIFY that the foregoing Transcript of Hearing before the Oil Conservation Division was reported by me; that the said transcript is a full, true, and correct record of the hearing, prepared by me to the best of my ability.

Sally W. Boyd CSR

I do hereby certify that the foregoing is a complete record of the proceedings in the Examiner hearing of Case No. 7459, heard by me on 2-17 1982.

Richard L. Stamets, Examiner
Oil Conservation Division

SALLY W. BOYD, C.S.R.
Rt. 1 Box 193-B
Santa Fe, New Mexico 87501
Phone (505) 455-7409

STATE OF NEW MEXICO
ENERGY AND MINERALS DEPARTMENT
OIL CONSERVATION DIVISION
STATE LAND OFFICE BLDG.
SANTA FE, NEW MEXICO
20 January 1982

EXAMINER HEARING

IN THE MATTER OF:

Application of Red Mountain Associates for the Amendment of Order No. R-6538, McKinley County, New Mexico. — CASE 7459

BEFORE: Richard L. Stamets

TRANSCRIPT OF HEARING

A P P E A R A N C E S

For the Oil Conservation Division: W. Perry Pearce, Esq.
Legal Counsel to the Division
State Land Office Bldg.
Santa Fe, New Mexico 87501

For the Applicant: James Thomson, Esq.
Santa Fe, New Mexico 87501

I N D E X

E X H I B I T S

MR. STAMETS: We'll call next Case 7459.

MR. PEARCE: Application of Red MOuntain Associates for the amendment of Order No. R-6538, McKinley County, New Mexico.

MR. STAMETS: You may proceed.

MR. THOMSON: My name is James Thomson, T-H-O-M-S-O-N. I'm an attorney here in Santa Fe and I'm representing Red Mountain Associates, and we have one witness.

(Witness sworn.)

MOHAMED ZONATI

being called as a witness and being duly sworn upon his oath, testified as follows, to-wit:

DIRECT EXAMINATION

BY MR. THOMSON:

Q. Would you state your name, please?

A. Mohamed Zonati.

Q. And where do you live, sir?

A. 2626 Holly Street, Denver, Colorado.

Q. And what is your occupation?

A. Petroleum engineer.

Q Would you please give the Division and the Hearing Officer a brief background of your education and training as a petroleum engineer?

A. I graduated with a Bachelor of Science in 1973 and worked for, among others, the National Oil Corporation, and subsequently with Scientific Softwear, and Kiplinger and Associates for about four years.

Q Okay, where did you -- okay, go ahead.

A. I went to school at Colorado School of Mines, where I'm in the process of finishing a Phd.

Q How far along are you in your Phd?

A. I've completed the course work and the comprehensive exam and am in the process of writing my thesis.

Q Now, Mr. Zonati, did you appear before this Division for the purpose of obtaining the original waterflooding project approval?

A. Yes, I did.

Q And were you accepted as an expert and qualified as an expert?

A. Yes, I did.

MR. THOMSON: Mr. Stamets, we would tender Mr. Zonati as an expert.

MR. STAMETS: The witness is considered qualified.

MR. THOMSON: Thank you, sir.

Q Now, Mr. Zonati, the first item in this application, you've asked for extension of a pressure maintenance program. Could you please explain to the Hearing Officer why you are requesting an extension of the pressure maintenance program?

A. We presently are getting water into a very shallow field. It's an average of about 500 feet deep, and there's another zone at 300 feet.

It's a channel sand and because it is very irregular we do not know at the present time the exact location of the injection wells, but we're extending the field and we ask you to be able to designate the injection well through administrative order rather than through hearing.

Q Now, Mr. Zonati, are you also asking for an increase in the injection pressure from 68 pounds per square inch --

A. Yeah.

Q And why are you making this application for an increase in injection pressure?

A. We have some wells that would not take water and we need to increase the pressure to be able to maintain --

Q Okay.

A. -- a homogenous water bank.

Q. Do you have an opinion whether it is necessary in some wells to have this increased injection pressure in order to promote the program that you've undertaken?

A. Yes.

Q. And to what pressure would you request?

A. We're asking to be authorized to inject water up to 170 pounds surface pressure.

Q. And do you have an opinion whether that is probably sufficient?

A. Yeah, I --

Q. Okay, now do you have an opinion whether or not an increase to this pressure that you have requested would result in any fracturing of the confining strata?

A. I do not think so.

Q. Could you explain why?

A. By using an average overburden pressure gradient of 1 psi per foot we would end up with a bottom hole at 300 feet, the shallow zone that we're injecting into, with a frac pressure that would be greater or equal to -- to about 300 pounds.

With a pressure of 170 pounds of surface pressure and counting the weight of the column of water, we would be below the -- this pressure.

Q Is there any danger in your opinion to damage to the strata, the confining strata?

A. These water sand, or channel sand, they're very -- of very limited extent.

Q Now, have you had any what you describe as acidizing operations?

A. Yeah, we, from the records we conducted some acidizing operations and from what I've been able to notice is that the breakdown pressure was about 350 pounds.

Q That's per square inch?

A. Per square inch, uh-huh.

Q The last item that you've requested is a request that you inject through the casing.

A. That's right.

Q Could you please describe why you are making this request?

A. Presently we're injecting through tubing with a packer holding the tubing downhole, and we're asking to be able to inject through casing for the reason of cost and because we do not feel that that would change the injection, and it would not contaminate any water sands present in the area.

Q All right, do you believe that there --

it would not contaminate the water sands in the area?

A. Because of three things: We feel that after analyzing the water that we use for injection, there are no corrosive agents present in the water. The casing that we're using follow all the API standards, and we are also cementing the casing from TD to top of the hole. And the injection pressure that we -- that we would be injecting at are very small.

Q. Is this a closed system?

A. Yeah, so there is no oxygen introduced into the water, and I've attached a water analysis.

Q. Okay. Is anyone using this sand, this --

A. No.

Q. -- that you may contaminate?

A. Not that I know of. I know there is a few water sands but there's been no use of these water sands in the area.

Q. Just back to one point. Why did you pick the 170 pounds per square inch from 68?

A. We feel that with that pressure it will be enough to inject in all the wells, inject enough water in all the wells.

Q. Now is this a request -- or is this a change from your original request when we had the original hearing about waterflooding? What were you requesting at that time, or do you recall?

A. We were requesting 200 pounds bottom hole pressure.

Q. And how does that --

A. 200 pounds surface pressure.

Q. Okay, and how does that -- how does that relate to bottom pressure?

A. It would relate to about 320 to 350.

Q. Now, Mr. Zonati, did you prepare Exhibits One, Two, Three, Four, and Five for presentation at this hearing?

A. Yes, I did.

MR. THOMSON: We submit Exhibits One through Four, it is, and they're just summaries of what he's testified to.

MR. STAMETS: Okay, are those marked?

MR. THOMSON: Yes, sir.

MR. STAMETS: Well, let's take a look at them. Standard procedure would be to have those during the discussion.

MR. THOMSON: One, Two, Three, Four, Five. Yeah, there's Five of them.

(Thereupon a discussion was

had off the record.)

MR. STAMETS: Well, let's take some of these issues here.

CROSS EXAMINATION

BY MR. STAMETS:

Q First off, the expansion of project, Mr. Zonati, it would appear to me that the Division's general rules and regulations on project expansion would be sufficient. That could be done administratively without any -- anything special. You haven't asked for anything special at this hearing, so unless you had something particularly on your mind, it doesn't seem like we need to do anything there.

As to the pressure, now, that limitation is contained in paragraph four of Order R-6538, and it goes on to say, though, that the Division Director may authorize the higher surface injection pressure upon a satisfactory showing that such pressure will not result in fracturing of the confining strata.

So that could have been done administratively, and although you have testified to it, I -- I would like to see some evidence in the form of a step rate test or the record of the acid job to show what instantaneous shut-in pressure was following the breakdown in pressure at

350 to assure myself that indeed, that this half a pound per foot of depth is -- is the accurate pressure.

Then you've discussed water zones. What depth are we talking about for fresh water in this area?

A. I think that there's a zone at 200 feet.

Q. That's immediately above the injection interval.

A. Yeah.

Q. So it is --

A. About 100 feet above.

Q. So it's the sort of thing that it would be highly possible that if a person injected above frac pressure that the injection fluid could enter this shallow water zone.

A. No, you would have 200 -- you would have 100 feet of shale, and with that kind of frac pressure you would not be able to fracture the shales.

Q. Where would the fractures go, then?

A. Well, I don't think you would -- you would fracture, but it would take much more pressure to be able to fracture 100 feet of shale and contaminate the other sand.

Q. Are you certain that these shales don't contain native fractures?

A. I'm not certain, but because of the vertical permeability of the shale it's almost negligible.

Q. Well, that's true, but I'm certain we've all experienced fractured shales that some even would be oil and gas reservoirs.

A. There is no mention in the literature and all the work that has been done in the Menefee of fractured shale.

We have not --

Q. My problem, Mr. Zonati, is that you have offered a considerable amount of opinion and no evidence whatsoever, and I believe that based on the lack of evidence in this case, I would have no recourse but to deny the application and allow you to proceed under the provisions of the order as originally issued.

Now if you would like to continue this case and bring in some additional evidence, and perhaps that was in the original record. I did not hear that case so I'm not certain of that.

A. All right, how about the point that we raised, injecting through a casing instead of through tubing?

Q. I think in large measure that might depend on what the evidence was relative to the water zones in the area, their locations.

What size casing do you have in those wells?

A. 4-1/2.

Q. And --

A. (Inaudible)

Q. And the reason for not needing tubing is simply the well cost?

A. It was the well cost.

Q. So it's not a matter of injection volumes or anything?

A. No.

Q. Okay.

A. And, you know, when I talk about water sands, we have never analyzed these -- these waters, you know, for an operation of this size there's really -- you know, these wells of that depth, there is a lot of analysis that you would not conduct.

What I believe is, the water is probably brackish because judging from some of the water wells that were drilled in the area, and the water was not even suitable for -- for cattle.

Q. Well, again, that's opinion and I don't have any evidence of that, and we have a responsibility, both in State law and in our relationship with the Environmental

Protection Agency to protect any underground waters having total dissolved solids of less than 10,000 milligrams per liter.

And without more evidence than we have here today, I don't believe I could -- I could recommend approval of this application.

Would you -- would you like to have this case continued?

A. Yes, I would.

Q. Okay, would you like -- the next Examiner Hearing that I will be at will be February 17th. Is that an acceptable date?

A. No, I have other obligations then.

Q. The following hearing I will be the Examiner at should be March the 17th.

A. I'll change, then I'll try to make it on February 17th.

Q. All right. Then we will continue Case 7459 to that date and proceed.

I would suggest that you work with the Aztec District Office. I'm certain that if the evidence that you have is satisfactory to them, that we may not have any difficulty at the hearing.

MR. THOMSON: Thank you.

CERTIFICATE

I, SALLY W. BOYD, C.S.R., DO HEREBY CERTIFY that the foregoing Transcript of Hearing before the Oil Conservation Division was reported by me; that the said transcript is a full, true, and correct record of the hearing, prepared by me to the best of my ability.

Sally W. Boyd CSR

I do hereby certify that the foregoing is a [illegible] the [illegible] hearing of Case No. 7459, heard by me on 1-20 1982.

Richard L. Stamets, Examiner
Oil Conservation Division

SALLY W. BOYD, C.S.R.
Rt. 1 Box 193-B
Santa Fe, New Mexico 87501
Phone (505) 455-7409

STATE OF NEW MEXICO
ENERGY AND MINERALS DEPARTMENT
OIL CONSERVATION DIVISION
STATE LAND OFFICE BLDG.
SANTA FE, NEW MEXICO
6 January 1982

EXAMINER HEARING

IN THE MATTER OF:

Application of Red Ountain Associates for the Amendment of Order No. R-6538, McKinley County, New Mexico. CASE 7459

BEFORE: Daniel S. Nutter

TRANSCRIPT OF HEARING

A P P E A R A N C E S

For the Oil Conservation Division: W. Perry Pearce, Esq.
Legal Counsel to the Division
State Land Office Bldg.
Santa Fe, New Mexico 87501

For the Applicant:

MR. NUTTER: Call next Case Number 7459.

MR. PEARCE: Application of Red Mountain Associates for the amendment of Order No. R-6538, McKinley County, New Mexico.

MR. NUTTER: Applicant has requested continuance in this case.

Case Number 7459 will be continued to the Examiner Hearing scheduled to be held at this same place at 9:00 o'clock a. m. on January 20, 1982.

(Hearing concluded.)

CERTIFICATE

I, SALLY W. BOYD, C.S.R., DO HEREBY CERTIFY that the foregoing Transcript of Hearing before the Oil Conservation Division was reported by me; that the said transcript is a full, true, and correct record of the hearing, prepared by me to the best of my ability.

Sally W. Boyd CSR

I do ... the foregoing is ... heard by me on 1/6 ... 7459, ... 198 .

Oil Conservation Division, Examiner

SALLY W. BOYD, C.S.R.
Rt. 1 Box 193-B
Santa Fe, New Mexico 87501
Phone (505) 455-7409

STATE OF NEW MEXICO
ENERGY AND MINERALS DEPARTMENT
OIL CONSERVATION DIVISION

BRUCE KING
GOVERNOR
LARRY KEHOE
SECRETARY

POST OFFICE BOX 2088
STATE LAND OFFICE BUILDING
SANTA FE, NEW MEXICO 87501
(505) 827-2434

July 16, 1982

Mr. Ernest L. Padilla
Attorney at Law
P. O. Box 2523
Santa Fe, New Mexico 87502

Re: CASE NO. 7459
ORDER NO. R-6538-A

Applicant:

Red Mountain Associates

Dear Sir:

Enclosed herewith are two copies of the above-referenced Division order recently entered in the subject case.

Yours very truly,

JOE D. RAMEY
Director

JDR/fd

Copy of order also sent to:

Hobbs OCD x
Artesia OCD x
Aztec OCD x

Other

STATE OF NEW MEXICO
ENERGY AND MINERALS DEPARTMENT
OIL CONSERVATION DIVISION

IN THE MATTER OF THE HEARING CALLED BY THE OIL CONSERVATION DIVISION FOR THE PURPOSE OF CONSIDERING:

CASE NO. 7459
Order No. R-6538-A

APPLICATION OF RED MOUNTAIN ASSOCIATES FOR THE AMENDMENT OF ORDER NO. R-6538, McKINLEY COUNTY, NEW MEXICO.

ORDER OF THE DIVISION

BY THE DIVISION:

This cause came on for hearing at 9 a.m. on February 17 and March 16, 1982, at Santa Fe, New Mexico, before Examiner Richard L. Stamets.

NOW, on this 16th day of July, 1982, the Division Director, having considered the testimony, the record, and the recommendations of the Examiner, and being fully advised in the premises,

FINDS:

(1) That due public notice having been given as required by law, the Division has jurisdiction of this cause and the subject matter thereof.

(2) That the applicant, Red Mountain Associates, seeks the amendment of Order No. R-6538, which authorized applicant to conduct waterflood operations in the Chaco Wash-Mesaverde Oil Pool. Applicant seeks approval for the injection of water through various other wells than those originally approved, seeks deletion of the requirement for packers in injection wells, and seeks an increase in the previously authorized 68-pound limitation on injection pressure.

(3) That the applicant failed to present any substantial evidence in this case upon which the proposed amendments to said Order No. R-6538 could be based.

(4) That the application should be denied.

IT IS THEREFORE ORDERED:

(1) That the application of Red Mountain Associates for amendment of Division Order No. R-6538 is hereby denied.

(2) That jurisdiction of this cause is retained for the entry of such further orders as the Division may deem necessary.

DONE at Santa Fe, New Mexico, on the day and year hereinabove designated.

STATE OF NEW MEXICO
OIL CONSERVATION DIVISION

Joe D. Ramey

JOE D. RAMEY
Director

S E A L

fd/

A. EXTENSION OF PRESSURE MAINTENANCE PROGRAM

Since August 1981, several wells were completed, put on production in the Chaco Wash field. Those are #20, #23, #24, #22. Drilling permits were approved for three more wells in the same area: #25, #26, #27, in late 1981, and are being presently drilled.

Red Mountain Associates intends to extend the pressure maintenance program by injecting water thru one or more wells.

Exhibit I

B. INCREASE OF INJECTION PRESSURE

Presently the injection pressure is limited at 68 psi surface pressure which gives an approximate bottom hole pressure of 198 psi.

Using an average overburden pressure gradient of 1 psi/ft, this would indicate that at a reservoir depth of 300', the oberburden pressure is 300 psi. The frac pressure is greater or equal to the present bottom hole pressure.

This shows that surface injection pressure could be increased up to 170 psi with the bottom-hole injection pressure remaining well under the frac pressure, considering friction losses in the pipe and the compressive strength of the reservoir sand and the pressure drop in the perforations.

Furthermore, it was observed during acidizing operations that the same formation would break down at a surface pressure of no less than 350 psi.

Exhibit II

B. INCREASE OF INJECTION PRESSURE

Presently the injection pressure is limited at 68 psi surface pressure which gives an approximate bottom hole pressure of 198 psi.

Using an average overburden pressure gradient of 1 psi/ft, this would indicate that at a reservoir depth of 300', the oberburden pressure is 300 psi. The frac pressure is greater or equal to the present bottom hole pressure.

This shows that surface injection pressure could be increased up to 170 psi with the bottom-hole injection pressure remaining well under the frac pressure, considering friction losses in the pipe and the compressive strength of the reservoir sand and the pressure drop in the perforations.

Furthermore, it was observed during acidizing operations that the same formation would break down at a surface pressure of no less than 350 psi.

Exhibit II

C. INJECTION THRU CASING

The factor limiting injection of fluids thru casing is a casing leak resulting in contamination of water sands that may be present in the area.

The injection wells are completed at 500 ft in the Menefee formation. The Menefee is a sand-shale sequence of about 1500 ft of thickness in the area. Those sands are channel sands of limited areal extent and not interconnected.

Furthermore, the probability of a casing leak developing as a result of injection operation is very small considering the composition of the water injected, the type of completion and the pressure.

An analysis of the injection water is included in the Appendix. It shows the absence of any acid gas or other corrosive agents. Furthermore, no oxygen is introduced since the injection system is closed.

The casing run into the well is new and conforms to API standards. This casing is cemented from TD to the surface. The cement also conforms to API standard.

Furthermore, it has been observed that in operating the Red Mountain field waterflood using the same water supply, that no failure due to corrosion was noted in the unprotected injection lines in more than 8 years of operations.

Exhibit III

NATIONAL CEMENTERS CORPORATION
DIVISION LABORATORY
GRAND JUNCTION, COLORADO

LABORATORY WATER ANALYSIS

Report No. W-FR03-80

To: Red Mountain Associates
209 Hawthorn Rd.
Baltimore, MD 21210

Date: Oct. 8, 1980

Submitted By: Mohamed Zenati   Date Received: Oct. 7, 1980

Well No. ______ Depth: ______ Formation: ______

Location: Water from supply well

Resistivity	70	
Temperature	60.2°F	
Specific Gravity (Sp.Gr.)	1.000	
pH	7.763	
Total Dissolved Solids	less than 2,900	parts per million*
Calcium (Ca)	less than 50	parts per million
Magnesium (Mg)	negative	parts per million
Chlorides (Cl)	472	parts per million
Bicarbonates (HCO_3)	420	parts per million
Sulfates (SO_4)	750	parts per million
Iron (Fe)	negative	parts per million
Potassium (K)	negative	parts per million
Stability Index (SI)		

REMARKS:

* indicates - parts per million by weight; uncorrected for Specific Gravity.

LABORATORY ANALYST:

Pahler & Dolberg

Respectfully submitted,
National Cementers, Corporation

By: Thomas Eapen
Thomas Eapen, Field Chemist

EXhibiT IV

CUSTOMER National Park Services
ATTENTION Gary Moore
ADDRESS P. O. Box 728
CITY Santa Fe, New Mexico 87501
INVOICE NO. 09148

SAMPLES RECEIVED 9/18/72 | CUSTOMER ORDER NUMBER PX-7000-3-0049

TYPE OF ANALYSIS Water Quality Analysis - 1 Sample

Sample Identification

Chaco Canyon, NM
"Field's Well" -3100 ft.

NOTE: Sample Collected After 24 hr. Artesian Flow at 165 GPM

Analysis	Report	Units
Arsenic	0.001	mg/l
Bicarbonate (as $CaCO_3$)	200	mg/l
Carbonate (as $CaCO_3$)	0	mg/l
Hardness (as $CaCO_3$)	39.3	mg/l
Sulfate	577	mg/l
Chloride	44.1	mg/l
Fluoride	1.54	mg/l
Nitrate	0.7	mg/l
Phosphate (as Phosphorus)	1.63	mg/l
Silica	22.1	mg/l
Calcium	12.1	mg/l
Iron	0.56	mg/l
Magnesium	2.21	mg/l
Manganese	<0.01	mg/l
Potassium	4.40	mg/l
Sodium	67.0	mg/l
pH	8.14	
Total Solids	1775	mg/l
Color	30 True Color Units	
Conductivity	2600	uMho

APPROVED BY

James J. Mueller, President
9/27/72

PAGE 1 OF 1 PAGE

Controls for Environmental Pollution, Inc.

Exhibit

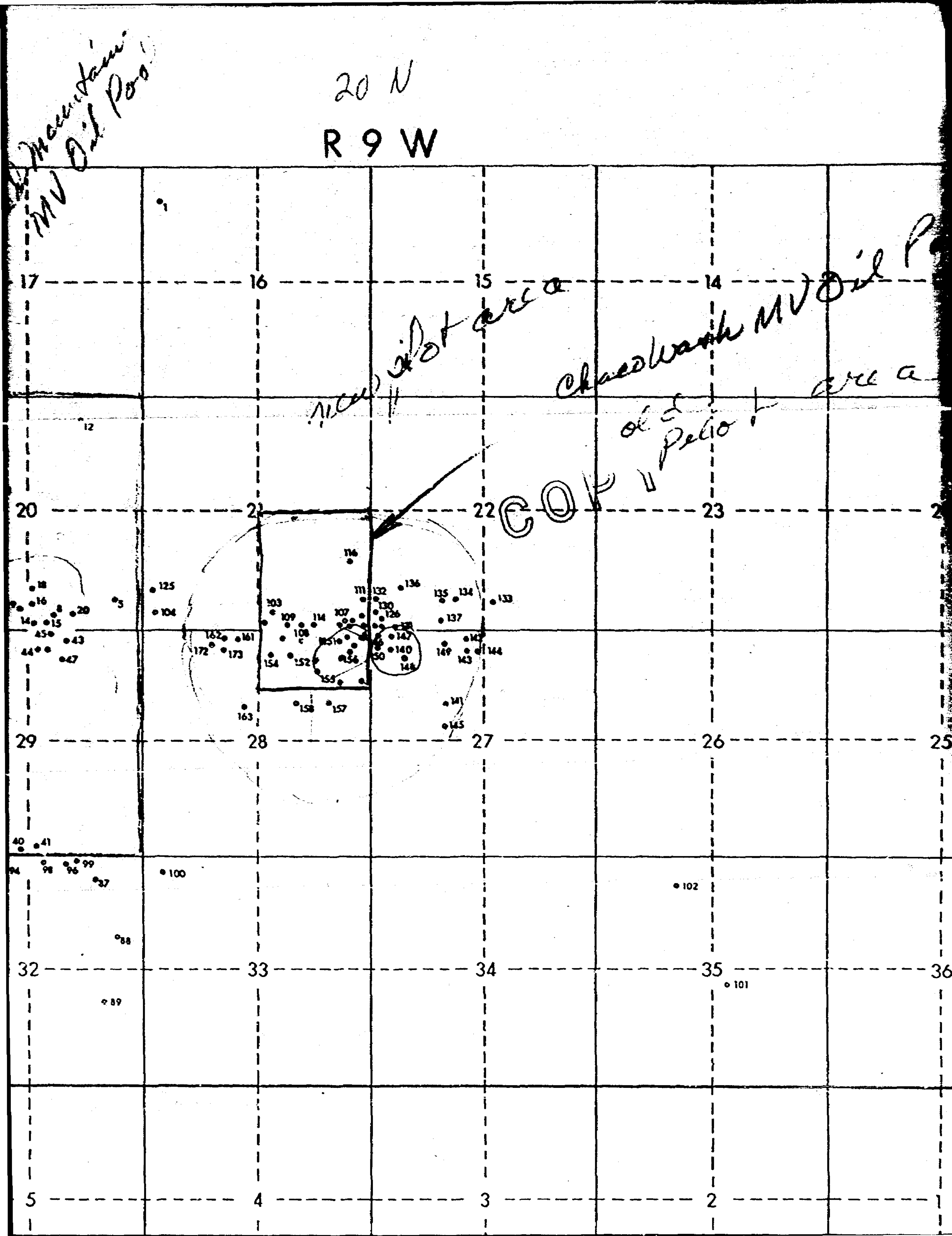
20 N
R 9 W
MV Oil Pool
new pilot area
MV Oil P
old pilot area
COPY
17
16
15
14
20
21
22
23
29
28
27
26
25
32
33
34
35
36
5
4
3
2
1

FRACTURE PRESSURE

The theory and practice of hydraulic fracturing has shown that the rock will fracture where the tensile stress equals the tensile of the rock. (Ref 1)

Let P_{wi} : initiating fracture pressure

P_{we} : expansion fracture pressure

For Horizontal fractures:

$$P_{wi} = P_{ob} + S_{tv}$$

$$P_{we} = P_{ob}$$

For Vertical fractures.

$$P_{wi} = \frac{2\nu}{1-\nu} \cdot (P_{ob} - P_p) + P_p + S_{th}$$

$$P_{we} = \frac{\nu}{1-\nu} \cdot (P_{ob} - P_p) + P_p$$

Calculations:

The overburden pressure gradient is about equal to 1 psi/ft. Ref 2,3

The Poisson's ratio for

Shales $.01 < \nu \leq .15$

Consolidated Sand $.15 \leq \nu \leq .27$

Unconsolidated Sand $.28 \leq \nu \leq .45$

BEFORE EXAMINER STAMETS
OIL CONSERVATION DIVISION
EXHIBIT NO.
CASE NO. 7459
2/18/82
Ex 1

Ex. 1

FRACTURE CONTAINEMENT

As theoretical investigatio[ns] have shown, the vertical fracture will be contained if the stiffness of the barrier formation (or the shear modulus) is greater than the stiffness of the pay zo[ne]

The intensity factor is defined as *

$$K = .8 * \Delta P * \sqrt{H}$$

Critical stress intensity factors for different rocks have been measured

For shales $K_c \simeq 1200$ psi inch$^{1/2}$

Chaco Wash case

$\Delta P \leq 200$ psi

$H \leq 10$

$K = 480 < K_c$

- Hydraulic fracture geometry: fracture containement in layered formation by H.A. Eebelen SPE 9261

* Optimization of stimulation design through the use of in-situ stress determination
M.D. Voegle & A.H Jones SPE 10308

1. Well Design ~~: Production~~ Drilling & Production
B.C. Craft, W.R. Holden & E.D. Graves Prentice Hall Inc

2. Laboratory Investigation of Fracture initiation Pressure and orientation.
W.L. Medlin & L. Masse SPE 6087

3. Effect of Poisson's ratios on rock properties
J. Kumar SPE 6094

4. Containment of Massive Hydraulic Fractures
E.R. Simonson
A.S. Aboo Sayed
R.J. Clinton

SPE

Society of Petroleum Engineers of AIME

SPE 9254

THE PREDICTION OF FRACTURE PRESSURES FOR WILDCAT WELLS

BEFORE EXAMINER STAMETS
OIL CONSERVATION DIVISION
EXHIBIT NO. 1A + B
CASE NO. 7459
Submitted by
Hearing Date 2/16/82

by Stephen R. Daines, Exploration Logging, Inc.

This paper was presented at the 55th Annual Fall Technical Conference and Exhibition of the Society of Petroleum Engineers of AIME, held in Dallas, Texas, September 21-24, 1980. The material is subject to correction by the author. Permission to copy is restricted to an abstract of not more than 300 words. Write: 6200 N. Central Expwy., Dallas, Texas 75206.

ABSTRACT

To date, the prediction of fracture pressures has been accomplished through the use of Gulf Coast-derived empirical formulae.[1-3] Now that exploration is extending to high latitudes and deep waters, the cost of these wells is becoming exceedingly high. The inability of the empirical relationships to adequately predict fracture pressures in areas other than the Gulf Coast to an acceptable degree of accuracy has prompted a reevaluation of the problem. Utilizing laboratory-derived physical properties of typical sedimentary rocks, and taking Hubbert and Willis'[4] Minimum Fracture Pressure Model a step further, an hypothesis is proposed that has the capability of predicting fracture pressures in a wildcat well subsequent to the first fracture test in compact formation.

The model requires that pore pressures, overburden pressures and lithology are known, and with this information fracture pressures may be accurately predicted at any point within the drilled hole. If the overburden pressure gradient can be extrapolated and pore pressures estimated, and if lithologies are continuously available, fracture pressures may actually be predicted a lag-time after the formation has been drilled. Initial testing of the model indicates that an accuracy greater than 95 percent may be consistently obtained, and the data is presented to substantiate this.

It is thus anticipated that this model may allow greater drilling efficiency, particularly in geopressured zones, thereby making the exploration effort safer and more economical.

INTRODUCTION

With drilling now extending to deep waters and high latitudes, the cost of these wells is becoming exceedingly high. Deep wildcatting in areas of poor geological control can be extremely hazardous and costly for lack of adequate pore pressure and fracture pressure information. If abnormally high pore pressures are encountered, a further casing string may be necessary; and if the pressure zone is shallow in relation to the target, completion of the well could be jeopardized.

Of prime importance in these wells is an accurate assessment of kick tolerance. For this to be achieved, knowledge of the fracture pressures at any depth in the open hole is necessary. The prediction of fracture pressures in the Gulf Coast and other areas that have undergone extensive drilling is accomplished by the use of empirical formulae.[1-3] These can be applied with confidence in other areas of similar geological and tectonic regime only when sufficient drilling has allowed the calculations of the necessary empirical constants. However, the absence of any method by which fracture pressures may be predicted outside these areas has necessitated the use of these empirical formulae, with the general result that actual fracture pressures can be very different from calculated pressures. This is mainly due to the application of the empirically derived constants, usually represently the "stress ratio," which are unrelated to the wildcat area. Accurate information on the in-situ principal stresses is vital for the solution of the fracture pressure problem. None of the empirical formulae can accurately predict stresses in poorly explored regions. A hypothesis is proposed that has the capacity to resolve and extrapolate the local principal stresses, subsequent to the first fracture test in compace formation. Compace is defined here as the point at which the sediment can transmit an applied stress through the grain contacts. Along with other pertinent data usually calculated on rank wildcats, i.e. overburden gradients and pore pressures, fracture pressures can then be obtained for any point within the drilled hole. Kick tolerance calculations then become realistic when they are based on fracture pressure calculations for that specific well, so that in the event that abnormal hole conditions are encountered, the chances of completing the well are greater than if reliance is placed on formulae containing unrelated empirical constants.

In order to hydraulically fracture the formation, it is necessary to overcome the minimum compressive stress. General formulae describe the minimum horizontal compressive effective stress as a function of the effective overburden pressure, which is empirically derived:

References and illustrations at end of paper.

Ex 1A

SPE 9254

THE PREDICTION OF FRACTURE PRESSURES FOR WILDCAT WELLS

BEFORE EXAMINER STAMETS
OIL CONSERVATION DIVISION
EXHIBIT NO. 1A + B
CASE NO. 7459
Submitted by
Hearing Date 2/16/82

by Stephen R. Daines, Exploration Logging, Inc.

This paper was presented at the 55th Annual Fall Technical Conference and Exhibition of the Society of Petroleum Engineers of AIME, held in Dallas, Texas, September 21-24, 1980. The material is subject to correction by the author. Permission to copy is restricted to an abstract of not more than 300 words. Write: 6200 N. Central Expwy., Dallas, Texas 75206.

ABSTRACT

To date, the prediction of fracture pressures has been accomplished through the use of Gulf Coast-derived empirical formulae.[1-3] Now that exploration is extending to high latitudes and deep waters, the cost of these wells is becoming exceedingly high. The inability of the empirical relationships to adequately predict fracture pressures in areas other than the Gulf Coast to an acceptable degree of accuracy has prompted a reevaluation of the problem. Utilizing laboratory-derived physical properties of typical sedimentary rocks, and taking Hubbert and Willis'[4] Minimum Fracture Pressure Model a step further, an hypothesis is proposed that has the capability of predicting fracture pressures in a wildcat well subsequent to the first fracture test in compact formation.

The model requires that pore pressures, overburden pressures and lithology are known, and with this information fracture pressures may be accurately predicted at any point within the drilled hole. If the overburden pressure gradient can be extrapolated and pore pressures estimated, and if lithologies are continuously available, fracture pressures may actually be predicted a lag-time after the formation has been drilled. Initial testing of the model indicates that an accuracy greater than 95 percent may be consistently obtained, and the data is presented to substantiate this.

It is thus anticipated that this model may allow greater drilling efficiency, particularly in geopressured zones, thereby making the exploration effort safer and more economical.

INTRODUCTION

With drilling now extending to deep waters and high latitudes, the cost of these wells is becoming exceedingly high. Deep wildcatting in areas of poor geological control can be extremely hazardous and costly for lack of adequate pore pressure and fracture pressure information. If abnormally high pore pressures are encountered, a further casing string may be necessary; and if the pressure zone is shallow in relation to the target, completion of the well could be jeopardized.

Of prime importance in these wells is an accurate assessment of kick tolerance. For this to be achieved, knowledge of the fracture pressures at any depth in the open hole is necessary. The prediction of fracture pressures in the Gulf Coast and other areas that have undergone extensive drilling is accomplished by the use of empirical formulae.[1-3] These can be applied with confidence in other areas of similar geological and tectonic regime only when sufficient drilling has allowed the calculations of the necessary empirical constants. However, the absence of any method by which fracture pressures may be predicted outside these areas has necessitated the use of these empirical formulae, with the general result that actual fracture pressures can be very different from calculated pressures. This is mainly due to the application of the empirically derived constants, usually represently the "stress ratio," which are unrelated to the wildcat area. Accurate information on the in-situ principal stresses is vital for the solution of the fracture pressure problem. None of the empirical formulae can accurately predict stresses in poorly explored regions. A hypothesis is proposed that has the capacity to resolve and extrapolate the local principal stresses, subsequent to the first fracture test in compace formation. Compace is defined here as the point at which the sediment can transmit an applied stress through the grain contacts. Along with other pertinent data usually calculated on rank wildcats, i.e. overburden gradients and pore pressures, fracture pressures can then be obtained for any point within the drilled hole. Kick tolerance calculations then become realistic when they are based on fracture pressure calculations for that specific well, so that in the event that abnormal hole conditions are encountered, the chances of completing the well are greater than if reliance is placed on formulae containing unrelated empirical constants.

In order to hydraulically fracture the formation, it is necessary to overcome the minimum compressive stress. General formulae describe the minimum horizontal compressive effective stress as a function of the effective overburden pressure, which is empirically derived:

References and illustrations at end of paper.

Ex 1A

$$P = \sigma_3' + p$$

where

$$\sigma_3' = K(S-p)$$

The minimum effective stress can be calculated from:

$$\sigma_3' = \sigma_t + \sigma_1' \left(\frac{\nu}{1-\nu}\right) \qquad (1)$$

where

$$S = \int_0^z g\rho(z)\ dz \text{ [5]} \qquad (2)$$

$$\sigma_1' = S - p$$

and

$$\sigma_t/\sigma_1' = \delta \qquad (3)$$

SUBSURFACE STRESS STATES

Effective Stresses

The concept of effective stresses was first introduced by Texarghi in 1923 and has subsequently been used extensively in mechanical applications. Basically, a hydrostatic stress (p) within a pore fluid has no influence on deformation, which is controlled by the effective stresses. This hydrostatic stress is thus a "neutral" stress, one that acts in all directions and in the same amount. This stress is regarded to exist in both the solid and the liquid, so the effective stresses arise exclusively from the solid skeleton. Major studies on rock deformation[6] have shown that fracture is controlled by the effective stresses, provided the rocks have a connected pore system:

$$\sigma_1' = \sigma_1 - p,\ \sigma_2' = \sigma_2 - p,\ \sigma_3' = \sigma_3 - p$$

where

$\sigma_1, \sigma_2, \sigma_3$ = principal maximum, intermediate and minimum compressive stresses

p = pore pressure

$\sigma_1', \sigma_2', \sigma_3'$ = principal compressive effective stresses

To apply this concept to a subsurface environment it must be assumed that the permeability is sufficient to allow movement of fluid and that the pore fluid is inert, so that the effects are purely mechanical.

[TH]EORETICAL SUBSURFACE STRESS STATES

There are two major schools of thought regarding the state of stress within the earth's crust:

1. That the stress state is hydrostatic - the three principal stresses are equal.

2. The horizontal principal stresses are a function of the effective vertical stress and Poisson's ratio.

The first hypothesis is generally termed Heim's rule and was later described as the "standard state."[7] It was stated in the form that stresses in rock tend to become equal because of the ability of the rocks to creep, such that any stress difference will eventually become alleviated. This hypothesis might be best illustrated by visualizing a scale model of the earth.[8] Although the earth as a whole has the strength of cold steel, if it is modeled as a 4-ft (1.22 m) diameter sphere, it would have the strength of pancake batter and a viscosity about twice that of honey, and would weigh 6.6 tons (5.99 t).

The second hypothesis describes the state of stress in an elastic, flay-lying strata of semi-infinite extent that is laterally constrained. If the weight of the overlying strata is the only source of stress, and the elongation in the horizontal directions are zero, then the relation

$$\sigma_H = \sigma_1'\left(\frac{\nu}{1-\nu}\right) \qquad (4)$$

is derived, where σ_H and σ_1' represent the horizontal and vertical effective stress components, respectively, and ν is Poisson's ratio. If, for example, Poisson's ratio for a particular rock type is 0.25, then the horizontal stresses would be one-third that of the vertical stress, provided the theoretical conditions were satisfied. In contrast, Heim's rule states that the horizontal stresses should be equal to the vertical stress.

Common to both theoretical discussions are the assumptions that one principal total stress is vertical and equal to the weight per unit area of the overlying rocks, and that the horizontal normal total stress is the same in any direction in the horizontal principal plane.

That the crustal stress state is largely not hydrostatic is illustrated by the number of structures and deformation processes that necessitate unequal stress states for their formation and maintenance. Jeffreys[9] suggested that significant stress differences occur within the upper 50 km of the earth's crust due to the existence of mountains and deep oceans. The occurrence of large-scale structures such as grabens, shear zones, dike swarms, nappes, folds, thrust and transcurrent faults suggest that not only did large stress differences occur in the past, but that stresses are still in a state of flux, as suggested by the occurrence of earthquakes. Some external stress, or tectonic stress, is necessary to produce these types of structures. Even in seismically inactive areas it is possible to infer a particular orientation of a tectonic stress, and it is reasonable to assume that even in the absence of tectonic structures and seismicity,[5] a region may be subject to some tectonic stress.

Hafner[10] showed that in order to obtain a hydrostatic type stress system (or "standard state") within a flat-lying strata of infinite horizontal extent in which lateral extension is prevented, the stress system is composed of two parts:

1. The effect of gravity, described by the second hypothesis above

2. A superposed horizontal stress which is constant in any horizontal plane but increasing uniformly with depth

Moreover, for faulting and folding to occur, the superposed horizontal stress must occur in a particular orientation within the horizontal plane. If it exists, and as such would be a tectonic stress, it would also increase uniformly with depth, assuming that the strata were isotropic and elastic.

The horizontal stress can thus be a minimum when there is no tectonic stress, such that

$$\sigma'_3 = \sigma'_1\left(\frac{\nu}{1-\nu}\right) \qquad (5)$$

where σ'_3 is the minimum principal horizontal effective stress, σ'_1 is the maximum principal stress which is equal to the effective weight of the overlying rocks, and ν is Poisson's ratio for the particular rock type. The largest magnitude that the horizontal stresses can reach is approximately three times the vertical stress, at which point failure occurs in the form of reverse faulting.[11]

The superposed horizontal tectonic stress, σ_t, can thus vary between the limits:

$$0 \le \sigma_t \le 3\sigma'_1 - \sigma'_1\left(\frac{\nu}{1-\nu}\right)$$

Since σ'_1 is calculated by subtracting the pore pressure from the total weight of the overlying strata, it is known for any point in the drilled hole. The superposed horizontal stress, if present, will increase uniformly with depth, or with σ'_1. Hence it may be assumed that the σ_t/σ'_1 ratio remains constant.

Ideally, Poisson's ratio for the rock type that is being drilled should be known at that moment in time, but this is not possible. However, Poisson's ratio has been experimentally measured for many rock types and is shown to be unique for a particular lithology.[12] Poisson's ratio cannot be measured for each and every rock type, but if it is possible to divide lithological types into a grouping that can be described by a Poisson's ratio, then there exists a means by which experimental results may be applied to the same lithological types in situ.

To be able to describe the minimum horizontal stress, it is necessary to measure the magnitude of the superposed tectonic stress σ_t. This can be achieved by a fracture test. Hence, after σ_t has been determined, the horizontal minimum effective stress state can be extrapolated to any point in the drilled hole.

THE ZERO TENSILE STRENGTH CONCEPT

The prediction of actual tensile strengths of subsurface sediments is probably impossible. Fortunately, this problem disappears if the common assumption, that any interval of sediment is intersected by joints and partings, is employed. Across these natural discontinuities the tensile strength is effectively zero.[4] However, the occurrence of open joints or fissures is generally quite rare and may be restricted to a particular zone or lithology. Cracks in competent sediments form during compaction and diagenetic processes as a result of very localized stress differences. Microcracks are also formed due to the drilling process and the resultant stress-release at the borehole walls. Cracks that are held closed by the in-situ compressive stresses require a pressure within the borehole equal to the compressive stress, so that the pressure holding the crack closed is reduced to zero. A further slight increase in pressure in the borehole should allow entrance of fluid into the crack so that pressure is transmitted to the sides. This pressure will extend the crack indefinitely, provided it can be transmitted to the leading edge.

This phenomena can be illustrated by considering a perfectly smooth, cylindrical borehole within an elastic medium, in which a crack extends to the wall of the hole. Upon an application of stress within the borehole that is slightly greater than the stress acting normal to the crack, a tensile stress is developed at the tip of the crack that approaches an infinite magnitude,[4] as illustrated in Figure 1.

The minimum pressure (F) necessary within the borehole to hold open and extend an existing fracture is therefore very slightly in excess of the regional horizontal stress normal to the plane of the fracture:

$$F = \sigma_t + \sigma'_1\left(\frac{\nu}{1-\nu}\right) + p \qquad (6)$$

where

p = pore pressure

The plane along which a fracture will start to form will be that plane across which the compressive stress is a minimum, and thus will first be reduced to zero with increasing pressure in the borehole. In the case where the horizontal compressive stress is less than the vertical compressive stress, this plane will be vertical; if the horizontal stresses are greater than the vertical stress, the plane would be horizontal.

THE FRACTURE TEST

Fracture tests are normally conducted after setting casing. The result of this test, when converted to an equivalent mudweight, is taken to be the maximum mudweight that the next hole section can withstand without losing circulation.

Examination of the principals involved suggests that this assumption is valid only in a certain set of circumstances. If the last casing shoe was cemented in an abnormally high pore pressure zone and the pore pressure then decreases significantly with depth, the fracture pressure will decrease also. Limestone has a high Poisson's ratio, which will result in a higher fracture pressure than if the casing shoe was set in a rock with a lower Poisson's ratio. Drilling out of a limestone into a sand at the same or lower pore pressure will result in a lower fracture pressure.

Generally, the point in any section of borehole that has the lowest fracture pressure will be that which has the lowest pore pressure and lowest Poisson's ratio. Maximum mudweights for further drilling are thus dependent on these parameters, not on a unique value that was determined at the casing shoe.

Once the formation has been fractured, it will be necessary to apply that same fracture pressure to cause fracturing again. On any fracture test, the point at which the horizontal stresses become balanced by the pressure within the borehole will be the same, whether the test is a repeat or not. However, if a permeable formation is being tested, the fracture pressure plot will probably not be linear:

the volume increase produces a smaller pressure increase, due to the invasion of fluid into the formation. This has the effect of raising the pore pressure of the formation immediately adjacent to the borehold. The increase in pore pressure has the result of reducing the stress concentration at the borehole wall, in turn resulting in a lower pressure necessary for initiating fracturing. Once the fracture is started and is extending into the undisturbed stress field, the pressure required for this extension is the same as if no invasion occurred.[4]

Fracture tests conducted offshore at shallow depths in unconsolidated clays can produce apparently abnormally high fracture pressures. Wet clays may behave as liquids, so that Poisson's ratio would be approaching 0.5 Also, as the pore water and adsorbed water may surround each clay platelet, the platelets will not themselves be in contact with one another, but will be supported by the water. These clay types have negligible shear strength. The effective pore pressure would thus be approaching the pressure exerted by the weight of the overlying sediments; when combined with a very high Poisson's ratio, it will be seen that calculated fracture pressures may exceed the overburden pressure by a significant amount. In these instances a horizontal fracture will form, lifting the overburden, so that the fracture pressure will approximately be equal to the overburden pressure.

At some depth, the weight of the overburden will squeeze out sufficient pore water so that the clay platelets become in contact with one another. When this occurs, the sediment can support a superposed horizontal stress. Poisson's ratio for the clay at this stage may be very similar to that of a more compact clay. Fracture tests in a clay which is at this stage of dewatering can be used for the calculation of the horizontal stresses.

Unconsolidated sands at shallow depths having a very good permeability may cause lost-circulation problems. Although the sand may be unconsolidated, the individual grains will be in contact so that a superposed stress can be supported independent of the pore pressure. Poisson's ratio will be normal, depending on the sand type. Consider that if an unconsolidated sand is drilled at 2000 ft. (609.6 m) the overburden pressure is 1453 psi (10018 kPa), and the pore pressure is normal at 892 psi (6150 kPa). For a fossiliferous sandstone, Poisson's ratio is 0.01. (Table 1) Assuming that the horizontal stress ratio is 'normal', i.e. σ_t/σ_1' is 0.2, then the calculated fracture pressure for these parameters is

$$F = \left[(1453-892)0.2 + (1453-892)\frac{0.01}{0.99}\right] + 892$$

$$F = 1010 \text{ psi, or } 9.7 \text{ lb/gal } (6963 \text{ kPa, or } 1162 \text{ kg m}^3)$$

It can be seen that in shallow, unconsolidated sediments with high water content, normally encountered offshore, fracture pressures can vary from overburden magnitudes in wet clays to only a little more than the pore pressure in unconsolidated sands.

A typical fracture-test plot is shown in Figure 2. The linear portion of the curve, AB, indicates elastic properties: pressure increase (stress) is directly proportional to volume pumped (strain). At point B, the pressure within the borehole is equal to the pore pressure plus the total minimum horizontal effective stress. All cracks, joints and partings within the section of borehole that is being tested, that lie on a vertical plane normal to this minimum horizontal stress, now have no compressional forces holding them closed. From B to C, the stress/strain proportionality no longer exists, such that for unit stress a greater proportion of strain is produced. The pressure difference, C - B, is that pressure necessary to push fluid into the cracks, apply pressure to the walls, and to apply pressure to the leading edge (close to the tip) of the cracks. When the pressure within the borehole is approximately 5 percent greater than the total minimum horizontal stress, an almost infinite tensile stress occurs at the tips of the crack. At this point, the cracks extend rapidly along the path of minimum resistance, i.e. in a vertical plane, normal to the minimum compressive stress (in a vertical borehole, with horizontal beds). If the pump is stopped at that moment, fracture propagation will cease and the pressure will fall to D. When the pressure in the borehole has falled (due to the increase in volume caused by the fractures) to a pressure equal to the pore pressure plus the total minimum horizontal stress, it should stabilize at a pressure equal to B. When the excess pressure is bled off, the amount of returning mud should be almost equal to the amount pumped. If the shut-in pressure (D) is lower than B, then it would be reasonable to assume that the fractures are still open, possibly being propped open by mud contaminants or cuttings. The larger volume produced by the open fractures causes a larger decrease in pressure, such that B - D >0. In this case, the amount of mud returned or bled off is less than the amount pumped. If this occurs in permeable formations, then possibly significant mud losses may occur due to the highly increased surface area in the fractured zone.

PREDICTION OF FRACTURE PRESSURE

All the data necessary to predice fracture pressures can be obtained from interpretation of the first fracture test in compact formation, parameters that are normally measured or calculated when drilling wildcat wells, and typical values for Poisson's ratio. Values of Poisson's ratio, as shown in Table 1, were obtained by sonic testing.[12] Poisson's ratio is not measured directly, but is calculated from the modulus of elasticity and modulus of rigidity:

$$\text{Poisson's ratio, } \nu = \frac{\text{Modulus of Elasticity}}{2(\text{Modulus of Rigidity})} - 1$$

The calculated ratio is a dynamic result and may differ from static elastic properties. This may be explained by pointing out that dynamic results which differ markedly from the static results are indicative of zones of weakness, anisotropy, or directional differences in the properties of the material.[13] These dynamic ratios should be more realistic when attempting to determine horizontal stresses at depth because of observed anisotropies, rather than static Poisson's ratios determined on carefully selected and prepared specimens. Each rock type (particularly in situ) has its own unique Poisson's ratio (and other mechanical properties), and this will vary when the influencing parameters change. Thus the tabulated values are presented only as an approximate guide; however, they should serve to provide a reasonable estimate. When two or more minerals are intermixed, i.e. sandy clay, shaley sand, the matrix-forming rock type must be determined. If the lithology is a sand with the grains in contact with one another, and clay is the matrix (clay content $\leq$ 30%), the Poisson's ratio is dependent on the sand type. If the clay content is greater than 30% so that the sand grains are not in contact but are supported in the clay matrix, then Poisson's ratio is dependent on the clay type. Likewise, if a clay is highly calcareous (>50%), the carbonate content may have a significant effect on the mechanical properties, so the Poisson'r ratio for shaley limestone should be used. Greater than 80% carbonate content in a shale, or rather 20% clay in a calcareous lithology, indicates that the gradation has progressed essentially from shale to micrite or fine limestone. Careful analysis and interpretation of cuttings and logs should provide a sound basis for selecting the correct Poisson's ratio. The weakest interval in the borehole will be that which has the lowest pore pressure and lowest Poisson's ratio with depth. A low pore pressure in a zone that has a higher Poisson's ratio may have a higher calculated fracture pressure than another zone that has a higher pore pressure and a lower Poisson's ratio. Fracture pressures calculated at changes in lithology and pore pressures will show the weakest interval in the borehole.

The result of the first fracture test in compact formations is used to calculate the effective stress ratio of the superposed tectonic stress, if present:

$$\sigma_t = F - \sigma_1'\left(\frac{\nu}{1-\nu}\right) + p \qquad (7)$$

σ_t remains directly proportional to σ_1', providing the strata remain close to the horizontal and the basin structure does not change significantly with depth.

Since

$$\sigma_t/\sigma_1' = \beta \qquad (3)$$

where β defines the stress ratio of σ_t to σ_1', and remains constant with depth,

then as σ_1' is known at any point within the drilled hole,

$$\sigma_1' = S - p \qquad (8)$$

where S and p are the overburden pressure and pore pressure, respectively:

$$\sigma_t = \sigma_1' \cdot \beta$$

The overburden pressure, S, should be accurately determined from a density log or measured bulk densities for the first fracture pressure test. It is particularly important on offshore wildcats to take into account the air gap and water depth.[14] Pore pressures can be reliably calculated from drilling exponent plots, mudweight/gas relationships, and sonic logs.

Accuracy of the parameters when obtaining σ_t from the first fracture test is of prime consideration, as any significant error at this point will render false predicted fracture pressures with depth.

Since the effective stress ratio has now been found for that particular well location, fracture pressures can be calculated as the well progresses, as changes in lithology. (Poisson's ratio), pore pressure, and overburden pressure occur:

$$F = \sigma_t + \sigma_1'\left(\frac{\nu}{1-\nu}\right) + p \qquad (6)$$

Between log runs the overburden gradient may be extrapolated with a reasonable degree of accuracy by plotting overburden pressure with depth (Figure 3). It will be seen that the relation is approximately linear, except for the upper portion of the curve which is affected by water depth, uncompacted sediments and the air gap. Linear extrapolation of the trend may be achieved with confidence, providing the upper overburden gradient obtained from logs or bulk densities was accurate. Correction of the extrapolated trend must be accomplished after subsequent logging runs, or continuously updated from bulk density measurements.

A continuous, real-time plot of calculated fracture pressures with depth is thus made possible, providing the various Poisson's ratios can be adequately determined from the cuttings. If complex or interrelated lithologies are encountered, assignment of a unique Poisson's ratio may not be immediately apparent: of the several lithologies that may occur in the same sample, that which has the lowest Poisson's ratio should be used until confirmation is obtained from logs. If the pore pressure gradient remains constant with depth, then the σ_1', σ_t and σ_H (with constant lithology) gradients are constant (Figure 4). Fluctuating pore pressure causes significant changes in all the stress gradients (Figure 5).

Several factors affect fracture test pressures, aside from formation characteristics:

1. Higher mudweights appear to cause higher fracture pressures,[15] although this may be due to a related increase in viscosity.

2. Smaller hole diameters may cause higher fracture pressures.[16]

3. The rate of pressurization affects fracture pressures: high pump rates produce inflated fracture pressures.[16] This effect is smaller than that in (2) above.

4. High mud gel strengths require higher pressures to initiate circulation. Correction for this pressure loss can be obtained from Chenevert and McClure.[17]

5. Hole deviation significantly affects fracture pressures.[18,19]

6. Rig and sensor instrumentation probably is accurate to within 5%.[20] Accuracy of predicted fracture pressures is therefore limited to this range.

7. Mud penetrability does not alter the actual breakdown pressure, but it will affect the shape of the fracture pressure plot such that the point at which the total horizontal minimum stress is balanced may be obscured.

A combination of these mechanisms is probably responsible for a considerable scatter of data points. However, if fracture test procedures are kept as consistent as possible on any one well, then the results obtained should lie within the 5% instrument error margin.

SUMMARY

A theoretical model is put forward that attempts to describe the principal stress system within a basin of simple topography and structure. If a well is drilled nearly vertically, then the well should be approximately parallel to one of the principal stresses, which is equal to the effective weight of the overlying strata. The horizontal stresses are a combination of the stress caused by gravity and a superposed horizontal tectonic stress. The latter may be nonexistent or may reach a maximum of two to three times the vertical stress.[4] The minimum horizontal stress is measured by the first fracture test in compact formation. As the vertical stress increases approximately linearly with depth, then the tectonic horizontal stress will increase linearly with depth also, defined by a constant stress ratio, β. Since this ratio is obtained from the first fracture test, then at any subsequent depths the fracture pressures may be calculated providing pore pressures, overburden pressures and lithological relationships are known. Fracture pressure test data from some rank wildcat wells are shown in Table 2 where a comparison is made between actual fracture pressures and calculated fracture pressures. The results are within the 5% minimum error margin caused by rig instrumentation.

CONCLUSIONS

1. Fracture pressures may be predicted when drilling rank wildcat wells to an accuracy of 95%.

2. Fracture pressures are dependent on the total minimum horizontal stress (a combination of a stress caused by gravity and a superposed tectonic stress) and the pore pressure.

3. Factors affecting actual fracture pressures may be minimized by conducting fracture tests as consistently as possible. A correction is available for gel strength (usually < 0.1 lb/gal, 11.98 kg m^{3}), but changes in mud types or large changes in properties may cause significant deviation from calculated fracture pressures. It is also suggested that at least one circulation is affected prior to conducting a fracture test, in order to minimize any inconsistencies in the mud column.

4. The theoretical fracture pressure formula provides an explanation for fracture pressures that equal the overburden pressure in shallow wet clays, and also indicates that if a sandstone reservoir is fractured, the fracture should not extend into or through the seal. Probably an inherent property of a permeability seal is a relatively high Poisson's ratio: these rock types require a higher pressure within the borehole to balance the horizontal compressive stress, so a hydraulic fracture within an underlying permeable strata should be confined to that strata.

NOMENCLATURE

F = fracture pressure

g = acceleration due to gravity

k = empirical "stress ratio" constant

ν = Poisson's ratio

OBG = overburden gradient

p = pore pressure

β = σ_t/σ'_1

ρ = density

σ_1 = maximum compressive principal stress

σ_2 = intermediate compressive principal stress

σ_3 = minimum compressive principal stress

σ'_1 = maximum compressive effective stress

σ'_2 = intermediate compressive effective stress

σ'_3 = minimum compressive effective stress

σ_t = superposed horizontal tectonic stress

σ_g = $\sigma'_1\left(\frac{\nu}{1-\nu}\right)$ = horizontal stress component caused by gravity

S = overburden pressure

Compressive stresses are positive.

ACKNOWLEDGMENTS

I would like to thank the management of Exploration Logging Inc. for their permission to publish this paper. The permission granted from the oil companies concerned for inclusion of their fracture data is gratefully acknowledged. Thanks are also due to Judy Cross, Alun Whittaker, Jerry Knobla and Dorette Carbone for their assistance in preparing and improving the manuscript.

REFERENCES

1. Matthews, W.R., and J. Kelley, 1967, How to Predict Formation Pressure and Fracture Gradient, O&G J., Feb. 20.

2. Eaton, B.A., 1969, Fracture Gradient Prediction and Its Application in Oilfield Operations, J. Pet. Tech., Oct.

3. Anderson, R.A., D.S. Ingram and A.M. Zanier, 1973, Determining Fracture Pressure Gradients from Well Logs, J. Pet. Tech., Nov.

4. Hubbert, M.K. and D.G. Willis, 1957, Mechanics of Hydraulic Fracturing, Trans. AIME, v. 210.

5. Jaeger, J.C. and N.G.W. Cook, 1976, Fundamentals of Rock Mechanics, Chapman and Hall, 2nd ed., London.

6. Handin, J. et al, 1963, Experimental Deformation of Sedimentary Rocks Under Confining Pressure: Pore Pressure Texts, Bull. AAPG, v. 47, n.5.

7. Anderson, E.M., 1942, The Dynamics of Faulting, Oliver and Boyd, London.

8. Hubbert, M.K., 1945, Strength of the Earth, bull. AAPG, v.29, n.11.

9. Jeffreys, H., 1952, The Earth, Cambridge, 3rd ed.

10. Hafner, W., 1951, Stress Distributions and Faulting, Bull. Geol. Soc. Am., v. 62.

11. Hubbert, M. K., 1951, Mechanical Basis for Certain Familiar Geologic Structures, Bull. Geol. Soc. Am., v. 62.

12. Weurker, R.G., 1963, Annotated Tables of Strength and Elastic Properties of Rocks, SPE Reprint Series, n. 6.

13. U. S. Bureau of Reclamation, 1953, Physical Properties of Some Typical Foundation Rocks, Concrete Laboratory Rpt. SP-39.

14. Christman, S.A., 1973, Offshore Fracture Gradients, J. Pet. Tech., SPE Paper 4133.

15. MacPherson, L.A. and L.N. Berry, 1972, Prediction of Fracture Gradients from Log Derived Moduli, The Log Analyst, Sep-Oct.

16. Haimson, B. and C. Fairhurst, 1969, Hydraulic Fracturing in Porous-Permeable Materials, J. Pet. Tech., SPE Paper 2354.

17. Chenevert, M.E. and L.J. McClure, 1978, How to Run Casing and Open Hole Pressure Tests, O&G J., Mar.

18. Bradley, W.B., 1979, Mathematical Concept -- Stress Cloud -- Can Predict Borehole Failure, O&G J., Feb.

19. Bradley, W.B., 1979, Predicting Borehole Failure Near Salt Domes, O&G J., Apr.

20. Taylor, D.B. and T.K. Smith, 1970, New Fracture Gradients Help Cut Costs Offshore, World Oil, Jun.

Table 1

Suggested poisson's ratios for different lithologies (12)

Rock Type		Poisson's Ratio
Clay, very wet		0.50
Clay		0.17
Conglomerate		0.20
Dolomite		0.21
Greywacke:	coarse	0.07
	fine	0.23
	medium	0.24
Limestone:	fine, micritic	0.28
	medium, calcarenitic	0.31
	porous	0.20
	stylolitic	0.27
	fossiliferous	0.09
	bedded fossils	0.17
	shaley	0.17
Sandstone:	coarse	0.05
	coarse, cemented	0.10
	fine	0.03
	very fine	0.04
	medium	0.06
	poorly sorted, clayey	0.24
	fossiliferous	0.01
Shale:	calcareous (<50% $CaCO_3$)	0.14
	dolomitic	0.28
	siliceous	0.12
	silty (<70% silt)	0.[illegible]7
	sandy (<70% sand)	0.12
	kerogenaceous	0.25
Siltstone		0.08
Slate		0.13
Tuff:	glass	0.34

156-40

Table 2

Fracture test data from six offshore wildcat wells

Well Number	1		2			3		4		5			6			
Fracture Test Number	1	2	1	2	3	1	2	1	2	1	2	3	1	2	3	4
(1) Depth of Weakest Formation, ft.	5,423	11,034	1,220	3,684	8,321	1,617	5,015	1,315	4,515	1,365	2,505	6,012	362	3,208	8,987	9,700
(2) Overburden Pressure psi	4,531	10,390	1,023	3,518	8,686	547	2,307	932	3,983	1,086	2,034	8,434	536	2,478	8,382	9,142
(3) Pore Pressure, psi	2,430	5,430	551	1,683	3,660	401	1,361	578	2,064	603	1,105	3,005	447	1,647	5,836	5,034
(4) Effective Vertical Stress, σ_1', psi	2,093	4,960	471	1,854	4,026	195	945	404	2,010	483	929	5,429	89	832	542	4,158
Lithology	Porous Limestone	clay	Sandy Fossils	Subgraywacke	Homogeneous Shale	Marlite	Clay	Silty Clay	Siltstone	Unconsolidated Clay	Clay	Siltstone	Unconsolidated Clay	Calcareous clay	Calcareous clay	Calcareous clay
(5) Poisson's Ratio, ν	0.20	0.17	0.01	0.24	0.25	0.20	0.17	0.17	0.00	0.5	0.17	0.00	0.5	0.14	0.14	0.14
(6) σ_H, psi	523	1,016	4.8	585	1,042	41	193	82	174	483	180	290	89	135	98	672
(7) σ_1, psi	530	[illegible]	[illegible]	[illegible]	1,401	64	322	200	933		703	2,017		471	387	2,336
(8) σ_3/σ_1	0.444	0.444	0.325	0.325	0.325	0.611	0.511	0.494	0.494		0.763	0.763		[illegible]	[illegible]	0.566
(9) Calculated Fracture Pressure, psi		8,847		2,852	7,133		2,133		3,152	1,005		5,921	536		6,234	8,642
(10) Actual Fracture Pressure, psi	3,891	8,647	709	2,906	>7,001	587	2,065	861	3,210	1,055	2,005	5,785	552	2,253	6,187	8,606
(11) Percent Difference		2.27%		1.87%	<1.85%		3.14%		1.79%	4.89%		2.85%	2.8%		0.75%	0.44%

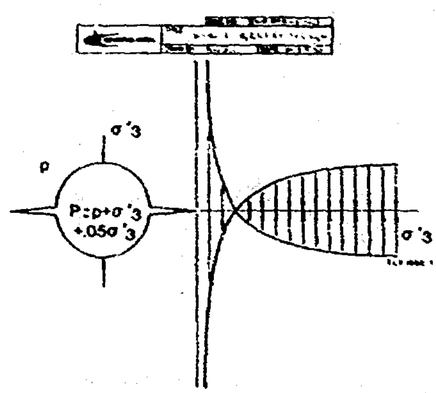

Fig. 1 - Extremely high tensile stress produced at the tip of a crack[4].

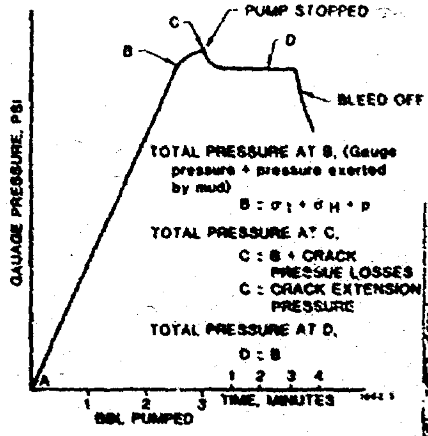

Fig. 2 - Typical fracture test curve.

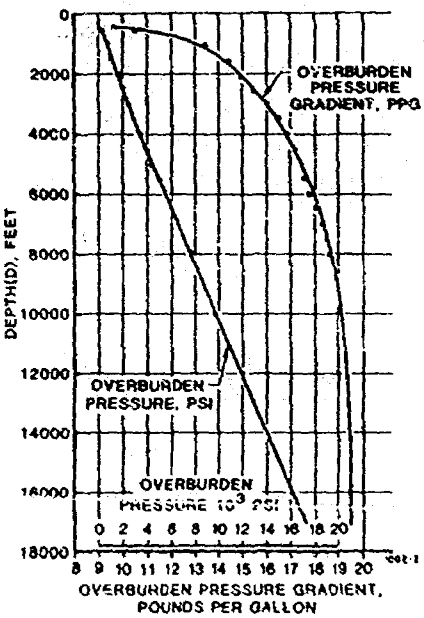

Fig. 3 - Typical overburden curves from an offshore well.

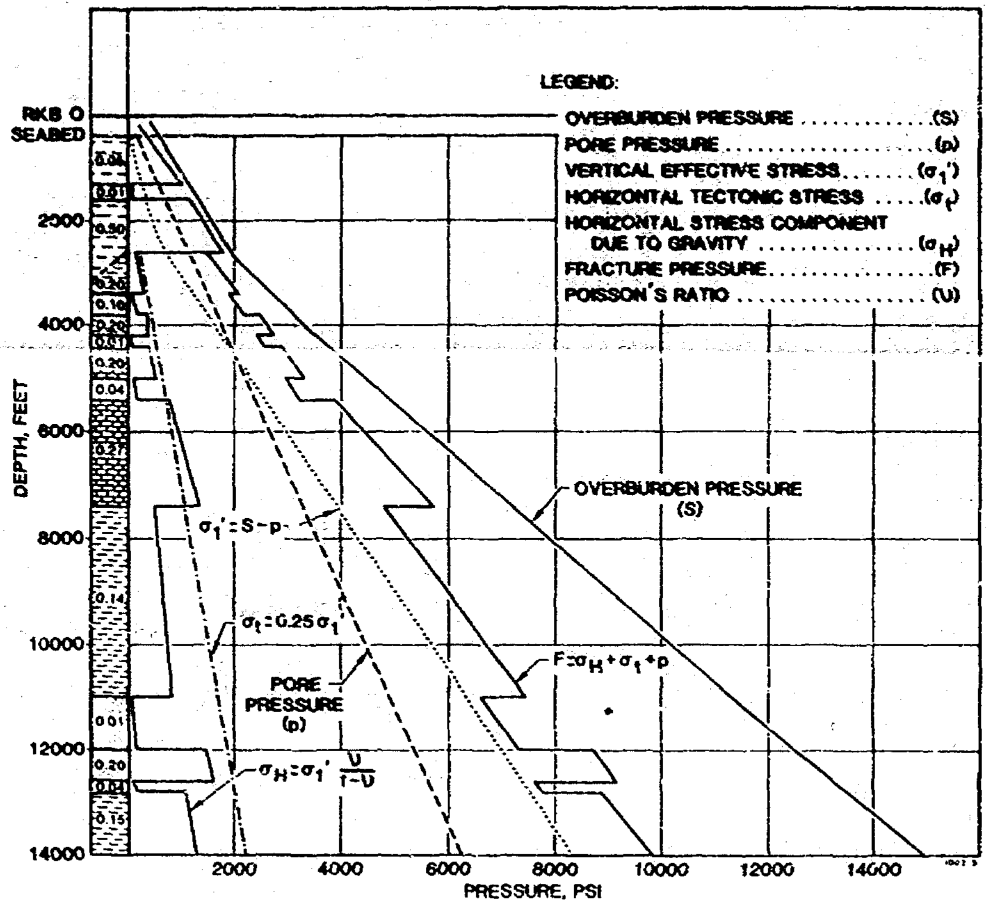

Fig. 4 – Hypothetical changes in σ_1, σ_t, and σ_H with depth and constant pore pressure.

SPE 9259

SPE
Society of Petroleum Engineers of AIME

COMPREHENSIVE DESIGN FORMULAE FOR HYDRAULIC FRACTURING

by Michael P. Cleary, Massachusetts
Institute of Technology

This paper was presented at the 55th Annual Fall Technical Conference and Exhibition of the Society of Petroleum Engineers of AIME, held in Dallas, Texas, September 21-24, 1980. The material is subject to correction by the author. Permission to copy is restricted to an abstract of not more than 300 words. Write: 6200 N. Central Expwy., Dallas, Texas 75206.

ABSTRACT

This paper provides a number of comprehensive algebraic formulae, with readily determinable coefficients, which can be used to predict the extent and width of fractures produced by fluid injection at specified rates or borehole pressures, when these are reasonably well-behaved functions of time. The fracture geometries described include as special cases the models currently in use for industrial design of hydraulic fractures, but extensions to allow variable fracture height are readily achieved. The formulae serve both to simplify the implementation of conventional models and to allow development of more realistic simulations which contain the rather idealised concepts of those models in their rightful place as components of a more general three-dimensional description. One such pseudo-3-D model is described in its simplest form; it allows physically credible tracing of length, height and width distributions under conditions of slow vertical spreading which a desirable stimulation treatment would achieve. All of the models admit quite general reservoir properties and frac-fluid behavior. A few popular applications are used to illustrate their power and simplicity.

INTRODUCTION

Over the past two decades, a considerable amount of effort has been expended on the development of models intended to describe the effects of a hydraulic fracturing treatment and to aid in the design of pumping sequences aimed at optimisation of the return on considerable investments in equipment, labour, and materials employed in a typical field operation. Various analyses and numerical routines have emerged from this activity (e.g. 1-8), but it seems fair to say that few of the authors would claim a satisfactory level of realism for their simulation capabilities, except perhaps in cases of unusually favourable circumstances in the reservoir being fractured. This state of affairs can be readily explained by the exceptionally difficult combined character of the phenomena which must be represented. A renewed effort has been underway over the past few years (e.g. 9-16) to obtain more realistic descriptions of the hydrofrac process; many insights have resulted from this activity, but a worthwhile fully three-dimensional simulator will require a few more years of concentrated endeavor. Numerous models may appear in the meantime, superficially embodying a 3-D capability; they will certainly be lacking many of the complex features which recent work (e.g. 9-10) has shown to be so essential for a physically realistic representation of the process involved in even the simplest reservoir geometries.

In the absence of such an acceptable comprehensive simulation capability, it appears necessary to have at least some approximate means of determining in a credible way what the general features will be for a fracture produced by fluid injection through a borehole, particularly as to effective length, width, and height. While it is true that these quantities are not yet measured accurately in the field,[7] it is certainly possible to make sufficiently good deductions from reservoir data in order to establish what the overall character of hydrofrac evolution will be and thus eliminate some of the more ridiculous models. Indeed, it is also possible to achieve scaled laboratory versions of increasingly complicated reservoir structures and the theoretical predictions should at least agree with the fracture growth observed in these.[17] Although the geometry assumed in almost any model, no matter how simple, can actually be generated in the laboratory, one must recognise and account for the complicated shapes which develop when test conditions approximate those found in the various geological circumstances where oil and gas are present. Thus, any acceptable working models should at least be capable of incorporating major features anticipated on the basis of laboratory observations and/or physical reasoning from core data, logging, structural geology etc.; a major purpose of this paper is to provide the basis for such approxi-

References and illustrations at end of paper.

Ex 1 B

mate models.

OUTLINE OF CONTENTS

The contents of the paper may be divided into five broad sections. Since the details of the paper may initially appear somewhat "theoretical" in nature, it is important to emphasise that the goals are entirely practical: the simplest possible realistic models and associated design formulae are being sought. To demonstrate this, it is noted that all known previous design procedures of the industry are included as special cases of the equations which are presented in the second and third sections; although the results here are not as detailed as those of numerical schemes typically applied[2-8] to solve the equations, they seem to be more transparent and are considered adequate for the level of accuracy involved in the assumptions on which the industrial models are based[5,7]. As well, they allow much greater generality in encompassing arbitrary wellbore conditions, and permitting height to vary in any specified fashion during the operation.

There is a twin motivation for simplifying the analysis of the popularly assumed geometries in this way. On the one hand, this makes it very easy to understand and implement in designs the essential features of the models which are currently employed in the industry. On the other hand, it renders the formulae simple enough that they can become the components of more realistic geometric descriptors which incorporate these elementary models into a framework where they begin to have real physical appeal. Thus, in Section 4, the paper proceeds to describe a model which allows such realistic simulation to be achieved, with reasonable three-dimensional evolution in fracture geometry -- using just the formulae already developed. This pseudo-three-dimensional hydrofrac (P3DH) model is picked for illustration here because we have found it readily amenable to both analytical and numerical solution; it also seems to have the capability for credible design in many typical field situations. Indeed, it certainly has more value than unwieldy fully three-dimensional simulators will have if they leave out many of the important reservoir features.

Other models of this pseudo-three-dimensional kind can be generated as the application demands, but all of these models must be kept in perspective, despite their apparently general applicability to varied rock response, fluid behavior and injection sequences. The paper tries to emphasise this by adopting the following layout:

1. First we present a reasonably general set of equations which would have to be solved for a complete 3-D simulation of hydraulic fracturing. The difficulty lies in solving these simultaneously, and marching out the solution stably in time,[10] not in finding schemes to solve them individually.[13] The equations both indicate the main features which must be incorporated in any worthwhile model and also serve as a reference frame for the various specialisations adopted later in solving them. [See figure 1]

2. Next we obtain approximate solutions of the governing equations in Section 1, assuming unidirectional fracture propagation along z (viz. normal to the long axis of the fracture). This idealisation is very like that of Christianovich,[1] Geertsma and deKlerk[3] and Daneshy[5] (-so that we term these CGDD-type models-) except that we regard it as generally more appropriate for describing the vertical spreading of the fracture (Figure 2) rather than the lateral extension for which it has typically been employed in design codes. The results are provided as simple algebraic formulae covering most reasonable behavior of specified pressure or injection rate driving the fracture; these contain only three simple coefficients which can be estimated approximately or more precisely determined by computer routines that we have developed.

3. The alternate extreme of propagation along the long axis x (Figure 3) is also analysed; these models reduce to that of Perkins and Kern[2] and Nordgren[4] when the height and wellbore flowrate are assumed constant (so that we call them generalised PKN models). Here there are just two coefficients to be determined numerically and good estimates can be obtained analytically.

4. The concepts of Sections 2 and 3 are now combined to give a pseudo-three-dimensional model of hydrofract evolution (P3DH). A CGDD-type model (figure 2) is used to describe vertical propagation while a generalised PKN model is employed to represent the lateral flow and fracture extension. (figure 4)

5. The formulae derived in foregoing sections are applied to the prediction of results for some typical field operations. Only a few simple examples are presented mainly because of the limited data available for the calculations needed and the fact that no case studies have yet been completed with the more complex models. However, the availability of these new models should stimulate the determination of reservoir quantities inherent in making the calculations; an example is the contrast in material properties and in-situ stress between strata.

1. GENERAL EQUATIONS GOVERNING HYDRAULIC FRACTURING

The equations governing opening and propagation of hydraulic fractures may be phrased in the following forms, which are typical of the approach being taken in some of our hydraulic fracture simulation[9-11] and, therefore, serve to introduce relevant parameters and variables. (See also the list of Notation at the end.) First there is the requirement of mass conservation, which can be written in the differential form

$$\nabla^S \cdot (\rho q \delta) + \frac{\partial}{\partial t}(\rho \delta) + \rho q_L \cdot n = 0 \qquad (1a)$$

for any point on the fracture surface (Figure 1), with associated normal n and gradient operator ∇^S in the tangent plane. For many practical purposes, fluid compressibility has tended to be neglected, by comparison with overall fracture compliance; non-constant density ρ may be quite important in operations such as foam fracturing. Special versions of eqn. (1a) pertain to unidirectional flow (along x) or to radial flow (along r), when the equation takes either of the forms

$$\frac{\partial}{\partial x}(\rho q \delta) = - \frac{\partial}{\partial t}(\rho \delta) - \rho q_L \quad (1b)$$

$$= \frac{1}{r} \frac{\partial}{\partial r}(r \rho q \delta) \quad . \quad (1c)$$

The second required equation is that relating crack opening δ to the pressure distribution; we will refer to the effective opening stress $\sigma(x_0)$, for any point x_0 on the crack surface, as the excess of internal frac-fluid pressure p_f over normal confining stress caused both by tectonic processes (which induce σ_T) and by back-stresses (σ_B) induced in the operation of fracturing[18], e.g., by alteration of pore-pressures around the fracture and by inelastic deformation of all kinds. An efficient and general integral equation scheme for numerically obtaining δ, for any given σ (or vice-versa), has been provided by the author[9,10]; this can be applied to fairly realistic material and geometric structure in the reservoir, so it constitutes an improvement over previous formulations, which have been limited to linear isotropic homogeneous time-independent media[3,5,13]. Greater generality might be achieved with an unwieldy full finite-element or finite-difference solution of the rock deformation equations throughout the reservoir; that level of detail is not warranted by the potentially available data on structural properties, and it would quickly render undoable a complete hydrofrac simulation. Indeed, a simple version of the general integral equation formulation will be adequate for purposes of this paper, namely one which neglects (e.g., consolidation) time-dependence of the porous medium (except as very importantly contained in the back-stresses σ_B); thus we concentrate on opening δ caused by stress normal to the fracture, namely

$$\sigma(x_0,t) \equiv p_f - \sigma_T - \sigma_B \equiv p_f - \sigma_c$$

$$= \int_{-\infty}^{t} d\tau \int_{S_c(\tau)} dS \, \Gamma(x_0,x;t,\tau) \cdot \nabla^S \delta(x,\tau) \quad . \quad (2a)$$

We will, therefore, remove the time-dependence in the influence function Γ and it will be most useful to have versions of such an equation which apply to one-dimensional or circularly symmetric fracture spreading, namely

$$\sigma(z_0,t;x) = \int_{-\ell_1(t)}^{\ell_2(t)} dz \, \Gamma(z_0,z;x)\delta'(z,t;x) \quad . \quad (2b)$$

Here we allow the possibility of two unequal crack wings ℓ_1 and ℓ_2 (which are both set equal to the fracture radius for a circular crack) and we include an additional position parameter x for application in the fourth section of the paper. Eqn. (2b) can be solved for the opening δ by straightforward numerical routines[10], for any of the numerous influence functions Γ which have been worked out over the years[3,10].

Solution by means of eqn. (2a) immediately allows the rock decohesion criteria to be imposed around the current perimeter of the fracture surface[9]. Specifically, for instance, if we adopt a model with critical stress-intensity factor K_c, then the form of the displacement gradient must be

$$\nabla^S \delta = m K_c / \bar{E}\sqrt{\pi m \cdot (x_p - x)} \quad (2c)$$

at a point x sufficiently close to the perimeter location x_p with associated normal m; for an isotropic material, $\bar{E} = G/2(1-\nu)$, but the relation (2c) applies more generally.

Thirdly, we must write a relation describing fluid flow in response to the pressure-gradients which drive it; the complex rheology of typical fracturing fluids makes this a forbidding task and many important[22] features must be accounted separately[12] from the calculations presented here or even those used in current industrial models. However, many established fluid characteristics can be incorporated in a "channel-flow" law of the form

$$q q^{m-1} = - \delta^{2n-m+1} \nabla p_f / \bar{\eta} \, , \quad \bar{\eta} \equiv \hat{\eta}/\gamma_4 \quad (3)$$

which allows both non-Newtonian behavior ($m=n\neq1$) and also permits regimes of turbulent flow ($m=2,n=1$). To provide a feeling for the parameters, we note the Newtonian fluid response when $\hat{\eta}$ is viscosity and γ_4 is the channel factor (1/12).

Lastly, it is necessary to write an equation governing exchange of fluid between the fracture and its surroundings. A very efficient surface integral representation may be written, relating p_f to the history of q_L through an equation of the kind connecting σ and δ in eqn. (2a) - and coupled to the history of δ through pore-pressures induced by stresses caused by fracturing; however, this compact appealing approach (developed in ref. 15) is limited to reservoirs amenable to linearisation and homogenisation of the pore-fluid flow equations, and thus may be regarded as a simplified simulation tool, useful for phenomenological simulations rather than detailed practical design. In actual design-oriented models, the fluid exchange (viz. the loss q_L in eqn. (1) and the influx of pore-fluid to the near-perimeter region not yet penetrated by frac-fluid) should be computed with the most suitable of the many available arbitrarily complex reservoir simulators (e.g. 14); this can be run simultaneously with the solution of eqns. (1, 2, 3) for the pressurised opening and spreading of fracture surfaces; (which provides the boundary conditions on the reservoir model). The pore-pressure and thermal profiles in the reservoir at each instant then allow a calculation of the back-stress σ_B in (2a).

Models which do not take account of at least the main features isolated by the foregoing equations and discussion do not promise much potential for worthwhile descriptions of fracturing in typical reservoirs; especially, they should incorporate the dominant material heterogeneity and porous medium effects. They may not have to be very unwieldy numerical simulators in order to do this.

A major simplification of the governing equations (1, 2, 3) may be achieved by assuming a fracture shape and adopting what amounts to a spatial averaging approach, which allows their reduction to simple ordinary differential equations on time. Although this procedure seemed suspect when we first conceived it[12], it turns out to retain most of the essential ingredients needed for first-order estimates of hydrofac opening and propagation, provided that the fluid injection sequence is not too complex; especially, it allows good descriptions for monotonic downhole pressure or pumping rate and it encompasses all previous design models[2-7] as special cases. In fact, its justification is firmly rooted in the concept of self-similar profiles of crack-opening as the fracture propagates; indeed, more complex sequencing of the hydrofrac operation can be captured by a numerical implementation of this self-similar concept, which also provides the numerical values for some coefficients used below. Thus, the self-similar assumption provides a short-cut approach, for modelling of fairly well-behaved fracturing sequences, avoiding the full unsteady propagation analyses which will be needed in more complex circumstances.

We have applied this self-similarity-based spatial averaging to a fairly broad variety of assumed geometries[12] but this paper will be limited to the CGDD-type[1,3,5] and generalised PKN[2,4] models which have been popular in the literature and also turn out to be basic for development of more realistic descriptions.

2. SELF-SIMILAR SOLUTIONS FOR CGDD-TYPE MODELS

The essence of the procedure we have employed may be understood by writing the averaged consequences of eqns. (2b) and (1b), respectively, for unidirectional flow in a propagating crack of length $\ell(t)$ as shown in figure 2; using carats for suitable averages, we get

$$\Delta \approx \hat{\sigma}\ell, \hat{\sigma} \equiv \gamma_1 \sigma^B/\bar{E}\ , \quad \sigma^B \equiv p_f^B - \sigma_c^B \tag{4a}$$

$$\dot{w} - \dot{w}_L \equiv \rho_B(q_B\Delta - \ell\hat{q}_L) = d(\gamma_3\rho_B\Delta\ell)/dt \quad . \tag{4b}$$

We have introduced the central crack opening Δ and we now employ it in the fluid-flow law of eqn. (3) to achieve a correspondingly simple equation for mass of fluid injected at the wellbore

$$q_B^m\Delta^m \approx \gamma_5^m(\hat{\sigma}\ell)^{2n+2}/\ell^2 \tag{4c}$$

$$\gamma_5^m \equiv \gamma_2\bar{E}/\gamma_1\bar{n}_B \quad . \tag{4d}$$

Here the coefficient γ_2 has been introduced to represent (fig. 2) the slope of the fluid pressure curve at the centre, namely, $\partial p_f/\partial z = \gamma_2\sigma/\ell$. This is less amenable to approximate estimation, without some guiding numerical results, than are the other undetermined coefficients γ_1 and γ_3 (as defined in Notation); all three will be sensitive to confining stress $\sigma_T + \sigma_B$, variation of wellbore excess pressure σ_w, etc. but the latter two are much less so for typical reservoir conditions. It is now straightforward to integrate eqns. (4b,c) in conjunction leading to a formula for crack volume as follows:

$$\left.\frac{(\gamma_3\rho_B\hat{\sigma}\ell^2)^{1-n/m}}{1-n/m}\right|_0^t \rightarrow \ell n\left[\frac{\gamma_3\rho_B\hat{\sigma}\ell^2}{\gamma_3^0\rho_B^0\hat{\sigma}_0\ell_0^2}\right]_{m=n}$$

$$= \int_0^t dt\, \frac{\rho_B^{1-n/m}}{\gamma_3^{n/m}}\left[\gamma_5^m\hat{\sigma}^{n+2} - \frac{(\ell\hat{q}_L)^m}{\hat{\sigma}^n\ell^{2n}}\right]^{\frac{1}{m}} \quad . \tag{5}$$

Perhaps surprisingly, no approximations have yet been made in obtaining this apparent solution to the governing equations (1b, 2b, 3). For any specified time-dependence of the effective excess pressure $\hat{\sigma}$, and for a computed or estimated average loss per unit area $\hat{q}_L$, eqn. (4e) provides a direct means of calculating the crack-length $\ell(t)$. Of course, the coefficients γ_1 to γ_5 may actually vary and must be determined as[1] functions of time; this is readily accounted in a more precise numerical implementation of the self-similar concept which we have also developed. However, it will often be convenient and adequate to regard them as constants, especially for purposes of writing simple formulae in this paper.

It is even more straightforward to establish the consequences of eqns. (4b,c) for conditions of specified pumping rate, $\dot{w}$ per unit length normal to the fracture, namely

$$\ell = \frac{w-w_L}{\gamma_3\rho_B\Delta}, \quad \Delta^{2n+2} = \frac{\dot{w}^m\ell^2}{\rho_B^m\gamma_5^m} \tag{6a}$$

$$w \equiv \int_0^t \rho_B q_B \Delta\, dt, \quad w_L \equiv \int_0^t \rho_B \ell\hat{q}_L\, dt \quad . \tag{6b}$$

These results show that mass balance very simply dictates the extent of fracturing. They also quantify the well-appreciated fact that fracture width can be increased by raising both pumping rate and fluid viscosity; the latter enters through γ_5 (eqn. (4d)), as does γ_2 - and there is a relatively weak dependence on both, so that precise numerical determination is not required. Indeed, it is also interesting to note[20] that a comparison can be made with the width which the crack would have if it were under uniform pressure great enough only to provide a fracture propagation energy G_{eq} at its perimeter: the corresponding crack opening may be written in the form

$$\Delta^2 \approx \ell G_{eq}/\alpha_1\bar{E} \quad . \tag{7a}$$

Here α_1 is a factor of order $\pi/4$, which is exactly its value for an isotropic homogeneous time-independent material. By comparing eqns. (6a, 7a) we can now derive an expression for the equivalent energy, namely

$$G_{eq}^{n+1} = \frac{\gamma_1}{\gamma_2}\alpha_1^{n+1}\left(\frac{\ell}{\bar{E}}\right)^{1-n}\bar{n}_B\bar{E}\left(\frac{\dot{w}}{\rho_B}\right)^m \quad . \tag{7b}$$

Calculations with typical field values of $\dot{w}$, $\bar{n}_B$ and $\bar{E}$ (see Section 5) show that this energy is usually much greater (by factors of order 10^2) than the true decohesion energy of most rock materials. Thus we observe that wide enough fractures (e.g., for proppant transport and prevention of sand-out) are possible in many jobs only because of the artificially high resistance to fracture propagation provided by the confining stresses $\sigma_T + \sigma_B$ in the near-perimeter region where frac-fluid has not yet penetrated, as denoted by $\omega\ell$ in figure 2. Indeed, this resistance overwhelms the role of natural rock toughness for typical pumping conditions and/or fracture sizes in the field, and this observation has led us to an efficient means of repeatedly simulating hydraulic fractures by pumping fluid into interfaces between carefully prepared blocks of suitable material in the laboratory[17]; these experiments serve both to test the character of predictions in eqns. (4) and to check the actual values of numerically determined coefficients.

It is also interesting to note the pressure behavior implied by any specified pumping history, from eqns. (4a, 6a), namely

$$\hat{\sigma}^{n+2} = \gamma_3^n \rho^{n-m} \dot{w}^m/(w-w_L)^n \gamma_5^m \quad . \tag{8a}$$

For instance, if we neglect fluid loss, w_L and if we assume either a power law or exponential dependence on time of pumping rate, we get the following expressions

$$w = w_0[t^\psi,\ e^{\chi(t)}],\ w_0 \equiv \rho\, q_0 \tag{8b}$$

$$\hat{\sigma}^{n+2} = \gamma_3^n q_0^{m-n}[\psi^m t^{\psi(m-n)-m},\ \dot{\chi}^m e^{(m-n)\chi}]/\gamma_5^m \ , \tag{8c}$$

This leads to the curious result, for $m = n$, that excess pressure is actually independent of all except the exponent in the pumping rate and behaves like $t^{-m/(n+2)}$ for power-law injection. Previous researchers have appreciated the feature of falling pressure for constant pumping rate in the CGDD models, but we now see that the same pressure behavior pertains to all power-law injection rates. Any other form of the pressure vs. time relation leads in general to an exponential injection rate, increasing with time only if the pressure power (called β) is greater than $-m/(n+2)$; if β is less than $-m/(n+2)$, the fracture is predicted to eventually reach a constant volume condition (eqn. (5)), so injection rate decreases exponentially to eventually reach a shut-in condition. Thus, although the foregoing solutions are not physically exact, except for constant ratios of confining stress to excess pressure $\hat{\sigma}$, they do serve to provide a complete and adequate picture of behavior to be expected from CGDD-type models.

3. SELF-SIMILAR SOLUTIONS FOR GENERALISED PKN MODELS

To permit a direct incorporation of equations already written for the CGDD models and to provide a natural transition to the P3DH model in the next section, we will vary and generalise the treatment typically provided[2,4,8] for the classical PK concepts. (See figure 3 for schematic.) The primary feature is that width of fracture will be dictated by height, which is expressed by a rewrite of eqn. (4a)

$$\Delta = \hat{\sigma}H,\ \hat{\sigma} \equiv \Gamma_1 \sigma^B/\bar{E} \quad . \tag{9a}$$

The mass conservation condition of eqn. (1b) is integrated along the height of the fracture to get

$$\frac{\partial}{\partial x}(\rho Q) + \frac{\partial}{\partial t}(2\Gamma_3 \rho H \Delta) + 2\rho H \hat{q}_L = 0 \tag{9b}$$

Lastly, the fluid flow law of eqn. (3) is also written in an integrated form

$$(Q/2H)^m = -\Gamma_4 \Delta^{2n+1}(\partial p_f/\partial x)/\hat{n} \ . \tag{9c}$$

Here Γ_4 must contain the effect of integrating the flow law across the height and averaging; rough estimates for Γ_4 (which are readily improved) may be deduced from Appendix 1 of ref. 2.

The argument of self-similar propagation now again allows us to write integrated averages along x (over the fracture length L), analogous to eqns. (4b,c,d), as follows:

$$\rho_W Q_L/2 + d(\Gamma_3 \rho_W \hat{\sigma}_W L H^2)/dt = \rho_W Q_W/2 \tag{10a}$$

$$= \rho_W H \Gamma_5 [(\hat{\sigma}_W H)^{2n+2}/LH]^{1/m},\ \Gamma_5^m \equiv \Gamma_2 \Gamma_4 E/\Gamma_1 \hat{n}_W \tag{10b}$$

$$\rho_W \hat{q}_L \equiv \int_0^L 2\rho H \hat{q}_L\, dx \ . \tag{10c}$$

Integration on time now allows a complete solution. Justification for the approximations used (especially use of a slope Γ_2 on the pressure curve, figure 3) is provided by the analytical solutions worked out in Appendix 1. The simplest case to handle is that where pumping rate Q_W is specified for the wing: this permits immediate solution for pressure and opening width, from eqn. (10b),

$$\Delta \equiv \hat{\sigma}_W H = [(Q_W/2\Gamma_5 H)^m L H]^{1/(2n+2)} \quad . \tag{11a}$$

Using this we can determine the fracture extent from eqn. (10a),

$$(LH)^{2n+3} = \left(\frac{W-W_L}{2\Gamma_3 \rho_W}\right)^{2n+2} \left(\frac{\Gamma_5 H}{Q_W/2}\right)^m \ , \tag{11b}$$

where the weights of pumped and lost fluid, respectively, are

$$W = \int_0^t \rho_W Q_W dt,\ W_L = \int_0^t \rho_W Q_L dt. \tag{11c}$$

We have not placed any restriction on the behavior of fracture height H as yet. Any specified history $H(t)$ or any relation between H and L can be accommodated in the expressions provided. However, it is most convenient to decide on the character of the height behavior before embarking on solutions for conditions of controlled downhole pressure; for instance, we suppose either that height H has a similar functional time-dependence as length L or that it is a specified function of time $h(t)$, or some combination of these possibilities. Thus we examine the class of fracture geometries for which

$$H = hL^\mu,\ h = h(t) \quad . \tag{12a}$$

Insertion into eqns. (10a,b) allows extraction of the solution

$$(\Gamma_3 \rho_W \hat{\sigma}_W L H^2)^F/F = \int_0^t \frac{dt}{\Gamma_3^{1-F}} \left[\Gamma_5 \rho_W^F h^E \hat{\sigma}_W^P - \frac{\rho_W^F Q_L/2}{(\hat{\sigma}_W L H^2)^{1-F}}\right] \tag{12b}$$

in which the powers are defined by

$$F \equiv [\mu(2m-2n) + (m+1)(1-\mu)]/m(2\mu+1) \tag{12c}$$

$$P \equiv [(2n+3)(\mu+1) - m\mu]/m(2\mu+1) \tag{12d}$$

$$E \equiv (2n+3+m)/m(2\mu+1) \tag{12e}$$

In fact, clearly, all of the gamma coefficients, densities, pressure, loss and height can still vary in a completely arbitrary fashion. Still, it is now worthwhile to explore the consequences of a few special assumptions: for illustration, we fix coefficients and densities, neglect fluid loss and allow time-dependence in height, pressure and/or injection rate only. Firstly, consider a power-law behavior of the latter three variables

$$h = h_0 t^{\phi}, \; \hat{\sigma}_W = \hat{\sigma}_W^0 t^{\beta}, \; Q_W = Q_W^0 t^{\psi} \quad . \tag{13a}$$

Insertion of H and Q_W into eqn. (11b) leads to

$$\left(\frac{L}{h_0}\right)^{2n+3} = \frac{\Gamma_5^m}{h_0^2}\left[\frac{Q_W^0 t/2h_0^2}{\Gamma_3(\psi+1)}\right]^{2n+2}$$

$$\times (2h_0/Q_W^0)^m t^{\psi(2n+2-m)-\phi(2n+3-m)} \tag{13b}$$

in which we have structured the result to display the special condition of constant height and constant pumping rate ($\phi=0=\psi$) for which the model has typically been used in the past[2,4,8]. On the other hand, insertion of H and $\hat{\sigma}_W$ into eqn. (12b) produces a fracture length given by

$$\left[\frac{L^{2\phi+1}}{h_0}\right]^F = \frac{\Gamma_5 h_0^{E-3F} F t}{\Gamma_3(E\phi+P\beta+1)}(\hat{\sigma}_W^0 t^{\beta})^{P-F} t^{(E-2F)\phi} . \tag{13c}$$

Again, the special case of constant height and pressure ($\mu=\phi=0=\beta$) is readily deducible (giving $L \sim t^{m/(m+1)}$). It is also interesting to note that the fracture will not propagate - indeed, it will formally reduce in length according to the present theory - unless the power of pressure satisfies

$$\beta \geq \frac{(2F-E)\phi-1}{P-F} = \left.\frac{-m}{2n+2-m}\right|_{\phi=0=\mu} \quad . \tag{13d}$$

The observation in eqn. (13d) naturally introduces the need for an alternative to power-law spreading of the height H. Reference back to the result of the computation for propagation for a long, straight crack perimeter, as deduced in eqns. (5,6), shows that there occurs a power-law for ℓ vs. t (for $m=n$) only if pressure has the form $\ln \hat{\sigma}_W \sim -m\ell nt/(n+2)$; eqn. (8c) then demonstrates that pumping rate also follows an arbitrary power-law. Otherwise, length is exponential in time; since those results are directly applicable to the computation of H (as is argued more generally for the P3DH model in section 4), it is necessary now to provide some calculations based on an exponential growth of height H. First, suppose that $\hat{\sigma}_W$ has a power-law behavior in time (eqn. (13a)) so that the solution of eqn. (5) is

$$H^2 = \frac{\hat{\sigma}_0 H_0^2}{\hat{\sigma}_W^0 t^{\beta}} \exp\left[\frac{\gamma_5 \hat{\sigma}_W^{0\,M}}{\gamma_3(M\beta+1)} t^{M\beta+1}\right], \; M = \frac{n+2}{m} . \tag{14a}$$

We note that $\hat{\sigma}_0$ and $\hat{\sigma}_W^0$ do not coincide except for a constant pressure ($\beta=0$), so that an exponential form of pressure may be preferred:

$$\hat{\sigma}_W = \hat{\sigma}_W^0 e^{\beta t}, \; H^2 = H_0^2 \exp(-\beta t)\exp[\quad] \tag{14b}$$

$$-[\quad] \equiv D - De^{\beta M t}, \; D \equiv \gamma_5 \hat{\sigma}_W^{0\,M}/\beta M \gamma_3 \quad . \tag{14c}$$

Insertion of (14a,b) into eqn. (12b) produces integrals of the form

$$I_P = \int t^B \exp t^{A+1}, \; I_E = \int \exp Bt \exp[D \exp At] \tag{14c}$$

where the coefficients appearing may be written in conjunction with the condition for perfect integrability

$$\beta M \equiv A = B \equiv P\beta - E\beta/2 + C, \; C = \beta(1+m)/2m. \tag{14d}$$

The coefficient C has been added just to satisfy the integrability condition and could, for instance, arise from a time-dependence in $\rho_W \Gamma_5(\rho_W \Gamma_3)^{F-1}$ of the form $\exp Ct$. Of course, the integrals can be performed anyway by repeated integration, or by numerical methods, but we focus on the perfect integrability result because it produces a dramatic demonstration of the relation between L and H; besides, it is apparently valid for reasonable operating conditions, such as constant specified pressure. The remarkable result is that, for any of the height growth laws in eqns. (14a,b), the aspect ratio of the fracture will take the form

$$\left(\frac{L}{H}\right)^{m+1} = \left[\frac{2\Gamma_5^0 \gamma_3}{3\gamma_5 \Gamma_3^0}\right]^m = \left(\frac{2\gamma_3}{3\Gamma_3}\right)^m \left(\frac{\Gamma_2\Gamma_4}{\gamma_2\gamma_4}\right) \tag{14e}$$

which follows directly on performing the integrals in (14c) and using values of F,P,E (with $\mu=0$) from eqns. (12c,d,e).

Slow variations in time may be superposed on eqn. (14e), arising from separate time-dependence of $\rho_W \Gamma_3$, but the essence of the result is still contained in the multiplying coefficient; this effectively implies that the aspect ratio is dictated by the ratio of slopes in the pressure curve, as is recognised by introducing eqns. (4d, 10b) for γ_5 and Γ^0 (the coefficient in a time-variable Γ_5). Cancellation of $\Gamma_1\hat{n}$ with $\gamma_1\hat{n}$ is reasonably assumed, but Γ_3 and Γ_4 will typically be somewhat smaller than γ_3 and γ_4. To achieve a length appreciably greater than height, our only resort is through the slope ratio Γ_2/γ_2 (figures 2,3). The vertical pressure slope γ_2 can be calculated with numerical models, for a given profile of rock properties at any particular vertical section in the reservoir (see Section 5 for discussion of typical values); the computation incorporates both vertical fluid flow in the fracture and, *sine qua non*, the mechanics of rock deformation and separation near the upper or lower perimeter. The lateral slope Γ_2 may also be calculated for a more detailed model of flow according to eqns. (9), in a fashion somewhat akin to (but more general than) previous approaches[2,4,8] (see Appendix 1). However, the mechanics of fracturing near the front of such a moving channel must be incorporated to correctly calculate $L(t)$; this will change the whole complexion of the solutions obtained, especially removing the possibility of self-similar lateral pressure profiles and rendering untenable all existing analyses (algebraic and numerical).

4. A PSEUDO-THREE DIMENSIONAL HYDROFRAC MODEL (P3DH)

To improve upon and go beyond the approximations of the previous sections, it is now possible to combine the governing equations for the various subelements described there, and thus generate a fairly general and realistic model which may describe many practical circumstances very adequately. Here we describe one such *pseudo-three-dimensional hydrofac* model (mnemonically called P3DH). The backbone of this model (Figure 4) is still the use of the height-wise integrated one-dimensional equations (9) for the main-stream lateral flow of fracturing fluid; but now a vital supporting framework is provided by the additional equations (1b,2b,3), approximated in eqns. (4a, b,c), for the behavior of the fracture height at any vertical cross-section.

To obtain a compact description of the primary structure in the P3DH model, the lateral flow equations (9) may first be combined to obtain a single governing equation on pressure $\hat{\sigma}$; we note that $\hat{\sigma}$ can actually also incorporate a nonlinear contribution to opening, (e.g. Δ_S, arising from frictional slippage figure 4). A convenient resulting form is:

$$\frac{\partial}{\partial t}(\rho\hat{\Gamma}_3 H^2\hat{\sigma}) - \rho H q_L - \frac{\partial}{\partial x}\left(\frac{\rho Q}{2}\right) \qquad (15a)$$

$$= \frac{\partial}{\partial x}\left[-\rho^m(\hat{\sigma}H)^{2n+1}H^m\frac{\Gamma_4}{\hat{\eta}}\frac{\partial p_f}{\partial x}\right]^{\frac{1}{m}} \qquad (15b)$$

$$\simeq \frac{\partial}{\partial x}\left[\rho\overline{\Gamma}_5\left(-\frac{\partial f}{\partial x}\right)^{\frac{1}{m}}\right], \quad \hat{f} \equiv \hat{\sigma}^{2n+2} \qquad (15c)$$

in which the transmissivity $\overline{\Gamma}_5$ is thereby found to be

$$\overline{\Gamma}_5 \equiv \Gamma_4\,\overline{E}H^{2n+1+m}/(2n+2)\Gamma_1\hat{\eta} \quad . \qquad (15d)$$

It may be emphasised that the vertical fracture spreading need not be symmetric upward and downwards; the total fracture height $H_U + H_L$ (figure 4) is called 2H purely for convenience, without loss of generality.

The transition from $\partial p_f/\partial x$ to $\partial\hat{\sigma}/\partial x$ is achieved when the other contributions to $\hat{\sigma}$ (from σ_T, σ_B and Δ_S) are independent of x, an approximation that will suffice for the purposes of this paper. Solutions to these equations (15a,b) may be obtained for any specified behavior of H, sometimes analytically (Appendix 1) but certainly numerically; in general, they constitute a nonlinear diffusion process along x, over a domain which expands continually in time. The classical circumstances[2,4,8] of constant H are included and they emphasise that a contribution to the fluid storage term $\partial(\hat{\Gamma}_3\rho\hat{\sigma}H^2)/\partial t$ (eqn. (15i) later) does arise from the increase of $\hat{\sigma}$ with time at any fixed point along x; this tends to be a secondary source of fluid take-up (by comparison to dL/dt and q_L) in the conventional solution and it was actually neglected in early work[2], with quite acceptable results[4]. However, the possibility of varying H now renders the storage of greater importance in solving eqns. (15a-c).

To proceed with the solution, we need to decide on boundary values near the wellbore and near the moving outer boundary; it may be assumed that the values of variables Q or σ are known:

$$x = L_0 \rightarrow \hat{\sigma} = \hat{\sigma}_W \;\underline{\text{or}}\; \overline{\Gamma}_5^m\,\partial\hat{f}/\partial x = -(Q_W/2)^m \qquad (15e)$$

$$x = (1-\omega)L \rightarrow \hat{\sigma} = \hat{\sigma}_F \;\underline{\text{or}}\; Q = Q_F(t) \quad . \qquad (15f)$$

Here Q_W is the wellbore injection rate for the particular wing of the fracture in question and any solutions must satisfy overall mass conservation

$$\frac{\rho_W Q_W}{2} = \frac{d}{dt}\int_0^L dx\,\hat{\Gamma}_3\,\rho H\Delta + \int_0^L dx\,\rho H q_L \quad . \qquad (15g)$$

With reference to an integration of eqns. (15a,b), and by use of the Leibnitz rule[21], this condition can be rephrased to get the rate of fracture extension

$$dL/dt = Q_F/[2\hat{\Gamma}_3 H\Delta]_{X=L(1-\omega)} \quad . \qquad (15h)$$

In conventional models, eqns. (15a,h) serve to determine dL/dt uniquely because the boundary value σ_F is typically assumed; this has always been set equal to zero and we note immediately the difficulty that $\Delta(X=L) = 0 = Q_F$ (presumably), so that the numerical calculation of eqn. (15h) is likely to give poor results. However, the model can readily be made more physically and computationally appealing as follows.

Firstly, we have made two adjustments to the conventional boundary conditons: the wellbore end may be at a finite initiation distance L_0 (for instance, to allow the possibility that L is exponential in time, as suggested by eqn. (14e)) and the pressure or flow rate at $X = L - \omega L$ may have quite general values (as against $\hat{\sigma}_F = 0$ or $Q_F = 0$, typically assigned[2,4,7,8]). These latter adjustments of the boundary conditions at the terminus of the fracture (figures 3, 4), constitute a major re-rationalisation of this whole PKN-type model for lateral flow: the values $\hat{\sigma}_F$ and Q_F are not (usually) determined simply from the fluid flow laws but are governed rather by the overall mechanics of rock separation at the front of the fracture. We have coined the suggestive title of *leading edge model* for the calculation which produces a relation between $\hat{\sigma}_F$ and dL/dt (or Q_F); when coupled to the flow described by eqns. (15a,b), the values of $\hat{\sigma}_F$ and dL/dt can be computed at each stage in the fracturing process.

The leading edge model must, of course, adequately capture the complex crack opening and frac-fluid penetration which occurs around the outer perimeter of the fracture. Rigorously implemented, it would require a full 3-D solution of the equations (1a,2a,c, 3); this is still much less computationally demanding than a 3-D simulation of the whole fracture as it spreads, and developing 3-D capabilities[9,10] may be applied to the task in the near future. However, for practical purposes, a simpler model can often adequately be used to make the computation; this takes advantage of the similarity in character between the extension of the outer perimeter and the spreading of upper and lower perimeters of the fracture, while recognising the corrections required for geometric differences between the two processes. The correction factors may be determined by laboratory experiments and/or eventually by 3-D numerical simulators. Thus, for illustration, we will implement the models described by eqns. (1b,2b,3), or their approximation in eqns. (4a,b, c), to describe the propagation dℓ/dt of the leading edge at the front of the lateral fracture spreading.

These same CGDD-type models are also the essence of the secondary structure, describing the evolution of fracture height $H(x,t)$ at any point along x. Their predictions are used to compute the contribution of $\partial H/\partial t$ in the fluid storage term

$$\frac{\partial}{\partial t}(\hat{\Gamma}_3\rho\hat{\sigma}H^2) = \hat{\Gamma}_3H^2\frac{\partial}{\partial t}(\rho\hat{\sigma}) + \rho\hat{\sigma}\frac{\partial}{\partial t}(\hat{\Gamma}_3H^2) \quad (15i)$$

of eqn. (15a), and also to update the value of the effective transmissivity $\bar{\Gamma}_5$ at each stage in the solution of the lateral fluid flow equations. This $\partial H/\partial t$ calculation can be arbitrarily accurate, depending on the complexity of the injection sequence in the field operation and on the level of confidence in the available data on reservoir structure and material properties. It may involve a complete unsteady-state simulation of fluid penetration and perimeter propagation, for which the required numerical capability is just now becoming available[10], or it may be a less complex numerical representation which we have also developed, based on self-similar kinds of assumptions; the latter proved adequate for many practical pumping sequences.

For illustration here, we will adopt the much simpler approximate solutions which were developed in eqns. (4); these immediately provide an expression for the whole of the storage term in eqn. (15i), a fact which greatly simplifies the procedure of solving (15a,b). However, we note that the separation in eqn. (15i) should more generally be maintained, in order to allow the possibility (e.g., for constant H) that the dominant storage term is in $\partial(\rho\hat{\sigma})/\partial t$; this will generally have to be computed from the lateral flow equations, since the vertical propagation model has no way of calculating the actual pressure at the cross-section in question - but rather requires it as an input for each next step in time.

For instance, then, an equation from which the excess pressure $\hat{\sigma}$ can be calculated is derived by employing the results from eqns. (4,5) to get the following more tractable version of eqns. (15a,b):

$$\frac{\partial}{\partial x}\left[\rho\bar{\Gamma}_5\left(-\frac{\partial\hat{f}}{\partial x}\right)^{\frac{1}{m}}\right] + \rho\gamma_5 H^{\frac{2n}{m}}\hat{f}^{\frac{1}{m}} = 0 \quad . \quad (16a)$$

It is interesting to note that when $m = 1$ this becomes a linear differential equation, with variable coefficients decided by $H(x,t)$, so that solutions can be extracted by superposition; this serves, therefore, as a convenient test case for verifying numerical results. It seems that time enters only as a parameter (through H) but, of course, the boundary-conditions in eqns. (15e,f) dictate the fracture extension in time - through eqn. (15g) for Q_W. In implementing the latter, we note that a relation of the kind in (15h) will typically produce results of lower accuracy than the kinds of overall mass conservation statements that we are able to use when self-similar solutions are possible (Appendix 1).

The form of such self-similar solutions may always be employed in the model of eqn. (16a), since no time-derivative appears there; thus the time-dependence in $H(x,t)$ can be transformed to a dependence on dimensionless position $X \equiv x/L$, with time as parameter. This can be written into transmissivity as follows:

$$H = H_0 g(X;t), \; \bar{\Gamma}_5 = \bar{\Gamma}_5^0 H^R, \; mR \equiv 2n+1+m \quad , \quad (16b)$$

and then eqn. (16a) takes the following form, neglecting density variations,

$$[\bar{\Gamma}_5^0 g^R(-\hat{f}')^{\frac{1}{m}}]' + \gamma_5(L/H_0)^{\frac{m+1}{m}} g^{\frac{2n}{m}}\hat{f}^{\frac{1}{m}} = 0 \quad . \quad (16c)$$

where prime denotes differentiation on X.

This equation can be solved for any reasonable form of $g(X)$, but a flavour of the results can be obtained by noting that assumption of $g=1=m$ (constant height and Newtonian fluid) allows the simple exponential solutions

$$\hat{f} = \sum_{+-} \pm(\hat{\sigma}_F^{2n+2} - e^{\mp d}\hat{\sigma}_W^{2n+2})e^{\pm dX}/(e^d - e^{-d}) \quad (16d)$$

$$d^2 \equiv \gamma_5(L/H_0)^2/\bar{\Gamma}_5^0 \quad . \quad (16e)$$

It is clear that the solutions cannot be truly self-similar, since the time-dependent length appears in the "inverse characteristic distance" d. It is interesting to note also the resulting injection rate, in terms of well-bore and crack front pressures:

$$Q_W = 2\sqrt{\gamma_5\bar{\Gamma}_5^0}\,[\hat{\sigma}_W^{2n+2}(e^d+e^{-d}) - 2\hat{\sigma}_F^{2n+2}]\,\frac{H_0^{2n+1}}{e^d - e^{-d}} \quad (16f)$$

For large d, the injection rate and pressure would have essentially the same functional behavior in time; with constant Q_W for instance, this contrasts strongly with the falling pressure $\sigma_W \sim t^{-n/(n+2)}$ of the CGDD-type models (eqns. (4a,6a) and with the rising pressure $\hat{\sigma}_W \sim t^{1/(2n+3)}$ of the conventional PKN model (eqns. (11a,b)). Roughly speaking, the fluid is being supplied partly to a PKN lateral extension and partly to CGDD vertical spreading.

Indeed, the fracture extension rate may now also be computed, a unique opportunity to use eqn. (15h) with precision. The result

$$\frac{dL}{dt} = \sqrt{\frac{\gamma_5\bar{\Gamma}_5^0}{\Gamma_3^2}}\left[\frac{2\hat{\sigma}_W^{2n+2} - \hat{\sigma}_F^{2n+2}(e^d+e^{-d})}{(e^d - e^{-d})\hat{\sigma}_F\,H_0^{1-2n}}\right] \quad (16g)$$

has a very revealing character: for large d especially, propagation of the fracture front dominantly depends on the excess pressure there, which must bear a suitable relation to the specified well-bore pressure or injection rate. This points up both the sensitivity to σ_F of the calculation in eqn. (15h) and also the need for an additional propagation criterion to determine this hitherto free variable at the fracture front. Both of the difficulties illustrated by eqn. (16g) may be alleviated effectively by introducing the model of a leading edge to decide the rate of crack extension at each stage in the process. The essence of this new feature is captured also by the approximate models for which solutions were worked out in eqns. (4,5) but their implications must be stated in a somewhat different way for the leading edge, since this does not actually increase appreciably in size during the propagation. Thus the calculation is for $d\ell/dt$, not for $d(\hat{\sigma}\ell^2)/dt$, and a suitable form may be obtained by inspection of eqn. (4c), namely

$$dL/dt = q_F = \gamma_5^T[\hat{\sigma}_F^{2n+2-m}(\omega L)^{2n-m}]^{1/m} \quad . \qquad (17a)$$

The γ_5^T employed here will need to have an appreciably larger value than that pertaining to the vertical propagation applications discussed in eqns. (14), certainly in reservoirs where long narrow fractures are to be produced.

The propagation rate implied by the equations for the main body of the fracture must now match that dictated by the mechanics of the leading edge; for instance, if eqns. (16g,17a) are to be compatible, then the following relation of front pressure to wellbore pressure must hold

$$\hat{\sigma}_F^{2n+2} = \hat{\sigma}_W^{2n+2}/[\Omega \sinh d + \cosh d] \qquad (17b)$$

$$\Omega \equiv \Gamma_3 \gamma_5^T \bar{\omega}^{2n-1}/\sqrt{\gamma_5 \Gamma_5^0}, \; \bar{\omega} \equiv \omega L/H_0 \quad . \qquad (17c)$$

Clearly, the excess pressure σ_F decays quite rapidly to zero with increasing aspect ratio L/H_0 (as represented in d, eqn. (16e)), so that it can be neglected eventually: effectively, the long path of fluid flow through the main body becomes a far greater resistance to propagation than the need for an excess to drive the leading edge. In addition, conditions may be such that Ω is very large, due to favourable propagation conditions near the front (e.g., very low confining stress or compliant rock, which will generate large γ_5^T). The dimension ωL has been converted to $\bar{\omega}H_0$ for very good physical reasons: the fracture opening transforms, from a simple relation to fracture height H (eqn. (9a)), to a dependence on distance from the real fracture front $x = L$ (figs. 3,4), when $L - x$ becomes comparable to H. Thus, ω is of order unity; it can be evaluated by laboratory experiments or by detailed modelling of the processes involved in the leading edge.

The pressure driving the leading edge, $\hat{\sigma}_F$ in eqn. (17b), can now be substituted back into eqn. (17a) and integration yields a complete analytical result for the fracture extent $L(t)$; we omit this because it would be unrealistic to assume a constant fracture height throughout a process governed by an equation (16a)) which vests its storage terms in the precept of steadily varying height. Although the formulae in eqns. (16d-g, 17b,c) are limited in this respect, they do convey in a compact transparent way, the structure of the more realistic solutions which can be obtained with this very appealing model of eqns. (16a-c).

Without presenting these more general results, it is possible to indicate[22] some primary practical implications of the new ingredients in models of the kind described by eqns. (15,16); these may warrant a complete re-assessment of field data, including the few cases where a thorough analysis has already been done with old models.

SAMPLE APPLICATIONS TO FIELD OPERATIONS

The simplest possible implementation of foregoing formulae can be achieved for the case of fixed fracture heights, an assumption common to all preceding design procedures[2-8]. Numerous such worked examples exist in the literature and, of course, innumerable case-histories are available in stimulation proposals regularly submitted to operators of the many oil and gas production companies throughout the world. Despite the limited realism of such special fixed height models, they will serve adequately here to demonstrate the general procedure to be followed in making computations with the more comprehensive formulae that we have presented. The current inability to satisfactorily verify predictions made after a stimulation treatment based on these, and suggested remedies for this - including the performance of more complex credible calculations, on the basis of the models in Section 4 - are matters which will have to be considered in separate work.

As a first example, we employ the formulae appropriate to a specified total wellbore pumping rate Q_W into a fracture with the conventional PKN[2,4] geometry. The width and length may then be determined from eqns. (11a,b), provided the coefficients Γ_5, Γ_3 can be determined. The first of these, Γ_5, contains a number of components (eqn. (10b)): $\bar{E}/\Gamma_1$ is dependent on the surrounding rock response - for instance, an isotropic homogeneous linear elastic medium gives the simplest behavior

$$\bar{E} = G/2(1-\nu), \; \Gamma_1 = 1 \quad . \qquad (18a)$$

The averaged channel-flow resistance $\hat{\eta}_W/\Gamma_4$ may be determined by integrating the nonlinear-flow equations across the height, viz. accounting for the vertically variable channel width; however, an adequate estimate[2] for this quantity is one which will allow direct comparison with conventional models[2,4,7]

$$\frac{\hat{\eta}_W}{\Gamma_4} = \frac{16}{3\pi}\frac{\hat{\eta}_W}{\gamma_4} = \frac{32}{3\pi}K'\left(4+\frac{2}{n}\right)^n \qquad (18b)$$

The shape factor Γ_3 expresses the ratio of total volume in the fracture to that which would pertain if crack opening δ were uniformly equal to $\Delta(x=0)$ everywhere (figure 3); a good estimate for it is, therefore

$$\Gamma_3 = \hat{\Gamma}_3/(1+\Gamma_2), \; \hat{\Gamma}_3 = \pi/4 \quad , \qquad (18c)$$

if we assume an elliptical opening along z and a $(1-x/L)^{\Gamma_2}$ profile along x.

The only appreciable difficulty arises in determining the slope of the pressure curve at the wellbore, Γ_2; Appendix 1 shows that a good estimate for this curve, when height is fixed and the leading edge is neglected (e.g. for low confining stress in the region), may be written as

$$\sigma = \sigma_W[1-U(X)]^{\Gamma_2^0}, \; \Gamma_2^0 = 1/(2n+2-m) \qquad (19a)$$

$$U(X) = \int_0^X ds\; [\alpha X + \bar{\alpha}(1-X)]^m/U_F^0 \qquad (19b)$$

$$U_F^0 = \frac{\alpha^{m+1} - \bar{\alpha}^{m+1}}{(m+1)(\alpha-\bar{\alpha})}, \quad \bar{\alpha} = \frac{\alpha+\beta}{1+\Gamma_2} \tag{19c}$$

Here α, β are the powers in the time-dependence of length L and excess pressure σ_w, respectively; for constant pumping rate, these powers are

$$\alpha = (2n+2)/(2n+3), \quad \beta = 1/(2n+3) \tag{19d}$$

The slope Γ_2 can now be deduced in the form

$$\Gamma_2 = \Gamma_2^0 U'(0) = \frac{\bar{\alpha}^m (m+1)(\alpha-\bar{\alpha})}{(2n+2-m)(\alpha^{m+1} - \bar{\alpha}^{m+1})} \tag{19e}$$

As a guide, in the above equations, $U(X)$ may be thought of as X and Γ_2 as Γ_2^0; these approximations would serve quite well for most practical purposes. Clearly, a little iteration on eqns. (19c,e) may be performed to improve the accuracy of the Γ_2 determination, but exhaustive computation to get fine precision is not justified by the accuracy of the model or the role which Γ_2 plays in eqns. (11a,b). To illustrate, for the special case $m = n = 1$, we start with $\Gamma_2 = 1/3$ and immediately get the converged estimate for constant pumping rate,

$$U_F^0 = 0.775 \rightarrow \Gamma_2 = 0.323 \quad . \tag{19f}$$

This corresponds with the value (roughly $\Gamma_2 = 0.33$) which can be deduced from the numerical solutions of Nordgren[4] (either as the slope of his figure 4 at $X = 0$ or by back-calculating from his eqn. (20) what Γ_2 would have to be for consistency of his results with eqns. (11a,b)). The value is higher than that resulting from the conventional assumption[2] of constant flow rate, namely $\Gamma_2 = 1/(2n+2) = 0.25$, which neglects the storage terms $\partial\Delta/\partial t$ that cause all the difficulty in Appendix 1.

Interestingly, the approximation $\Gamma_2 \approx \Gamma_2^0 = 1/(2n+2-m)$ proves to be increasingly good with decreasing $n = m < 1$, and this value will be adopted here. Our argument has concentrated on the regime of dominant accumulation but similar arguments (Appendix 1) may be made for the alternate extreme of dominant loss; these are borne out again by the numerical solutions of Nordgren[4], which verify our deductions that Γ_2^0 can be used as a good estimate for the pressure slope in making practical calculations over the whole regime of a typical fracturing treatment. Crack-opening Δ is relatively insensitive to Γ_2 (and to γ_2 in the next application, with CGDD models), because of the 2n+2 root that is taken in eqn. (11a); thus, small changes in Γ_2 (e.g., during transition from accumulation to loss) may be ignored if a good average value has been determined. These observations are the key to the simple application of our formulae which is presented here.

To facilitate calculations, we rephrase eqns. (11a,b) for constant specified pumping rate in the form

$$\Delta^{2n+2} = \Gamma_1 \hat{n}_W \, LH \, Q_W^m / 4^m H^m \Gamma_2 \Gamma_4 \bar{E} \tag{20a}$$

$$Q_W t = W_L/\rho_W + 2\Gamma_3 \, LH\Delta \quad , \tag{20b}$$

$$\left(\frac{Q_W t}{2LH}\right)^2 - \left[\left(\frac{\pi k_L^W}{\alpha+0.5}\right)^2 + \frac{\bar{\Delta} Q_W}{LH}\right] t + \bar{\Delta}^2 = 0, \quad \bar{\Delta} = \Delta_{sp} + \Gamma_3 \Delta \tag{20c}$$

Here we have introduced the conventional spurt loss and square-root loss assumption $q_L = k_L^W/\sqrt{t-\tau}$, for comparison purposes, although any other law is readily incorporated for W_L in the formulae; the result, eqn. (20c), is a straightforward quadratic equation for the treatment time t needed to achieve any desired length L (with accompanying width Δ in eqn. (20b)), which is assumed to vary as $L \sim t^\alpha$. The parameter α must be varied slightly to correspond with the growth regime in question, going from $\alpha = (2n+2)/(2n+3)$ for dominant accumulation to 0.5 for dominant loss; the value chosen may be decided by comparing loss to accumulation on a quick first pass through eqn (20c) - but, again, excess fussiness is not warranted by the inherent approximations in the model itself.

A number of illustrative results are shown in Table 1; these are all chosen deliberately to allow comparison with existing calculations in the literature particularly the compendium provided in ref. 7. The agreement, with calculations ascribed[7] to Nordgren's model (denoted by N) is generally good for linear fluids and the few deviations can probably be explained by small errors in calculations or differences in minor details of our models such as the weighting of the loss function in eqn. (20c). For nonlinear fluids, much better agreement is found with the calculations[7] based on Perkins and Kerns model (denoted by PK), because the linearisation needed to implement Nordgren's solutions works quite poorly; obviously, the careful implementation of eqns. (20a, b,c) now provides the proper extension of such detailed solutions to the nonlinear range. These simple formulae can therefore supplant all foregoing tedious or approximate analyses.

An entirely analogous procedure can be followed for calculations based on the CGDD-type models. The relevant equations are now (6a,b) which can be rephrased in the form

$$\Delta^{2n+2} = \gamma_1 \hat{n}_W \ell^2 \, Q_W^m / 4^m H^m \, \gamma_2 \gamma_4 \, \bar{E} \tag{21a}$$

$$Q_W t = W_L/\rho_W + 2\gamma_3 \ell H \Delta \quad . \tag{21b}$$

The latter reduces to exactly the form of eqn. (20c) when γ_3 is substituted for Γ_3 and ℓ is interpreted as the length L of the fracture for the present context. The major difference from PKN models is the appearance of ℓ^2 (rather than LH) in the expression for crack-opening Δ; fractures with ℓ shorter/longer than H therefore obviously tend to have narrower/wider aperatures than those predicted by PKN.

The simpler parameters needed for the calculations are $\gamma_1/\bar{E}$ ($\approx \Gamma_1/\bar{E}$, eqn. (18a)), $\gamma_3 (\approx \hat{\Gamma}_3$, eqn. (18c)) and $\hat{n}_W/\gamma_4$ (eqn. (18b)). Again, the greatest difficulty appears in deciding on values for the slope of the pressure curve γ_2: this must be determined numerically, with the aid of self-similar propagation routines which we have developed. These resemble the schemes formulated by Geertsma and deKlerk[3] and Daneshy[5], but they do not assume constant flow rate along the fracture, viz. storage or loss terms corresponding to $\partial\delta/\partial t$ and q_L in eqn. (1b) are precisely taken into account; as well, quite general rock/fluid properties and injection sequences can be accommodated. A special application is that of constant pumping rate and isotropic homogeneous rock, which allows comparison with previous predictions[3,5,7]; we find that incorporation of these more realistic descriptions leads to considerable alteration of the predictions conventionally made with these models.

In particular, the value of γ_2 does not seem to be nearly so high as that implied by the results of previous workers [3,5,7]. For instance, it is easy to show that the formulae in ref. 3 implicitly represent a value $\gamma_2 = 4\pi/14$, independently of the confining stress (provided this is large enough to justify the approximations made in deducing their formulae). We find values this high only for very low confining stress (of order one-third of the total fracturing pressure) and γ_2 drops quite dramatically with increased confining stress, as much as an order of magnitude up to stresses typical of relatively deep hydrofrac operations. However, we will use the value $4\pi/14$ for reference purpose in making our comparative calculations here (Table 2): this serves to check the predictions of preceding work[3,5,7] and allows the estimates for Δ to be readily altered (keeping all else fixed in eqn. (21a)) for any new γ_2 determined numerically.

Clearly, the agreement in Table 2, with results cited in ref. 7 is quite good. Our stimulation time estimates are consistently lower but this may be explained by our more rigorous implementation of space and time integration in the final form used for the loss function (eqn. (20c)). Sometimes, the Geertsma results (G) for Δ are lower than ours, (implying an even higher γ_2?) so we use Daneshy (D) for comparison; both are used (GD) when they agree. Sometimes, the Δ of Daneshy is appreciably higher, so we use the Geertsma results (G); this means that Daneshy does find lower γ_2 and may provide a more reasonable estimate. However, all of these results must be corrected to account for the effects of storage terms, confining stress and more realistic rock properties. The result will typically be a somewhat larger crack-opening Δ (smaller γ_2) and longer stimulation time t to reach any desired length, for this particular CGDD model.

Of course, we have argued that both these CGDD-type and the foregoing PKN models should really be incorporated in a more realistic simulator (such as P3DH); this immediately brings in the need for more general injection sequences (such as specified pressure), rather than constant pumping rate. Such calculations (e.g., using eqns. (5, 12b)) can also readily be performed. The more general calculations, e.g. for P3DH, become appreciably more complicated and inherently numerical - except for special analytical results of the kind cited in Section 4. Thus, the many other possible calculations with these simple geometries and more detailed applications of these new pseudo-3-D models clearly warrant a separate presentation and will not be pursued further here.

CONCLUSIONS

From a practical point of view, there are probably just three main conclusions to be taken from the material in this paper:

1. It is possible to employ straightforward algebraic formulae for analysis and design with conventional CGDD and PKN industrial models of the hydraulic fracturing process. These adequately capture the predictions made by more complex numerical simulators, for the typical assumptions of specified (e.g. constant) pumping rate; they also encompass more general injection sequences (such as specified pressure) and allow a broad range of frac-fluid or rock properties.

2. The formulae incorporate the capability for describing variation of fracture heights during the stimulation treatment. This vertical spreading may be either specified, in the simplest descriptions, or it may be allowed to evolve in a manner consistent with the (specified or deduced) pressures driving the lateral propagation.

3. The formulae for the CGDD and PKN models are simple enough that they can be combined to achieve various more realistic descriptions of the hydrofrac processes which are believed to develop in the field. One particular P3DH model has been described, to illustrate that resulting governing equations and solutions may sometimes be simpler than these for the conventional descriptions presently in use; it also helps to crystallise and remedy the numerous shortcomings in these currently available models.

The paper has aimed mainly at providing an overview of the great potential which is offered by simplification and integration of the various components which have been developed over the past few years. Only a sampling of the many amenable geometric idealisations has been presented and this has concentrated mainly on the currently popular models; it is hoped that this choice will provide the greatest motivation for industrial interest in the method, since the formulae can be immediately tested against available simulators, and extensions can be made as desired.

Although not presented exactly in this manner, it will be observed that the heart of the formulae can be extracted very simply by a non-dimensionalisation of the governing equations; the remainder just involves a good physico-mathematical choice of the undetermined coefficients. The results could be presented in the usual format of design charts, based on dimensionless groups extracted, but these can readily be generated from the formulae as desired; a more appealing procedure may be to program the solutions for a suitable pocket calculator, with the separately determinable γ or Γ coefficients and job parameters as input.

Despite the great appeal and considerable improvements in simulation capability wrought by these simple formulae, the paper emphasises that they may be severe idealisations for many practical applications; of course, they are still more desirable than fully 3-D simulators with equally idealised assumptions of a different kind. However, it is possible to extend their realm of relevance by astute combination of the kind indicated in Sections 3 and 4. Indeed, we have been able to develop quite realistic quasi-analytic and numerical models of the fracture evolution in typical geological structures, based simply on equations of the kind outlined in Section 4; these again just hybridise the conventional one-dimensional lateral flow description with the two-dimensional vertical spreading models that we have generated. The result is an effectively three-dimensional description of the operation, without the many details and expense needed for a truly 3-D numerical simulation. There will be circumstances and, eventually, sufficient reservoir information to merit such rigorous 3-D capabilities. However, the "half-way-house" models of the kind described in this paper will at least constitute acceptably realistic intermediate stop-gaps. Their allowance of a varied level of complexity, from the very simple equations in Section 4 to the full numerical simulation of multiple vertical and horizontal cross-sections, matching the level of confidence in data available for the reservoir, may make them popular for some time to come.

NOTATION

a,b	=	Arbitrary powers in growth laws
B	=	Subscript or superscript denotes evaluation of variable in main body of fracture (fig.2)
C	=	Arbitrary constant, e.g., eqn. (14d)
d,D	=	Inverse characteristic lengths, eqn. (A2.1)
E,F	=	Powers used in growth laws, eqns. (12c,e)
$\bar{E}$	=	Plane-strain modulus of reservoir rock
f	=	Arbitrary function (e.g., excess pressure in fracture, σ^{2n+2})
$G;G_j$	=	Shear modulus; values in region j
g	=	Acceleration due to gravity on earth
$\mathcal{G};\mathcal{G}_{eq}$	=	Fracture energies of material; equivalent value for typical hydrofrac operations
h,h_0	=	Parameters appearing in expressions for fracture height
H,H_0	=	Half-heights of fracture, formation pay zone, etc.
k	=	Permeability of porous medium
k_L,k_L^W	=	Fluid loss coefficient, value at the well-bore
K'	=	Effective consistency of frac-fluid for pure shearing deformation rate
K,K_c	=	Stress intensity factor; critical value for propagation
ℓ	=	Generic length of fracture, lateral extent or height
L,L_0	=	Lateral extent of fracture, coefficient or initial value
m,n	=	Power laws for flow of fluid within fracture
$\mathbf{m},\mathbf{n}$	=	Unit vectors normal to crack perimeter, or normal to fracture surface
M,N	=	Powers used in solutions, eqns. (14a,A1.4c)
p,p_T	=	Pore-pressure, tectonic value
p_f,p_f^W, p_f^B,p_f^f	=	Pressure in fracturing fluid; value at the well-bore, or in main body of fracture or at front of frac-fluid (e.g., for vertical cross-section of lateral flow model, fig.2)
P	=	Power used in growth law, eq. (12d)
$\mathbf{q},q$; q_w,q_F	=	Velocity, speed of fluid flow in fracture or porous medium; values at the well-bore and fracture front
$\mathbf{q}_L,q_L$	=	Flow rate for fluid loss from fracture
$Q;Q_W$, $Q_F;Q_W^T$	=	Integrated volume flow rate of fluid laterally along fracture; value at the well-bore, fracture front; total injection at wellbore.
r,r_w	=	Radial position co-ordinate, radius of well-bore
t	=	Time measured from beginning of process
u,u_k	=	Generic displacement, component in k direction
v,v_k	=	Generic velocity, components in k direction
w,w_ℓ	=	Mass of fluid injected, lost to formation (per unit length, figure 2)
W,W_L	=	Mass of fluid injected, lost to formation (total for one wing of fracture)
$\mathbf{x},\mathbf{x}_0$	=	Position vector of any point, specific point of evaluation
x,y,z	=	Distances along reference axes to any point
X	=	Dimensionless position laterally along fracture, $X = x/L$.
$(\dot{\ })$	=	Time derivative of quantity in parentheses
$(\ )'$	=	Spatial derivative of quantity in parentheses, usually along x or z
α,β	=	Powers or exponents in the variation of crack length, excess pressure vs. time
α_k,β_k	=	Coefficients for various uses (e.g., power of near-tip singularity, material dependence)
γ	=	Power used in fluid loss law, eqn. (A1.1a)
γ_1,Γ_1	=	Ratio of crack opening at center to that for uniform pressure
$\gamma_2;\Gamma_2$	=	Slope of pressure curve in CGDD-type model (fig. 2); slope at the wellbore in PKN-type lateral flow model (fig. 3)
$\gamma_3;\Gamma_3$	=	Ratio of fracture volume to that for uniform opening in CGDD-type model; same ratio along generalised PKN model (sometimes $\gamma_3 = \Gamma_3$)
$\gamma_4;\Gamma_4$	=	Channel-flow factor in CGDD-type model; same in general PKN-type lateral flow model
γ_5	=	Combination of foregoing γ factors, eqn. (4d)
Γ_5	=	Combination of foregoing Γ factors, eqn. (10b)
$\Gamma(\mathbf{x}_0,\mathbf{x})$	=	This is an "influence function" describing the stress at point $\mathbf{x}_0$, due to a dislocation or other disturbance at point $\mathbf{x}$
δ	=	Crack opening displacement at any point
$\delta',\nabla\delta$	=	Spatial derivative of crack opening, often called the dislocation density
$\Delta;\Delta_s$	=	Maximum value or suitable average of crack-opening, e.g., for any vertical cross-section of PKN-type model; inelastic slippage
Δ_{sp}	=	Spurt loss, as equivalent crack width
$\epsilon_{k\ell}$	=	Components of second-order strain tensor
$\hat{\eta};\bar{\eta}$	=	Consistency of frac-fluid used in flow between fracture walls; incorporation of channel-flow factor, e.g., eqn. (18b)
θ	=	Power or exponent in fracture's storage parameter dependence on time (eqn. (A1.1c)). Often also used for angle in polar or spherical co-ordinates
κ	=	Power or exponent in variable height models
μ	=	Power or exponent, sometimes friction factor
ν,ν_u	=	Drained, undrained Poisson ratio for porous reservoir rock
τ	=	General time value, e.g., elapsed time
τ_c	=	Characteristic time, e.g., in growth laws for hydraulic fracture
ρ,ρ_w	=	Density of fluid, value at the wellbore
σ_{ij}	=	Components of second-order stress tensor
σ_V,σ_H	=	In-situ principal stresses -- "vertical, horizontal maximum and minimum;
$\sigma_M;\sigma_T$, σ_T^W,σ_T^B	=	General symbol for tectonic stress normal to fracture, values at wellbore or on main body of any cross-section (fig.2)
σ^B	=	Value of excess pressure σ in the main body of any vertical cross-section (not to be confused with back-stress σ_B)

σ_B, σ_B^W = Back-stress on fracture surface due to pore-pressure alteration, inelastic deformation, thermal stress induction, etc., caused by the fracturing operation

σ_c, σ_c^W = Total confining stress on fracture surface ($\sigma_T + \sigma_B$), value at the wellbore

σ, σ_W = Excess pressure ($p_f - \sigma_c$) driving fracture, value at wellbore

$\hat{\sigma}; \hat{\sigma}_F$ = Dimensionless value of excess pressure, $\hat{\sigma} = \gamma_1 \sigma / \bar{E}$; value at fracture front.

ϕ = Power or exponent in height growth

χ = Power or exponent in injection rate

ψ = Power or exponent in injection rate

$\omega; \Omega$ = Dimensionless amplitude of non fluid-penetrated length near crack-tip or size of decohesion zone; eqns. (17a,c).

∇, ∇^S = Gradient operator in 3-D, or along fracture surface

REFERENCES

1. Christianovich, S. A. and Zheltov, Yu. P., "Formation of vertical fractures by means of a highly viscous fluid," Proc. 4th World Petroleum Congress, 2, 579-586, 1955.

2. Perkins, T. K. and L. R. Kern, "Widths of hydraulic fractures", J. Pet. Technology, 937-949, 1961.

3. Geertsma, J. and F. deKlerk, "A rapid method of predicting width and extent of hydraulically-induced fractures," J. Pet. Technology, p. 1517, Dec. 1969.

4. Nordgren, R. P., "Propagation of a vertical hydraulic fracture," J. Soc. Pet. Engrs, p. 306, 1972.

5. Daneshy, A. A., "On the design of vertical hydraulic fractures," J. Pet. Technology, 83-93, 1973.

6. Howard, G. C. and C. R. Fast, "Hydraulic fracturing," SPE Monograph, 1970.

7. Geertsma, J. and R. Haafkens, "A Comparison of the theories for predicting width and extent of vertical hydraulically-induced fractures," J. Energy Resources Technology, 101, 8-19, March 1979.

8. Nolte, K. G., "Determination of fracture parameters from fracturing pressure decline," Paper No. SPE 8341, 1979.

9. Cleary, M. P., "Primary factors governing hydraulic fractures in heterogeneous stratified porous formations," ASME Paper No. 78-Pet-47, 1978.

10. Cleary, M. P., Petersen, D. R. and S. H. Wong, Quarterly Reports from M.I.T. to Lawrence Livermore Laboratories (contained in ref. 11) Jan. 1978 - April 1980. [See also D. R. Petersen, "Numerical Analysis of Hydraulic Fracturing and Related Crack Problems", M.S. Thesis, M.I.T., Jan. 1980.]

11. Hanson, M. E., et. al., "LLL gas stimulation program", Quarterly Reports of Lawrence Livermore Laboratory, UCRL-50036, 78-1 to 80-2, 1978-1980.

12. Cleary, M. P., "Underground fracturing for enhanced recovery of oil and gas," Report to Marathon Oil Co., February, 1980.

13. Clifton, R. J. and A. S. Abou-Sayed, "On the computation of the three-dimensional geometry of hydraulic fractures", Paper No. SPE 7943, 1979.

14. Settari, A., "Simulation of hydraulic fracturing processes," Paper No. SPE 7693, 5th SPE Symposium on Numerical Simulation, Denver, 1979.

15. Cleary, M. P., "Fundamental solutions for fluid-saturated porous media and application to localised rupture phenomena," Ph.D. thesis, Brown University, 1975.

16. Advani, S. H., "Finite element model simulations associated with hydraulic fracturing," Paper No. SPE/DOE, 8941 (presented at Unconventional Gas Recovery Symposium, Pittsburgh), May 1980.

17. Papadopoulos, J. M. and M. P. Cleary, "Laboratory simulation of hydraulic fracturing," in preparation, 1980. [Preliminary report in ref. 11, April 1980].

18. Nolte, K. G. and M. B. Smith, "Interpretation of fracturing pressures," Paper No. SPE 8297, 1979.

19. Cleary, M. P., "Rate and structure sensitivity in hydraulic fracturing of fluid-saturated porous media," Proc. 20th U.S. Symposium on Rock Mech., pps. 227-242, 1979.

20. Settari, A. and M. P. Cleary, Private Communications, 1979-1980.

21. Abramowitz, M. and I. A. Segun, "Handbook of Mathematical Functions", Dover, 1965.

22. Cleary, M. P., "Analysis of mechanisms and procedures for producing favorable shapes of hydraulic fracture", Paper No. SPE 9260. 1980.

ACKNOWLEDGEMENTS

This paper represents a portion of my research on underground fracturing at M.I.T., which has been supported by a number of sources. I am especially grateful to Marathon Oil Company, Denver Research Center, where my interest in this area was heightened during a University Fellowship period, Summer 1978.

The award of a Carl Richard Soderberg Career Development Chair has helped me to continue my work and develop our facilities at M.I.T. As well, I express my appreciation for an unrestricted grant from Chevron Oil Field Research Co., Le Habra, California. Support for our more general modelling[10,17] from U. S. Dept. of Energy (through Lawrence Livermore Laboratory) is also gratefully acknowledged.

My sincere appreciation to M & N Toscano for their assistance in the preparation of this manuscript.

Discussions with a number of people have helped me to improve my ideas on the subject of underground fracturing; they know that I am grateful for their time and interest.

APPENDIX 1 SAMPLE SOLUTIONS OF GENERALISED PKN EQUATIONS

The starting point for a detailed (analytical or numerical) solution of the lateral flow equations is the combination of eqn. (9a,b,c) written in eqns. (15a,c). Our objective here is just to provide the self-similar solutions which were implicit in the derivation of the formulae in eqns. (10-14) of the main text. Two distinct forms of $H(t)$, $\ell(t)$ are used, namely the power laws assumed in eqn. (12,13) and the exponential behavior treated in eqn. (14). A completely general self-similar analysis has been worked out, but it seems more informative here just to describe the special cases used in the paper.

The existence of power-law self-similar solutions may be established by adopting the following structure of the variables

$$\hat{\sigma}^{2n+2} = f(X)t^{\overline{\beta}},\ H = H_0 f^{\xi}\tau^{\phi},\ q_L = k_L\tau^{-\gamma} \quad , \qquad \text{(A1.1a)}$$

where τ is time elapsed since the front of the fracture reached the point in question; we scale position to the overall fracture length, which is assumed to have a power-law dependence on time, so that

$$X = x/L,\ L = L_0 t^{\alpha},\ \tau = (1-X^{1/\alpha})t \quad . \qquad \text{(A1.1b)}$$

In addition, we assign their own power-law dependencies to the transmissivity $\overline{\Gamma}_5$ and storage parameter $\Gamma_3 H^2$, namely

$$\rho\overline{\Gamma}_5 = \Gamma_5^0 f^{\kappa}\tau^{\lambda},\ \rho\hat{\Gamma}_3 H^2 = \Gamma_3^0 \sigma^{\zeta}\tau^{\theta} \quad . \qquad \text{(A1.1c)}$$

Insertion of these assumptions into eqns. (15a,c) leads to

$$[\Gamma_5^0(1-X^{1/\alpha})^{\lambda} f^{\kappa}(-f')^{1/m}]'\ t^{a}/L_0^{1+1/m} \qquad \text{(A1.2a)}$$

$$+\ \Gamma_3^0\left(b-\alpha X\frac{d}{dX}\right)\overline{f}t^{b-1} + H_0 k_L f^{\xi}(1-X^{1/\alpha})^{\phi-\gamma} = 0,$$

$$\overline{f} \equiv (1-X^{1/\alpha})^{\theta}\ f^{(\zeta+1)/(2n+2)} \quad . \qquad \text{(A1.2b)}$$

The dependence on time can be removed if the powers match

$$\beta(\zeta+1) + \theta - 1 \equiv b - 1 = a = \phi - \gamma \qquad \text{(A1.2c)}$$

$$a \equiv (\overline{\beta}-\alpha)/m + \lambda - \alpha,\ \overline{\beta} \equiv \beta(2n+2) \quad . \qquad \text{(A1.2d)}$$

Obviously, all three conditions cannot be satisfied simultaneously by the (strictly) one undetermined parameter α. However, values of either β and/or ϕ,λ,θ (which are strongly related through eqns. (15d, A1.1a,c)) can be found which allow satisfaction of eqn. (A1.2c) for any appropriate value of the fluid loss power γ; for instance, a complete self-similar solution pertains to the constant height solution ($\zeta=\xi=0=\lambda=\theta$) when $\beta = 1-\gamma$, namely when specified excess pressure increases as $t^{1-\gamma}$ (so that eqn. (A1.6b) implies a pumping rate of the form $t^{\psi}, \psi(m+1) = 2n+2-\gamma(2n+3)$).

Of course, verification of a self-similar solution requires the further step of finding a reasonable solution for f, having assumed consistency of the power laws in eqn. (A1.2c). This involves considerable work to do it exactly but some tractable manipulations allow us to extract the essence of the results needed. First we perform an integration by parts on the second term and thereby establish an expression for flow rate along the fracture (which has the power ψ on time),

$$\Gamma_5^0(1-X^{1/\alpha})^{\lambda} f^{\kappa}(-f')^{1/m}/L_0^{1+1/m}$$

$$= \Gamma_3^0\,\alpha\,X\overline{f} + \overline{\alpha}\int_X^{1-\omega} ds\ \Gamma_3^0\overline{f}(s) \qquad \text{(A1.3a)}$$

$$+ \int_X^{1-\omega} ds\ k_L\ H_0 f^{\xi}(1-S^{1/\alpha})^{\phi-\gamma} = \rho Q/2t^{\psi}L_0 \ ,$$

in which the new terminology is defined by

$$\overline{\alpha} \equiv \alpha + b,\ \psi = a + \alpha \quad . \qquad \text{(A1.3b)}$$

Note that the constant in the integration was determined by the overall condition of mass conservation for fluid injection, eqn. (15g); the quantity ω is introduced (fig. 3) to allow for a region near the front where either the fluid has not penetrated or the model of crack opening should be altered from eqn. (9a). It is interesting to note that the variation of flow-rate along the fracture is readily deduced from eqn. (A1.3a), especially if $\overline{f}$ has almost a constant slope until it dips sharply to zero at the front (as the final solution will show): for instance, Q has essentially the same behavior as $\overline{f}$ for constant pressure ($\overline{\alpha} = \alpha$, neglect k_L and θ), while it varies almost linearly and then drops off sharply in other cases. Thus there are various degrees of error in typical assumptions[2,7,8] of constant Q or of linearly varying Q, which is remedied by the formulae provided here.

A further integration of (A1.3a) is now possible to get an implicit solution for f as follows:

$$f^N = f_W^N - NL_0^{m+1}U_F(X) \qquad \text{(A1.4a)}$$

$$U_F(X) \equiv \int_0^X ds\ \left[\frac{\Gamma_3^0(\alpha s+\alpha U_A^P)+H_0U_B^P}{\Gamma_5^0(1-s^{1/\alpha})^{\lambda-\theta(1,0)}}\right]^m \qquad \text{(A1.4b)}$$

$$N \equiv 1 + m\kappa - [m(\zeta+1)/(2n+2),0] \quad . \qquad \text{(A1.4c)}$$

The functions U_A^P and U_B^P are conveniently chosen to be

$$\Gamma_3^0U_A^P(X) \equiv \int_X^{1-\omega} ds\ \Gamma_3^0\,\frac{\overline{f}(s)}{\overline{f}(X)} \approx \frac{1-X-\varepsilon}{1+\Gamma_2}\,\Gamma_3^0 \ , \qquad \text{(A1.4d)}$$

$$H_0 U_B^P(X) \equiv \int_X^{1-\omega} ds\; k_L\, f^{\xi}/(1-s^{1/\alpha})^{\gamma-\phi}\bar{f}^{(1,0)}(X), \quad \text{(A1.4e)}$$

in which we have assumed U_A^P can be adequately evaluated by adopting a form of $\bar{f} \sim (1-\varepsilon-X)^{\Gamma_2}$, perhaps with small ε to capture near-front behavior; U_B^P is obviously of the form $[\pi/2-\mathrm{Sin}^{-1}X/(1-\omega)]/\bar{f}^{(0,1)}$ for the classical square-root law $\gamma = 0.5 = \alpha$, but can be evaluated more generally. The optional zeroes in parentheses are provided to allow for the simplification which arises when the loss cerms (associated with k_L) dominate the accumulation terms (associated with Γ_3^0).

The solution is now completed by imposing the boundary condition on f at $X = 1-\omega$, as in Eqn. (15f); eqn. (A1.4a) then becomes

$$f^N = f_W^N - (f_W^N - f_F^N)U(X), U(X) \equiv U_F(X)/U_F(1-\omega), \quad \text{(A1.5a)}$$

and equivalence with (A1.4a) automatically produces the desired estimate of the length parameter L_0 in eqn. (A1.10), namely

$$L_0^{m+1} = (f_W^N - f_F^N)/NU_F(1-\omega) \quad . \quad \text{(A1.5b)}$$

This is the final formal result if excess pressure $\hat{\sigma}_W$ is specified at the wellbore. However, if pumping rate $Q_W^0 t^{\psi}$ is imposed instead, then we must employ eqns. (A1.5a,b) in eqn. (A1.3a) to get (neglecting f_F for simplicity)

$$\rho_W Q_W^0/2L_0 = \int_0^{1-\omega} ds\; k_L f^{\xi}(1-s^{1/\alpha})^{\phi-\gamma} \quad \text{(A1.5c)}$$

$$+\ \bar{\alpha}\int_0^{1-\omega} ds\; \Gamma_3^0(1-s^{1/\alpha})^{\theta}\left[L_0^{m+1}U_F\Big|_s^{1-\omega}\right]^{\frac{\zeta+1}{N(2n+2)}} .$$

Use of the definitions provided for U_F^N, N etc. in eqns. (A1.4) now allow an implicit determination of L_0 [Note that we leave f^{ξ}, which contains L_0 also, for brevity.]

Before preceeding to special cases, we note some interesting general features of the result. The first concerns the characteristic power α in the growth law of eqn. (A1.1b), which is deduced from eqns. (A1.2c,3b):

$$\alpha = \bar{\beta} + m(\lambda-\psi) \quad . \quad \text{(A1.6a)}$$

Since the pressure (power β) and flow rate (power ψ) cannot be specified simultaneously, it is necessary to solve further between β and ψ; if the first of (A1.2c) is adopted, viz. if flow rated is certainly consistent with accumulation arising from height and pressure changes at each section of the fracture, then the relation is

$$\beta = (m\psi+\zeta-m\lambda-\theta)/(2n+3+\zeta) . \quad . \quad \text{(A1.6b)}$$

On the other hand, if the last of (A1.2c) is employed, corresponding to a flow rate consistent with fluid loss (and perhaps simultaneous accumulation), then

$$\bar{\beta} = m\psi + \psi - m\lambda - \phi + \gamma \quad . \quad \text{(A1.6c)}$$

A short calculation (using $m\lambda = (2n+1+m)\phi$ and $\theta = 2\phi$) shows that eqns. (A1.6a,b) are consistent with the powers of time in eqns. (13b,c) when $\mu = 0$ (in eqns. (12c,d,e)). Indeed, eqn. (A1.5b) now establishes the more complete results, which allows the identification of the pressure slope Γ_2 used in Γ_5 of eqns. (13b,c) and also produces the formulae relevant to dominant loss. It is worth listing such a comprehensive formulae here, in a form directly comparable to eqns. (13b,c); for specified pressure (neglecting f_F again) we obtain

$$\left(\frac{L}{h_0}\right)^{m+1} = \frac{\Gamma_5^m h_0^{2n-2m}\sigma_\omega^{(2n+2)N}}{N(2n+2)\Gamma_2\hat{\Gamma}_3^m U_F^0}\, t^{(\ldots)} \quad . \quad \text{(A1.7a)}$$

This allows us to make a direct calculation of the quantity Γ_2 first employed in eqn. (10b), namely

$$\Gamma_2 = \Gamma_3^m(E\mu+P\beta+1)^m/F^m(2n+2-m)\hat{\Gamma}_3^m U_F^0 \quad . \quad \text{(A1.7b)}$$

Here the coefficient U_F^0 has been used to describe

$$U_F^0 = \int_0^{1-\omega} ds[\alpha s+\bar{\alpha}U_A+H_0U_B/\Gamma_3^0]^m/(1-s^{1/\alpha})^{\lambda-\theta(1,0)} . \quad \text{(A1.7c)}$$

Clearly, the roles of U_B and U_A could be reversed in the foregoing formulae if we were more interested in the regime of dominant loss (rather than accumulation).

A major observation must now be made concerning U_F and the importance of ω in foregoing models. Notice that, if $m(\lambda-\theta) = (2n+1-m)\phi > 1$, the value of U_F^0 formally goes to infinity (and $\Gamma_2 \to 0$) as $\omega \to 0$; physically, this corresponds to the effect of a more strongly vanishing transmissivity ($H \to 0$ in Γ_5) than storage constant ($\Gamma_3 H^2$). Of course, the width model $\Lambda = \sigma H$ breaks down at points very close to the fracture front and a leading edge model must be substituted. However, it requires quite a complex analysis, beyond the scope of discussion here, to decide exactly how ω is to be chosen. Thus, we restrict attention to models which give a bounded U_F^0 as $\omega \to 0$, that is where ϕ is sufficiently small, viz. slowly varying (or constant) height H.

The dilemma of unbounded U_F^0 is actually avoided by a second class of solutions to eqns. (15a,c), namely those which are exponential in time, as discussed in eqns. (14). The most readily analysable group of this potentially broad class of mixed powers and exponents can be described (with reference to eqn. (14)) by the following structure

$$\hat{\sigma}^{2n+2} = f(X)e^{\bar{\beta}t},\ L = L_0 e^{\alpha t}\ , \qquad \text{(A1.8a)}$$

$$H^2 = H_0^2\, e^{-\beta\tau}\exp[D \exp \beta M\tau D] \equiv H_0^2 g_0^2(X) \qquad \text{(A1.8b)}$$

$$g(X) = X^{\beta/2\alpha}/\exp[D(1-X^{-M\beta/\alpha})/2]\ . \qquad \text{(A1.8c)}$$

With these assumed forms, we can now again write a separated equation analogous to (A1.2a), namely (with $\bar{\Gamma}_5 = \Gamma_5^0\, f^{\kappa}H^{\lambda}$, $\Gamma_3 H^2 = \Gamma_3^0\, f^{\zeta}H^{\theta}, \bar{b} \equiv b - \theta$)

$$[\Gamma_5^0 g^{\lambda} f^{\kappa}(-f')^{1/m}]'\ e^{(\bar{\beta}-\alpha-m\alpha)t/m}/L_0^{1+m}$$

$$= - \Gamma_3^0(\bar{b}-\alpha X \frac{d}{dX})(g^{\theta}\ f^{\frac{\zeta+1}{2n+2}})e^{\beta(\zeta+1)t} \qquad \text{(A1.8d)}$$

$$- H_0 k_L g(X)\ [\ell n X^{-1/\alpha}]^{-\gamma} = (\rho Q)'/2L_0\ e^{\psi t}\ .$$

The remainder of the analysis follows foregoing steps for the power-law solutions. Matching of powers gives, instead of eqns. (A1.6a,b,c),

$$\bar{\beta} - \alpha = m\psi,\ [2n+3+\zeta, 2n+2]\beta = (m+1)\psi\ , \qquad \text{(A1.9a)}$$

which shows that the relation of pressure exponent β to pumping rate exponent ψ changes very little in going from dominant accumulation (first option in parentheses) to dominant loss (second option). Indeed, the exponent α describing crack extension has also a very simple relation to these exponents

$$\begin{bmatrix} 2n+2+m\zeta+m \\ \\ 2n+2 \end{bmatrix} \frac{\beta}{m+1} = \alpha = \begin{bmatrix} 2n+2-m-m\zeta \\ \\ 2n+3+\zeta \end{bmatrix} \frac{\psi}{2n+3+\zeta}\ . \qquad \text{(A1.9b)}$$

Note that either constant pressure (β=0) or pumping rate (ψ=0) gives α = 0; this, of course, means a weaker growth in time, namely the power laws extracted in eqns. (A2.6). The self-similar solution with exponential $H(x,t)$ is then no longer possible but results in eqns. (14) retain an approximate characterisation value.

The overall solution is exactly the same as in (A1.4a), except that we need the following redefinitions,

$$U_F(X) = \int_0^X ds \left[\frac{\Gamma_3^0(\alpha s+\bar{\alpha}U_A^E)+H_0 U_B^E}{\Gamma_5^0 g^{\lambda-\theta}\hat{f}^{(1,0)}} \right]^m \qquad \text{(A1.10a)}$$

$$U_A^E = U_A^P\ \{\hat{f} \equiv g^{\theta} f^{\frac{(\zeta+1)}{2n+2}}\},\ \ \bar{\alpha} \equiv \alpha + \beta \qquad \text{(A1.10b)}$$

$$U_B^E \equiv \int_X^{1-\omega} ds\ k_L g(X)/[(-\ell n X)/\alpha]^{\gamma}\hat{f}^{(1,0)}\ . \qquad \text{(A1.10c)}$$

The expression for U_F^0 (replacing that in eqn. (A1.7c)) is now obtained from (A1.10a) by direct specialisation. Indeed, a solution like eqn. (A1.7a) is again entirely valid, with this new definition of U_F^0 and $\exp(\alpha m t)$ replacing $t^{\alpha m}$.

APPENDIX 2 ILLUSTRATIVE SOLUTION FOR P3DH MODEL

Although presentation of general realistic simulation, based on eqns. (15,16), must be postponed, it is worthwhile to show one simple example which illustrates the various manipulations that can be performed to extract interesting solutions of eqns. (16a,c) with variable height. For simplicity, this starts from the governing equation for Newtonian fluid flow and transforms it as follows

$$(g^4\hat{f}')'-d^2g^2\hat{f}=0=g^2[(g^2\hat{f})''-D^2(g^2\hat{f})] \qquad \text{(A2.1)}$$

where D is any constant coefficient, parameterising the class of solutions. This can be achieved if the height-variation function g (eqn. (16b)) itself satisfies the following differential equation

$$(g^2)'' - D^2g^2 = - d^2 \qquad \text{(A2.2)}$$

The solutions which satisfies the condition $H = H_0$ at $X = 1$ are then

$$g = \pm \frac{d}{D}\ [1-e^{\pm d(1-X)}] + e^{\pm D(1-X)}\ . \qquad \text{(A2.3)}$$

The complete solution for the pressure distribution now follows that in eqn. (16d), namely

$$g^2\hat{f} = \sum_{+-}\pm(\hat{\sigma}_F^{2n+2}-g_W^2 e^{\mp D}\hat{\sigma}_W^{2n+2})e^{\pm DX}/(e^D-D^D) \qquad \text{(A2.4)}$$

where the height at the wellbore is given by

$$H_W = g_W H_0,\ g_W = \pm\, d/D + (1\mp d/D)e^{\pm D}\ . \qquad \text{(A2.5)}$$

By suitable choice of the parameter D, we can obviously model a fairly general set of fracture shapes, especially reasonable amounts of vertical spreading at the wellbore, with the solutions just obtained. That these shapes (sketched on the left in figure 3) may correspond to those which would evolve naturally in at least some reservoirs, can be appreciated with reference to the forms rationalised in eqns. (A1.8b,c). The same steps, as those in eqns. (16f,g,17b,c), may now be followed to get estimates for injection rate Q_W and lateral fracture extension rates dL/dt; the latter may now quite reasonably be integrated on time to get the whole expression for $L(t)$, with any specified $\hat{\sigma}_W$ or Q_W.

TABLE 1

n $= m$	$\hat{\eta}_W/\gamma_4$ $[N\text{-}s^n/m^2]$	L $[m]$	Δ $[mm]$		t $[sec]$	
1.0	0.12	38	2.11	(2.0^N)	350	(330)
1.0	0.12	181	3.12	(2.6^N)	6150	(6000)
1.0	1.2	180	5.55	(5.1^N)	6500	(6000)
1.0	1.2	153	9.45	(8.8^N)	6350	(6000)
0.63	1.46	180	3.63	(3.6^{PK})	6530	(6500)
0.464	5.34	31	2.9	(2.8^{PK})	341	(350)
0.464	5.34	180	5.2	(5.1^{PK})	7400	(7000)
0.28	2.26	140	16.5	(16.0^{PK})	7971	(8000)

Sample calculations of crack widths Δ and required stimulation treatment time t, to achieve a fracture length L, for comparison with values cited in the literature[7] (as shown in parentheses and superscripted); computations are based on a PKN-type model (figure 5(a)) and other parameters are the same as those used in Ref. 7, namely fracture height $2H = 30.5m$ (=100 ft.), pumping rate 10 bbℓ/min. ($Q_W/2H = 4.37\ cm^2/sec$), loss coefficient $k_L = .059\ mm/\sqrt{sec}$. ($.0015\ ft/\sqrt{min}$), spurt loss $\Delta_{sp} = 0.41$ mm (.01 gal/ft²) and modulus $\bar{E} = 7796\ MN/m^2$ (viz. $G = 2.6 \times 10^6$ psi, $\nu = 0.15$).

TABLE 2

1.0	0.12	26.5	1.52	(1.5^{GD})	227	(300)
1.0	0.12	152.0	3.63	(3.4^G)	5303	(6000)
1.0	1.2	23.1	2.51	(2.5^D)	245	(300)
1.0	1.2	139.0	6.17	(6.0^G)	5567	(6000)
1.0	12.0	20.1	4.17	(4.0^D)	282	(300)
1.0	12.0	152.0	3.63	(3.4^G)	5118	(6000)
0.63	1.46	25.6	1.76	(1.8^D)	232	(300)
0.63	1.46	152.0	5.25	(5.0^G)	6009	(6000)
0.464	5.34	24.0	1.98	(1.9^{GD})	225	(300)
0.464	5.34	140.0	6.6	(6.3^G)	5799	(6000)
0.28	226.0	19.2	5.12	(4.5^{GD})	307	(300)
0.28	226.0	88.0	16.8	(17.0^D)	5394	(6000)

Illustrative calculations of crack widths Δ and required stimulation time t to achieve a fracture length L, based on CGDD-type models (figure 5(b)). Comparison is made with results cited in Ref. 7, and other required fluid, rock and fracture parameters are the same as those used in Table 1; a value of $\gamma_2 = 4\pi/14$ is used throughout, for reference and ease of modification.

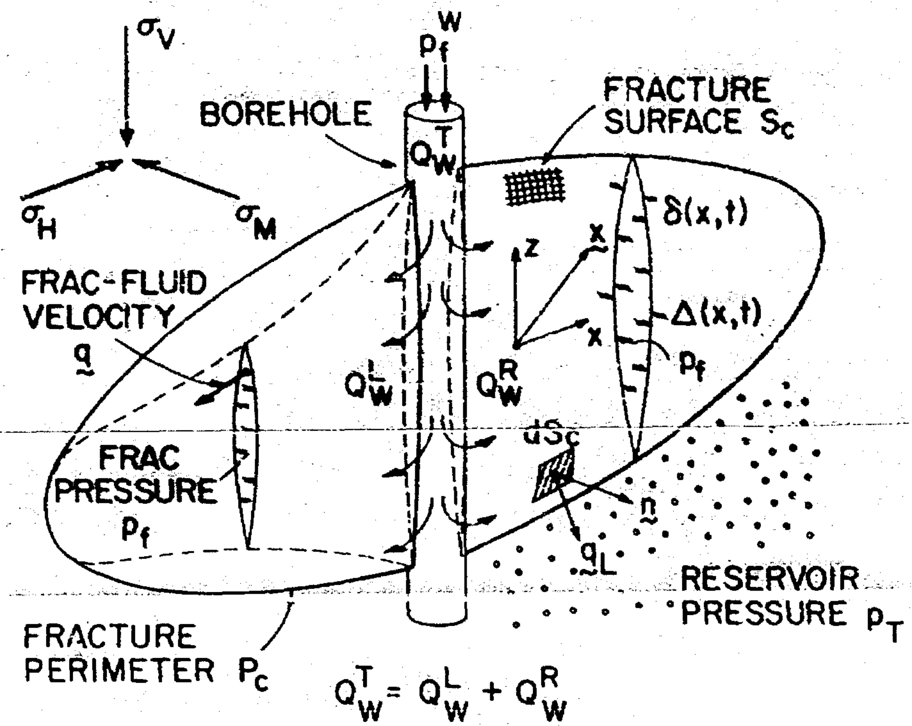

Fig. 1 - Schematic of geometry and variables in a typical hydraulic fracturing operation.

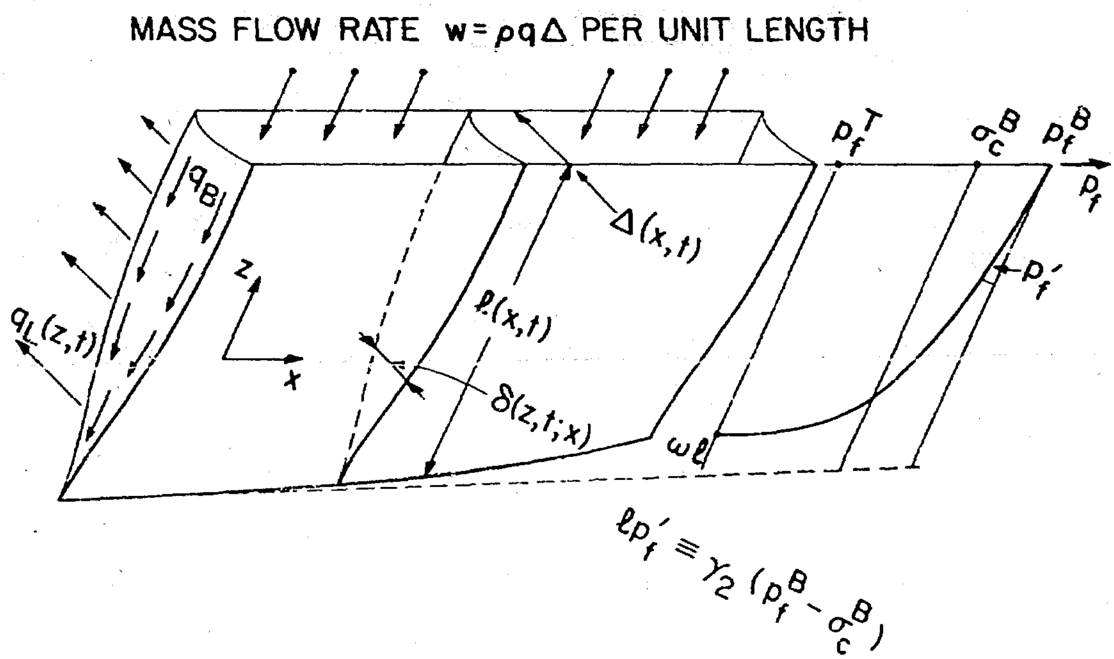

Fig. 2 - Isolation of geometry which can be described by CGDD-type hydraulic fracturing models: Vertical cross-section of fracture during predominantly lateral extension (see inset Fig. 4).

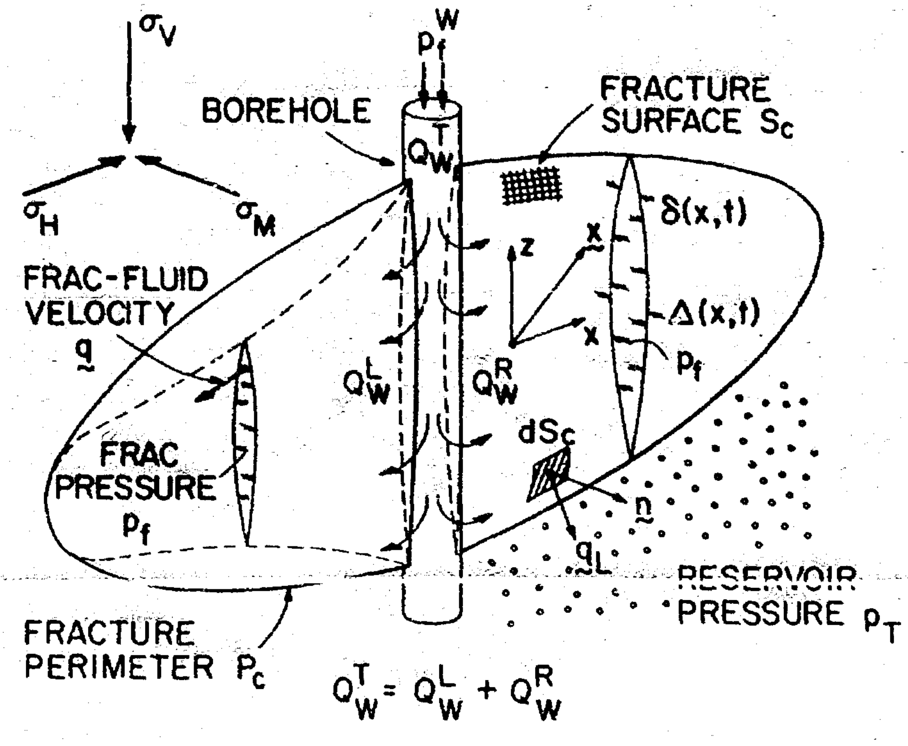

Fig. 1 - Schematic of geometry and variables in a typical hydraulic fracturing operation.

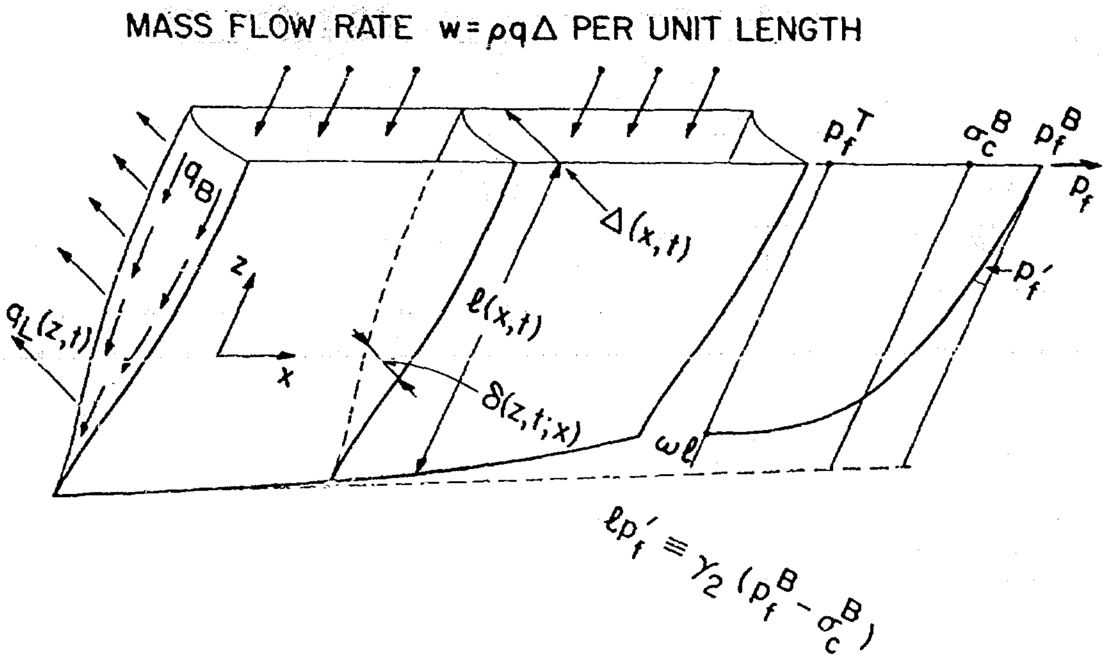

Fig. 2 - Isolation of geometry which can be described by CGDD-type hydraulic fracturing models: Vertical cross-section of fracture during predominantly lateral extension (see inset Fig. 4).

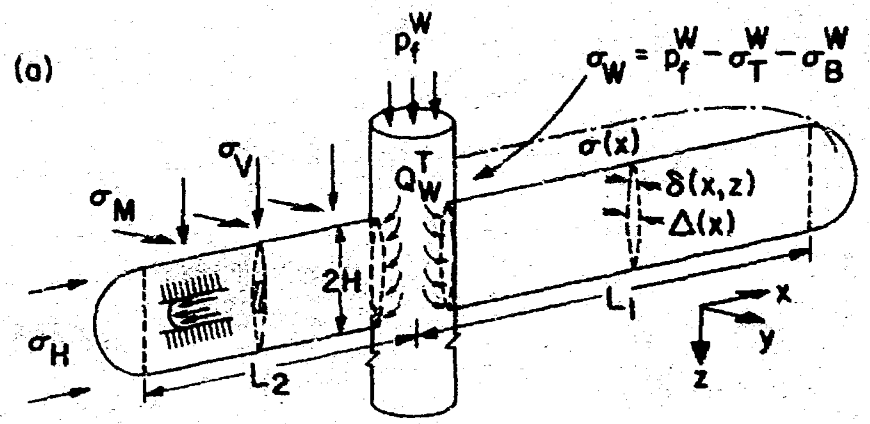

Fig. 5a- Schematic of conventional PKN geometry used in making sample calculations for field applications (Table 1).

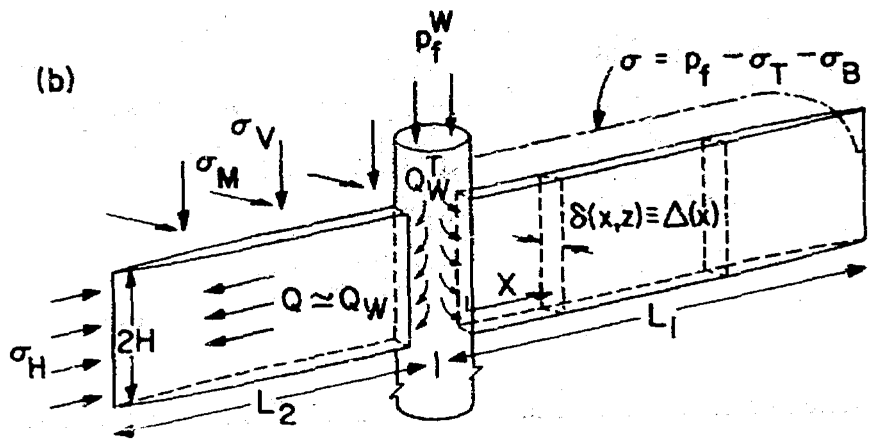

Fig. 5b- Demonstrates conventional implementation of CGDD model for computation of lateral extent in field operations (Table 2).

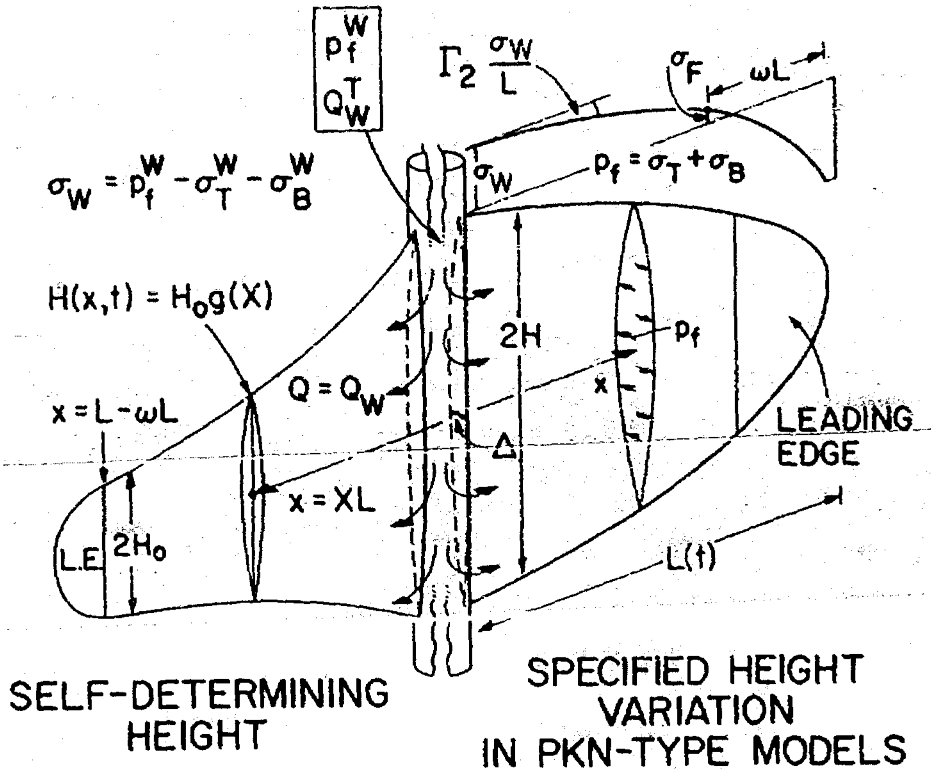

Fig. 3 - Schematic of fracture shapes which can be described by PKN-type models for for lateral extension, showing two distinct kinds of vertical height profiles.

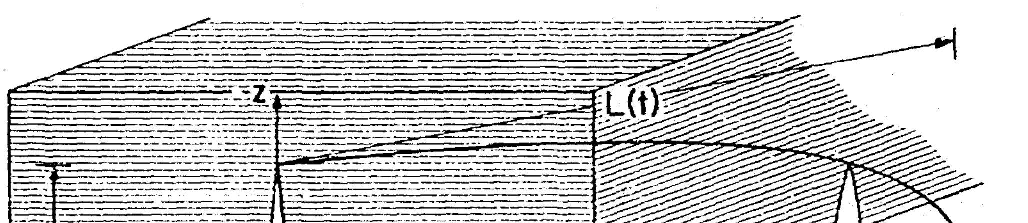

Fig. 4 - Illustration of concepts in pseudo-three-dimensional hydrofrac (P3DH) models.

Society of Petroleum Engineers of AIME
6200 N. Central Expwy.
Dallas, Tex. 75206

PAPER
NUMBER SPE 6094

The Effect of Poisson's Ratio on Rock Properties

By

J. Kumar, Member SPE-AIME, Associated Regulatory Consultants, Inc.

THIS PAPER IS SUBJECT TO CORRECTION

ABSTRACT

This paper presents various relationships between Poisson's ratio and other rock properties such as overburden pressure, bulk compressibility, Young's modulus, modulus of rigidity, compressive and tensile strength, porosity, density, wave velocities, modulus of resilience, modulus of rupture, fractures, drillability, and hardness. Thus, it points out the importance of Poisson's ratio in the understanding of some of the questions in rock mechanics.

INTRODUCTION

Though the change in Poisson's ratio for various types of rocks is small in general, sometimes this change can be significant. Assumption of a constant value of Poisson's ratio in some cases may result in serious errors. Unfortunately, the importance of Poisson's ratio in the understanding of other rock properties is not fully realized and very little work, both theoretical and practical, has been done on this subject. This paper presents various relationships between Poisson's ratio and other rock properties such as overburden pressure, bulk compressibility, Young's modulus, modulus of rigidity, compressive and tensile strength, porosity, density, wave velocities, modulus of resilience, modulus of rupture, fractures, drillability, and hardness. Thus, it points out the importance of Poisson's ratio in the understanding of some of the questions in rock mechanics.

References and illustrations at end of paper.

POISSON'S RATIO

When a force is applied to a body, at right angles to the force, a certain amount of lateral (transverse) expansion or contraction takes place. This phenomenon is shown in Fig. 1. In other words, it can be said that, if a solid body is subjected to an axial tension, it contracts laterally; on the other hand, if it is compressed, the material expands sidewise.

So the definition of Poisson's ratio can be stated as the ratio of transverse strain to axial strain induced by unconfined axial deformation. Poisson's ratio can be expressed as

$$\nu = \frac{\text{lateral strain}}{\text{axial strain}} = \frac{\epsilon_x}{\epsilon_z}, \quad \ldots\ldots (1)$$

where the strains are caused by uniaxial strain only.

Generally, values of Poisson's ratio vary between 0.25 and 0.35. In some extreme cases

Ex 2A

values can be as low as 0.1 for some concretes and 0.2 for some glasses. On the other hand, the values can be as high as 0.43 for lead and 0.25 for rubber. The highest possible value cannot be more than 0.5 due to theoretical reasons (Love[1]). Although negative values are not theoretically impossible, values less than zero have never been reported for isotropic materials. For rocks, generally the value is taken as 0.25 to 0.27.

EFFECT OF PRESSURE ON POISSON'S RATIO

Birch[2] has shown that under pressure Poisson's ratio increases, but not very strikingly. For example, if a substance having Poisson's ratio initially equal to 0.250 is subjected to a pressure sufficiently high to decrease compressibility by 10 percent and rigidity by 8 percent, Poisson's ratio changes by less than 2 percent, namely, to 0.254.

The change of Poisson's ratio with pressure is shown in Fig. 2. In this figure the total increase in Poisson's ratio caused by pressure is only about 10 to 15 percent.[3]

Adams and Williamson[4] have noticed that, at depths greater than about 50 km, ν is very nearly constant and is equal to 0.27. At relatively shallow depths ν is very significantly less than 0.27. At this point, the role of Poisson's ratio in seismic calculations may be important. A small error in the assumed value of ν will have a considerable effect upon the value of wave velocity calculated from compressibility measurements alone; e.g., changing ν from 0.27 to 0.26 will increase V_p by 1 percent and V_s by 2.5 percent, the compressibility remaining the same.

Somerton et al.[5] have also reported that Poisson's ratio increases with increased uniaxial stress. Cleary[6] has reported that there is evidently a relation between Poisson's ratio and the mean effective stress.

Table 1 shows the mean values obtained when the mean effective stress was less than 2,000 lb/sq in. and the mean values under stress conditions greater than 2,000 lb/sq in. With one exception, the mean values are greater for conditions of greater mean effective stress.

EFFECT OF POISSON'S RATIO ON ROCK PROPERTIES

Very little work has been done on this subject and not very much appears in the literature regarding the role of Poisson's ratio, as the number of authors have taken the value of ν nearly constant. Now we shall try to see how Poisson's ratio can affect the various rock properties.

1. Bulk Compressibility - We know the following relation.

$$1/\beta = K = \frac{2(1+\nu)G}{3(1-2\nu)} = \frac{E}{3(1-2\nu)} \quad \ldots\ldots (2)$$

From these relations we can see that bulk modulus increases with Poisson's ratio; i.e., with the increase in Poisson's ratio, the bulk compressibility decreases.

2. Young's Modulus - The following relation exists between Young's modulus, E, and Poisson's ratio.

$$E = 3K(1-2\nu) \quad \ldots\ldots (3)$$

From this relation we see that with K as constant, E increases with decreasing Poisson's ratio.

The work done by D'Andrea et al.[7] has also confirmed this (see Fig. 3). They also found a simple correlation coefficient by linear analysis between Young's modulus and Poisson's ratio to be -0.487. The results of the work of Wilhelmi and Somerton[8] also verified this. The results are given in Table 2.

Using the data presented by Wuerker[9] in Tables 3 and 4, the author determined the correlation between Poisson's ratio and Young's modulus from dynamic tests as

$$E_{(dynamic)} = \frac{\nu}{0.012 + 0.06\nu} \quad \ldots\ldots (4)$$

The correlation coefficient of the above equation was determined to be -0.355. This equation also confirms the above findings of D'Andrea et al.[7] The relation between Poisson's ratio and Young's modulus under static tests was determined to be

$$E_{(static)} = \frac{1}{0.74 - 2.37\nu} \quad \ldots\ldots (5)$$

This relation suggests that E increases with Poisson's ratio.

3. Modulus of Rigidity - The relation between rigidity G and Poisson's ratio is

$$G = \frac{E}{2(1+\nu)} \quad \ldots\ldots (6)$$

This relation suggests that, with decreasing Poisson's ratio, rigidity increases when Young's modulus is constant. This was confirmed by the results of the work of Wilhelmi and Somerton.[8] The results are given in Table 5. The works of D'Andrea et al.[7] have also confirmed this (see Fig. 4). The correlation coefficient found by them between rigidity and Poisson's ratio was -0.465.

Using the data of Table 3, the relation between G and ν was found by the author to be

$$G = \frac{\nu}{0.02 + 0.2\nu} \quad . \quad . \quad . \quad . \quad . \quad . \quad . \quad . \quad . \quad (7)$$

The coefficient of correlation of the above equation was -0.173.

4. Compressive Strength - D'Andrea et al.[7] have plotted compressive strength as a function of Poisson's ratio. Though no definite relation seems to exist, it can be said that compressive strength decreases with the increase in Poisson's ratio. The correlation coefficient found was -0.451 (see Fig. 5). The following relation was found by the author using the data of Table 4.

$$\sigma_c = 1598 + 55360\nu \quad . \quad . \quad . \quad . \quad . \quad . \quad . \quad . \quad . \quad (8)$$

with a correlation coefficient of 0.241. The above equation suggests that the compressive strength increases with the increasing Poisson's ratio.

5. Tensile Strength - D'Andrea et al. have plotted Poisson's ratio vs tensile strength. See Fig. 6. No definite correlation can be found from the figure, but by linear analysis, they have found the correlation coefficient to be - 0.491. This negative coefficient suggests that tensile strength decreases with the increasing Poisson's ratio.

6. Porosity - Wylie et al.[3] have shown in a plot (see Fig. 7) that porosity increases with Poisson's ratio. The total change plotted is rather small, from about 0.19 at zero porosity to about 0.27 at a porosity of 35 percent. In other words, we can say that, with a small change in Poisson's ratio, there is a big change in porosity.

Walsh[10] has given a formula for the change of porosity in terms of Poisson's ratio, Young's modulus, and original porosity.

$$\frac{d\phi}{dp} = \frac{-9(1 - \nu)}{2E} \times \frac{\phi}{(1 - \phi)} \quad . \quad . \quad . \quad . \quad (9)$$

Using the data of Table 9, the following relation between porosity and Poisson's ratio was found with a correlation coefficient of 0.15.

$$\phi = 2.9 + \frac{0.61}{\nu} \quad . \quad . \quad . \quad . \quad . \quad . \quad . \quad . \quad . \quad (10)$$

7. Density - D'Andrea et al. have plotted Poisson's ratio vs specific gravity. See Fig. 8. The density seems to decrease with the increase in Poisson's ratio. The correlation coefficient found between these parameters was -0.361. Gutenberg[11] has given a table showing the values of Poisson's ratio and density (see Table 6). Using the data of Table 6, the author found the following relationship between density and Poisson's ratio.

$$\rho = 1/(0.47 - 0.585\nu) \quad . \quad . \quad . \quad . \quad . \quad . \quad (11)$$

The following relation between density and Poisson's ratio was determined using the data of Table 4.

$$\rho = 2.25 + 1.56\nu \quad . \quad . \quad . \quad . \quad . \quad . \quad . \quad . \quad (12)$$

8. Wave Velocities - The velocity V_p of longitudinal waves and the velocity V_s of transverse waves transmitted through a material are related to the density and elastic constants of the material according to the following equations:

$$V_p = \sqrt{\frac{3(1 - \nu)}{(1 + \nu)\beta\rho}} \quad . \quad . \quad . \quad . \quad . \quad . \quad . \quad . \quad . \quad (13)$$

$$V_s = \sqrt{\frac{3(1 - 2\nu)}{2(1 + \nu)\beta\rho}} \quad . \quad . \quad . \quad . \quad . \quad . \quad . \quad . \quad . \quad (14)$$

These relations suggest that both the velocities should decrease with the increase in Poisson's ratio.

Birch and Bancroft[12] have given the values of Poisson's ratio and waves velocities that are tabulated in Table 7. Using the data of Table 7, the author found the following relations:

$$V_s = \frac{1}{0.226 + 0.148\nu} \quad . \quad . \quad . \quad . \quad . \quad . \quad . \quad . \quad (15)$$

$$V_p = 7.35 - 0.139/\nu \quad . \quad . \quad . \quad . \quad . \quad . \quad . \quad (16)$$

Using the data of Table 3, the following relation was found with a correlation coefficient of 0.32.

$$V_p = 18.05 - 0.505/\nu \quad . \quad . \quad . \quad . \quad . \quad (17)$$

The above equations suggest that the velocity of longitudinal waves, V_p, increases, whereas the velocity of transverse waves V_s decreases with the increase in Poisson's ratio.

When dealing with wave velocities and elastic constants, Gutenberg[11] suggests using the following relation between longitudinal and transverse wave velocities.

$$\frac{V_s}{V_p} = \frac{1 - 2\nu}{2(1 - \nu)} \quad . \quad . \quad . \quad . \quad . \quad . \quad . \quad . \quad . \quad . \quad (18)$$

The values of this ratio between V_s and V_p are given as a function of Poisson's ratio and are given in Table 8. From Table 8, we can observe that the ratio between the two velocities decreases with the increase in Poisson's ratio.

Using the data of Table 8, it was found by the author that

$$\frac{V_s}{V_p} = 0.739 - 0.653\nu \quad \ldots\ldots \quad (19)$$

The above relation has a correlation coefficient of -0.99.

Dobrynin[13] has plotted the calculated values of longitudinal waves vs pressure. See Fig. 9. The solid lines on the figure show the plot when ν is constant. If the Poisson ratio changes, e.g., from 0.15 to 0.20, the effect on the calculated values of V_p would be as shown by the dashed curves. These curves also indicate that, with the increase in Poisson's ratio, the velocity of the waves decreases.

D'Andrea et al.[7] have also plotted Poisson's ratio vs shear velocity and vs longitudinal velocity. See Figs. 10 and 11. From these figures also, it can be noticed that velocities decrease with the increase in Poisson's ratio. They also found the correlation coefficient between longitudinal velocity and Poisson's ratio equal to -0.462 and between shear velocity and Poisson's ratio equal to -0.568.

9. Modulus of Resilience - The modulus of resilience is defined as the amount of energy absorbed by, or work done on, a unit volume of material in being stressed to the proportional limit.

Using the data of Table 3, the author determined the following relation between the modulus of resilience and Poisson's ratio.

$$M_r = \frac{1}{0.0185 + 0.022\nu} \quad \ldots\ldots \quad (20)$$

10. Quartz Content of the Rocks - As pointed out by Birch and Bancroft,[12] Voigt's measurements on the elasticity of quartz indicate that Poisson's ratio should be 0.07 for pure quartz aggregate. The average value of ν for granite is 0.23. This lower value for granite is undoubtedly connected with the content of quartz in these rocks. Incidentally, it may be noted that the influence on V_s of the low Poisson's ratio for quartz is so great that, despite the relatively low compressibility of quartz, V_s in rocks increases sharply with an increase in quartz content.

The value of Poisson's ratio and quartz content are given in Table 9 for various rocks. From Table 9, we can notice that, with the decrease in Poisson's ratio, the quartz content increases.

11. Cracks in Rocks - Generally, due to the presence of cracks in the rocks, their strengths are much lower than the theoretical strengths. Griffith's theory[14,15] of crack formation assumes a large number of cracks in the material, rupture being primarily conditioned by the extension of an already existing crack and not by the formation of a new one.

Now we shall see how Poisson's ratio figures in Griffith's theory. For mathematical reasons, Griffith has confined his theoretical treatment of the problem in two dimensions. Considering the crack as an ellipse of vanishing minor axis (see Fig. 12) and assuming the validity of Hook's law to the corners of the crack, he finds that rupture will occur when the stress normal to crack reaches the critical value given by the following equation.

$$\sigma_{crit} = \sqrt{\frac{2E}{C(1-\nu^2)}} \quad \ldots\ldots \quad (21)$$

We can see that σ_{crit} will increase with the increasing Poisson's ratio if other terms are constant. In other words, we can say that rocks with many cracks would have a low Poisson's ratio; whereas, those with few cracks would have correspondingly higher values.

Sack[16] extended Griffith's theory to three dimensions. He considers the number of plane circular cracks oriented in a manner such that the principal stress acts normally to the plane of one of these cracks. This normal principal stress must be tensile; otherwise, the faces of the crack will be pressed together and can exert traction on each other.

He calculated the total free energy contribution due to a crack and it is given by the following equation.

$$W_{total} = 2\Pi\gamma c^2 - \frac{8(1-\nu^2)\,\sigma^2 c^3}{E} \quad \ldots \quad (22)$$

This relation suggests that total free energy increases with Poisson's ratio.

Sack[16] has also given a relation for the minimum pressure necessary to extend a fracture in rock.

$$(P_m - \sigma) = \frac{E}{2(1-\nu^2)r} \quad \ldots\ldots \quad (23)$$

This equation predicts that minimum fracture extension pressure increases with the increase in Poisson's ratio.

Sneddon[17] has shown that the volume of a radially symmetrical crack with a uniform pressure P acting in the crack is given by the equation

$$V = \frac{16(1-\nu^2)c^3\ (P-\sigma)}{3E} \quad \ldots\ldots \quad (24)$$

The volume of crack will decrease with the increase in Poisson's ratio if other parameters remain constant.

The equation for the width of a penny-shaped crack is given by Sneddon.[17]

$$W_m = \frac{8(P-\sigma)(1-\nu^2)c}{\Pi E} \quad \ldots\ldots\ldots (25)$$

The width of the crack also decreases with the increasing Poisson's ratio.

Walsh[10] has given the relations for calculating the effective compressibility of cracks in various cases.

Penny-shaped crack (Snack)[16]:

$$\beta_{eff} = (1 + 16/9 \times \frac{(1-\nu^2)}{(1-2\nu)} \frac{\bar{c}^3}{\bar{v}}) \quad \ldots (26)$$

Elliptical crack in plane strain (Griffith)[14]:

$$\beta_{eff} = \beta(1 + \Pi/3 \times \frac{(1-\nu^2)}{(1-2\nu)} \frac{\bar{c}^3}{\bar{v}}) \quad \ldots (27)$$

Elliptical crack in plane stress (Griffith)[14]:

$$\beta_{eff} = \beta(1 + \frac{4\Pi}{3(1-2\nu)} \frac{\bar{c}^3}{\bar{v}}) \quad \ldots\ldots (28)$$

In these three cases, β_{eff} increases with Poisson's ratio. He has also given a relation for the pressure required to close the penny-shaped cracks.

$$P_c = \frac{\Pi E \alpha}{4(1-\nu^2)} \quad \ldots\ldots\ldots (29)$$

This equation suggests that the pressure required to close the crack increases with Poisson's ratio.

12. Modulus of Rupture - The quantity obtained in the bending test is commonly used in the discussion of the behavior of rock in flexure. Using the data of Table 3, the author found the following relation between the modulus of rupture and Poisson's ratio with a correlation coefficient of 0.77.

$$M.R. = \frac{\nu}{0.11 - 0.38\nu} \quad \ldots\ldots\ldots (30)$$

The above equation suggests that the modulus of rupture increases with Poisson's ratio.

13. Rock Drillability - Gstalder and Raynal[18] performed the experiments to determine the relationship of rock drillability and mechanical properties of rocks. They measured Young's modulus by "punch-test," in which they used punches of various sizes and shapes. For calculating Young's modulus from this test, they used the following equation.

$$E = \frac{(1-\nu^2)\,F_e}{Dh_e} \quad \ldots\ldots\ldots (31)$$

Fig. 13 shows the attempt to correlate hardness of the rocks to Young's modulus. From this figure it is obvious that the greater is Young's modulus, the greater is the hardness of rock; i.e., hardness of rocks increases with the decrease in Poisson's ratio.

The correlation between Young's modulus and the drilling rate is shown in Fig. 14, a. and b. We can conclude from these figures that increase in Poisson's ratio (decrease in Young's modulus) results in the increased drillability of rocks.

Moh's hardness, abrasion hardness and impact toughness are some of the other rock properties that are helpful in ascertaining the ~~drillability of rocks.~~ Using the data of Table 3, the following relationships were determined by the author.

Moh's hardness and Poisson's ratio:

$$H_m = \frac{\nu}{0.028 + 0.182\nu} \quad \ldots\ldots\ldots (32)$$

Abrasion hardness and Poisson's ratio:

$$H_a = \frac{1}{0.082 - 0.104\nu} \quad \ldots\ldots\ldots (33)$$

Impact toughness and Poisson's ratio:

$$I_t = 3.37 + 40.6\nu \quad \ldots\ldots\ldots (34)$$

CONCLUSIONS

Though the change in Poisson's ratio for various rocks is small in general, sometimes this change can be significant. Then this change in the value of Poisson's ratio may alter other properties of rocks significantly. The proper understanding of this property of rocks may lead to the solution of various questions in rock mechanics. Its understanding may be helpful in determining rock drillability, behavior of rocks under stress and fractures, log analysis, and a general understanding of other aspects of rock mechanics.

NOMENCLATURE

ν = Poisson's ratio
β = bulk compressibility
K = bulk modulus
E = Young's modulus
G = modulus of rigidity
ϕ = porosity
P,p = pressure
V_p = longitudinal velocity
V_s = shear velocity
ρ = density
σ = stress
σ_{crit} = critical stress
γ = surface energy
W_{total} = total free energy due to crack
P_m = minimum fracture extension pressure, psi
W_m = width of crack
α = ratio of minor to major axis of crack
M_r = modulus of resilience
H_m = Moh's hardness

H_a = abrasion hardness
I_t = impact toughness
C = length of crack, if located on the surface, or half this value if located in the interior
$\bar{c}$ = average crack length
$\bar{v}$ = average region volume of crack
r = fracture radius
Fe = load at elastic limit, kg
he = displacement of punch at elastic limit, mm
D = diameter of punch, mm

ACKNOWLEDGMENTS

The author wishes to express his gratitude to W. H. Somerton of the U. of California, Berkeley for his data as well as for his valuable guidance and suggestions. The author is also thankful to his secretary, Constance Hayes, for her patience in typing the manuscript.

REFERENCES

1. Love, A. E. R.: A Treatise on the Mathematical Theory of Elasticity, Fourth Ed., Dover Publications.
2. Birch, F.: "The Effect of Pressure Upon the Elastic Properties of Isotropic Solids, According to Murnaghan's Theory of Finite Strain," J. Appl. Phys. (1938) 9, 279.
3. Wyllie, M. R. J., Gardner, G. H. F., and Gregory, A. R.: "Studies of Elastic Wave Attenuation in Porous Media," Geophysics (Oct. 1962) 27, No. 5, 569.
4. Adams, L. H. and Williamson, E. D.: "The Compressibility of Minerals and Rocks at High Pressures," J. Franklin Inst. (1923) 195, 475.
5. Somerton, W. H., Timur, A., and Gray, D. H.: "Stress Behavior of Rock Under Drilling Loading Conditions," paper SPE 166, Oct. 1961.
6. Cleary, J. M.: Hydraulic Fracture Theory - Part III, Elastic Properties of Sandstone, Div. of the Illinois State Geological Survey.
7. D'Andrea, D. V., Fischer, R. L., and Fogelson, D. E.: "Prediction of Compressive Strength from Other Rock Properties," RI 6702, USBM, Washington (1965).
8. Wilhelmi, B. and Somerton, W. H.: "Simultaneous Measurement of Pore and Elastic Properties of Rocks Under Triaxial Stress Conditions," paper SPE 1706.
9. Wuerker, R. G.: Annotated Tables of Strength and Elastic Properties of Rocks, AIME (Dec. 1956).
10. Walsh, J. B.: "The Effect of Cracks on the Compressibility of Rock," J. of Geophys. Res. (Jan. 15, 1965) 70, No. 2, 381.
11. Gutenberg, B.: Internal Constitution of the Earth, Second Ed., Dover Publications.
12. Birch, F. and Bancroft, D.: "The Effect of Pressure on the Rigidity of Rocks, I," J. of Geology (1938) 46, 59; II, Ibid (1938) 46, 113.
13. Dobrynin, V. M.: "Effect of Overburden Pressure on Some Properties of Sandstone," Trans., AIME (1962) 225, 360.
14. Griffith, A. A.: "The Phenomena of Rupture and Flow in Solids," Phil. Trans., Roy. Soc., London (1921) Series A, 221, 198, 163.
15. Griffith, A. A.: "The Theory of Rupture," Proc., Int. Cong. Appl. Mech., Delft (1924) 55.
16. Sack, R. A.: "Extension of Griffith's Theory to Three-Dimensions," Proc., Phys. Soc., London (1946) 58, 729-736.
17. Sneddon, I. N.: "The Distribution of Stress in the Neighborhood of a Crack in Elastic Solid," Proc., Roy Soc. (1946) A, 187, 229.
18. Gstalder, S. and Raynal, J.: "Measurement of Some Mechanical Properties of Rocks and Their Relationship to Rock Drillability," J. Pet. Tech. (Aug. 1966) 991.

TABLE 1: EXPERIMENTAL VALUES OF POISSON'S RATIO

Sample	Mean value for 2,000 psi	Mean value for 2,000 psi	Mean of all experimental values
1	.15	.218	.185
3	.071	.145	.108
4	.045	.109	.077
5	.147	.168	.157
6	.124	.112	.118

TABLE 2: EXPERIMENTAL VALUES FOR BEREA SANDSTONE

Poisson's ratio	Young's Modulus
0.47	3.7×10^6 psi
0.28	3.9×10^6 psi
0.26	4.1×10^6 psi

TABLE 3: TYPES AND PROPERTIES OF ROCKS

Rock Type	Poisson's Ratio	Dynamic Modulus of Elasticity 10^6 psi	Modulus of Rigidity Shear 10^6 psi	Longitudinal Bar Velocity 10^3 ft/sec	Modulus of Rupture 10^3 x psi	Impact Toughness in/in^2	Abrasive Hardness	Modulus of Resilience in-lb/in^3	Moh's Hardness
Amphibolite	0.14	15.1	6.64	19.0	7.4	16.0	40.0	124.5	6.21
Amphibolite	0.325	6.74	2.54	12.9	4.0	33.0	-	117.0	5.47
Diabase	0.281	13.9	5.41	18.7	8.0	24.0	37.0	78.1	6.21
Basalt	0.26	12.4	4.91	17.6	6.6	7.9	29.0	60.9	5.32
Diorite	0.26	11.6	4.61	17.80	-	9.7	23.0	70.6	5.74
Diorite, Gneiss	0.27	15.0	5.9	18.2	—	5.2	16.0	33.6	6.37
Diorite, Gneiss	0.24	9.74	3.93	15.7	-	3.9	17.9	27.8	5.8
Graywack, Coarse grain	0.06	3.8	1.9	20.0	-	-	—	18.4	-
Graywack, Medium grain	0.29	3.6	1.4	20.0	-	-	—	19.3	-
Limestone	0.20	9.43	4.93	15.9	2.2	2.5	9.3	41.7	4.11
Limestone	0.21	9.56	3.96	16.4	1.9	2.5	9.6	27.7	4.58
Limestone	0.17	9.53	4.07	15.6	2.4	7.4	15.0	64.0	-
Marlstone	0.45	2.87	1.0	9.9	3.6	4.6	13.0	18.8	3.84
Quartzite	0.10	12.3	5.6	3.0	3.4	4.6	39.0	39.5	5.75
Sandstone	0.04	2.1	1.02	8.4	0.42	-	-	31.4	-
Shale	0.09	8.44	3.86	14.9	2.5	6.0	7.0	58.0	4.42
Shale	0.17	9.53	4.07	15.6	2.4	7.4	15.0	64.0	4.74
Tactite	0.11	8.9	4.02	15.1	2.7	4.8	12.0	87.2	4.79
Basalt	0.15	8.92	3.89	15.2	3.8	13.0	15.0	60.0	5.0
Basalt	0.09	5.9	2.68	2.68	2.1	9.0	9.2	58.0	3.95
Amphibolite	0.395	3.3	4.77	18.1	5.0	34.0	39.0	88.4	-
Basalt	0.15	8.92	3.89	15.2	3.8	13.0	15.0	62.8	-
Basalt, Altered	0.09	5.9	2.68	12.7	4.1	8.8	25.0	141.0	-
Diorite	0.165	12.6	5.4	17.6	2.9	20.0	18.0	62.7	5.2

TABLE 4: TYPES AND PROPERTIES OF ROCKS

Rock Type	Poisson's Ratio	Density	Porosity Percent	Strength, psi	Static Modulus of Elasticity 10^6 psi
Andensite Hypensthine	0.16	2.57	4.8	19,150	5.6
Basalt	0.22	2.72	4.5	24,450	6.7
Diorite	0.15	2.50	2.7	12,670	4.2
Diorite	0.11	2.86	4.9	10,000	10.3
Granite	0.12	2.63	1.00	10,460	3.9
Granite	0.20	2.61	2.36	9,400	1.6
Graywack, Coarse grain	0.07	2.46	10.3	7,900	1.8
Graywack, Coarse grain	0.12	2.49	9.7	4,400	1.5
Graywack, Fine grain	0.12	2.41	13.0	7,200	1.5
Graywack, Medium grain	0.09	2.44	11.5	7,080	1.9
Graywack, Medium grain	0.08	2.49	9.7	7,350	1.5
Monzonite	0.18	2.57	2.32	11,140	6.2
Phyllite	0.06	2.18	22.4	1,360	1.3
Sandstone	0.17	2.28	16.4	8,810	3.2
Schist	0.08	2.68	1.44	7,750	6.0
Schist	0.20	2.75	0.52	17,000	9.9
Schist	0.12	2.47	11.4	2,180	1.3
Shale	0.07	2.69	6.6	17,770	2.0
Siltstone	0.12	2.50	10.3	3,500	1.9
Tuff	0.11	1.45	12.17	530	0.20
Limestone, Fine grain	0.25	2.71	3.4	11,660	9.9
Limestone, Medium grain	0.23	2.68	4.7	18,480	5.2
Limestone, Porous	0.22	2.44	13.9	19,320	3.0
Limestone	0.22	2.60	5.4	15,580	8.8
Limestone	0.16	2.25	16.0	4,960	5.4
Limestone	0.13	1.82	1.82	860	1.2
Limestone	0.23	2.73	4.7	3,080	3.0

TABLE 5: EXPERIMENTAL RESULTS FOR BANDERA SANDSTONE

Poisson's ratio	Modulus of Rigidity
0.36	0.70×10^6 psi
0.29	0.71×10^6 psi
0.25	0.73×10^6 psi
0.22	0.85×10^6 psi
For Berea Sandstone	
0.47	1.29×10^6 psi
0.28	1.50×10^6 psi
0.26	1.69×10^6 psi

TABLE 6: EXPERIMENTAL VALUES OF POISSON'S RATIO & DENSITY

Rock Type	Poisson's Ratio	Density
Syenite	0.26	2.61
Granite L	0.24	2.64
Granite H	0.22	2.65
Granodiorite	0.24	2.71
Quartz diorite	0.25	2.73
Diorite	0.26	2.76
Gabbro	0.27	3.04
Olivine Gabbro	0.27	3.21
Peridotite	0.27	3.35
Dunite B	0.27	3.29
Dunite H	0.27	3.40
Pallasite	0.27	5.65
Siderite	0.28	7.9
Amphibolite	0.26	3.08
Anorthorite	0.27	2.72
Orthopyroxenite	0.24	3.42
Quartzite	0.10	2.65
Marble	0.29	2.71

TABLE 7: POISSON'S RATIO & WAVE VELOCITIES FOR VARIOUS ROCKS AT 4000 BARS AND 30° C

Rock type	Poisson's ratio	V_p km/sec	V_s km/sec
Quartzitic S.St.	0.118	6.08	4.00
Solenhofen L.St.	0.276	5.54	3.08
Vermont marble	0.229	6.51	3.49
Granite			
Quincy 1	0.229	6.08	3.61
Rockport	0.243	6.24	3.59
Syenite, Ontario	0.274	6.04	3.36
North, Sudbury 2	0.268	6.49	3.65
Diabase			
Vinal Haven	0.277	6.97	3.88
Maryland	0.281	6.96	3.83
Gabbro			
Mellen	0.302	6.96	3.71
French Creek	0.270	7.15	3.98
Pyroxenite			
Hypersthenite	0.230	7.83	4.58
Bronzitite	0.249	7.86	4.55
Dunite	0.262	8.05	4.57

TABLE 8: EXPERIMENTAL VALUES OF POISSON'S RATIO AND V_s/V_p RATIO

Poisson's ratio	V_s/V_p
0.10	0.667
0.11	0.662
.12	.657
.13	.652
.14	.647
.15	.642
.16	.636
.17	.630
.18	.625
.19	.619
.20	.612
.21	.606
.22	.599
.23	.592
.24	.585
.25	.577
.26	.569
.27	.561
.28	.553
.29	.544
.30	.535

TABLE 9: EXPERIMENTAL VALUES OF POISSON'S RATIO AND QUARTZ CONTENT

Rock type	Poisson's ratio	Quartz content
Syenite	0.26	5%
Granite L	0.24	20%
Granite H	0.22	35%
Grandiorite	0.24	25%
Diorite	0.26	15%

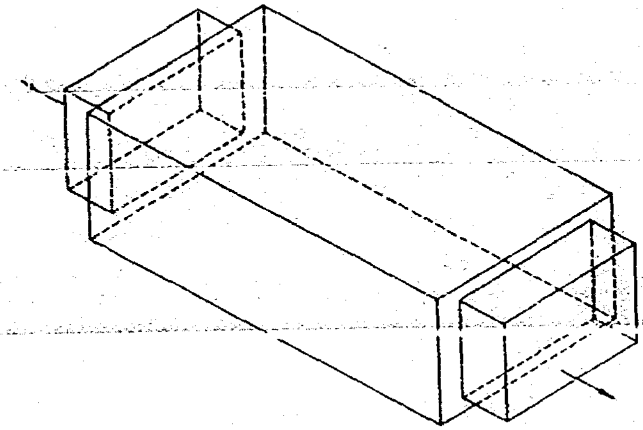

Fig. 1 - Presentation of Poisson's ratio.

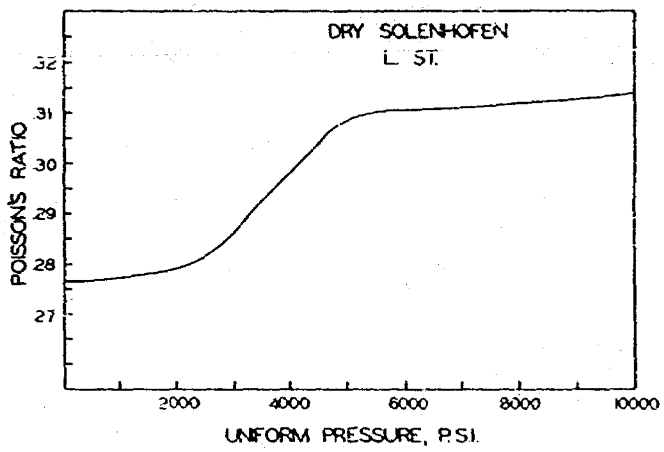

Fig. 2 - Change of Poisson's ratio with pressure.

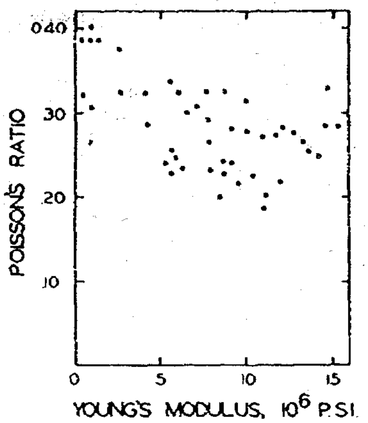

Fig. 3 - Poisson's ratio vs Young's modulus.

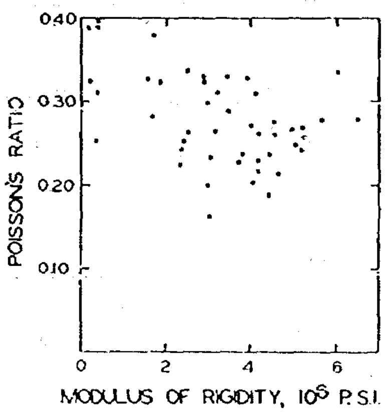

Fig. 4 - Poisson's ratio vs modulus of rigidity.

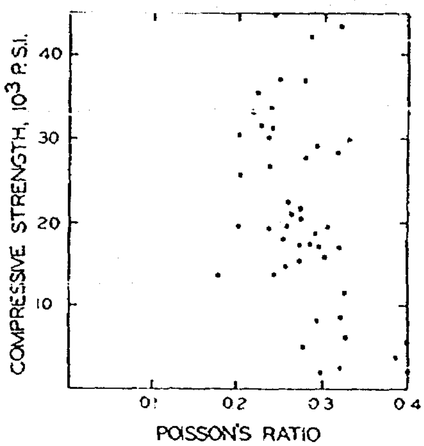

Fig. 5 - Compressive strength vs Poisson's ratio.

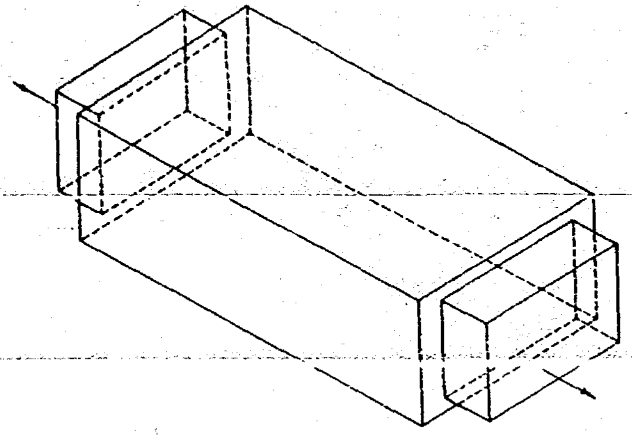

Fig. 1 - Presentation of Poisson's ratio.

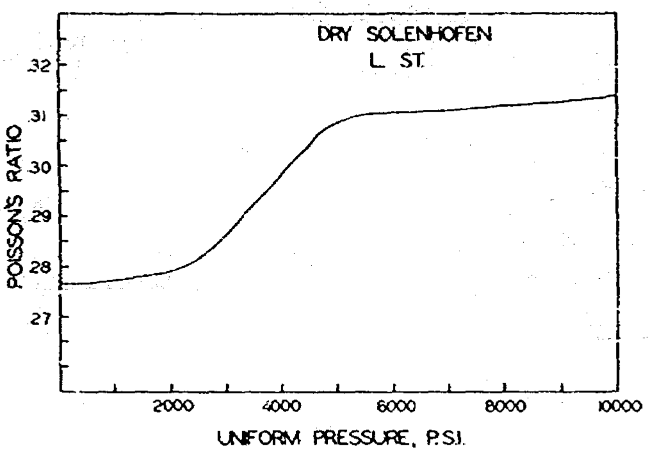

Fig. 2 - Change of Poisson's ratio with pressure.

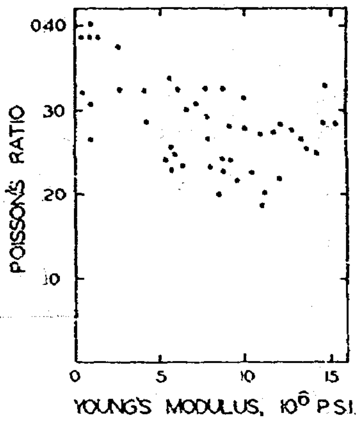

Fig. 3 - Poisson's ratio vs Young's modulus.

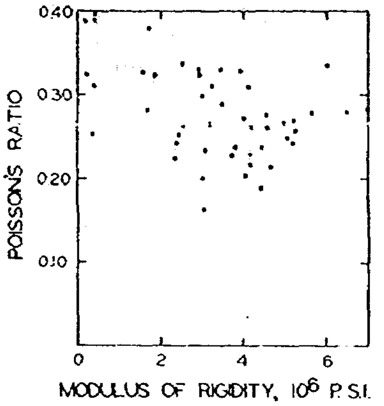

Fig. 4 - Poisson's ratio vs modulus of rigidity.

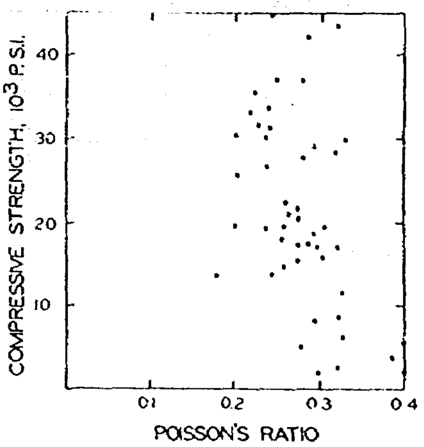

Fig. 5 - Compressive strength vs Poisson's ratio.

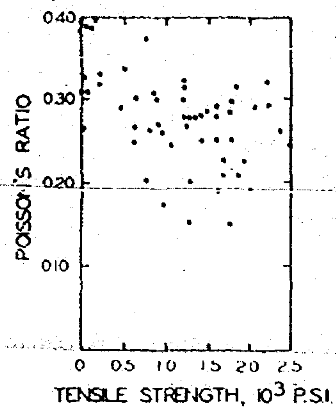

Fig. 6 - Poisson's ratio vs tensile strength.

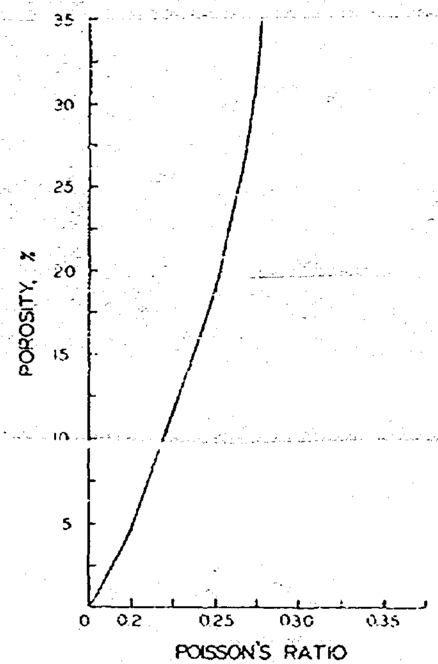

Fig. 7 - Porosity vs Poisson's ratio.

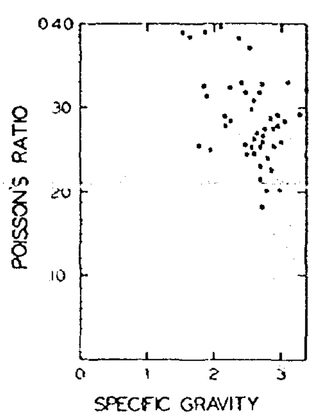

Fig. 8 - Poisson's ratio vs specific gravity.

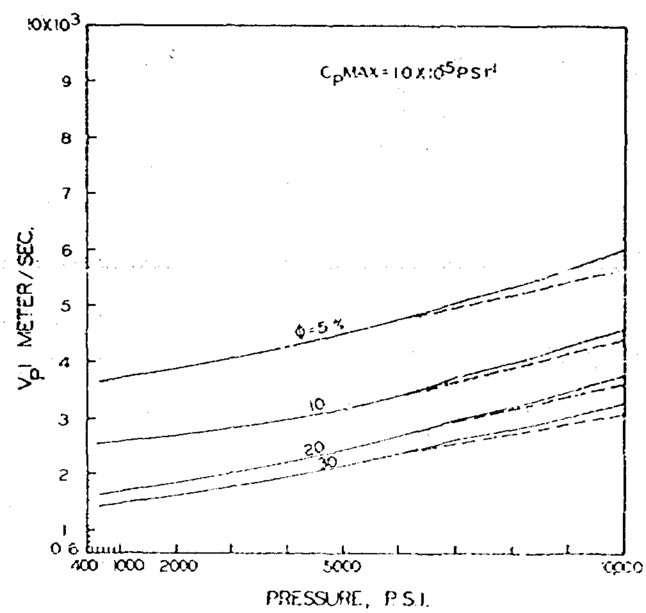

Fig. 9 - Longitudinal wave velocity vs pressure.

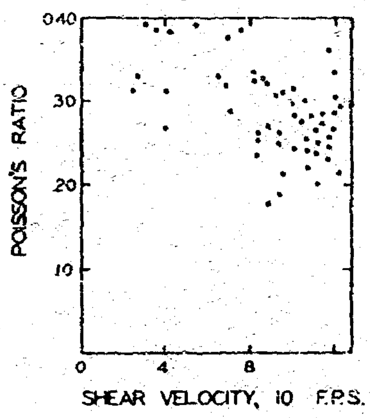

Fig. 10 - Poisson's ratio vs shear velocity.

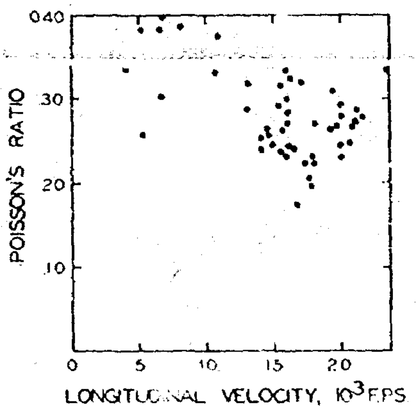

Fig. 11 - Poisson's ratio and longitudinal velocity.

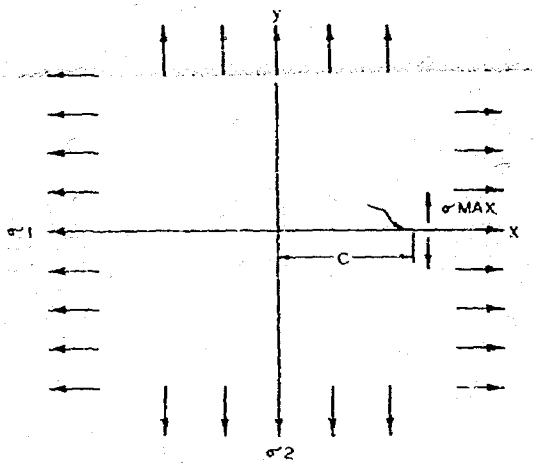

Fig. 12 - Griffith's theoretical treatment of crack formation.

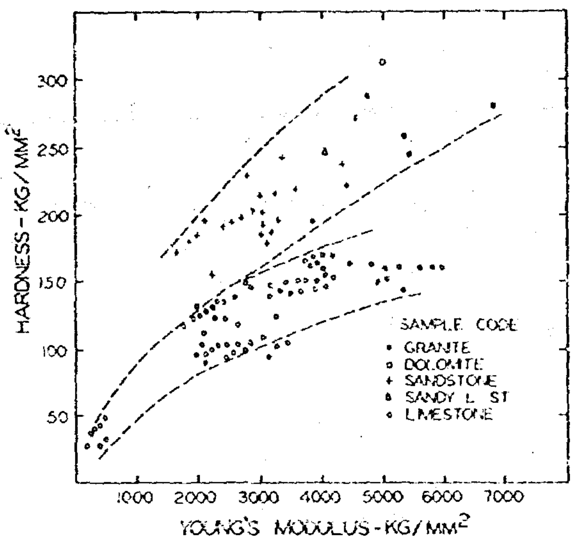

Fig. 13 - Hardness vs Young's modulus.

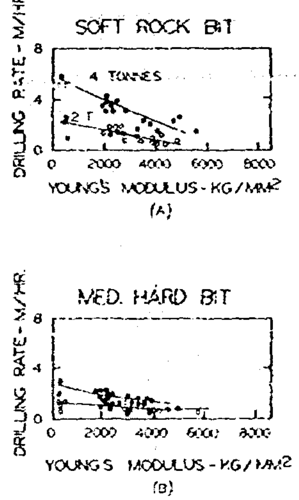

Fig. 14 - Drilling rate vs Young's modulus.

Society of Petroleum Engineers of AIME
6200 N. Central Expwy.
Dallas, Tex. 75206

PAPER NUMBER SPE 6087

Laboratory Investigation of Fracture Initiation Pressure and Orientation

By

W. L. Medlin, Member SPE-AIME, and L. Masse', Mobil Research and Development Corp.

ABSTRACT

The mechanics of hydraulic fracture initiation has been investigated in a combined experimental-theoretical study. Theory was developed assuming poro-elastic behavior. Experiments were conducted with 4 inch diameter cores containing spherical and cylindrical cavities and loaded in a triaxial cell under variable confining pressure, end load and pore pressure. Experimental results agreed with theory for non-penetrating frac fluid over limited ranges of hydrostatic confining stresses for four kinds of rock. With penetrating frac fluids the theory was only partially confirmed. Under non-hydrostatic stress conditions, reproducibility of measurements was too poor to evaluate the theory. Fracture orientation was controlled predominantly by stress conditions and cavity geometry. Notching of cylindrical cavities gave failure through notch extension only if the notch depth exceeded the value predicted approximately by a simple Griffith theory equation. Field applications of all results are discussed.

INTRODUCTION

This paper describes a combined theoretical-experimental investigation of the mechanics of hydraulic fracture initiation. We have considered fracture initiation pressure, fracture orientation and mode of failure for various stress conditions and wellbore geometries. Our intention has been to develop theory applicable to both field and laboratory conditions, to test it by laboratory experiments and to apply it to field problems.

The laboratory experiments have been designed not to duplicate field conditions so much as to provide a critical test of the theory. Some field data are examined but it is impractical to learn much about fracture initiation from field experiments because of the limited number of quantities which can be measured.

The theory presented here is as much a generalization of earlier work as a development of new theory. It provides a completely general treatment

Ex 2 B

of fracture initiation in spherical and cylindrical cavities for poro-elastic materials. An extension of this theory to porous materials with non-elastic behavior has already been developed by M. A. Biot and will be referred to later.

The paper begins with development of the theory for fracture initiation in spherical and cylindrical cavities. This development is followed by descriptions of laboratory results which test the equations for failure pressure in these geometries under various stress conditions, using penetrating and non-penetrating frac fluids. Effects of notching in cylindrical cavities is then considered and a simple model based on Griffith crack theory is developed to explain experimental results. Field applications of all results are then taken up and discussed in detail.

THEORY OF FRACTURE INITIATION

The theory of hydraulic fracture initiation in rock materials has been treated in successive degrees of refinement[1-6]. Cases of interest are hollow sphere and long cylinder geometry with penetrating and non-penetrating fracturing fluids. References 1-6 consider various parts of the overall picture but none presents a general treatment including analysis of scaling effects between laboratory experiments and field work. Reference 6 gives the most complete analysis but invokes analogies between thermoelasticity and poroelasticity which obscure the physics of the problem somewhat. We present here a general treatment based on Biot's theory of elasticity for fluid-saturated, porous solids[7,8] which includes evaluation of scaling effects.

We start with Biot's stress-strain relations for a fluid saturated porous solid:

$$\tau_{ij} = -2\mu e_{ij} - (\lambda e - \alpha p)\,\delta_{ij} \qquad (1)$$

The strain components are:

$$e_{ij} = \tfrac{1}{2}\left(\frac{\partial u_i}{\partial x_j} + \frac{\partial u_j}{\partial x_i}\right) \qquad (2)$$

and the dilation is:

$$e = \sum_{i=1}^{3} \frac{\partial u_i}{\partial x_i} = \sum_{i=1}^{3} e_{ii} \qquad (3)$$

We show in Appendix A that Equation (1), under the usual equilibrium conditions, leads to a displacement potential which satisfies the relation

$$\nabla^2\phi = \frac{\alpha}{\lambda + 2\mu}\, p(r,t) + C(t) = e \qquad (4)$$

The effective stress components are also shown to be

$$\tau'_{ij} = -2\mu e_{ij} - (\lambda A + \beta) p\,\delta_{ij} - \lambda C(t) \qquad (5)$$

Equations (2)-(5) include all of the equations needed to relate fracture initiation pressure to stress conditions for various wellbore cavity geometries and for penetrating or non-penetrating fracturing fluids. Equations (2)-(5) can be used to determine stresses produced by applying pressure in the wellbore cavity. By superposing the stresses due to overburden and tectonic loading, we can find the total stress components. A fracture will be initiated when the tangential component $\tau_{\theta\theta}$ at the wellbore cavity wall is just equal to the tensile strength of the rock. This procedure provides an equation which gives fracture initiation pressure in terms of external stress conditions and rock tensile strength.

Hollow Sphere Geometry

Using the above procedure, we show in Appendix B that fracture initiation pressure for the hollow sphere geometry of Figure 1 is given by the following:

Non-Penetrating Fluid

$$p_f = 2\,(T + \tau_t) \qquad (6)$$

Penetrating Fluid

$$p_f = \frac{2\,(T + \tau_t)}{3 - 2\alpha\left(\frac{1-2\nu}{1-\nu}\right)} \qquad (7)$$

where

$$\tau_t = \frac{3}{2\,(7-5\nu)}\left[(9-5\nu)\,\sigma_1 - (1+5\nu)\,\sigma_2 + (-1+5\nu)\,\sigma_3\right] \qquad (8)$$

with $\sigma_1 \le \sigma_3 \le \sigma_2$. These results apply to both the field case (infinite medium) and the lab case. We show in Appendix B that Equation (7) is an approximation for the lab case and is only valid when the following conditions are met: (1) $b^3 \gg 2a^3$, (2) frac fluid penetration has not gone far enough to raise the pore pressure significantly at the outer boundary, and (3) injection pressure has been increased linearly with time up to the fracturing pressure.

Long Hollow Cylinder Geometry

Appendix C shows that fracture initiation pressure for the long hollow cylinder geometry of Figure 2 is given by the following:

Non-Penetrating Fluid

$$P_f = T + \tau_t \qquad (9)$$

Penetrating Fluid

$$P_f = \frac{T + \tau_t}{2 - \alpha\left(\frac{1-2\nu}{1-\nu}\right)} \qquad (10)$$

where $\tau_t = -\sigma_1 + 3\sigma_2$ with $\sigma_2 > \sigma_1$. These results again apply to both the field case and the lab case. Equation (10) is again an approximation for the lab case and is only valid when $b^2 \gg a^2$, frac fluid penetration has not reached the outer boundary and injection pressure has been increased at a constant rate up to the fracturing pressure.

EXPERIMENTAL PROCEDURE

Purpose of our experimental procedure was to use laboratory measurements to test the above relations, to investigate fracture orientation and mode of failure, and to interpret all of these results in terms of field applications.

All measurements were made using rock cores of 4 inch diameter and 5 inch length. Rock materials included four common types of limestone quarry rock: Carthage, Indiana, Lueders, and Austin, selected for their homogeneity and ranging in mechanical properties from hard-brittle to soft-plastic. A summary of their physical properties is given in Table 1. Spherical and cylindrical cavities of 1/8 inch diameter were used to give $b = 32a$.

Figure 3 shows the experimental arrangement using a core prepared with a spherical cavity. External stress was applied to the cores using a conventional triaxial cell arrangement. Horizontal stress was applied by means of oil pressure acting against a plastic sleeve. Vertical load was applied between the upper, moveable piston and lower anvil by means of the servo-controlled actuator which provided either hydrostatic or biaxial stress on the core. For biaxial stress, the servo system used the load cell shown in Figure 3 as sensor. In this way piston load could be set to give an end stress greater or less than the lateral stress. Extra end load was applied by forcing the lower anvil against the cell bottom. For reduced end loading, the servo system allowed the piston to move out of the cell until the outer sleeve, shown in Figure 3, contacted the cell lid and absorbed some fraction of the piston load. For hydrostatic stress the outer sleeve was removed and the ram was controlled by a position sensor which allowed the piston to move out of the cell until it butted against the load cell.

The core shown in Figure 3 contains a spherical cavity. It was prepared by sealing a $\frac{1}{4}$ inch O.D. x 1/8 inch I.D. steel tube into the core with epoxy. A 1/8 inch diameter burring tool was used to drill a hemispherical cup into the rock beyond the tube as shown. Cylindrical cavities of two types were prepared which we designate A & B. Type A cavities were prepared by shortening the length of the steel tube to 1 inch and drilling a 1/8 inch diameter hole to within 1 inch of the bottom of the core. Type B cavities were prepared without steel tubes. A 1/8 inch diameter hole was drilled completely through the core and 1 inch diameter patches were painted around the hole on each end to provide sealing surfaces for O-rings in the piston and anvil faces.

The non-penetrating fluid case was simulated by using heavy grease as frac fluid and additionally sealing the cavity walls with epoxy paint in some cases. The epoxy paint seal gave anomalous results in Carthage cores and did not completely prevent fluid penetration in Indiana cores. Grease penetration was measured by looking through a low power microscope at cross sections cleaved through dry cores. In all but Indiana cores, penetration was no greater than one cavity diameter in unsealed cavities. In epoxy sealed cavities penetration was undetectable except in Indiana cores where it was as much as five cavity diameters in regions where partial rupturing of the paint seal occurred. One effect of the epoxy paint coatings was to increase the apparent rock tensile strength as will be discussed later. Experiments with cavity liners made of plastic or rubber tubing gave erratic results which were discarded.

To assure uniform loading, the ends of all cores were ground flat and parallel to within .002 inch. Fracturing fluid was injected into the core cavities through a port in the piston as shown in Figure 3. A second port in the piston was used to apply pore pressure at one end of the core through annular and diametral grooves machines into the piston face.

Confining pressure in the triaxial cell was supplied by an air-driven hydraulic pump. The air regulator on this pump was driven by a variable speed motor to give linear buildup of confining pressure with time. Injection pressure was provided by a motor driven hydraulic pump in series with a 10:1 intensifier. A hydraulic regulator between pump and intensifier gave pressure control to within one percent up to 50,000 psi. A variable speed motor drive attached to this regulator produced linear buildup of injection pressure with time. The motor speed control gave buildup rates between 500 psi/min and 20,000 psi/min. Pore pressure was supplied by a second motor driven pump with hydraulic pressure regulator.

Pressure transducers were used to measure confining pressure, injection pressure and pore pressure. The injection and pore pressure transducers were located as close as possible to the piston ports. A linear motion transducer was linked with the piston of the injection pressure intensifier to measure its displacement. This displacement was multiplied by piston area and corrected for fluid compressibility to get the volume of fluid injected into the cavity during buildup of injection pressure. We recorded injection pressure, p_i, confining pressure, σ_h, pore pressure, σ_p, displaced volume in the injection pressure intensifier, v_i, and end load on the core.

The procedure for fracturing a core was as follows. Confining pressure was built up at a rate of 1000 psi/min with appropriate end stress. In cores where pore pressure was applied, it was built up simultaneously with confining pressure. After buildup of confining pressure a 15-20 minute period was allowed for equilibrium to be established. Then injection pressure in the cavity was raised at a linear rate until fracture occurred.

Fracturing data were obtained in both oil saturated and dry cores. Pore pressure was applied only in the case of saturated cores. In cores where no pore pressure was applied, the pore pressure port was left open during buildup of σ_h and during the equilibrium period which followed. This allowed excess fluid, produced by reduction of pore volume, to bleed off. For the penetrating fluid case, where the injection fluid was the same oil used for saturation, the injection pressure port was also left open during buildup of σ_h. This prevented oil forced out of pores from moving into the injection cavity and diluting the grease.

Comparison of p_i and v_i recordings provided information about failure mode. Brittle fracture initiation was indicated by a sudden drop in p_i accompanied by a sharp rise in v_i. Failure involving plastic behavior gave a bending over of the p_i curve and a bending up of the v_i curve. The rate of bending served as a measure of degree of plasticity. In some cases plastic failure was indicated by a series of inflections in the p_i and v_i curves due to stepwise fracturing.

To assure single phase flow in experiments with penetrating frac fluid, we used a rigorous core saturating procedure. The oven dried cores were placed in a vacuum-tight cell with 21 core capacity and pumped to a vacuum better than 5 microns for 48-96 hours. The saturating fluid, which was 150 cp vacuum pump oil, was degassed in a second cell by pumping to better than 5 microns for 24 hours. The cell containing cores was filled with the degassed vacuum pump oil, and then pressure in this cell was raised to 600 psi by a vacuum tight air-driven pump. Saturation was assumed to be complete when the valve to this pump could be cut off for 24 hours with no decline in pressure.

EXPERIMENTAL RESULTS

p_f Measurements: Hydrostatic Stress

Measurements of p_f have been compiled for hollow sphere and long hollow cylinder geometries (types A & B) in dry and saturated cores for penetrating and non-penetrating frac fluids with and without pore pressure.

Figure 4 shows results for saturated Lueders cores at zero pore pressure over a range of hydrostatic stress, p_o, from 0 to 16,000 psi. Curves (a) and (b) represent long hollow cylinder geometries and (c) represents hollow sphere geometry. In (a) the cavities are type B coated with epoxy paint to prevent frac fluid penetration, in (b) the cavities are type B but uncoated, in (c) the spherical cavities are also uncoated. The frac fluid in all three cases was heavy grease.

Plotted in Figure 4 are the theoretical lines of slope 3 and slope 2 predicted by Equations (6) and (9) for hollow sphere and long hollow cylinder geometry, respectively, using non-penetrating frac fluid under hydrostatic stress conditions. Over the p_o range 0-2000 psi, the experimental points fall on the theoretical slopes. At higher p_o the p_f values are lower than predicted. According to (9), the p_f intercept of 4100 psi is T, the tensile strength for fracture initiation. For (a) points the intercept is somewhat higher, consistent with an increase in tensile strength due to the epoxy paint coating. The close match between (b) and (c) points indicates that the heavy grease frac fluid behaves practically as a non-penetrating fluid in Lueders rock. Visual inspection of the cores leads to the same conclusion. The p_f intercept for (c) points should be 2T or 8200 psi according to Equation (6) but is actually only 7200 psi. This discrepancy is well within expected limits since the spherical cavities are not ideal because of weakening effects of the hole drilled for the steel injection tube (cf Figure 3).

Figure 5 compares results for penetrating and non-penetrating frac fluids in saturated Lueders cores with long hollow cylinder geometry at zero pore pressure. We used type A cavities in this case to minimize end effects from fluid penetration through the borehole wall. The (a) points were obtained with heavy grease frac fluid in uncoated cavities. They correspond to the (b) points in Figure 4 except for the type A vs type B cavity configurations. The (b) points were obtained using 150 cp vacuum pump oil as the frac fluid, the same oil used as saturating fluid. Equation (10) predicts that the p_f intercept and the slope of p_f vs p_o should be reduced by the same factor due to fluid penetration. The results in Figure 5 show a 30% reduction in p_f intercept but no apparent reduction in slope. Therefore, results are not consistent with theory in this case.

The type A configuration used for the Figure 5 experiments was designed to allow frac fluid penetration to reach the ends of the core only a little before it reached the outer diameter. Cores were fractured in all of the Figure 5 experiments before fluid had penetrated to the top end of the core. This was verified by monitoring pressure at the pore pressure inlet. We determined in this way that 10,000 psi/min was an appropriate build-up rate to keep p(b) = 0 up to fracture initiation for Lueders cores. The 20% mismatch between p_f intercepts for the (b) points of Figure 4 and the (a) points of Figure 5 is probably due to the non-ideal geometry of the type A cavities.

Figure 6 shows p_f vs p_o measurements for dry Lueders cores with long hollow cylinder geometry using non-penetrating frac fluid. The (a) points represent type B cavities coated with epoxy paint and the (b) points are for uncoated type B cavities. Heavy grease was the frac fluid in all cases. Dry cores give about the same p_f behavior as saturated cores indicating that the oil saturation had little effect on rock properties.

Reproducibility of p_f measurements was fairly good in all of the Lueders experiments. Most of the points plotted in Figures 4-6 represent averages of 3 or 4 measurements. The maximum variation in p_f value for a particular point was typically 5-10% for cylindrical cavities and 10-15% for spherical cavities.

Figure 7 shows results for Carthage cores with long hollow cylinder geometry using non-penetrating frac fluid. All of these measurements were made using heavy grease as the frac fluid in type B cavities. The (a) points were obtained in saturated cores and the (b) points in dry cores. The saturated core measurements give a good fit to Equation (9) from p_o = 0 to 12,000 psi with T = 5000 psi. The (b) points give a poorer fit from p_o = 0 to 6000 psi with T = 7000 psi. These results are consistent with reduction of T and extension of the stress range of elastic behavior by saturating with oil. Note that the (b) point for p_o = 0 is considerably above the projected intercept of points at higher p_o. This effect corresponds to a lowering of tensile strength in dry cores by compression. When dry cores are fractured at p_o = 0 after first loading them to p_o = 4000 psi, the p_f values fall about where they belong as shown by the square symbol in Figure 7. This result is suggestive of hysteresis effects commonly observed in stress-strain curves under compressive loading. It does not occur in saturated Carthage cores as shown by the good agreement between the open square and open circle measurements obtained by the same procedure.

Reproducibility of Carthage core measurements was poorer than those for Lueders. The points in Figure 7 represent averages of 3-4 measurements in which the maximum spread was typically 10-20%.

Figure 8 shows results for Indiana cores. Here we used saturated cores to investigate spherical cavities with non-penetrating fluid and cylindrical cavities with both penetrating and non-penetrating fluids. Also, we investigated cylindrical cavities in dry cores using non-penetrating fluid.

The (a) points in Figure 8 correspond to hollow sphere geometry using saturated cores with non-penetrating fluid. The fit to Equation (6) is good out to p_o = 6000 psi with T = 6000 psi. The (b) points represent saturated cores with type A cylindrical cavities using non-penetrating frac fluid. The results fit Equation (9) out to p_o = 6000 psi with T = 6000 psi in good agreement with the (a) results. The (c) points represent saturated cores with type A cylindrical cavities using penetrating frac fluid which was the same 150 cp vacuum pump oil that the cores were saturated with. By injecting at a pressure buildup rate of 20,000 psi/min, we were able to maintain p(b) = 0 until fracture initiation. Equation (10) predicts reduction in p_f intercept and slope by the same factor between the (b) and (c) points. Instead, we find a 40% reduction in p_f intercept but no detectable reduction in slope. In this respect the Indiana results are in agreement with the Lueders results of Figure 5.

The (d) points in Figure 8 show results for dry Indiana cores with heavy grease as the frac fluid in type B cylindrical cavities. They show, in comparison with the (b) points, that oil saturation lowers the tensile strength T somewhat but otherwise has little effect on fracture initiation behavior.

Reproducibility of measurements was good in the Indiana cores. Total spread in p_f measurements at a given p_o was typically 3-5% for cylindrical cavities and 15-20% for spherical cavities. We attribute the consistently poorer reproducibility of spherical cavity measurements in all rock materials to localized inhomogeneities in the rock samples. These inhomogeneities are averaged out much better over the long cylindrical cavities than over the small spherical cavities.

Figure 9 shows results for dry and saturated Austin cores with spherical and hollow cylinder geometry. The heavy grease used for non-penetrating frac fluid gave insignificant penetration in these cores, and there was little difference between results for coated and uncoated cavities. This is shown by comparing the (a) and (b) points of Figure 9 which represent dry cores containing coated and uncoated type B cylindrical cavities, respectively. The p_f intercepts are about the same, indicating that the epoxy coating adds little to the tensile strength. The slopes are about equal also. There is no range of data points which fit a line of slope 2, indicating non-elastic behavior at all confining stresses.

Points (c) and (d), which represent saturated cores, show what may be a small range of elastic behavior at low p_o. The (c) points correspond to type A, uncoated, cylindrical cavities and the (d) points represent uncoated spherical cavities. Non-penetrating grease is the frac fluid in both cases. Lines drawn through both sets of points intercept the $p_o = 0$ axis above the corresponding measured values. This result suggests that, over a limited p_o range, the slopes could be 3 for (c) points and 2 for (d) points. However, precision of the measurements is too poor to verify this result by measurements over smaller p_o intervals. Reproducibility of measurements for (d) points was poorer than usual. Vertical bars show probable errors for 7 measurements made at each point. Reproducibility of measurements for (a)-(c) points was comparable with Lueders and Carthage measurements.

All of the above measurements were made at zero pore pressure. That is, pore pressure, σ_p, at the outer core boundary was kept at zero by leaving the pore pressure port open (see Figure 3). We investigated effects of elevated pore pressure at the core boundaries by repeating several of the measurements of Figures 4-7 at $\sigma_p = 4000$ psi. These measurements verify the effective stress relation of Equation (5). There is good agreement between measurements at $\sigma_p = 4000$ and $\sigma_p = 0$ when results are plotted as $p_f - \sigma_p$ vs $p_o - \sigma_p$ as required by Equation (5). Figure 10 compares measurements of this kind in Indiana and Austin cores. Points labeled (a) are a reproduction of the (b) points of Figure 8 for Indiana cores with $\sigma_p = 0$. Points labeled (b) correspond to Indiana cores fractured from the same block of material, under the same conditions, except with $\sigma_p = 4000$ psi. Points labeled (c) are a reproduction of points labeled (a) in Figure 9 for Austin cores with $\sigma_p =$ 0. Points labeled (d) correspond to Austin cores from the same block, measured under the same conditions but with $\sigma_p = 4000$ psi. The match in both cases is well within limits of reproducibility of the measurements.

The p_1 and v_1 recordings described earlier showed that failure mode included increasing degrees of plastic failure at stresses above the elastic behavior range in Figures 4-8. In Austin cores some plastic failure was evident even at zero confining stress.

p_f Measurements: Non-Hydrostatic Stress

Investigation of p_f behavior under non-hydrostatic stress was limited to hollow sphere geometry. For this geometry we were able to make measurements for the case $\sigma_3 = \sigma_2 \neq \sigma_1$ (Figure 1 notation). Hollow cylinder geometry could not be investigated because, with the arrangement shown in Figure 3, we could not readily orient the borehole of the core to give $\sigma_1 \neq \sigma_2$ (Figure 2 notation).

The hollow sphere measurements gave inconclusive results because of extremely poor reproducibility of measurements. A typical example is given in Figure 11 which shows results for 23 Indiana cores fractured under confining stress, $\sigma_2 = \sigma_3 = 4000$ psi and end stress, $\sigma_1 = 2000$, 4000, and 6000 psi, respectively. The theoretical lines plotted in Figure 11 were computed from Equation (6) using $\nu = 0.16$ from

Table I and T = 8000 psi as determined from p_f measurements at zero confining stress. The large spread in p_f measurements makes it impossible to assess the validity of the theory although the match appears to be poor.

A poor match to theory would most likely be due to non-ideal geometry of the experiments in which a spherical outer boundary is represented by a cylindrical one. Poor reproducibility is probably due to mechanical damage produced in the rock cores during application of unequal stresses. Our procedure was to first load the cores hydrostatically, then apply excess end load or lateral load. Even under the slowest loading rates available with our servo system, we were applying excess stress at rates of the order of 100 psi/sec. Strains produced under these loading rates could be expected to produce microcracks and other flaws which could easily affect p_f.

Fracture Orientation

Fracture orientation was measured for hollow sphere and hollow cylinder geometry under hydrostatic and non-hydrostatic stress conditions. We also investigated effects of notching in hollow cylinder wellbores. Results can be summarized as follows.

In the case of hollow cylinder geometry, we were unable to investigate effects of stress conditions on azimuthal orientation. Reference 6 gives results of work on this problem. Here we consider only inclinations of the fracture plane with respect to the wellbore. Our results showed that, under all stress conditions, fractures intersected and were aligned with the cylindrical cavity. This result was observed in dry and saturated samples, using penetrating and non-penetrating fluids with various stress-pore pressure combinations in the effective stress range 1,000-16,000 psi. It applies up to a maximum σ_3/σ_2 ratio of 2 (Figure 2 notation) which was the limit of our triaxial apparatus. It should be noted that Daneshy[9] has reported fractures inclined to the wellbore for $\sigma_3/\sigma_2 < 2$ the external stress field has little to do with fracture inclination in hollow cylinder geometry. It is the stress concentrating nature of the wellbore cavity which dominates and produces vertical fractures in all cases.

In the case of hollow sphere geometry, our results showed that fracture orientation is controlled almost completely by stress conditions. This result is illustrated in Table 2 where fracture angle θ is measured with respect to the $\sigma_2 - \sigma_3$ plane (Figure 1 notation). The results given here were obtained at $\sigma_2 - \sigma_3 = 8000$ psi and $\sigma_p = 4000$ psi using non-penetrating grease as the frac fluid. Similar results were obtained under other stress conditions and with penetrating frac fluid. A less complete set of measurements in Carthage cores also gave results consistent with those in Table 2.

It is clear from these results that external stress conditions are dominant in determining fracture orientation for hollow sphere geometry except when they are nearly hydrostatic. Under hydrostatic conditions orientation appears to be random and is undoubtedly controlled by local inhomogeneities in the rock at the cavity wall. A 10-20% departure from hydrostatic conditions seems to be sufficient to control orientation almost completely.

Notched Borehole Experiments

To investigate effects of borehole notching we prepared cores with type B hollow cylinder geometry containing machined notches. The notches were formed by means of an elliptically shaped tungsten carbide bit welded on the end of a two inch length by 1/8 inch drill rod. Cores with $\frac{1}{2}$ inch diameter boreholes were mounted in a lathe and the bit was used to machine a notch in the borehole wall 1 $\frac{1}{2}$ inches from one end of the core. In this case b was 2 inches, a was 0.25 inches, and c, the notch depth measured from the wellbore wall, was a maximum of 0.45 inches.

Initial experiments using non-penetrating grease showed that such notches have no effect on either p_f or fracture orientation if c is small enough. Measurements in dry, shallow-notched Lueders and Carthage cores under hydrostatic confining stress p_o gave vertical fractures through the wellbore at p_f values consistent with those of Figures 4-8. With deeper notches, we obtained vertical fractures at low p_o and horizontal fractures at high p_o.

These results lead to the formulation of a simple theory of fracture initiation in notched wellbores based on Griffith crack theory. Neglecting wellbore effects, the Griffith theory predicts that pressure required to extend an elliptical crack under hydrostatic stress p_o without fluid penetration is,[10,11]

$$p_e = \sqrt{\frac{\pi E s}{2c(1-\nu^2)}} + p_o. \tag{11}$$

At low p_o this extension pressure will exceed the hollow cylinder fracture initiation pressure which is given by (9) if we neglect effects of the notch, i.e.,

$$p_f = \frac{b^2 - a^2}{b^2 + a^2} T + \frac{2b^2}{b^2 + a^2} p_o \approx T + 2p_o \tag{12}$$

The slope of p_f vs p_o is twice that of p_e vs p_o. Therefore, as p_o is increased, Equation (11) will intersect Equation (12) and there will be a transition from hollow cylinder fracture initiation to notch extension.

This simple model seems to explain the notched borehole results fairly well as illustrated in Figures 12 and 13. Figure 12 shows results for dry Carthage cores prepared with type B hollow cylinder cavities notched with c = 0.32 inches and fractured with non-penetrating grease. The theoretical lines correspond to Equations (11) and (12). The Equation (11) plot assumes T = 5000 psi in agreement with results in Figure 11(b). The Equation (12) plot gives surface tension s = 2.1 psi = 1.4×10^5 dynes/cm^2 based on elastic constants listed in Table I for Carthage limestone. The points in Figure 12 represent averages of measurements on 2-3 cores. Open circles represent horizontal fractures in the plane of the notch tip and half closed circles represent mixtures of vertical and horizontal fractures.

Figure 13 shows similar results for Indiana cores with c = 0.23 inches. Grease penetration was significant in this case, especially around the notched region. But we found that coating the notch and borehole surfaces with "Neobon", a neoprene rubber paint, prevented grease penetration and did not increase tensile strength of the rock significantly. In this case, the theoretical hollow cylinder fracture line corresponds to T = 4200 psi in agreement with Figure 8(d). The upper intercept corresponds to s = 4.9 psi = 3.4×10^5 dynes/cm^2 for Indiana limestone.

This analysis is very approximate in that it neglects effects of the wellbore on notch extension and effects of the notch on wellbore rupture. Also, it is only applicable to elastic materials. Carthage limestone departs from elastic behavior above p_o = 12,000 psi (cf Figure 7) and Indiana above p_o = 8000 psi (cf Figure 8). These departure stresses are not far above the transition regions of Figures 12 and 13. The range of elastic behavior in Lueders and Austin is too limited to apply the analysis to them. However, notch experiments with these materials showed that qualitatively their behavior is not unlike that of Figures 12 and 13.

Notch extension in these experiments was enhanced by making $\sigma_3 < \sigma_1 = \sigma_2$ (Figure 2 notation). This was demonstrated in Carthage cores prepared like those of Figure 12 but with $\sigma_1 = \sigma_2 = 2\sigma_3$. Cores fractured with $\sigma_1 = \sigma_2$ ranging from 2,000 to 20,000 psi gave only horizontal notch extension fractures in all cases. Notch extension pressures were considerably lower than those of Figure 12 at $\sigma_1 = \sigma_2$ values corresponding to p_o in that figure. The p_e vs σ_1 slope was 1 in agreement with the notch extension region of Figure 12.

Additional notching experiments were conducted using a simulated notched casing arrangement. In this case 3/8 inch O.D. x ¼ inch I.D. brass tubing was sealed with epoxy into a ½ inch diameter borehole in two sections. A 1/8 inch gap was left between these sections 1 ½ inches from the end of the core. A rotating sand jetting tool was then used to cut a notch through the epoxy and into the rock core material. Notches of unlimited depth could be cut in this way but our experiments were limited to c values between 0.2 and 0.5 inches. These experiments gave results similar to open hole notching. That is, horizontal notch extension was only favored when the notches were deep. When we made $\sigma_3 > \sigma_2 = \sigma_1$, vertical fractures were obtained even with deep notches. Evidently shallow notches prepared in this way provide a geometry which approaches that of a hollow sphere because wellbore stresses which would favor vertical fractures are shielded from the wellbore wall by the casing.

FIELD APPLICATIONS

Results of this work have application to a variety of field problems associated with formation breakdown in hydraulic fracturing and drilling operations. The results of Figures 4-10 are difficult to compare with field experience, however, because accurate field measurements of fracture initiation pressures are scarce. Surface pressure measurements are commonly made during formation breakdown in connection with hydraulic fracturing treatments. But these measurements give severe damping of bottomhole pressure transients as shown by the experiments of Godbey and Hodges[12]. Accurate bottomhole breakdown pressure measurements by these authors and by van Dam and Horner[13] are plotted in Figure 14 as a function of depth for wells in Texas, Oklahoma, and South America. A line of slope ~ 1 fits these points reasonably well. This slope on a depth plot is roughly consistent with a slope of 2 on an effective stress plot since pore pressure gradients are normally about half of the 0.7-1.0 psi/ft normal stress gradients. So slope data like that of Figure 10 are roughly consistent with the field results of Figure 14. On the other hand, the projected intercept in Figure 14 would correspond to a tensile strength less than 1000 psi, much smaller than any of our lab measured values. The empirical correlations of Matthews and Kelly[14] also indicate near zero tensile strengths in the Gulf Coast formations they studied. These and other field results indicate that the large tensile strengths measured in our limestone samples are not characteristic of many reservoir rocks.

Formation breakdown prior to a hydraulic fracturing treatment can be aided by taking advantage of lowering p_f by fluid penetration. The use of acid as a breakdown fluid is already a well established technique which takes advantage of this effect. The importance of proper placement of the acid at the breakdown point is demonstrated by the results given here.

The same logic applies in a reverse sense to formation breakdown during drilling. The fracture gradient is lowered by use of penetrating drilling fluids. Therefore, rapid buildup of a thick mud cake is desirable. Once breakdown has occurred, the created fracture will be propagated at something like half the pressure required to initiate it, provided it is reasonably large and the formation does not exhibit much plasticity. This follows in a very approximate sense from Equations (9) and (11). After a sizeable crack is initiated, the T term and the factor 2 are lost in Equation (9) and the extension pressure is reduced by more than a factor 2. More refined fracture propagation theory[15] provides a more convincing argument. Propagation of sizeable cracks requires a fracture propagation pressure a little greater than the far field stress whereas initiation requires more than twice the far field stress. On the basis of these arguments, plugging of lost circulation zones will only be effective if the plug prevents application of wellbore pressure to most of the fractured surface area.

Fracture orientation results reported here show that initiation of any but vertical fractures in most wells is highly unlikely. This is most clearly the case for formation breakdown during drilling where the cavity is certainly cylindrical. In hydraulic fracturing through perforations, the common perforating patterns all approach cylindrical cavities if the perforated interval is more than a few wellbore diameters in length. The closest approach to a spherical cavity would be a single horizontal row of perforations[4].

Notching is effective for initiating a horizontal fracture provided the notch is deep enough. A minimum notch depth can be estimated from Equation (11) if modulus E and surface tension s of the formation rock are known. Our experimental results indicate that the minimum notch depth should be more than a few inches into the formation rock.

Most favorable geometry for initiating horizontal fractures is deep notching through cemented casing. A fracture initiated horizontally will turn toward a vertical orientation away from the wellbore if stress conditions favor a vertical fracture, as is usually the case. The rate of turning will depend on magnitude of the stress differences and cannot be predicted quantitatively from our results because of undetermined scaling effects.

CONCLUSIONS

Fracture initiation pressures in laboratory scale experiments are consistent with poro-elasticity theory for non-penetrating frac fluids over some range of hydrostatic stress. This stress range is highly variable with rock properties. In Carthage limestone it extends from 0 to 12,000 psi but in Austin Chalk it is no more than a few hundred psi at most. In Indiana limestone it goes from 0 to 8,000 psi and in Lueders limestone from 0 to 3,000 psi. Saturation of our samples with oil had only minor effects on fracture initiation mechanics.

In the stress range beyond elastic behavior, fractures are initiated at pressures lower than predicted for elastic behavior. Failure mode is partially plastic at these stresses and a non-linear failure analysis is required. Such an analysis has already been carried out by Biot[16] and is consistent with our experimental results.

Initiation pressures measured with penetrating frac fluid are not completely consistent with poro-elastic theory. The theory predicts that frac fluid penetration will reduce both intercept and slope of p_f vs p_o plots by the same factor. Experimental results show the reduction in intercept but not the reduction in slope.

Theoretical predictions for non-hydrostatic stress conditions could not be confirmed because of very poor reproducibility of measurements. This problem is one of experimental limitations rather than breakdown of the theory.

The dominant factors controlling fracture orientation and external stress conditions and wellbore geometry. In spherical cavities, stress conditions are the dominant factor. In cylindrical cavities stress conditions have no effect on fracture inclination except under extreme conditions. In reasonably homogenous rock, fractures align themselves with the wellbore axis and ignore minor wellbore flaws and shallow notches because of the overwhelming effects of stress concentrations developed by the wellbore. Even large flaws do not affect fracture orientation if they are very far removed from the wellbore. Rock anisotropy played an insignificant role in determining fracture orientation in rocks investigated here except in spherical cavities under hydrostatic stress. Anisotropy also had no detectable effect on fracture initiation pressure in our experiments.

Notching has predictable effects on fracture initiation pressure and orientation. However, laboratory notching experiments present some scaling problems because notch depths required are not small compared to outer dimensions of practical size cores. A simple Griffith theory of crack extension is roughly consistent with laboratory results. For field applications it is critical that notch depth exceed a minimum value of the order of inches to generate horizontal fractures in a cylindrical cavity. The most favorable geometry for horizontal fractures is a deep notch cut through well cemented casing. A shallow notch in poorly cemented casing is likely to be ineffective.

There was considerable variation in physical appearance of fractures in rocks investigated here. Austin cores gave smooth fracture surfaces and Indiana cores gave very rough surfaces with Lueders and Carthage as intermediate cases. Proppant transport would be significantly influenced by these differences. In all cases the fracture surfaces were much smoother than those produced by mechanical cleaving. Typical fractures were planar, but fractures which changed direction away from the wellbore did occur in some cases under hydrostatic stress, mostly in Austin and Indiana cores.

In general, our experimental results on fracture initiation pressure and orientation are consistent with those reported by others[17-19].

NOMENCLATURE

- a = radius of spherical or cylindrical cavity
- A = poro-elastic parameter = $\alpha/(2\mu + \lambda)$
- b = outer radius of hollow sphere or cylinder
- c = notch depth measured from wellbore wall
- C = integration constant and arbitrary function of t
- e = dilatation
- E = Youngs modulus
- e_{ij} = strain components
- f = rock porosity
- k = rock permeability
- K = inverse bulk modulus = $3/(3\lambda + 2\mu)$
- m = injection pressure buildup rate
- M = Biot constant defined by Equation (B-13)
- p = $p(r,t)$ = variable pore pressure
- p_e = pressure at which notch extension occurs
- p_f = fracture initiation pressure
- p_i = injection pressure
- r = radial coordinate
- s = surface tension
- S = axial stress
- t = time
- T = rock tensile strength
- $\bar{u}$ = displacement vector
- u_i = ith component of displacement vector
- v_i = volume of frac fluid injected
- x_i = space coordinate
- α = Biot constant = $1 - (K_{bulk}/K_{matrix})$
- β = $1 - \alpha$
- δ_{ij} = Kronecker Delta
- ϕ = displacement potential
- ζ = pore fluid compressibility
- η = frac fluid viscosity
- θ = spherical or cylindrical coordinate (Figures 1 and 2)
- κ = flow parameter defined by Equation (B-12)
- λ,μ = Lame' constants
- ν = Poisson ratio
- σ_i = ith component of external stress
- σ_h = confining pressure in triaxial cell
- σ_p = pore pressure
- τ_{ij} = stress components
- τ'_{ij} = effective stress components
- τ_t = tangential stress produced at spherical or cylindrical cavity wall by external loading
- ψ = spherical coordinate

ACKNOWLEDGEMENTS

The authors wish to thank M. A. Biot for helpful discussions and Mobil Research and Development Corporation for permission to publish this paper.

REFERENCES

1. Hubbert, M. K. & Willis D. G., "Mechanics of Hydraulic Fracturing," Trans. AIME Vol. 210 (1957) 153-166.
2. Scheidegger, A. E., "On the Connection Between Tectonic Stresses and Well Fracturing Data," Jour. Pure & Applied Phys. Vol. 46 (1960) 66-76.
3. Kehle, R. O., "The Determination of Tectonic Stresses Through Analysis of Hydraulic Well Fracturing," Jour. Geophys. Res. Vol. 69 (1964) 259-273.
4. Le Tirant, P. & Baron, G., "Hydraulic Rupture in Sedimentary Rocks," Proc. First Congress Int. Soc. Rock Mech. Vol. 1 (1966) 577-583.
5. Geertsma, J., "Problems of Rock Mechanics in Petroleum Production Engineering," Proc. First Congress Int. Soc. Rock Mech. Vol. 1 (1966) 585-594.

6. Haimson, B. & Fairhurst, C., "Hydraulic Fracturing in Porous-Permeable Materials," Jour. Pet. Tech. (July 1969) 811-817.
7. Biot, M. A., "General Solutions of the Equations of Elasticity and Consolidation for a Porous Material," Jour. Appl. Mech. Vol. 23 (1956) 91-96.
8. Biot, M. A., "Mechanics of Deformation & Acoustic Propagation in Porous Media," Jour. Appl. Phys., Vol. 33 (1962) 1482-1498.
9. Daneshy, A. A., "Experimental Investigation of Hydraulic Fracturing Through Perforations," SPE Paper 4333, 5th Ann. Offshore Tech. Conf., Houston, Tex., Apr. 29-May 2, 1973.
10. Sack, R. A., "Extension of Griffith's Theory of Rupture to Three Dimensions," Proc. Phys. Soc. London, Vol. 58 (1946) 729-736.
11. Sneddon, I. N., "The Distribution of Stress in the Neighborhood of a Crack in an Elastic Solid," Proc. Roy. Soc. Vol. 187A (1946) 229-260.
12. Godbey, J. K. and Hodges, H. D., "Pressure Measurements During Formation Fracturing Operations," Trans. AIME Vol. 213 (1958) 65-69.
13. van Dam, J. and Horner, D. R., Second Annual Venezuelan Meeting, AIME, Caracas (1957).
14. Matthews, W. R. and Kelly, J., "How to Predict Formation Pressure and Fracture Gradient," The Oil & Gas Journal, Feb. 20 (1967) 92-106.
15. Khristianovich, S. A. and Zheltov, V. P., "Formation of Vertical Fractures by Means of Highly Viscous Liquid," Proc. 4th World Petroleum Congress (1955) Vol. II, 579.
16. Biot, M. A., "Exact Simplified Non-Linear Stress and Fracture Analysis Around Cavities in Rock," Int. Jour. Rock. Mech. Min. Sci., Vol. 11 (1974) 261-266.
17. Haimson, B. C. and Edl, J. N., Jr., "Hydraulic Fracturing of Deep Wells," SPE Paper 4061, 47th Ann. Fall Meeting, SPE, San Antonio, Tex., Oct. 8-11, 1972.
18. Daneshy, A. A., "Study of Inclined Hydraulic Fractures," SPE Paper 4062, 47th Ann. Fall Meeting, SPE, San Antonio, Tex., Oct. 8-11, 1972.
19. Komar, C. A. and Frohne, K. H., "Factors Controlling Fracture Orientation in Sandstone," SPE Paper 4567, 48th Ann. Fall Meeting, SPE, Las Vegas, Nev., Sept. 30-Oct. 3, 1973.
20. Carslaw, H. S. and Jaeger, J. C., "Conduction of Heat in Solids," 2nd Ed., Clarendon Press, Oxford (1959), p. 247.
21. Ibid, p. 30.
22. Southwell, R. V. and Gough, H. J., "On the Concentration of Stress in the Neighborhood of a Small Spherical Flaw," Phil. Mag., Vol. 7 (1926) 71-97.
23. Carslaw, H. S. and Jaeger, J. C., op. cit. p. 335.
24. Timoshenko, S. and Goodier, J. N., "Theory of Elasticity," 2nd Ed. McGraw-Hill, New York (1951) p. 80.

APPENDIX A

When Equation (1) of the text is substituted into the usual differential equations of equilibrium,

$$\sum_{j=1}^{3} \frac{\partial \tau_{ij}}{\partial X_j} = 0 \tag{A-1}$$

we get

$$-2\mu \sum_{j=1}^{3} \frac{\partial e_{ij}}{\partial X_j} + \frac{\partial}{\partial X_j}(-\lambda e + \alpha p) = 0 \tag{A-2}$$

Substituting Equations (2) and (3) into (A-2) gives

$$\mu\nabla^2\bar{u} + (\mu + \lambda) \text{ grad } e - \alpha \text{ grad } p = 0 \tag{A-3}$$

As long as the displacements are irrotational, we can write $\bar{u}$ in terms of a displacement potential ϕ as follows

$$\bar{u} = \text{grad } \phi \tag{A-4}$$

With Equation (3), this gives

$$e = \nabla^2\phi \tag{A-5}$$

If we now substitute (A-4) and (A-5) into (A-3), we get

$$-\mu\nabla^2(\text{grad } \phi) + \text{grad}\left[-(\mu + \lambda)\nabla^2\phi + \alpha p(r)\right] = 0 \tag{A-6}$$

Integration of (A-6) over the space coordinates X_i gives Equation (4) of the text with C(t) an arbitrary function of t. From Equation (1), the effective stress components are

$$\tau'_{ij} = \tau_{ij} - P\delta_{ij} = 2\mu e_{ij} - (\lambda e + \beta P)\delta_{ij} \qquad \text{(A-7)}$$

where $\beta = 1 - \alpha$. Substituting (1) into (A-7) and letting

$$A = \frac{\alpha}{2\mu + \lambda}$$

gives Equation (5) of the text.

APPENDIX B

Consider the hollow sphere of Figure 1. When a pressure p(r,t) is applied to fluid in the spherical cavity, the resulting displacements will be irrotational and spherically symmetric. Thus, in spherical coordinates, ϕ will depend on r only and Equation (4) of the text will give

$$e = \nabla^2\phi = \frac{1}{r^2}\frac{\partial}{\partial r}\left(r^2\frac{\partial\phi}{\partial r}\right) = Ap(r,t) + C(t) \qquad \text{(B-1)}$$

Integration and differentiation gives

$$e_{rr} = \frac{\partial^2\phi}{\partial r^2} = Ap(r,t) - \frac{2A}{r^3}f(r,t) + \frac{1}{3}C - \frac{2K}{r^3} \qquad \text{(B-2)}$$

where K is an arbitrary function of t and

$$f(r,t) = \int r^2 p(r,t)dr \qquad \text{(B-3)}$$

Because of spherical symmetry $e_{\theta\theta} = e_{\psi\psi}$ and from (3) and (4)

$$e_{\theta\theta} = \tfrac{1}{2}Ap(r,t) + \tfrac{1}{2}C - \tfrac{1}{2}e_{rr} \qquad \text{(B-4)}$$

Substituting (4), (B-2) and (B-4) into Equation (5) gives

$$\tau'_{rr} = -(\tfrac{2}{3}\mu+\lambda)C - p(r,t) + \frac{4\mu Af(r,t)}{r^3} + \frac{4\mu K}{r^3} \qquad \text{(B-5)}$$

and

$$\tau'_{\theta\theta} = \tau'_{\psi\psi} = -\frac{2\mu Af(r,t)}{r^3} - (\tfrac{2}{3}\mu+\lambda)C-(\lambda A+\beta)p(r,t) - \frac{2\mu K}{r^3} \qquad \text{(B-6)}$$

These are the radial and tangential stresses developed by applying p(r,t). To get fracture initiation pressure, we need only tangential stress at r = a. The radial stress equation is used with boundary conditions to determine C and K.

For a non-penetrating fluid boundary conditions are:

$\tau'_{rr} = p(a,t)$ at $r = a$; $\tau'_{rr} = 0$ at $r = b$; $p(r,t) = f(r,t) = 0$.

These conditions are substituted into (B-5) to determine C and K and the result is substituted into (B-6) to give

$$\tau'_{\theta\theta} = -\frac{2a^3 + b^3}{2(b^3 - a^3)}\,p(a,t) \qquad \text{(B-7)}$$

Under field conditions $b \rightarrow \infty$, $C \rightarrow 0$ and at $r = a$,

$$\tau'_{\theta\theta} = -\tfrac{1}{2}p(a,t) \qquad \text{(B-8)}$$

This result is also a good approximation to the laboratory case as long as $b^3 >> 2a^3$.

For a penetrating fluid the boundary conditions are $\tau'_{rr} = 0$ at $r = a$ and $\tau'_{rr} = -p(b,t)$ at $r = b$.

Using these conditions in (B-5) to determine C and K and substituting the results in (B-6) gives

$$\tau'_{\theta\theta} = -\left[\frac{3}{2}\left(\frac{b^3}{b^3 - a^3}\right) - \alpha\left(\frac{1-2\nu}{1-\nu}\right)\right] p(a,t)$$

$$- \frac{3\alpha}{b^3 - a^3}\left(\frac{1-2\nu}{1-\nu}\right)\int_a^b r^2 p(r,t)\,dr \qquad \text{(B-9)}$$

where

$$f(b,t) - f(a,t) = \int_a^b r^2 p(r,t)\,dr$$

Again, under field conditions, $b \rightarrow \infty$, $C \rightarrow 0$ and at $r = a$,

$$\tau'_{\theta\theta} = -\left[\frac{3}{2} - \alpha\left(\frac{1-2\nu}{1-\nu}\right)\right] p(a,t) \qquad \text{(B-10)}$$

To determine $\tau'_{\theta\theta}$ for the lab case, we must evaluate the integral term in (B-9). We do this by considering flow into an infinite medium. We can estimate $p(r,t)$ in this way as long as frac fluid penetration has not gone far enough to raise the pore pressure $p(b,t)$ at the core boundary significantly before fracture.

In an infinite medium with constant pressure $p(a)$ in the spherical cavity, we have[20]

$$p(r,t) = \frac{a}{r}\,p(a)\ \text{erfc}\ \frac{r-a}{2\sqrt{\kappa t}} \qquad \text{(B-11)}$$

where

$$\kappa = \left[\frac{\eta}{k}\left(\frac{1}{M} + \frac{\alpha^2}{2\mu + \lambda}\right)\right]^{-1} \qquad \text{(B-12)}$$

with

$$M = \left[fc + K(1-\alpha)(\alpha - f)\right]^{-1} \qquad \text{(B-13)}$$

and

$$K = \frac{3}{3\lambda + 2\mu} \qquad \text{(B-14)}$$

For variable injection pressure $p(a,t)$ we can determine $p(r,t)$ by means of Duhamel's Theorem[21]

$$p(r,t) = \int_0^t F(r,\xi)\,\frac{\partial}{\partial t}\,p(a,t-\xi)\,d\xi \qquad \text{(B-15)}$$

where

$$F(r,\xi) = \frac{a}{r}\,\text{erfc}\left(\frac{r-a}{2\sqrt{\kappa\xi}}\right) \qquad \text{(B-16)}$$

A good approximation to the erfc is given by[7,8]

$$\text{erfc}\left(\frac{r-a}{2\sqrt{\kappa t}}\right)$$

$$\approx 1 - \frac{r-a}{3.36\sqrt{\kappa t}} \qquad r - a < 3.36\sqrt{\kappa t}$$

$$\approx 0 \qquad r - a \geq 3.36\sqrt{\kappa t}$$

Using this approximation in (B-16), substituting the result in (B-15) and integrating under the condition of constant pressure buildup rate, $p(a,t) = mt$ we get

$$\int_a^b r^2\, p(r,t)\,dr =$$

$$.747\, a^2 \sqrt{\kappa/m}\left[p(a,t)\right]^{\frac{3}{2}} + \frac{.471 a\kappa}{m}\left[p(a,t)\right]^2 \qquad \text{(B-17)}$$

In Lueders and Indiana cores where the penetrating frac fluid case was investigated, we used $m = 1.2 \times 10^7$ and 2.4×10^7 dyne/cm^2 - sec, respectively. Substitution of these values along with the κ values listed in Table I and $b = 5.08$cm $- 32a$ into (B-17) shows that the second term in (B-9) is always negligible compared to the first. Therefore, Equation (B-9) reduces approximately to (B-10) for the lab case provided the restrictions given above are met.

We get total tangential stress at $r = a$ by superposing on the stress components (B-8) and (B-10) the tangential stress due to external loading. We use the equations of Southwell and Gough[22] for a small spherical cavity in a large cylinder. Axial stress S produces stresses at $r = a$ given by

$$\tau''_{\psi\psi} = \frac{3S}{2(7-5\nu)}\left[-1 - 5\nu + 10\cos^2\psi\right] \qquad \text{(B-18)}$$

$$\tau''_{\theta\theta} = \frac{3S}{2(7-5\nu)}\left[-1 - 5\nu + 10\nu\cos^2\psi\right] \qquad \text{(B-19)}$$

The minimum tangential stress (least compressive stress) τ_t due to a triaxial load can be obtained from these equations by superposing the stresses τ'_t, τ''_t and τ'''_t which are produced by applying S along the directions of σ_1, σ_2, and σ_3, respectively, in Figure 1. Thus, τ'_t is obtained by letting $S = \sigma_1$ and replacing ψ by $\psi + \pi/2$ in (B-18) and τ'''_t by letting $S = \sigma_3$ and $\psi = 0$ in (B-19). The result for $\psi = 0$ or π and $\sigma_2 \geq \sigma_1$ is

$$\tau_t = \frac{3}{2(7-5\nu)}\Big[(9-5\nu)\sigma_1 - (1+5\nu)\sigma_2 + (-1+5\nu)\sigma_3\Big] \qquad \text{(B-20)}$$

This equation has its minimum value when $\sigma_1 \leq \sigma_3 \leq \sigma_2$, that is σ_2 and σ_1 are the maximum and minimum compressive stresses, respectively. Under these conditions (B-20) agrees with the result obtained by Scheidegger[2] by a different procedure.

Adding (B-20) to each of Equations (B-8) and (B-10), setting the result equal to $-T$ and solving for $p(a,t) = p_f$ gives Equations (6) and (7) of the text. When $\alpha = 1$, these equations agree with results obtained by Le Tirant and Baron[4] using theory of elasticity for a non-porous material.

APPENDIX C

The hollow cylinder of Figure 2 has axial symmetry in cylindrical coordinates so the potential ϕ does not depend on θ and from (4)

$$e = \nabla^2\phi = \frac{1}{r}\frac{\partial}{\partial r}\left(r\frac{\partial\phi}{\partial r}\right) = Ap(r,t) + C(t) \qquad \text{(C-1)}$$

From (C-1) we determine e_{rr} in the same way as before. We assume e_{zz} is small enough so that $e_{\theta\theta} = e - e_{rr}$ which can be used with (3) and (5) to get

$$\tau'_{rr} = \frac{2\mu A}{r^2} g(r,t) - p(r,t) - (\mu + \lambda)C + \frac{2\mu K}{r^2} \qquad \text{(C-2)}$$

and

$$\tau'_{\theta\theta} = -\frac{2\mu A}{r^2}\, g(r,t) -$$

$$(\lambda A + \beta)p(r,t) - (\mu + \lambda)C - \frac{2\mu K}{r^2}$$

(C-3)

where $g(r,t) = \int r\, p(r,t)dr$. C and K are determined as before from (C-2) and boundary conditions which are the same as for the hollow sphere case except $g(r,t)$ replaces $f(r,t)$. For non-penetrating fluids, we then get at $r = a$

$$\tau'_{\theta\theta} = -p(a,t) \qquad \text{(C-4)}$$

for both the field case and the lab case as long as $b^2 \gg a^2$.

For a penetrating fluid, we get at $r = a$

$$\tau'_{\theta\theta} = \frac{-2\alpha}{b^2 - a^2}\left(\frac{1 - 2\nu}{1 - \nu}\right)\int_a^b rp(r,t)dr -$$

$$\left[\frac{2b^2}{b^2 - a^2} - \alpha\left(\frac{1 - 2\nu}{1 - \nu}\right)\right] p(a,t)$$

(C-5)

For the field case where $b \rightarrow \infty$ (C-5) reduces to

$$\tau'_{\theta\theta} = -\left[2 - \alpha\left(\frac{1 - 2\nu}{1 - \nu}\right)\right] p(a,t)$$

(C-6)

But for the lab case, the integral term in (C-5) must again be evaluated. We again consider fluid flow for an infinite medium and require the same experimental restrictions as before. We have

$$p(r,t) = m\int_0^t F(r,\xi)d\xi \qquad \text{(C-7)}$$

where[23]

$$F(r,\xi) = 1 + \frac{2}{\pi}\int_0^\infty e^{-\kappa u^2 \xi}$$

$$\left[\frac{J_0(ur)Y_0(ua) - Y_0(ur)J_0(ua)}{J_0^{\,2}(ua) + Y_0^{\,2}(ua)}\right]\frac{du}{u}$$

(C-8)

Computer evaluations have been made of the integral term in (C-5) using (C-7) and (C-8) with κ values from Table 1 and m values given earlier. These results show that the integral term is never more than 2% of the second term in (C-5) and therefore can be neglected. Thus (C-6) is a good approximation for $\tau'_{\theta\theta}$ in our experiments.

As before, the tangential stresses developed at $r = a$ by external loading must be added to (C-4) and (C-6). For a long enough cylindrical cavity stress variations along z can be neglected and tangential stress at $r = a$ will be given by[24]

$$\tau_t = \frac{b^2}{b^2 - a^2}(\sigma_1 + \sigma_2) - d(\sigma_1 - \sigma_2)\cos 2\theta$$

(C-9)

where

$$d = 2\,\frac{b^8 + a^4b^4 + a^6b^2 + a^2b^6}{b^8 - 4a^2b^6 + 6a^4b^4 - 4a^6b^2 + a^8}$$

For $\sigma_2 \geq \sigma_1$ the maximum negative value of τ_t (maximum tensile stress) is at $\theta = 0,\pi$ where for $b^2 \gg a^2$

$$\tau_t = -\sigma_1 + 3\sigma_2 \qquad \text{(C-10)}$$

Adding (C-10) to each of Equations (C-4) and (C-6) gives Equations (9) and (10) of the text. Equation (9) was first derived by Hubbert and Willis[1] using theory of elasticity for non-porous materials. Equation (10) has been derived for the field case by Haimson and Fairhurst[6] using analogies with thermoelasticity theory. It is also consistent with a result given by Geertsma[5] for the stress field induced by fluid penetration around a borehole in an infinite medium. An equation not much different from (10) is given in reference 6 for the lab case based on evaluation of the integral term in (C-5) by use of the diffusion equation. The diffusion equation is not applicable to the lab case even as an approximation unless the restrictions given above for p(b,t) are met.

TABLE I

ELASTIC CONSTANTS AND ROCK PROPERTIES

ROCK	E-STATIC **(dynes/cm^2)	*E-DYNAMIC (dynes/cm^2)	ν	f	k (md)	K (cm^2/dyne)	M (dyne/cm^2)	κ (cm^2/sec)
Lueders	3.0×10^{11}	3.5×10^{11}	.25	.19	1.0	5.0×10^{-12}	7.2×10^{10}	.43
Carthage	6.9×10^{11}	8.3×10^{11}	.30	.03	.04	1.7×10^{-12}	4.3×10^{11}	.093
Indiana	2.4×10^{11}	5.7×10^{6}	.16	.14	2.0	8.6×10^{-12}	9.2×10^{10}	1.0
Austin	2.1×10^{11}	2.1×10^{6}	.28	.33	1.5	6.5×10^{-12}	4.4×10^{10}	.40

*E-Dynamic determined from measurements of pulse velocity v in 1.0 in. dia. x 2.5 in. long cores at 100 kHz assuming $E = \rho v^2$

**To convert dynes/cm^2 to psi multiply by 1.45×10^{-5}

TABLE 2

FRACTURE ORIENTATION MEASURED AS ANGLE OF INCLINATION TO

$\sigma_1 - \sigma_2$ PLANE VS. σ_3/σ_1 IN SPHERICAL CAVITIES

σ_3/σ_1	NUMBER OF CORES VS. FRACTURE PLANE ANGLE-DEGREES								
	0-10	10-20	20-30	30-40	40-50	50-60	60-70	70-80	80-90
					LUEDERS CORES				
0.6	6								
0.7	6								
0.8	5								
0.9	2	1	1					1	
1.0	7	2			1		1		
1.1			2	1		1		1	2
1.2								1	10
1.3									4
1.4									8
					INDIANA CORES				
0.6	3								
0.8	7								
0.9	6		1	1		1		4	
1.0	7	3			1		1		
1.1				1		1	1		4
1.2									7
1.4									7
					AUSTIN CORES				
0.6	5								
0.8	5								
0.9	6	2							
1.0	4	1	3	1	2		1	2	3
1.1		1			1			1	5
1.2									8
1.4									9

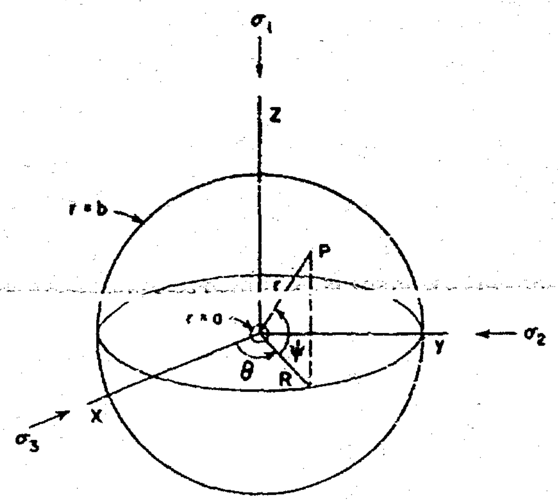

Fig. 1 - Hollow sphere representation of spherical cavity in a laboratory core or well.

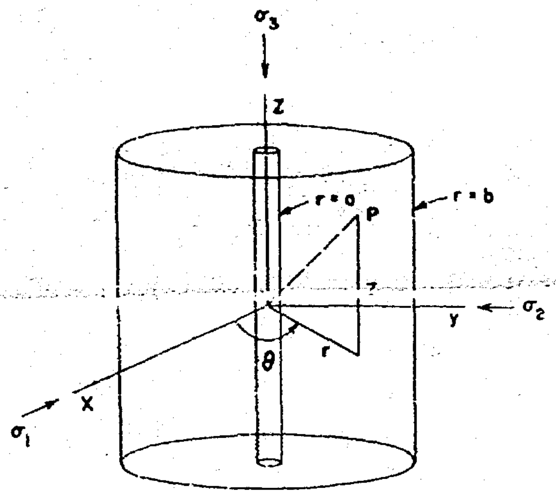

Fig. 2 - Long hollow cylinder representation of cylindrical cavity in a laboratory core or well.

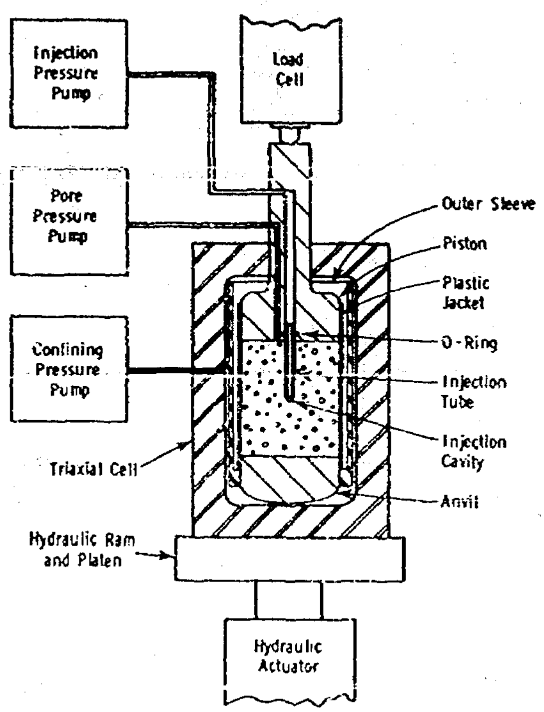

Fig. 3 - Experimental arrangement for applying confining pressure, end load, pore pressure and injection pressure to cores containing spherical or cylindrical cavities.

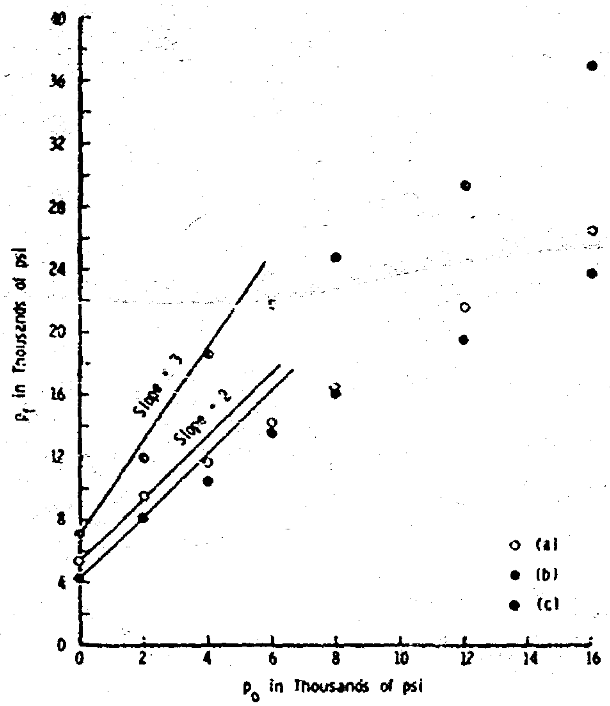

Fig. 4 - Fracture initiation pressure p_f vs hydrostatic confining stress p_o in saturated Lueders cores using non-penetrating heavy grease as frac fluid in: (a) type B cylindrical cavities coated with epoxy paint; (b) type B uncoated cylindrical cavities; (c) uncoated spherical cavities.

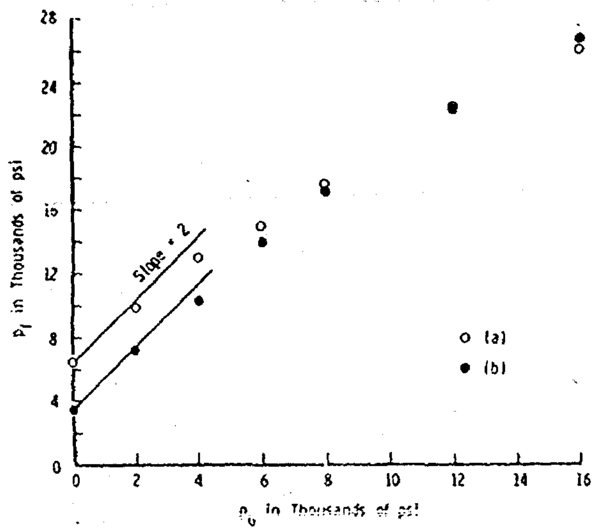

Fig. 5 - Fracture initiation pressure p_f vs hydrostatic confining stress p_o in saturated Lueders cores: (a) non-penetrating heavy grease as frac fluid; (b) penetrating vacuum pump oil as frac fluid.

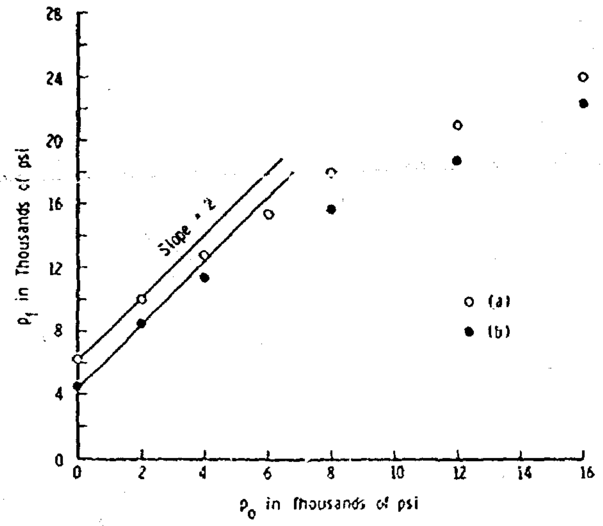

Fig. 6 - Fracture initiation pressure p_f vs hydrostatic confining stress p_o in dry Lueders cores with non-penetrating frac fluid in: (a) coated type B cylindrical cavities; (b) uncoated type B cylindrical cavities.

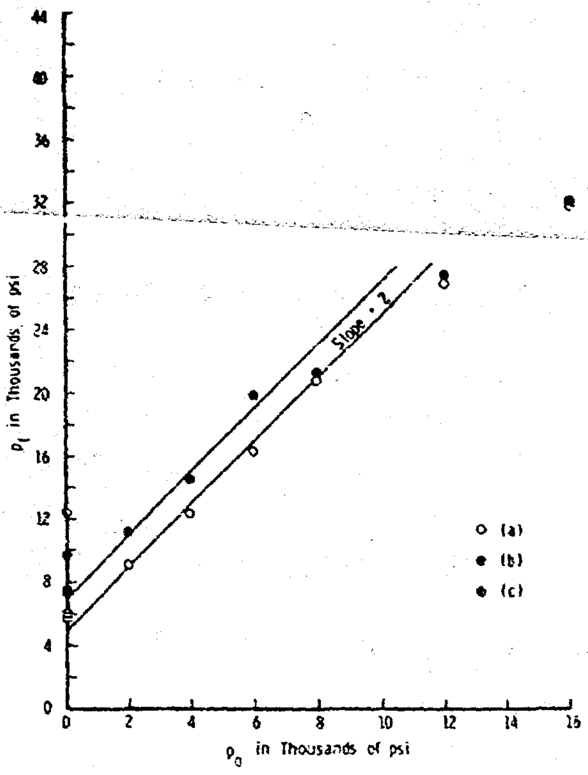

Fig. 7 - Fracture initiation pressure p_f vs hydrostatic confining stress p_o in carthage cores with non-penetrating frac fluid in type B cylindrical cavities: (a) saturated cores; (b) dry cores.

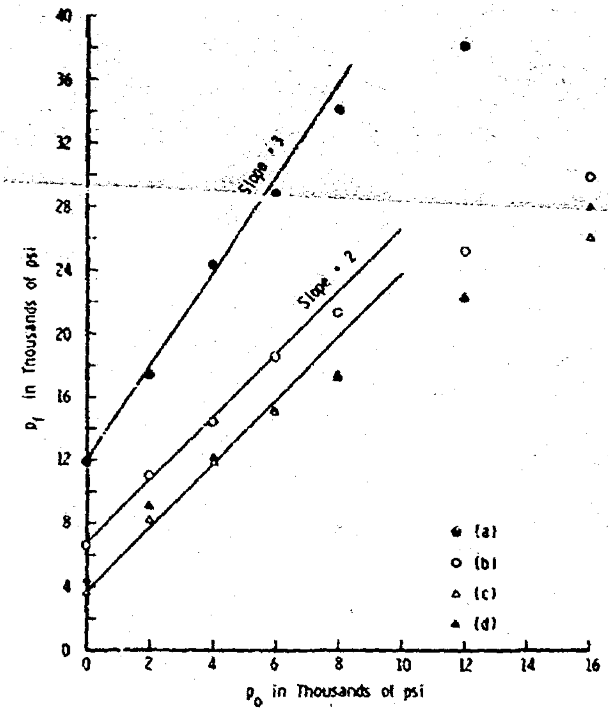

Fig. 8 - Fracture initiation pressure p_f vs hydrostatic confining stress p_o in Indiana cores: (a) non-penetrating frac fluid in saturated cores containing spherical cavities; (b) non-penetrating frac fluid in saturated cores containing type A cylindrical cavities; (c) Penetrating frac fluid in saturated cores containing type A cylindrical cavities; (d) non-penetrating frac fluid in dry cores containing type B cylindrical cavities.

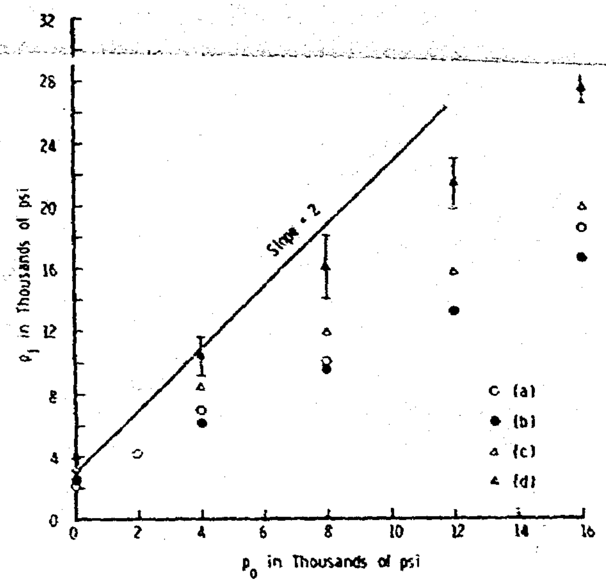

Fig. 9 - Fracture initiation pressure p_f vs hydrostatic confining stress p_o in Austin cores using non-penetrating frac fluid in (a) dry cores containing coated, type B cylindrical cavities; (b) dry cores containing uncoated, type B cylindrical cavities; (c) saturated cores containing type A, uncoated cylindrical cavities, (d) saturated cores containing uncoated spherical cavities.

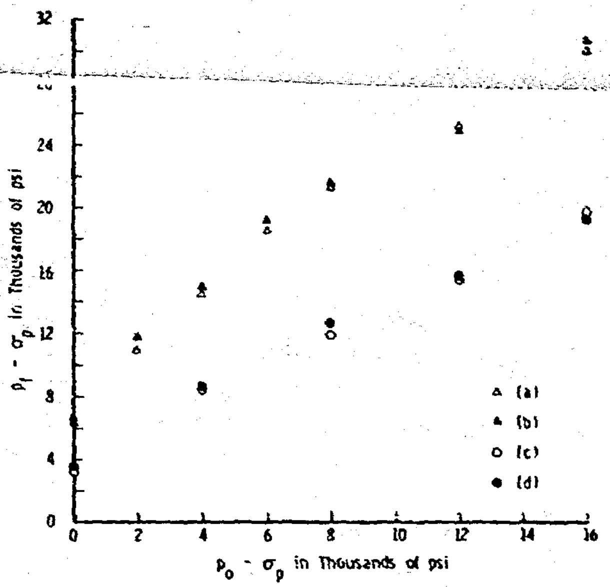

Fig. 10 - Effective fracture initiation pressure $p_f - \sigma_p$ vs effective hydrostatic confining stress $p_o - \sigma_p$ in experiments with pore pressure: (a) same as (b) points of figure 8 for Indiana cores with $\sigma_p = 0$; (b) - same as (a) except σ_p = 4000 psi; (c) same as (a) points of figure 9 for Austin cores with $\sigma_p = 0$; (d) same as (c) except with σ_p = 4000 psi.

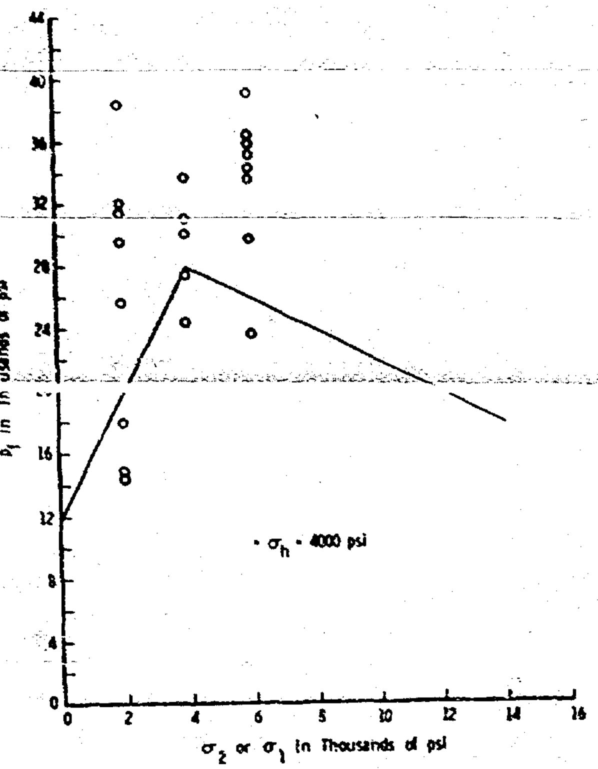

Fig. 11 - Fracture initiation pressure p_f vs end stress σ_1 in Indiana cores loaded under non-hydrostatic stress conditions with confining stress $\sigma_2 = \sigma_3 = 4000$ psi; theoritical ines computed from equations (6) and (8).

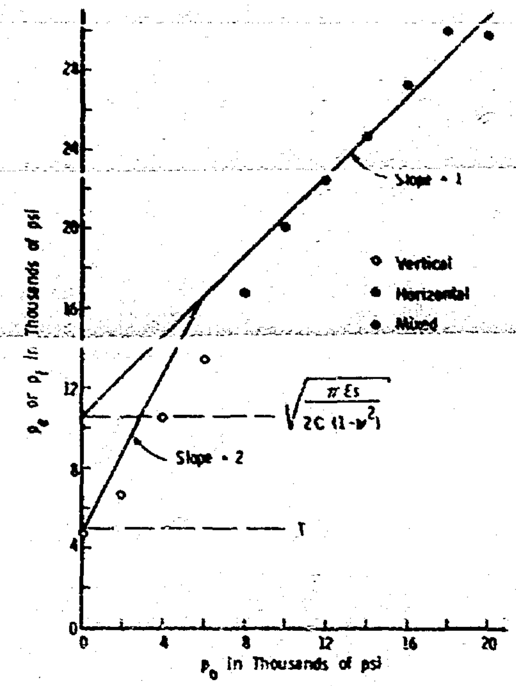

Fig. 12 - Failure pressure p_e or p_f vs hydrostatic confining stress p_o in dry carthage cores containing notched, type 8 cylindrical cavities.

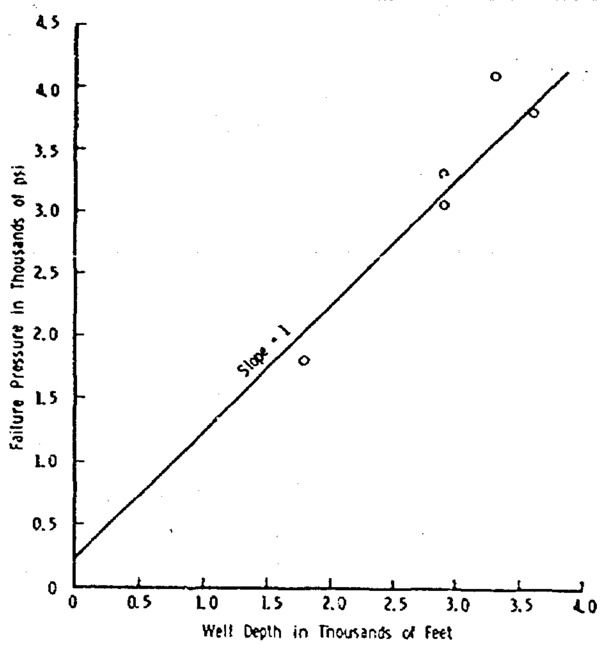

Fig. 13 - Failure pressure p_e or p_f vs hydrostatic confining stress p_o in dry Indiana cores containing notched, type B cylindrical cavities.

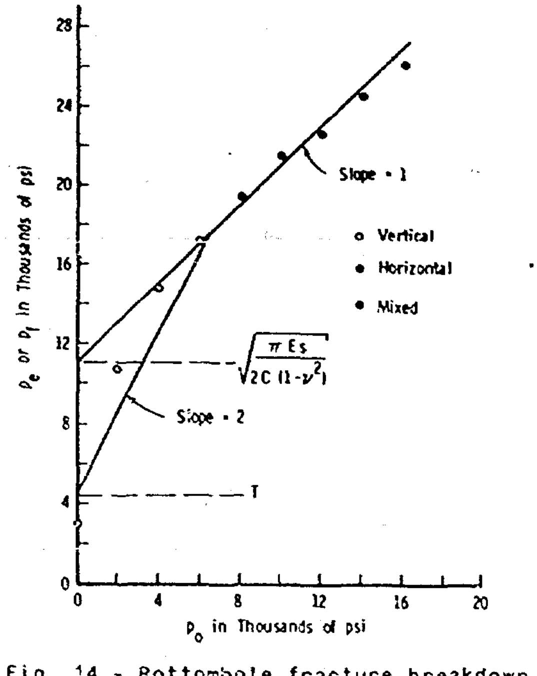

Fig. 14 - Bottomhole fracture breakdown measurements of Godbey and Hodges[12] and van Dam and Horner[13] vs depth.

SPE

Society of Petroleum Engineers of AIME

SPE 10308

BEFORE EXAMINER STAMETS
OIL CONSERVATION DIVISION
EXHIBIT NO. 3A+B+C
CASE NO. 7459
Submitted by
Hearing Date 3/16/82

Optimization of Stimulation Design Through the Use of In-Situ Stress Determination

by M.D. Voegele, A.S. Abou-Sayed,* and A.H. Jones,* Terra Tek, Inc.

*Member SPE-AIME

This paper was presented at the 56th Annual Fall Technical Conference and Exhibition of the Society of Petroleum Engineers of AIME, held in San Antonio, Texas, October 5-7, 1981. The material is subject to correction by the author. Permission to copy is restricted to an abstract of not more than 300 words. Write: 6200 N. Central Expressway, Dallas, Texas 75206.

ABSTRACT

The role of in-situ stresses in controlling hydraulic fracture geometry and extent has been widely recognized. This paper describes the results, and applications, of several research programs carried out over the past few years to optimize the design of hydraulic fracture stimulation treatments using information pertaining to in-situ stress action within the reservoir.

Initially started as fracture-mechanics based theoretical studies of propagation and containment of hydraulically induced fractures, these programs have grown into full-scale field demonstrations of the deduced principles. A review is provided of field measured in-situ stresses in the pay and confining formation. The existence of in-situ stress contrast between the pay zone and the bounding layers has been demonstrated in these field demonstrations. Furthermore, the results also showed the significant role of the in-situ contrasts in fracture containment. Unfortunately, however, a great variability in '' stress contrast from site to site has been observed. The field programs have been performed in both open hole and cased wells. Laboratory studies of hydraulically fractured large block samples have been carried out. Cubic samples up to one meter per side were subjected to triaxial stresses as high as 15 MPa. The results of these tests have been used to support the field efforts.

The programs described in the paper have indicated that successful stimulation design requires a knowledge of the in-situ stress field and contrasts within relatively narrow ranges at well depth where the stimulation treatment is to be performed. A general knowledge of the approximate regional stress fields and gradients is not a sufficient data base upon which design can be undertaken. Stimulation designs will have to be adapted to the in-situ stress contrasts to obtain deeply penetrating fractures. To minimize the costs of in-situ stress determinations on a well by well basis, a "wireline" operated hydraulic fracturing tool has been designed. The tool does not require a rig on the well in question; since it is entirely self-contained considerable cost savings will be possible when compared to the standard techniques of stress determination by hydraulic fracturing.

References and illustrations at end of paper.

INTRODUCTION

The design of fracturing treatments are generally based upon the assumption that the vertical height of the fracture is known, and that this height remains a constant from the wellbore to the point of deepest lateral penetration. This fracture geometry may be quite accurate in the presence of strong barriers to vertical fracture growth. In fact, MHF treatments with results consistent with deisng predictions, appear to be in reservoirs where the adjacent rock layers form effective barriers to vertical fracture growth (Murphy and Carney, 1977). One must expect, however, to encounter many situations in which natural barriers to vertical fracture migration do not exist.

The application of the fundamental principles of fracture mechanics has led to rapid development of both quantitative and qualitative predictions of hydraulic fracture growth and geometry based on knowledge of the in-situ material properties and in-situ stress. Recent studies of hydraulic fracturing (Simonson, et al., 1978) have delineated those factors that affect fracture geometry and fracture containment within the pay zone. These factors include (i) the contrast in material properties, (ii) the contrast in in-situ stress, (iii) the contrast in in-situ stress gradients and frac fluid density. Daneshy (1978), Cleary (1978) and Advani, et al, (1978) further discussed the effect of the contrast in material properties (including the interface) on the created fracture geometry. The material barrier concept (contrast in mechanical properties) appears to provide the basis of the success encountered in the Wattenberg experiment (Fast, et al., 1975). In this field, the pay zone had lower elastic moduli than the bounding shale layers. Table 1 summarizes the mechanical properties of the pay zone and bounding formation

Ex 3A

in various gas fields where MHF treatments had been performed. As is apparent from the data in the table, the *moduli* contrast, *does not* seem to prevail in many gas fields. While such data may be discouraging it does not necessarily follow that the lack of "material barriers" precludes the application of MHF treatments. An alternative, the stress barrier, shows significant promise in countering the lack of material barriers to contain an MHF within a pay zone. In fact, MHF appears very successful in the stimulation of the Cotton Valley Limestone, a formation which has no material-property barriers adjacent to the pay zone (Kozik and Holditch, 1981). In a case where there are no material barriers, the contrast in in-situ stress and stress gradient is essential to the treatment design. While absolute control of fracture growth within one zone would appear impossible, judicial pumping schedule design may provide the means of optimizing fracture growth within the pay zone, and guarantee a minimum excursion into the bounding layers.

ANALYSIS OF FRACTURE CONTAINMENT

The degree to which adjacent rock layers will impede the vertical growth of a hydraulic fracture being propagated in the pay zone is dependent upon contrasts or differences in elastic modulus and in-situ stress between layers. Simplified two dimensional analyses of the problem (Simonson, et al., 1978) indicate that as a fracture growing in the pay zone approaches the interface between the pay zone and the adjacent layer, its growth will be impeded if: (1) the shear modulus of the adjacent layer is greater than that of the pay zone; and, (2) if the minimum in-situ stress of the adjacent layer is greater than the minimum in-situ stress in the pay zone. Because the analyses of these conditions are generated using different simplifying assumptions of plane strain, their effects must be evaluated separately, and their cumulative effect cannot be assessed quantitatively. Methods of assessing their effects are summarized below from the work by Simonson, et al. (1978).

The Effect of Differing Material Properties

The effects of the variation in elastic properties between the pay and potential barrier layers on vertical fracture migration is best shown by examining the change in the stress intensity factor at the fracture tip, as it approaches the interface between the two distinct layers. This variation was first described by Simonson, et al. (1978), and it indicates that a bounding layer which has a higher shear modulus than the pay zone will impede the propagation of the fracture. This has since been supported by results from Advani (1978) and by Cleary (1978) who states that "the stiffer adjacent stratum does indeed present the greatest (and persistent) resistance to continued fracturing."

Table 1 summarizes the analysis of core samples recovered from various gas wells throughout the country. A review of the data indicates that in most cases, a strong contrast does not exist between elastic moduli of the rock forming the pay and adjacent layers. Furthermore, the large degree of scatter generally found in the elastic properties of rock, suggests that a material property barrier cannot be relied on to provide consistent resistance to fracture growth.

In-situ stress contrasts, on the other hand offer the advantage of being measured with relative ease in terms of effort expended (but, at the present time at considerable cost and downtime for a rig) in numerous positions throughout the length of a borehole. With the knowledge of the in-situ stresses in various pay zones within the same well, it is a simple matter to select those zones with favorable in-situ stress contrasts for concentration of MHF efforts.

The Effects of In-Situ Stress Contrasts on Fracture Containment

The analysis of the effect of different minimum horizontal in-situ stress conditions between adjacent layers is based upon a fracture which has already penetrated into the non-productive layer. Simonson, et al. (1978) present the solution to the following two dimensional problem (See Figure 1) where the minimum horizontal in-situ stress in the adjacent layers (σ_b) is greater than the minimum horizontal in-situ stress in the pay zone (σ_a). The effect of the stress difference can be shown by the variation in excess treating pressure, as in Equation 1.

$$(P - P_o) = \left(\frac{K_{Ic}}{\sqrt{\pi L}}\right)\left(\frac{1}{\sqrt{1+\varepsilon}} - 1\right) + \frac{2(\sigma_b - \sigma_a)}{\pi}\cos^{-1}\left(\frac{1}{1+\varepsilon}\right) \quad (1)$$

where P_o = Pressure required to extend the fracture to the pay zone/bounding layer interface.

P = Pressure required to extend the fracture when it has penetrated into the overstressed layer.

$2L$ = Height of the pay zone

2ℓ = Height of the fracture

$\varepsilon = \frac{\ell}{L} - 1$

K_{Ic} = Critical stress intensity factor of the adjacent layer.

The excess treating pressure as a function of fracture penetration into the barrier (for various stress contrasts) is shown in Figure 2. The figure shows that the initial penetration into the overstressed region requires a considerable increase in pressure (above the pay zone propagation pressure, P_o). Small fracture incursions into a bounding layer with a greater in-situ stress contrast (500 to 1000 psi) would require substantial increases in treating pressure.

Simonson, et al. (1978) suggest that the magnitude of the in-situ stress gradient might also be used to control vertical fracture propagation. By examining the stress intensity factors for the top and bottom of the fracture, one may generate the following expression.

$$K_{I\ BOTTOM} - K_{I\ TOP} = (g_{fluid} - g_{rock})\ \ell\sqrt{\pi\ell} \quad (2)$$

where K_I = Stress intensity factor

g_{fluid} = Pressure gradient of the fracturing fluid

g_{rock} = Gradient of the minimum in-situ stress

ℓ = Fracture height

Since propagation begins when K_I becomes greater than some critical value for the material (K_{Ic}), one can see that the downward (upward) growth will be favored if g_{fluid} is greater (less) than g_{rock}. This result suggests that frac fluid density can be used to help contain a fracture, if one of the bounding layers does not form an effective barrier.

IN-SITU STRESS DETERMINATION IN DEEP WELLS

At the present time the only technique which has been demonstrated to be viable for in-situ stress determinations at depths greater than a few hundred meters is a small scale hydraulic fracturing operation. The technique is well understood and frequently demonstrated for open hole operations (Haimson, 1978; Bredehoeft et al, 1976; Zoback and Pollard, 1978). Other techniques, utilizing for example strain relief or velocity birefringence, are proposed from time to time, but to date none have been successfully demonstrated in a deep hole. Furthermore, none of these proposed techniques could possibly work in a cased well. On the other hand, suggesting to an operator that one be allowed to emplace a tool in a portion of a hole that is open because it has not yet been cased, especially if the hole is deep, one is met with a look which has to be experienced to be believed.

The state-of-the-art then, today, is that a technique exists for stress determination at depth, but it is best understood for open hole conditions. Very little data has been published (Daneshy, 1973) with regard to stress determination in cased wells; however, because of the costs incurred if a tool should become jammed in an open portion of the hole, stress determinations must be typically carried out in cased wells.

A series of laboratory tests were thus performed to determine the feasibility of using the hydraulic fracturing technique as a means of in-situ stress determination in cased wellbores. The objective of these tests was to determine whether the stresses, in particular the minimum horizontal stress, applied to the specimens could be estimated by analysis of the pressure-time records obtained during the hydraulic fracturing of the specimens.

The majority of these tests were performed in 30 cm x 30 cm x 45 cm specimens of hydrostone Super-X loaded in triaxial compression. API standard 7 in. O.D. - 23 lb/ft casing was simulated using 28.6 mm x 26 mm steel tubing which was centered in the modl before casting. The samples and casing were perforated using a small right angle drive drill which was positioned inside the casing with a rod. These perforations were approximately 3 mm in diameter and extended approximately 8 mm into the hydrostone.

Two perforation configurations were used in these tests. These consisted of either: two perforations drilled 180° apart at the mid-point of the sample; or perforations drilled in a helical arrangement. The helical perforations were confined to the middle one-third of the specimen and were located 1.0 cm apart along the axis of the casing and 30° apart tangentially around the casing.

Samples with the 180° perforations were tested with the perforations oriented at 0° and 90° to the maximum horizontal stress. The purpose of these tests was to determine whether the fracture direction would be controlled by perforation orientation or, as suggested by Daneshy (1973), the fracture would be properly oriented parallel to the maximum stress) independent of perforation orientation.

It was found that the fractures always initiated through the perforations even when the perforations were oriented at 90° to the maximum stress. It was also found that these fractures re-oriented themselves as the extended. Even though these fractures became re-orientated, it was not possible to reliably estimate the applied stresses from the pressure-time records. This is not surprising in that the fracture paths were somewhat tortuous and that the pressures were measured in the wellbore and hence would be a measure of some average stress acting perpendicular to the fracture. It is also likely that the method used to create the perforations led to a more realistic simulation than that used by Daneshy. The post shut-in portion of the pressure-time records could, perhaps, yield information as to the state of stress acting perpendicularly to the fracture at various locations, however, such an analysis is beyond the present state-of-the-art and would require more work in numerical modeling and experimental verification before such an analysis could be considered valid.

By perforating the wellbore with a helical pattern, there is a very good chance that one perforation will be oriented in or very near to the direction of the maximum horizontal stress and as such the fracture would initiate in the proper orientation. Results of the tests performed with the helically perforated specimens show that this is indeed the case.

In general it was found that the induced fracture initiated from one perforation, in the proper orientation. There was some indication of several perforations being intersected by the induced fractures; however, this may be due to the rather close spacing of the perforations along the casing. For the most part the fractures were planar and oriented in the proper direction by the time they had propagated to several wellbore diameters into the rock mass.

For those cases where the preferred fracture orientation was vertical (the vertical stress was the intermediate or maximum principal stress) it was found that the instantaneous shut-in pressure was a reliable estimate of the minimum applied horizontal stress when analysis techniques based upon minimum reopening and shut-in pressures were utilized. The estimation of the maximum horizontal stress were not so straightforward; it must be borne in mind that the actual presence of the casing in the wellbore coupled with the cementing pressure history to which the casing has been subjected present a marked deviation from the standard open hole case upon which the interpretive theory is based. Nonetheless, it was found that for vertical fractures a reasonable estimate of the maximum horizontal stress could be estimated from the minimum reopening and shut-in pressures. This is not too surprising in light of the minimum level of interaction to be expected between the medium and the relatively flexible inclusion represented by the casing.

For those cases where the preferred fracture orientation was horizontal (the vertical stress was the minimum principal stress) the instantaneous shut-in pressure could not be always related directly to the minimum principal stress. For tests in larger blocks the relationship between instantaneous shut-in pressure and minimum principal stress was observed although the fracture had to be extended a significant distance from the wellbore before this was so. As expected the other two principal stresses were not calculable from the data since standard interpretive techniques are based upon stress concentrations around wellbores and fractures propagating parallel to the wellbore. A strictly correct interpretive technique for horizontal fractures would probably require an analysis based upon fracture growth in two directions.

APPLICATION OF IN-SITU STRESS DETERMINATION TO FRACTURE DESIGN

The stress state within a given region is typically consistent to the extent that at least its orientation remains fairly constant, as illustrated in Figure 3. This figure is a compilation based upon geologic evidence as well as in-situ stress measurements and illustrates the stress state in terms of stress regimes, each with a different potential for faulting. As can be seen in those areas where several data points exist the orientation is relatively constant; also, the boundaries between areas of relatively constant orientation are fairly well delineated. When magnitude as well is considered, however, a different picture emerges. Figure 4 is a compilation of data from publishable in-situ stress measurements; it is separated according to rock type. The stress difference axis is primarily an indication of preferred fracture plane; a positive stress difference indicates a preferential vertical fracture. Furthermore, a high differential stress is indicative of a stronger material. It is also a convenient axis to compare points from the same region to examine relative containment potential of the different horizons. For example, examine the cluster of data points at $\sigma_v = 90$, and $20 < (\sigma_v - \sigma_{HMIN}) < 30$; these six points are from two wells within 1 km of each other. Two interesting points can be observed, namely; (i) the stress differences between the shales and sandstones; and (ii) the scatter in the data. There is also an interesting trend in the figure which supports a qualitative correlation between stress difference and rock type (Figure 5) as suggested by Abou-Sayed, et al (1981). There is a strong theoretical basis for this correlation. General laboratory response of granites, sedimentary rocks and salt to applied loads implies that soft, high ductility material (higher principal strain ratio during inelastic flow) as well as materials not capable of sustaining large deviatoric stresses (low principal stress ratio in uniaxial strain tests) possess higher minimum horizontal stresses. In the elastic regime this response has widely been attributed to Poisson's ratio effects. Examination of Figures 6(a) through (e) illustrates that there is strong field evidence to support this qualitative observation. Close examination of Figure 6(e), however, illustrates an important point; although the general trend is seen to exist, it must be concluded that, owing to the overlap of the boundaries, it does not make sense to try to design for containment on the basis of lithology alone. This boundary overlap reinforces the requirement of in-situ stress measurement on a case by case basis.

To further illustrate the concepts discussed in this paper, it is illustrative to examine several case histories.

Fracture Containment Studies in the Devonian Shales

An extensive program to characterize the material properties and the in-situ stresses was conducted on Columbia Gas Wells #20402 and #20403. The results indicated that the elastic moduli of the various shale layers were comparable, and that although the gray shales were, in general, stiffer than the brown shales, the difference was not great enough for the gray shales to form fracture barriers. The in-situ stress was measured in the upper gray shale, and this measurement coupled with local geologic structure, field observation and elastic properties was used to calculate the following in-situ stress profiles (Jones et al., 1977). Figure 7 indicates that the brown shales will not impede the growth of fractures being propagated in the gray shales. This is supported by field evidence reported by McKetta (1977) who notes that a fracture initiated in the lower gray shale propagated upward into the middle brown shale. Analysis of the specific layers produced the following treating pressure limits. Because of the limited potential for fracture containment and possibility of subsequent connection of fractures created by multi-stage treatments, the best results should be obtained when the reservoir formation most suitable for fracture containment is fractured first.

Fracture Containment Analysis in the Benson Sandstone

A series of four in-situ stress measurements were conducted in Columbia Gas Well 20538-T. The minimum horizontal stress was measured in the lower shale, sandstone pay and upper shale. The measurements revealed a 480 psi (3.3 MPa) difference between the upper shale and the sandstone pay zone. The difference between the lower shale and pay zone was only 130 psi (0.9 MPa). The distribution of stress in the different layers is shown in Figure 8 (Abou-Sayed, et al, 1978). The core analysis on this well revealed that the moduli of the adjacent shale layers were comparable, or less than the Benson sandstone. Only the in-situ stress contrast would provide containment. The situation was subsequently analyzed to determine the maximum allowable treating pressure. A schematic representation of the analysis is shown in Figure 9 (Abou-Sayed, et al, 1978). This analysis incorporates both the in-situ stress contrast measured in Well 20538-T, and the effect of frac fluid density. The calculations were performed for three different types of fracturing fluids, used commonly in this area of the United States. Results of the calculations are summarized in Table III. The results indicate that although the upper shale does provide a degree of containment, the lower shale allows a downward migration of the fracture, roughly 5 to 7 times the degree of upward penetration. The bottom hole treating pressure must be controlled very closely to maintain any degree of containment; maximum pressure variation should be 50 to 185 psi (0.4 to 1.3 MPa) at the surface.

Fracture Design in the Pinedale Field

In-situ stress measurements were performed in Mountain Fuel Mesa Unit Wells #1 and #2 in the Pinedale Field; the wells are separated by a distance of approximately 1.0 km. Six measurements were carried out in the same pay sand and bounding shale layers. The wells were cased and later perforated using a helical arrangement. The measurement indicate the existence of a higher in-situ stress within the shale layers. A difference of 5.3 MPa exists between the stresses in the upper shale and the pay zone while the lower shale shows a 5.6 MPa higher stress than the pay sand. Such in-situ stress contrast is favorable for fracture containment. This data was analyzed to correlate the maximum allowable downhole treatment pressure with the total frcture height and penetration into the barrier layers. Figure 10 shows a profile for the minimum in-situ in Well #2 along with such correlation. Fracture treatment design was based on the information obtained in the field along with laboratory determined fracture conductivity tests (Ahmed, et al., 1981).

Application of Fracture Geometry to Thick or Massive Formations

Recent work by Abou-Sayed et al. (1978) illustrates the advancement of predictive capabilities in the field of hydraulic fracture analysis. This work applies to thick or massive formations, and predicts the effect of frac fluid gradients on the geometry of fractures being propagated in these formations. The type of geometry is shown in Figure 11 (Abou-Sayed et al., 1978b) as a function of relationship of minimum horizontal in-situ stress gradient (g_{rock}) versus frac fluid density pressure gradient (g_{fluid}). Abou-Sayed, et al (1978) noted that downward or upward fracture growth may be achieved (if enough measurements of in-situ stress have been made to characterize the minimum horizontal in-situ stress gradient within a thick or massive formation, and the density of the frac fluid is adjusted accordingly).

This geometric analysis has application to thick pay formations, which exhibit very localized gas concentrations. It may be advantageous to concentrate perforations at a particular depth in the formation so that the amount of fracture created in the productive portion of the pay formation can be optimized. As Figure 7 shows, the amount of fracture created in the producing zone is not appreciably different, even though the larger fracture is nearly twice the size of the smaller fracture.

CONCLUSION

The preceding examples have illustrated that there can indeed be significant variations, other than those due to gradient, of horizontal stresses within a given well as well as in different wells within a given region. To optimize the stimulation design in a well there is, of necessity, a requirement to determine the stress state, in-situ, of those horizons which are potential targets for massive stimulation. From the viewpoint of production, it can be far too costly to have a drilling rig and its crew standing by while stress measurements are made, so most measurements of this type are made when a workover rig is on the hole. The logistic problems associated with non-production people being on site running a non-standardized borehole test lead to delays and it is not unusual to expend several days time before the first data point is acquired. What is needed is a rapid method, similar conceptually to a production logging operation, whereby the in-situ stress state can be determined, rapidly, at multiple horizons along the borehole length. At the present time, it appears that the only way that this goal can be obtained is through the use of a wireline hydraulic fracturing logging tool. Such a tool design has recently been completed for DOE/METC by Terra Tek, Inc.

The design of any downhole tool is a complex process. The tool must be able to perform its function under a variety of harsh downhole conditions, thousands of feet deep inside a very expensive hole in the ground. If it is to be useful and therefore used regularly, it must be economically feasible to build, relatively quick and easy to use, and most importantly, it must be relible in that it can be removed from the borehole without damaging the well.

A list of the original design requirements for this particular tool reveals some of the problems to be solved:

1. Hole depths from near surface to 10,000 feet (3000 m) deep.

2. Boreholes that are dry or filled with water, drilling mud, or other liquids.

3. Corresponding variable working pressures from atmospheric to several hundred atmospheres.

4. Boreholes that are smooth, deteriorated, washed out, straight, crooked, cased or uncased through a wide variety of rock.

5. Downhole operating temperatures from surface conditions to geothermal (100°C).

6. If possible, the tool should be able to function on a standard cable currently used for other purposes.

Careful consideration of the requirements and possibilities for a wireline fracturing tool has consistently suggested that no single tool is the best solution to all possible downhole conditions. Indeed, the tool design should be selected based on the actual conditions for which it will be used most of the time. The major hole conditions that must be considered in selecting the tool are whether or not the hole is cased (which can affect the fracture detection device); whether or not the borehole is fluid filled (which dictates the need for a self-contained reservoir); and the most serious, the type of borehole fluid.

The tool design which is presented in this report meets or exceeds all of the original design requirements with the exception of number six. The preliminary design phase of this project indicated that it probably would not be possible to transmit sufficient electrical power downhole on a standard wireline cable, that these power levels would severely hamper the function of the downhole control circuitry, and insufficient pull strength would be available to pull the tool should it become jammed. Accordingly, the tool design is based upon a fluid wireline which will be used in conjunction with an armored electrical wireline.

The wireline hydraulic fracturing tool design is modular in nature, utilizes off-the-shelf components and is illustrated in Figure 13. The tool design is based upon a Lynes surface controlled inflatable production injection packer; the majority of other components facilitate downhole control of the tool. Fundamental to operation in this mode is a microprocessor based controller with a bidirectional communication line running to the surface (which also transmits power). Both the hardware and software of the controller exist as they were developed independently for another geophysical logging tool. In response to signals from the surface the controller manipulates valves and sends acquired data, mainly pressure/time history to the surface where it is recorded. Should the tool become jammed in the well the cable and conduit can be disconnected by exploding bolts and a standard API thread exposed for fishing. Finally, the tool design incorporates a radial differential temperature logging tool (Cooke, 1978) to be used in an attempt to locate fractures behind casing. The tool scans temperature circumferentially and it is felt that the temperature contrast between the strata and fluid from the surface will present an anomaly that should be detectable.

The availability of in-situ stress data and the knowledge of the role that it and other rock mechanics parameters have in the physical process of fracture growth and containment, has led to the initiation of comprehensive modeling programs which have as their goal the prediction of fracture geometry. A number of such efforts are presently underway; recent fracture geometry prediction simulators (c.f. Clifton and Abou-Sayed, 1981) represent an advanced level of modeling that incorporates three dimensional fracture geometry as well as variations in the stress field with depth. With the types of data which are now becoming available from field investigations coupled with laboratory measurements, better guidelines can now be provided for operations such as fracturing close to acquifers, limited entry methods for multiple sands (continuous and lenticular) and more economic treatments of lower permeability sands.

There is a demonstrated need for in-situ stress data and for a logging tool to perform in-situ stress determinations by hydraulic fracturing, on a routine basis, as an aid to optimizing stimulation design. The tool design is complete; the remaining challenge is to get the prototype tool into the field.

REFERENCES

Abou-Sayed, A.S., Brechtel, C.E. and Clifton, R.J., 1978a, "In-Situ Stress Determination by Hydrofracturing - A Fracture Mechanics Approach", Journal of Geophysical Research, Vol. 83, No. 86.

Abou-Sayed, A.S., Jones, A.H. and Simonson, E.R., 1978b, "On the Stimulation of Geothermal Reservoir by Downward Hydraulic Fracturing", ASME Paper 77 PET 81.

Abou-Sayed, A.S., Ahmed, U. and Jones, A., 1981, Systematic Approach to Massive Hydraulic Fracturing Design", SPE 9877.

Advani, S.H., Gangarao, H., Chang, H., Komar, C. and Khan, 1978, "Hydraulic Fracture Modeling for the Eastern Gas Shales Program", Second Eastern Gas Shales Symposium, Vol. 1, DOE/METC.

Ahmed, U., Schatz, J.F., Greenfield, H. and Jones, A.H., "Optimized Stimulation of Tight Sands in the Pinedale Field, Wyoming", Proceeding of the 16th Intersociety Energy Conversion Engineering Conference, Atlanta, Georgia, August, 1981.

Bredehoeft, J.D., Wolf, R., Keys, W. and Shuter, E., 1976, "Hydraulic Fracturing to Determine the Regional In-Situ Stress Field, Piceance Basin, Colorado", GSA Bul. 87, pp. 250-258.

Cleary, M.P., 1978, "Primary Factors Governing Hydraulic Fractures in Heterogeneous Stratified Porous Formations", ASME 78 PET 47.

Clifton, R.J., and Abou-Sayed, A.S., 1981, "A Variational Approach to the Prediction of the Three Dimensional Geometry of Hydraulic Fractures, SPE/DOE 9879.

Cooke, C., 1978, "Radial Differential Temperature Logging - A New Tool for Detecting and Treating Flow Behind Casing", SPE 7558.

Daneshy, A.A., 1973, "Experimental Investigation of Hydraulic Fracturing Through Perforations", JPT, October, pp. 1201-1207.

Daneshy, A.A., 1978, "Hydraulic Fracture Propagation in Layered Formations", JPT, Vol. 18, No. 1.

Fast, C.R., Holmar, G. and Covlin, R., 1975, "A Study of the Application of MHF to the Tight Muddy "J" Formation, Wattenberg Field, Adams and Weld Counties, Colorado", SPE 5624.

Haimson, B.C., 1978, "Crustal Stress in the Continental United States as Derived from Hydrofracturing Tests", in J.C. Heacock, ed: The Earth's Crust, Geophys. Monograph Series, Vol. 20 AGU.

Jones, A. Abou-Sayed, A.S. and Rogers, L., 1977, "Rock Mechanics Aspects of MHF Design in Eastern Devonian Shale Gas Reservoirs", Terra Tek Report TR 77-63.

Kozik, H.G. and Holditch, S., 1981, "A Case History for Massive Hydraulic Fracturing the Cotton Valley Lime Matrix Fallon and Personville Fields", JPT Vol. 33, pp. 229-244.

Lindner, E. and Halpern, J., 1978, "In-Situ Stress in North America: A Compilation", Int. Jour. Rock Mech. Min. Sci., Vol. 15, No. 4, pp 183-204.

McKetta, S., 1977, "Columbia Gas System Services, Personal Communication.

Murphy, D. and Carney, M., 1977, "Massive FRAC - A Second Look", Proc. of Massive Hydraulic Fracturing, University of Oklahoma.

Simonson, E.R., Abou-Sayed, A.S. and Jones, A.H., 1978, "Containment of Massive Hydraulic Fractures", JPT, Vol. 14, No. 1.

Swolfs, H.S., 1981, "The Triangular Stress Diagram, A Graphical Representation of Crustal Stress Measurements", USGS Professional Paper, In Press.

Zoback, M. and Pollard, D., 1978, "Hydraulic Fracture Propagation and Interpretation of Pressure Time Records for In-Situ Stress Determinations", 19th Symposium on Rock Mechanics, Stateline, NV.

Zoback, M. and Zoback, M., 1980, "State of Stress in Conterminous United States", Journal of Geophysical Research, Vol. 85, No. B-11, November

TABLE I

MODULI CONTRAST FOR TIGHT GAS RESERVOIRS

Well Name	Rock Type	Young's Modulus (10^6 psi)
Rio Blanco		
Upper Barrier	Siltstone	7.74
Pay Zone	Sandstone	6.97
Lower Barrier	Shale	8.63
Wagon Wheel		
Upper Barrier	Shale	1.04
Pay Zone	Sandstone	2.76
Lower Barrier	----	----
Proprietary #2		
Upper Barrier	Shale	4.98
Pay Zone	Sandstone	1.85
Lower Barrier	----	----
Berea #20342		
Upper Barrier	Shale	4.78
Pay Zone	Sandstone	5.71
Lower Barrier	Shale	5.10
Canyon Largo #256		
Upper Barrier	----	----
Pay Zone	Sandstone	4.32
Lower Barrier	Siltstone	1.09
Martin Well #20336		
Upper Barrier	Shale	4.92
Pay Zone	Shale	4.60
Lower Barrier	Shale	6.10
Proprietary #1		
Upper Barrier	Shale	5.65
Pay Zone	Sandstone	5.89
Lower Barrier	Slate	1.75

TABLE II

Recommended Treating Pressures for Fracturing in Columbia Wells #20402 and #20403

ZONE	MAXIMUM PRESSURE ABOVE ISIP* (psi)
Upper Brown	200
Middle Brown	400
Lower Gray	250
Lower Brown	250

* ISIP - Instantaneous Shut-In Pressure

TABLE III

RESULTS OF THE CONTAINMENT ANALYSIS CONDUCTED ON COLUMBIA WELL [illegible]

Fracturing Fluid Type and Gradient (psi/ft)	In-Formation Treatment Pressure (psi)	[illegible] Upper Shale (ft)	[illegible] Lower Shale (ft)	[illegible]
Foam, 75% Gas, 25% Water ([illegible])	1857	[illegible]	[illegible]	[illegible]
	2095	[illegible]	[illegible]	[illegible]
	2125	55	[illegible]	[illegible]
CO_2 Gelled Water, 25% CO_2 ([illegible])	1857	[illegible]	[illegible]	[illegible]
	[illegible]	7	[illegible]	[illegible]
	2125	[illegible]	[illegible]	[illegible]
Gelled Water ([illegible])	[illegible]	[illegible]	[illegible]	[illegible]
	[illegible]	[illegible]	[illegible]	[illegible]
	2125	[illegible]	[illegible]	[illegible]

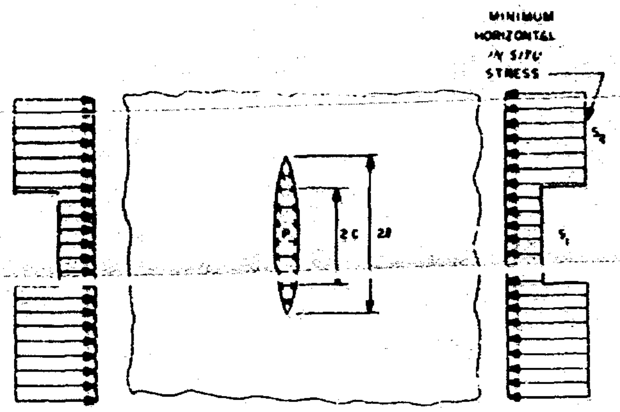

Fig. 1 – Vertical hydraulic fracture loaded under uniform pressure (P) with differing horizontal in-situ stress (Simonson, *et al.*, 1978).

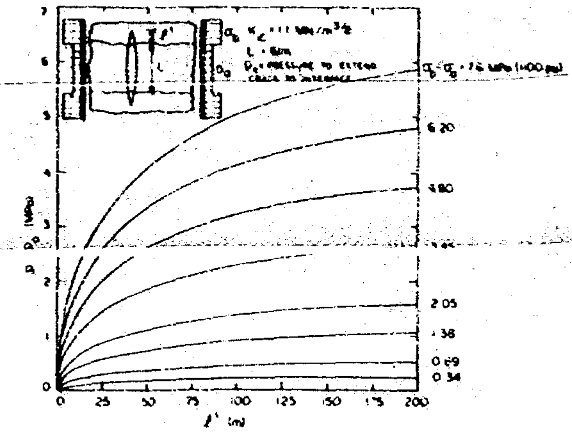

Fig. 2 – Plot of excess treating pressure ($P - P_a$) vs. extension into bounding layers as a function of contrast in the minimum horizontal stress in the confining layers.

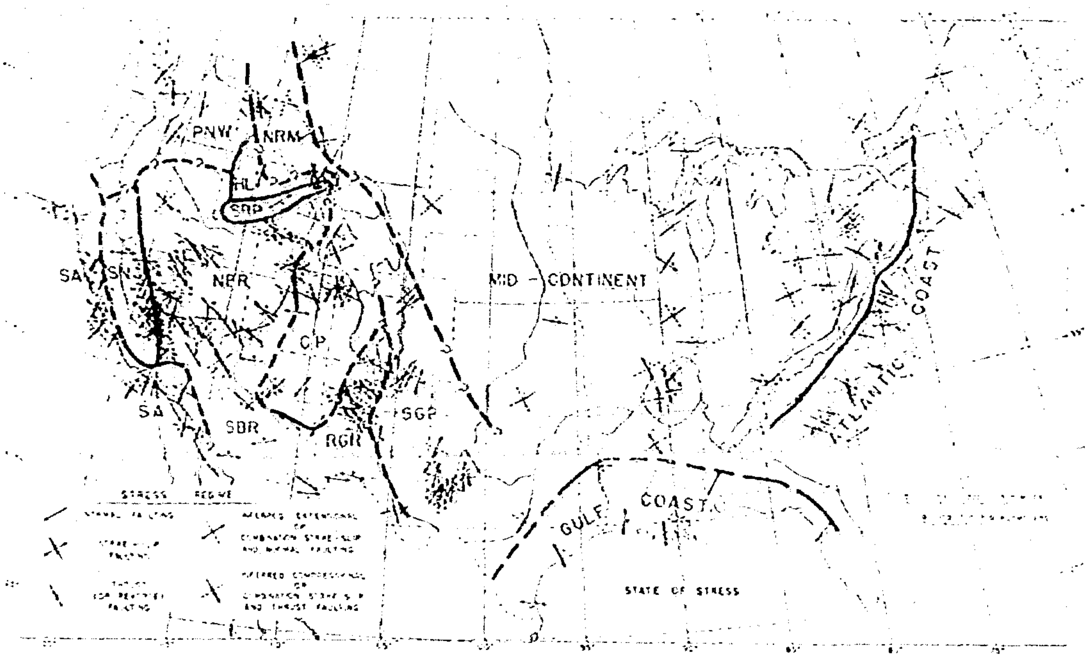

Fig. 3 – Stress regimes in the conterminous United States illustrating the consistency of orientation within a given regime (Zoback and Zoback, 1980).

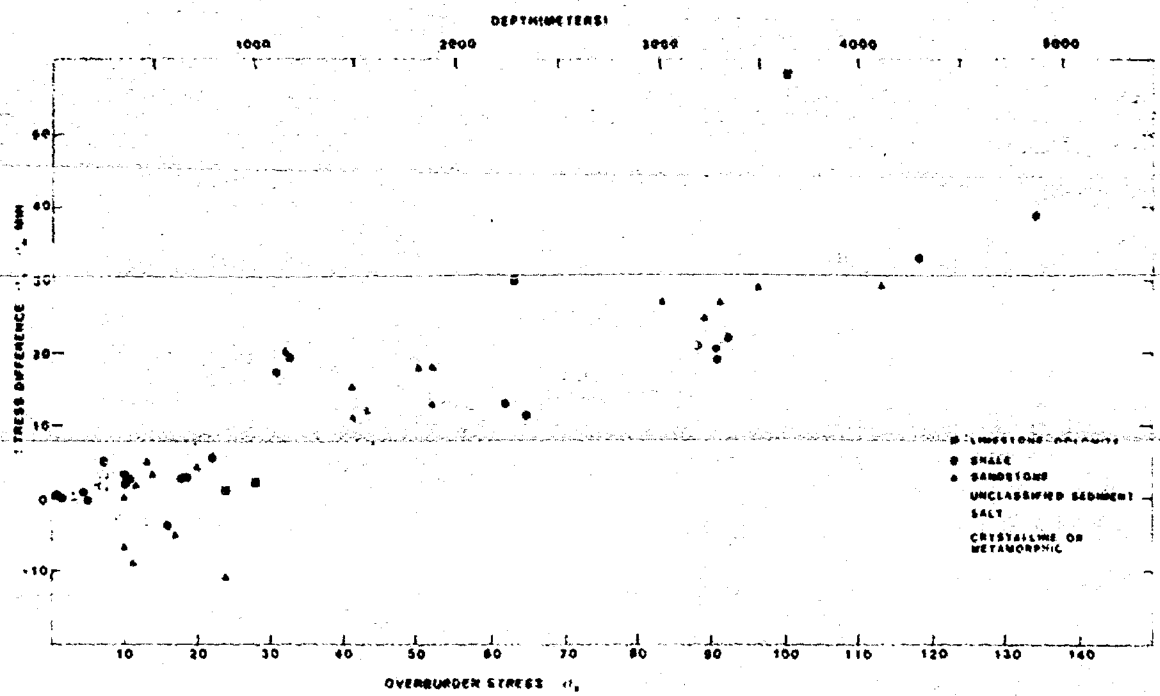

Fig. 4 – Data base of in-situ stress measurements plotted as to rock type (Lindner and Halpern, 1978; Swolfs, 1981; and Terra Tek Project Files), stress in MPa.

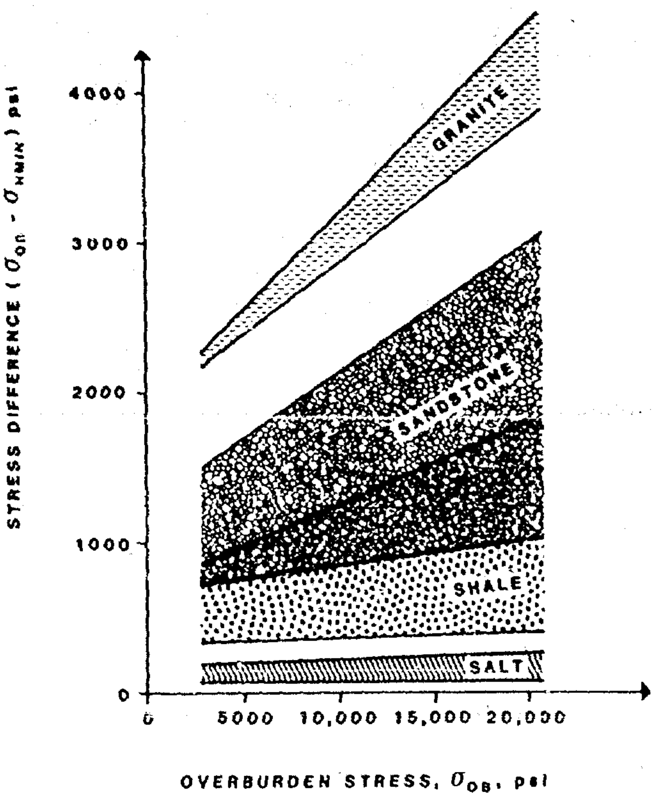

Fig. 5 – Qualitative correlation between stress difference ($\phi_{OB} - \phi_{H\,min}$) for various rock types (Abou-Sayed, *et al.*, 1981).

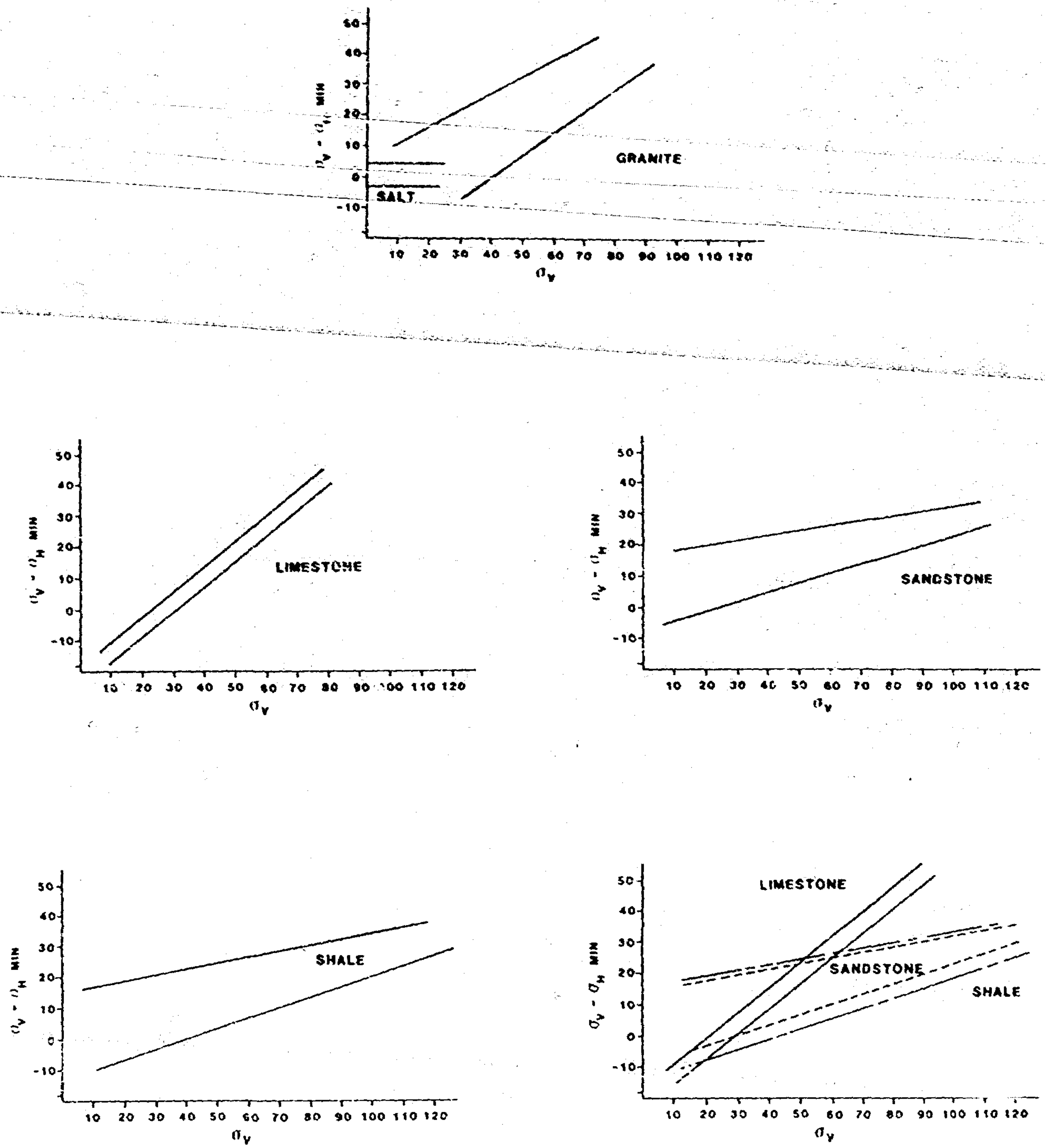

Fig. 6 – Stress difference as a function of depth and rock type; compare to theoretical relationship expressed in Fig. 5.

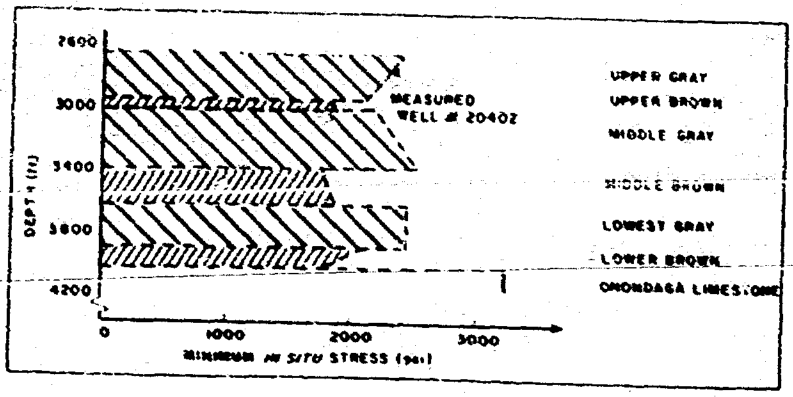

Fig. 7 – Derived minimum in-situ stresses correlated to measured stresses (x) at 2745 ft. in Well #20402, Columbia Gas (Jones, *et al.*, 1977).

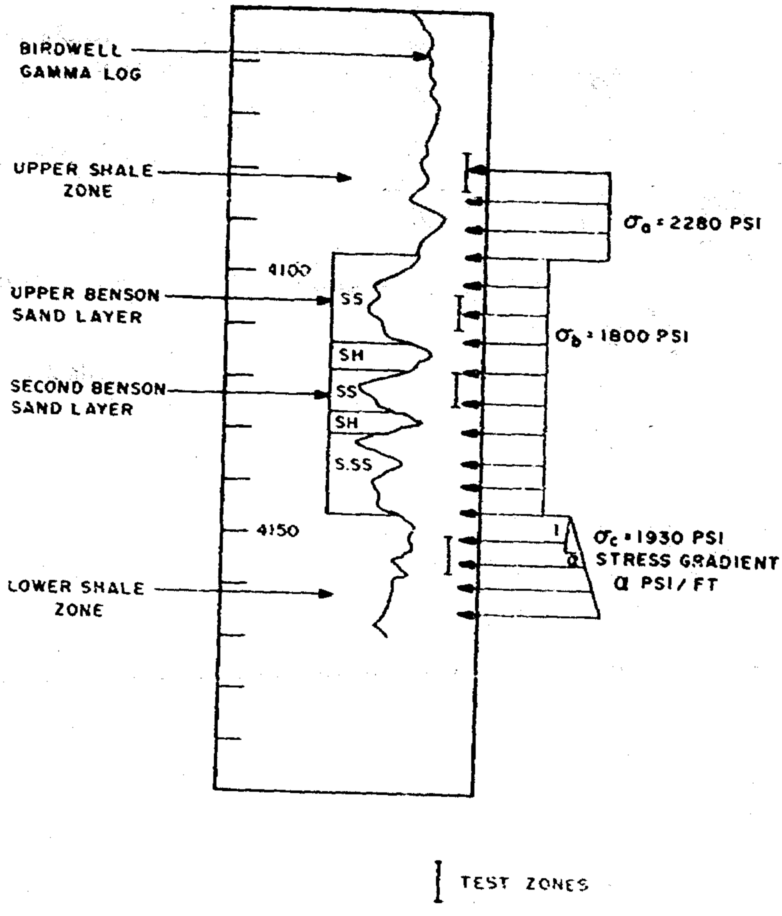

Fig. 8 – Variation of minimum in-situ stress in the Benson Sandstone and surrounding layers (Abou-Sayed, *et al.*, 1978a).

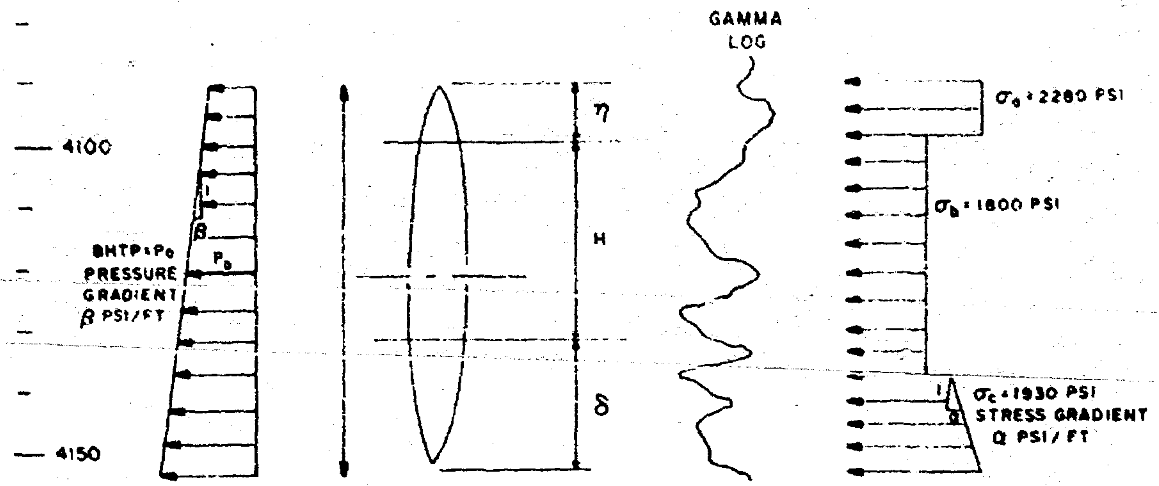

Fig. 9 – Schematic of fracture containment problem in Columbia Well 20538-T (Abou-Sayed, *et al.*, 1978a).

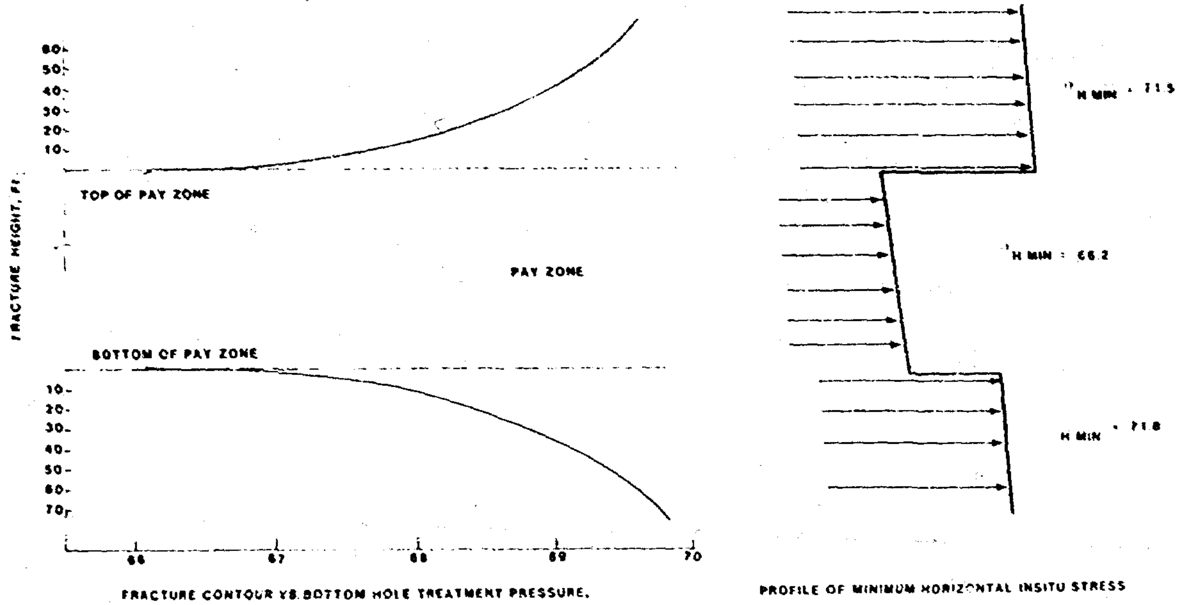

Fig. 10 – Minimum horizontal in-situ stress profile, downhole treatment pressure and fracture penetration into barrier layers for Mountain Fuel's Mesa Unit Well #2, stress in MPa.

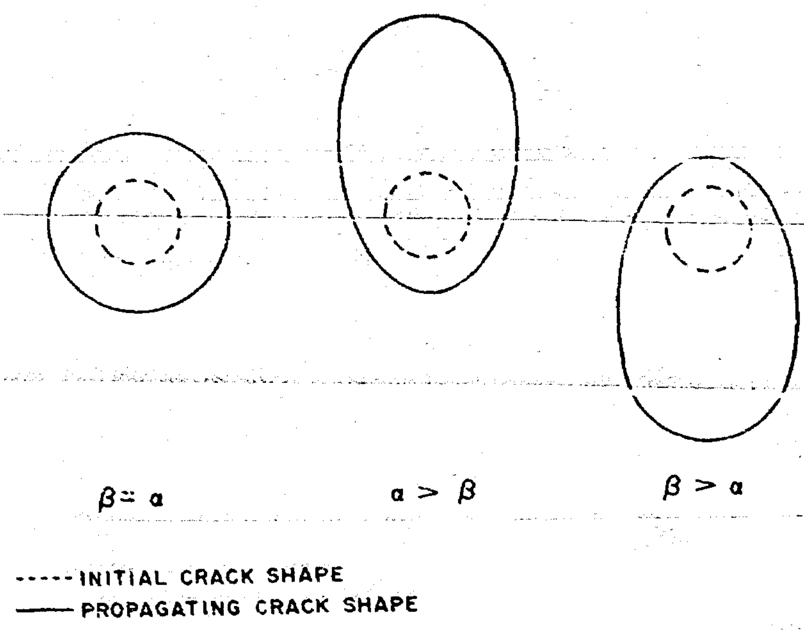

Fig. 11 – Geometry of vertically migrating fracture (Abou-Sayed, *et al.*, 1978b).

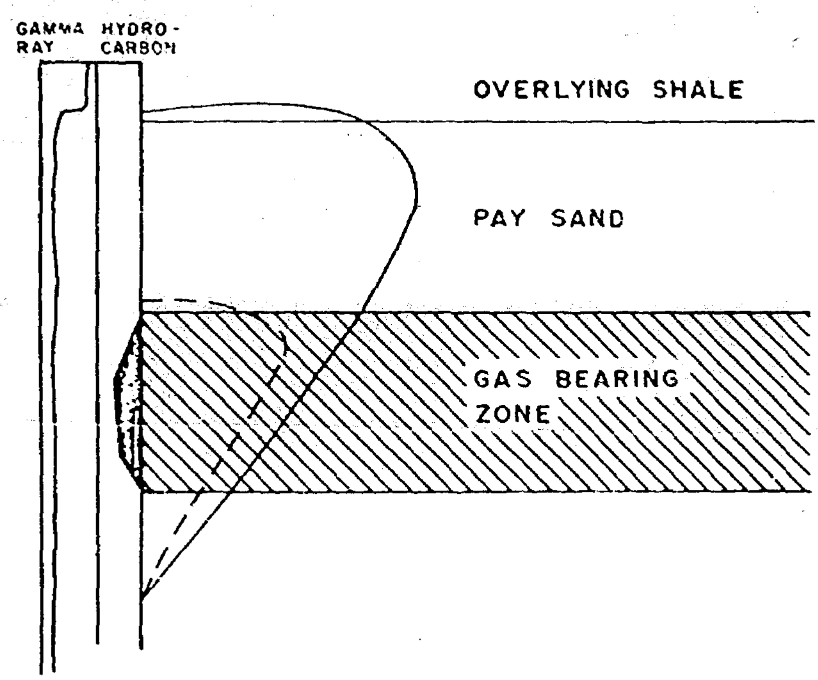

Fig. 12 – Upward growing fracture in a thick formation with localized porosity and gas concentrations.

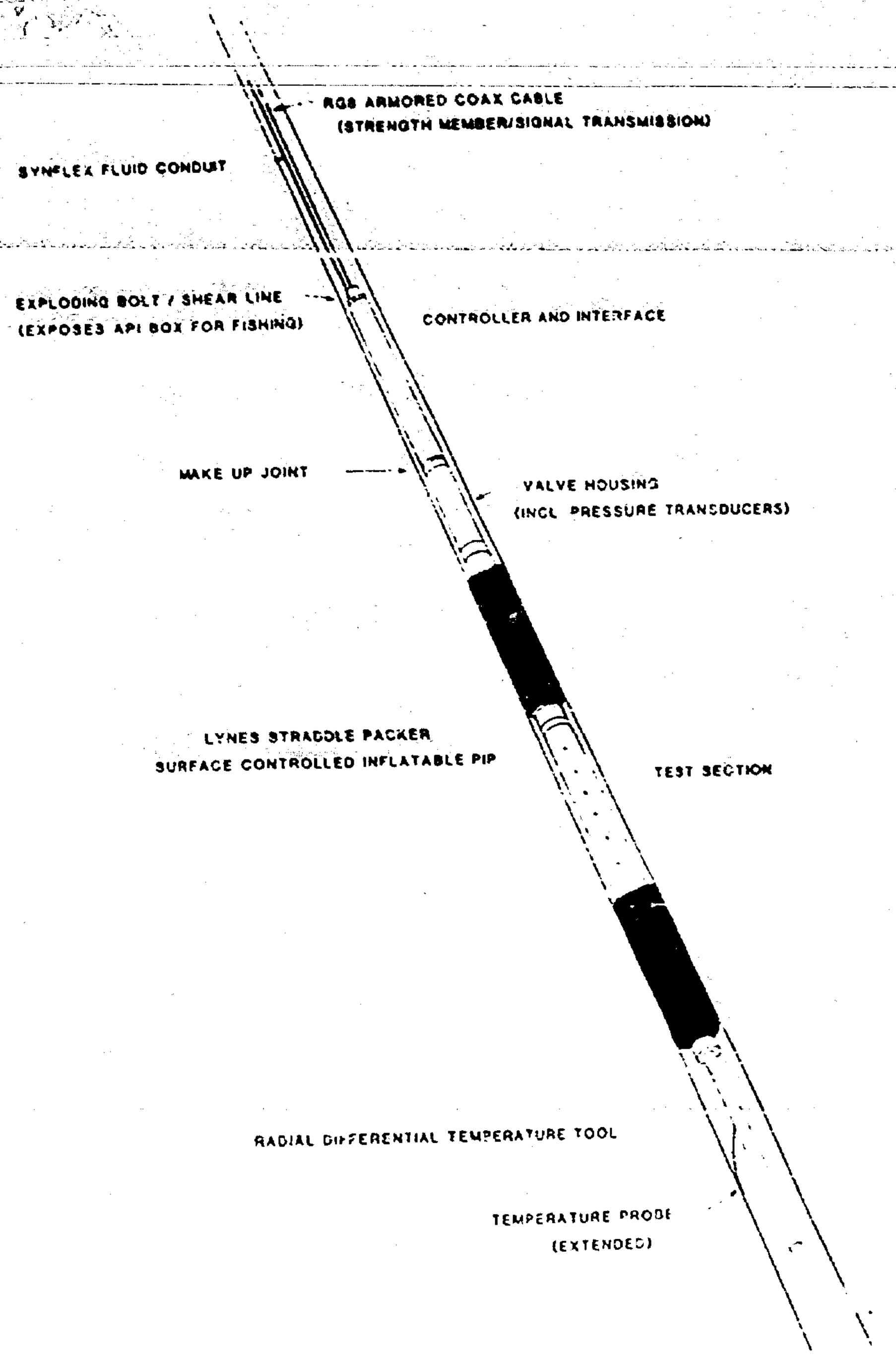

Fig. 13 – Schematic of wireline hydraulic fracturing tool components.

SPE 9261

SPE

Society of Petroleum Engineers of AIME

HYDRAULIC FRACTURE GEOMETRY: FRACTURE CONTAINMENT IN LAYERED FORMATIONS

by Hans A. Van Eekelen, Koninklijke/Shell,
Exploratie en Produktie Laboratorium

This paper was presented at the 55th Annual Fall Technical Conference and Exhibition of the Society of Petroleum Engineers of AIME, held in Dallas, Texas, September 21-24, 1980.

ABSTRACT

One of the main problems in hydraulic fracturing technology is the prediction of fracture height. In particular, the question of what constitutes a barrier to vertical fracture propagation is crucial to the success of field operations.

An analysis of hydraulic fracture containment effects has been performed. The main conclusion is that in most cases the fracture will penetrate into the layers adjoining the pay zone, the depth of penetration being determined by the differences in stiffness and in horizontal in-situ stress between the pay zone and the adjoining layers. For the case of a stiffness contrast, an estimate of the penetration depth is given.

INTRODUCTION

Present-day design procedures for hydraulic fracturing of oil and gas reservoirs are predominantly based on the fracturing theories of Perkins and Kern (Ref. 1), Nordgren (Ref.2) and Geertsma and de Klerk (Ref. 3). In the model proposed by Perkins and Kern, and improved by Nordgren, the formation stiffness is concentrated in vertical planes perpendicular to the direction of fracture propagation. The fracture cross-section in these planes is taken to be elliptical, and the stiffness of the formation in the horizontal plane is neglected. In the model proposed by Geertsma and de Klerk, the stiffness of the formation is concentrated in the horizontal plane. The fracture cross-section in the vertical plane is assumed to be rectangular, and the stiffness in the vertical plane is neglected. In both models, the fluid pressure is assumed to be a function of the distance from the borehole, independent of the transverse coordinates. The theory by Perkins and Kern is more appropriate (Ref. 4) for long fractures ($L/H \gtrsim 1$, where L and H are length and height of the fracture), whereas the model by Geertsma and de Klerk is applicable (Ref. 4) for short fractures, $L/H \lesssim 1$.

The main shortcoming of these fracture-design procedures is that they assume a constant, preassigned fracture height, H. The value of H has a strong influence on the results for fracture length, fracture width, and proppant transport. Usually, the estimated fracture height is based on assumed 'barrier action' of rock layers above and below the pay zone. This situation is rather unsatisfactory.

Moreover, if in reality these layers do not contain the fracture, large volumes of fracturing fluid may be lost in fracturing unproductive strata, and communication with unwanted formations may be opened up.

Whether an adjacent formation will act as a fracture barrier may depend on a number of factors. Among these are:

- differences in in-situ stress
- differences in elastic properties
- differences in fracture toughness
- differences in ductility
- differences in permeability
- the bonding at the interface.

In this paper we analyse these factors with respect to their relative influence on fracture containment.

Differences in in-situ stress and differences in elastic properties affect the 'global' or overall stress field around the fracture, and hence, the three-dimensional shape of the fracture. This shape, together with the horizontal and vertical fracture propagation rates, determines the fluid pressure distribution in the fracture which in turn affects the stress field around the fracture. Consequently, the elastic stress field, the fluid pressure field, and the fracture propagation pattern are intimately coupled, which makes the fracture propagation problem a complicated one.

Whether at a certain point of the fracture edge the fracture will propagate is determined by the intensity of the stress concentration at that point. This stress concentration depends on the global stress distribution in and around the fracture, but it is also directly affected by the local ductility, permeability, and elastic modulus in the tip region.

Ex 3B

For instance, idealised linear elastic fracture theory predicts that the 'stress intensity factor' goes to zero as a fracture approaches an interface with a layer of higher stiffness (higher shear modulus) (Refs. 5,6,7); this effect is independent of the fluid pressure distribution in the fracture. Similarly, the stress intensity factor effectively decreases when the fracture crosses into a layer of higher ductility (Ref. 8) or lower permeability (Ref. 9). Another class of local effects is due to the nature of the interface between two layers. For instance, if the layers are poorly bonded, slip may occur, leading to blunting of the crack tip and subsequent crack arrest. The effect of a 'smeared out' interface, where properties change gradually from one layer to the next, may differ from that of a more abrupt transition.

It will be shown in the next section that it is unlikely that the 'local' effects mentioned above are of primary importance in determining the geometry of hydraulic fractures. It is more probable that in-situ stress and stiffness differences between layers, through their influence on fracture cross-section and fluid pressure distribution, are the main factors determining fracture shape.

THE STRESS INTENSITY FACTOR

In the linear elastic theory of fracture, the stresses around the tip of a crack are singular with $r^{-1/2}$, where r is the distance to the crack tip. The strength of the singularity is 'measured' by means of the stress intensity factor, K, which for a tensile ('mode I') crack is defined as

$$K = \lim_{r \to 0} (2\pi r)^{1/2} \sigma_y ,$$

where σ_y is the tensile stress on the crack axis ahead of the tip. The value of the stress intensity factor K depends on the fracture geometry and on the load applied. For instance, for an infinitely long crack of height H, internally pressurised by a fluid and propagating through a homogeneous material, one has (Ref. 10)

$$K = 1.25\ \Delta p\sqrt{H}, \qquad (1)$$

while for a penny-shaped crack of radius H/2

$$K = 0.80\ \Delta p\sqrt{H}.$$

In these formulae, $\Delta p = p - S_h$, where p is the fluid pressure inside the crack and S_h is the formation stress normal to the plane of fracture.

The fracture propagates if the stress intensity factor K reaches a critical value K_c, which is a material property called critical stress intensity factor, fracture toughness, or facturability. Measured values of K_c, in MPa $m^{1/2}$ (psi $inch^{1/2}$), are

$1.04 < K_c < 1.81$
$(950 < K_c < 1650)$ for siltstone (Refs. 11,12)

$0.44 < K_c < 1.76$
$(400 < K_c < 1600)$ for sandstone (Refs. 11,12,13)

$0.44 < K_c < 1.04$
$(400 < K_c < 950)$ for limestone (Refs. 14,15,16,17)

$0.33 < K_c < 1.32$
$(300 < K_c < 1200)$ for shale (Refs. 11,12,15,18)

All of these values have been measured under low confining pressures; under downhole conditions, the fracture toughness may be somewhat higher, for instance (Ref. 14), a factor of 1.6 at 24 MPa (3500 psi). However, the main point is that the range of measured values of fracture toughness is very narrow - all but one of the values of K_c in Refs. 11 - 18 are within a factor of two from 0.88 MPa $m^{1/2}$ (800 psi $inch^{1/2}$).

As mentioned in the Introduction, existing theories of hydraulic fracturing assume a constant fracture height, H. Let us consider the case where the material is homogeneous, the fracture length L is much larger than H (as is the case in most fracturing designs), and the fluid pressure inside the crack is a function $p(x) = S_h + \Delta p(x)$ of the distance x to the borehole. The stress intensity factor at the upper and lower edges of the crack may then be approximated by

$$K(x) = 1.25\ \Delta p(x)\sqrt{H},$$

while the stress intensity factor at the crack front (x = L) will be slightly larger than that of a penny-shaped crack of radius H/2, say

$$K(L) = 1.00\ \Delta p_L \sqrt{H},$$

where Δp_L is some average value of $\Delta p(x)$ over the region close to the crack front.

If the fluid overpressure Δp were constant over the crack (independent of x), it would follow that the stress intensity factor at the upper and lower edges of the crack would be some 25 per cent higher than at the crack front (Clearly (Ref. 19) gives the ratio of stress intensity factors as $K(x)/K(L) = \sqrt{(2L/H)}$, which may be much larger than 1.25. His analysis is based on an elliptical cross-section in the x-z plane. It is more likely that a contained long crack would have an approximately semicircular end). Consequently, the crack would start propagating in the vertical direction, unless adjoining layers contain the fracture by decreasing the value of K or increasing the value of K_c. The width of the fracture would be given by

$$W = \frac{1-\nu}{G} H\ \Delta p \simeq \frac{1-\nu}{G} K_c \sqrt{H},$$

where G is the shear modulus and ν is Poisson's ratio for the formation. Taking a representative case with

K_c = 1 MPa $m^{1/2}$ (910 psi $inch^{1/2}$)
G = 10^4 MPa (1.45×10^6 psi)
ν = 0.25 and
H = 50 m (164 ft)

one obtains a fracture width $W = 0.50$ mm (0.02 inch), at a fluid overpressure $\Delta p \approx 0.14$ MPa (21 psi).

Obviously, a fracture 0.50 mm wide would not admit proppant. To increase fracture width, use is made of very viscous fracturing fluids and high pumping rates. In this way, a viscous pressure drop is created along the fracture, which forces the crack to open wider. Again taking a representative case, with

fluid viscosity $\eta = 0.1$ Pa s (a hundred times the viscosity of water)
pump rate $Q = 0.01$ m^3/s ([illegible]/min.)
fracture length $L = 200$ m,

Nordgren's theory without fluid loss gives for the fracture width at the well bore

$$W = 2.75 \left(\frac{1-\nu}{G} \eta Q L \right)^{1/4} = 7.7 \text{ mm (0.30 inch)}$$

and for the overpressure at the well bore

$$\Delta p = \frac{G}{1-\nu} \frac{W}{H} = 2.0 \text{ MPa (296 psi)}$$

However, with this value of Δp, the stress intensity factor at the upper and lower edges of the fracture would be

$$K = 18 \text{ MPa m}^{1/2} \text{ (16400 psi inch}^{1/2})$$

which is an order of magnitude larger than the critical value K_c. Of course, it is impossible for K to exceed K_c, and what really happens is that the crack edge continually keeps ahead of the fluid so that the overpressure Δp is not applied right up to the crack edge (in fact, in some laboratory tests (Ref. 20) the fluid was found to occupy only 60 - 70 per cent of fracture length). It will be clear that differences in fracture toughness K_c between layers will not contain such a fracture and that local effects which decrease the stress intensity factor K (ductility, permeability, stiffness contrast) will not reverse this situation - whenever K drops below K_c, the fluid catches up with the crack edge until K is again equal to K_c and the fracture edge starts moving again.

Thus, the problem of fracture containment in hydraulic fracturing operations may be summarised as follows. To obtain reasonable fracture widths that allow proppant to enter the fracture, use is made of highly viscous fluids and high pumping rates. The high pressures involved cause the stress intensity factor at the upper and lower edges of the fracture to be (potentially) an order of magnitude higher than the critical value K_c. Local effects around the fracture edge, which decrease K or increase K_c, will not be sufficient to contain such fractures within the 'pay zone'. Apart from interface slippage which is expected to occur only at shallow depths (see below), the only effects which might (partially) contain such fractures are those that influence the overall stress and deformation patterns around the fracture. These 'global' effects are differences between adjoining layers as regards (a) elastic stiffness and (b) in-situ stress.

LOCAL CONTAINMENT EFFECTS AROUND THE CRACK EDGE

In this section, a more detailed discussion is given of the 'local' effects which may change the (effective) stress intensity factor as a crack approaches an interface between two layers.

Ductility

According to the linear elastic theory of fracture, both stresses and strains around a fracture tip are singular with $r^{-1/2}$, where r is the distance to the crack tip. Singular strains correspond to a dislocation or discontinuity, but singular stresses are physically impossible. To eliminate the stress singularity, one can assume a plastic zone (Ref. 8) around the crack tip*, where the stresses are limited by a 'yield condition'.

A discussion of the role of plasticity in fracture mechanics has been given by Rice (Ref. 8), for the case of Mode III crack (out-of-plane shearing). The material is assumed to be linear elastic up to a certain 'yield' value of the shear stress, τ_o, or the shear strain γ_o. After yielding, the shear strain increases at constant shear stress; this is what happens in the plastic zone around Rice's crack tip. It is further assumed that the fracture propagates if the strain at a fixed microstructural distance ρ_s ahead of the crack tip reaches a value $\gamma_f = (1+D)\gamma_o$, where D is the ductility (by definition). It can be shown (Ref. 8) that the resistance to fracture propagation then increases with crack length until an asymptotic value is reached; the increase is larger for larger ductility D. In this way, a ductile material such as shale may, in principle, stop a running crack. In essence, the effect is due to energy dissipation in the plastic zone around the crack tip. It may be interpreted as a gradual increase of the (effective) fracture toughness K_c for a running crack.

The applicability of Rice's analysis to a Mode I (hydraulic fracturing) crack is uncertain, but it is clear that some plastic energy dissipation will occur. However, the question is whether this effect has not already been included in the measured values of fracture toughness K_c. The asymptotic fracture propagation pressure is reached when the crack length is large compared with the microstructural distance ρ_s. The microstructural distance will probably be of the order of millimetres or less, whereas the characteristic

* An alternative is to introduce cohesive forces in a small region behind the crack tip (Ref. 21); the 'critical stress intensity factor' is then replaced by a 'modulus of cohesion'. In the case of hydraulic fracturing, a simplified version of the cohesive force theory is obtained by assuming that the fracturing fluid (or the fracturing fluid pressure) does not extend all the way out to the crack tip (Ref. 22). The compressive in-situ stresses then act as cohesive forces around the crack tip. This concept has been used by Geertsma and de Klerk in their model of hydraulic fracturing. It deviates from the original cohesive force theory in that the modulus of cohesion (or fracture toughness) of the material itself is effectively put equal to zero.

crack length in fracture toughness tests is of the order of centimetres (Ref. 11). Hence, it seems likely that in these tests asymptotic fracture propagation is approached and that the measured value of fracture toughness would not increase substantially if the sample size were increased to, say, one metre. Although it would still be useful to investigate the dependence on sample size of the measured value of K_c in jacketed burst tests (Ref. 11), we conclude that the effect of ductility on fracture propagation has already been accounted for in the measured value of fracture toughness, and does not give a further contribution to fracture containment.

However, the difference between 'fast' and 'slow' (undrained and drained) propagation pressures should not be expected to be more than, say, a factor of two. Moreover, part if not all of the effect is already accounted for in the measured value of fracture toughness K_c. This applies especially for shales, for which the diffusivity is very low due to the low permeability and the value of va/c in the fracture toughness test will be large. Consequently, we conclude that a permeability contrast does not give a significant contribution to fracture containment beyond that which is already contained in the values of K_c.

Permeability

The simplest (linear elastic) description of the stress-strain behaviour of fluid-saturated porous rock is by means of 'poroelasticity' relations formulated by Biot (Ref. 23); a recent review has been given by Rice and Cleary (Ref. 24).

There are two limiting cases in which poroelastic response corresponds to the response of a classical elastic solid. For slow deformation (slow by comparison with the time scale for diffusive transport of pore fluid), the material deforms without changes in pore pressure and behaves as an elastic solid with shear modulus G and Poisson's ratio ν_d ('d' for drained). In the limit of very rapid deformation, there is no time for fluid flow and the material behaves as a massive impermeable solid with shear modulus G and Poisson's ratio ν_u ('u' for undrained). In general, $\nu_u > \nu_d$, which means that volumetric stiffness is larger for undrained than for drained deformation; the shear stiffness is the same. To give an idea of the magnitude of the effect, we quote (Ref. 24) three pairs of values for ν_u and ν_d:

Ruhr sandstone	$\nu_d = 0.12,\ \nu_u = 0.31$
Berea sandstone	$\nu_d = 0.20,\ \nu_u = 0.33$
Weber sandstone	$\nu_d = 0.15,\ \nu_u = 0.29$

Rice and Simons (Ref. 9) have solved the problem of a plane strain shear (Mode II) crack, which propagates at constant speed through a homogeneous poroelastic material; a short and lucid discussion of their results has been given by Rice (Ref. 25). It is found that the propagation pressure Δp is a function of va/c, where v is the crack speed, a the crack length, and c the poroelastic diffusivity (Ref. 24). The precise shape of the function depends on the assumed size of the 'process zone' around the crack tip. For our purpose, it is sufficient to note that the maximum increase in propagation pressure due to increasing crack speed is bounded as follows:

$$\left(\frac{1-\nu_d}{1-\nu_u}\right)^{1/2} < \frac{\Delta p_{fast}}{\Delta p_{slow}} < \frac{1-\nu_d}{1-\nu_u}$$

With the values of Poisson's ratio given above, the effect of crack speed on propagation pressure is less than 30 per cent. For a Mode I (hydraulic fracturing) crack, the effect may be somewhat larger because the volume stiffness plays a larger part in tensile cracking than in shear cracking.

Stiffness contrast

According to idealised linear elastic fracture theory, the stress intensity factor at the tip of a crack goes to zero if the crack approaches an interface with a stiffer material; an analytical derivation of this effect has been given by Hilton and Sih (Ref. 5). In fact, if the crack tip is located at the interface, the stress singularity is no longer of the form $r^{-0.5}$; for instance (Refs.6,7), if $\nu_2 = \nu_1 = 0.3$ and the stiffness ratio G_2/G_1 is equal to three, the stresses are singular with $r^{-0.4}$. It has been stated that this means that a crack would never cross an interface with a stiffer material (Ref. 26), but it is obvious that such a general statement cannot be correct.

If the stress intensity factor goes to zero when the crack tip approaches an (infinitely sharp) interface with a stiffer material, it is doubtful whether it is still correct to use a fracture propagation criterion $K = K_c$ which has been derived for homogeneous materials. Furthermore, the finite size of the process zone at the crack tip, the finite size of the transition zone between the layers, and the existence of natural flaws in the material, should all be taken into account. Finally, both laboratory (Ref. 20) and field (Refs. 27,28) tests indicate that fractures do indeed break through into layers with higher shear modulus. This conclusion has been confirmed in fracturing tests by the author on layered blocks of gelatin (unpublished), in which a stiffness contrast up to a factor of four did not act as a fracture barrier. In these and other (Refs. 20, 29) laboratory tests on layered systems, crack arrest at interfaces was caused by slippage due to poor bonding, rather than by stiffness contrast. It may be concluded (Refs. 27,28,30,31) that a stiffness contrast, by itself, does not constitute a barrier to propagation of fractures which are driven by viscous fluids at high pump rates.

As noted in the Introduction, however, a stiffness contrast between adjacent layers also has an influence on the overall stress field in and around the fracture and on the fracture width. This subject will be discussed in the next section, together with the effect of in-situ stress differences.

Interface slippage

As mentioned above, crack arrest at interfaces in laboratory tests on layered systems is usually caused by interface slippage. This phenomenon can be prevented by increasing the compressive stress normal to the interface, which improves the frictional resistance to slippage. For example, in tests on layered samples of Nugget sandstone (Ref. 29), a crack crossed both a rough and a smooth interface under a normal load of 6.9 MPa (1000 psi), it crossed only the rough interface at normal load of 4.3 MPa (625 psi), and it crossed neither the rough nor the smooth interface at a normal load of 3.4 MPa (500 psi). No bonding agent was used in these tests, so that the interface had no tensile strength.

In field operations, one may expect crack arrest by interface slippage to occur at shallow depths, if the layers are separated by a sharp interface. At greater depth, however, high frictional resistance due to the overburden load will probably prevent interface slippage, so that this crack arrest mechanism will not be operative.

GLOBAL CONTAINMENT EFFECT

In this section, a discussion will be given of 'global' containment effects, which are due to differences between adjoining layers as regards elastic stiffness and in-situ stress. These differences do not keep a fracture from crossing an interface between two layers but may restrict the depth of penetration into the adjoining layer.

Difference in elastic stiffness

Let us consider a fracture of constant height H and increasing length L, which propagates from a well bore into a homogeneous formation with shear modulus G and Poisson's ratio v. The fluid pressure p_w in the well bore is kept constant so that the flow rate Q varies with time; fluid loss into the sides of the fracture will be neglected.

For a long fracture (L > H), the fracture width at the well bore is constant and given by (Refs. 1,4)

$$W = H(1-v)\ \Delta p/G, \qquad (2)$$

where $\Delta p = p_w - S_h$, with S_h the formation stress perpendicular to the plane of fracture. Assuming that the fluid pressure at the end of the fracture is equal to S_h, the pressure drop Δp (for laminar, Newtonian flow) may be written, according to Nordgren (Refs. 2,4)

$$\Delta p = 2.75\ \left[\left(\frac{G}{1-v}\right)^3\ \eta\ Q\ L/H^4\right]^{1/4}, \qquad (3)$$

where η is the fluid viscosity. From (3), we find the flow rate Q(t) as a function of fracture length L(t). On the other hand, the flow rate is equal to the increase in fracture volume with time (Refs. 2,4)

$$Q = \frac{d}{dt}\ (0.59\ W\ H\ L) = 0.59\ H^2\ (1-v)\ \frac{\Delta p}{G}\ \frac{dL}{dt} \qquad (4)$$

Substituting Q from (3), we obtain the fracture-propagation rate

$$\frac{dL}{dt} = 0.030\ \frac{H^2}{L}\ (1-v)^2\ \frac{(\Delta p)^3}{\eta\ G^2}\ . \qquad (5)$$

For a short fracture (L < H), a similar derivation using the theory by Geertsma and de Klerk (Refs. 3,4) gives

$$\frac{dL}{dt} = 0.190\ L\ (1-v)^2\ \frac{(\Delta p)^3}{\eta\ G^2}\ . \qquad (6)$$

The two expressions for dL/dt agree for an almost square (two-winged) fracture with 2L/H = 0.8.

Comparing equations (5) and (6), we see that for Δp constant, the propagation rate for a short fracture increases with time or fracture length, whereas the propagation rate for a long fracture decreases with time or fracture length. For both short and long fractures, the propagation rate is inversily proportional to G^2. Other things being equal, this means that a fracture propagates four times faster in a layer with modulus G_1, than in a layer with modulus $G_2 = 2G_1$.

However, in most cases, other things will not be equal. To see this, we consider a vertical fracture in a formation consisting of a central layer of height h and modulus G_1, sandwiched between two layers with modulus $G_2 > G_1$ (see Fig. 1). If the fluid overpressure Δp is independent of the vertical co-ordinate z, a reasonable assumption for the maximum width of the fracture seems to be [see equation (2)]

$$W = (1-v)\Delta p\left(\frac{h}{G_1} + \frac{\Delta h}{G_2}\right) = (1-v)\ \Delta p\ \frac{h'}{G_1}$$

where the effective fracture height h' is equal to $h(1+G_1\ \Delta h/G_2 h)$. We note that W has the correct limits for $G_2 = G_1$ and $G_2 >> G_1$. Concerning the vertical cross-section of the fracture, we make two further assumptions:

1) In the central layer, the fracture is part of an ellipse with major axis h' and minor axis W.
2) In the outer layers, the fracture is part of an ellipse with major axis $h + \Delta h$, and minor axis given by the requirement of continuity at the interfaces.

One then finds that the shape of the fracture in the outer (G_2) layers is the same as if the material were homogeneous with shear modulus

$$G' = \left(G_1\ G_2\ \frac{1 + \Delta h/2h}{1 + G_1\ \Delta h/2G_2 h}\right)^{1/2} \qquad (7)$$

For small $\Delta h/h$, the crack width at the interface is a factor $\sqrt{G_1/G_2}$ smaller than it would be in a homogeneous material with modulus G_1, whereas it is a factor $\sqrt{G_2/G_1}$ larger than it would be in a homogeneous material with modulus G_2.

The above considerations will be used to obtain an estimate for the horizontal and vertical propagation rates of the fracture of total length 2L and height $H = h + \Delta h$ depicted in Fig. 1. We assume that $\Delta h < h$, and that the outer layers are appreciably stiffer than the central layer: $G_2 >> G_1$. In that case, the crack in the outer layers will be of small width and volume compared with the crack in the central layer. In addition, more than 80 per cent of the pressure drop in the horizontal direction occurs in the region $x > L/2$, where fracture penetration of the outer layers will be small or zero. Consequently, the horizontal crack propagation rate dL/dt will hardly be influenced by the crack in the outer layers, and will be given by equation (5) with $G = G_1$, h instead of H, and Δp the overpressure in the well bore.

Regarding fracture propagation in the vertical direction in the region around the well bore, we note that almost all of the pressure drop in this direction occurs in the outer layers where the crack is narrow and has the same shape as in a homogeneous material with modulus G'. For small $\Delta h/2h$, we have $G' = \sqrt{G_1/G_2}$ constant, and we may assume that the vertical propagation rate is approximately given by equation (6), with L replaces by H and G^2 by $G'^2 = G_1 G_2$. In that case, the ratio of the horizontal and vertical propagation rates is given by

$$\frac{dL}{dH} = \frac{3}{19}\frac{h^2}{LH}\frac{G_2}{G_1} \qquad (8)$$

which is idependent of Δp, and proportional to G_2/G_1, instead of $(G_2/G_1)^2$. Integration of (8) with the initial condition $2L = h$ at $H = h$ gives

$$2L = h\left[1 + \frac{24}{19}\frac{G_2}{G_1}\log\frac{H}{h}\right]^{1/2} \qquad (9)$$

A somewhat more accurate calculation, where we use the full expression (7) for G', modify equation (6) to take account of the fact that G' changes with H, and neglect $G_1\,\Delta h/2G_2 h$ in the expression for dL/dH, gives as a final result

$$2L = h\left[1 + \frac{12}{19}\frac{G_2}{G_1}\left\{\log\frac{H}{h} + \frac{1}{4}\left(3 + \frac{G_1}{G_2}\right)\left(\frac{H}{h} - 1\right)\right\}\right]^{1/2}$$

A plot of $2L/h$ against H/h is given in Fig. 2 for $G_2/G_1 = 10$. After the fracture has reached the interface ($2L = H = h$), it at first grows mainly in the horizontal direction. However, the more elongated the fracture becomes, the more favourable circumstances become for propagation in the vertical direction; as a consequence, $2L/H$ reaches a maximum value of 1.64 at $2L/h = 2.7$, after which it slowly declines. A plot of the maximum elongation $2L/H$ as a function of G_2/G_1 is given in Fig. 3. It is seen that, to obtain a fracture with elongation $2L/H = 3$, one needs a modulus contrast $G_2/G_1 > 35$.

Although the above results should be considered order-of-magnitude estimates (the expressions for horizontal and vertical propagation rates are only very approximate), they do indicate that the containing effect due to an elasticity contrast is not as strong as one might hope. Although in principle the propagation rate of a fracture at given overpressure Δp is proportional to G^{-2}, the actual effect in the geometry of the layered system is far smaller. One reason for this is that the crack width in the outer layers is estimated to be a factor $\sqrt{G_2/G_1}$ larger than it would be without the more compliant central layer. A second reason is that the crack in the outer layers is relatively long in the horizontal direction, so that transverse elasticity does not play a role and the crack becomes wider as it goes deeper. Consequently, vertical fracture growth at constant Δp is an accelerating process ($dH/dt \sim H$), whereas horizontal fracture growth is a decelerating process ($dL/dt \sim 1/L$).

We conclude that a stiffness contrast between the layer to be fractured and the adjoining layers will cause the fracture to assume a horizontally elongated shape. For reasonable stiffness ratios, however, the elongation ratio will probably not be larger than two or three.

Differences in in-situ stress

The effect on fracture geometry of a contrast in horizontal in-situ stress between the layer to be fractured and adjoining layers has not yet been analysed in any depth.

Consider an infinitely long fracture of height H in the geometry of Fig. 1, where we now assume that $G_2 = G_1$. If the horizontal in-situ stress perpendicular to the plane of the fracture is everywhere equal to S_1, and the fluid pressure p in the fracture is uniform, the fracture propagation pressure will be

$$p_{f,H} = S_1 + \frac{1}{1.25}\frac{K_c}{\sqrt{H}}, \qquad (10)$$

where K_c is the critical stress intensity factor or fracture toughness - see equation (1).

If, on the other hand, the in-situ stress in the outer layer is equal to $S_2 > S_1$, the fracture propagation pressure increases to

$$\hat{p}_{f,H} = S_1 + \frac{1}{1.25}\frac{K_c}{\sqrt{H}} + (S_2 - S_1)\frac{2}{\pi}\arccos\frac{h}{H}. \qquad (11)$$

The derivation of this expression is simple and is given in Ref. 32. The fracture propagation pressure $p_{f,h}$ for a fracture which just reaches the interface at $z = \pm 1/2\, h$ is given by (10) or (11) with $H = h$. From (11) we then have

$$\hat{p}_{f,H} - p_{f,h} = (S_2 - S_1)\frac{2}{\pi}\arccos\frac{h}{H} - \left(1 - \sqrt{\frac{h}{H}}\right)\frac{1}{1.25}\frac{K_c}{\sqrt{h}}$$

This equation gives the extra fluid pressure that is needed to propagate the fracture into the layer of higher in-situ stress as a function of penetration depth. For the case

K_c	=	1 MPa $m^{1/2}$	(910 psi inch$^{1/2}$)
G	=	10^4 MPa	(1.45×10^6 psi)
ν	=	0.25	
h	=	50 m	(164 ft)
$S_2 - S_1$	=	3 MPa	(435 psi)

one obtains 10 m (33 ft) penetration ($H = 70$ m), for an extra fluid pressure $\hat{p}_{f,H} - p_{f,h} = 1.46$ MPa (212 psi).

The drawback of the above analysis (Ref. 32) (which is the only one we are aware of) is that it is not really relevant to the problem in hand. For the case given above, the fracture propagation pressure $p_{f,h}$ at the interface is equal to S_1 plus 0.11 MPa (16 psi) and the full width of the fracture is approximately 0.4 mm (0.02 inch). As mentioned before, such a fracture would not admit proppant. In practice, fluid overpressures near the well bore are much higher than 16 psi, and the fracture edge keeps ahead of the fluid to prevent K exceeding K_c. The confining effect of an in-situ stress contrast derives from a reduction in fracture width in the outer layers, which impedes fluid flow and thereby reduces the vertical fracture-propagation rate dH/dt.

Consequently, the effect of an in-situ stress contrast on fracture geometry should be calculated from a coupled elasticity/fluid flow analysis. An estimate of the effect may be obtained by simple but very approximate calculations, as presented above for the case of a stiffness contrast. A more thorough evaluation requires a three-dimensional (numerical) analysis of the coupled fluid flow/elastic deformation problem in and around the fracture (Refs. 30, 31).

Until such calculations have been performed, it is not possible to estimate the effect of in-situ stress differences on fracture containment. However, the effect may well be quite appreciable. In fact, one of the reasons that shale layers often seem to contain hydraulic fractures may be that, owing to their higher ductility or tendency to creep, the horizontal stress in these shale layers may often be higher (closer to the overburden stress) than in adjoining layers. Some direct measurements of in-situ stress seem to confirm this notion (Ref.33).

It should be noted that an in-situ stress contrast may also be induced artificially by reducing the pore pressure in the pay zone by partial drainage of the reservoir around the borehole. If the drainage radius is much larger than the height of the pay zone, the resulting deformation field will have zero lateral strains, while the vertical stress remains equal to the overburden load. From the poroelasticity equations one then finds a linear relationship between change in horizontal in-situ stress in the pay zone, and change in pore pressure

$$\Delta S_{horiz} = (1-\beta)\,\frac{1-2\nu}{1-\nu}\,\Delta u \equiv \gamma\,\Delta u \qquad (12)$$

where

- u = pore pressure,
- β = ratio of rock grain to rock matrix compressibility, and
- ν = Poisson's ratio for the formation.

The parameter γ will usually have a value between 0.5 and 0.6. Experimental verification of equation (12) has been provided by Salz (Ref. 34), who found a linear relationship between fracture propagation pressure and pore pressure in the Vicksburg field in South Texas; his data scatter around a straight line of slope 0.51.

It should be noted that the Vicksburg field data refer to reservoir depletion over a number of years, in the course of commercial production from the field. It has recently been suggested (Ref. 31) that a massive hydraulic fracture be contained by fracturing in stages, allowing time for drainage after each fracturing stage to lower the pore pressure around the fracture. However, since fracturing is usually undertaken in tight (low-permeability) formations, the drainage times involved may well be excessive: as mentioned above, the process only works if the drainage radius is much larger than the height of the pay zone. The reason for this is that, owing to the requirement of stress equilibrium, a local reduction in horizontal (total) stress can only be achieved if part of the horizontal far-field stress is 'carried' by shear stresses at the interfaces with cap and base rock. Otherwise, the reduction in pore pressure will be compensated by an increase in horizontal effective stress, the total horizontal stress remaining unchanged.

SUMMARY AND CONCLUSIONS

This paper considers the problem of hydraulic fracture containment. It is shown that the concepts of 'stress intensity factor' and 'fracture toughness' have only limited applicability in the context of hydraulic fracturing of underground formations. As a consequence, 'local' containment effects around the upper and lower crack edge, which decrease the stress intensity factor or increase the fracture toughness, are of only minor importance as regards the ultimate shape of the fracture. Hence, in most cases, the fracture will penetrate into the layers adjoining the 'pay zone' which is being fractured. However, there is another class of ('global') containment effects which tend to limit the penetration depth of the fracture into these layers. These effects are due to contrasts in stiffness and in-situ stress between pay zone and adjoining layers. For the case of a stiffness contrast, an estimate of the penetration depth has been given. For the case of in-situ stress contrast, the necessary analysis (Refs. 30,31) has not yet been completed.

NOMENCLATURE

h	height of pay zone
p	fluid pressure
p_w	fluid pressure in borehole
Δp	fluid overpressure, $\Delta p = p - S$
G	shear modulus of formation
H	fracture height
K	stress intensify factor
K_c	critical stress intensity factor, fracture toughness
L	fracture (half-)length
Q	flow rate into (half) the fracture
S	horizontal in-situ stress perpendicular to plane of fracture
W	fracture width
η	fluid viscosity
ν	Poisson's ratio for formation

ACKNOWLEDGEMENT

This paper is based on work completed during an assignment to Shell Development Company, Bellaire Research Center, Houston, Texas. Permission to publish this work is gratefully acknowledged.

REFERENCES

1. Perkins, T.K., & Kern, L.R. (1961), 'Widths of Hydraulic Fractures', J. Pet. Techn., September, pp. 937.
2. Nordgren, R.P. (1972), 'Propagation of a Vertical Hydraulic Fracture', Soc. Pet. Eng. J., August, pp. 306.
3. Geertsma, J. & de Klerk, F. (1969), 'A Rapid Method of Predicting Width and Extent of Hydraulically Induced Fractures', J. Pet. Techn., December, pp. 1571.
4. Geertsma, J. & Haafkens, R. (1979), 'A Comparison of the Theories for Predicting Width and Extent of Vertical Hydraulically Induced Fractures', Transactions, ASME, 101, pp. 8-19.
5. Hilton, P.D. & Sih, G.C. (1971), 'A Laminate Composite with a Crack Normal to the Interfaces', Int. J. Solids Structures, 7, pp. 913-930.
6. Erdogan, F. (1974), 'Fracture Problems in a Non-homogeneous Medium', in 'Continuum Mechanics Aspects of Geodynamics and Rock Fracture Mechanics', Thoft-Christensen (Ed.), pp. 45-64 (Reidel Publishing Company, Dordrecht, Holland).
7. Comninou, M. & Dundurs, J. (1979), 'A Closed Crack Tip Terminating at an Interface', J. Appl. Mech., 46, pp. 97-100.
8. Rice, J.R. (1968), 'Mathematical Analysis in the Mechanics of Fracture', in 'Fracture, an Advanced Treatise', Vol. 12, Mathematical Fundamentals, H. Liebowitz (Ed.), Academic Press, pp. 191-311.
9. Rice, J.R. & Simons, D.A. (1976), 'The Stabilisation of Spreading Shear Faults by Coupled Deformation-Diffusion Effects in Fluid Infiltrated Porous Materials', J. Geophys. Res., 81, pp. 5322-5334.
10. Sih, G.C. (1973), 'Handbook of Stress Intensity Factors', Lehigh University.
11. Clifton, R.J., Simonson, E.R., Jones, A.H. & Green, S.J. (1976), 'Determination of the Critical Stress Intensity Factor from Internally Pressurized Thick-Walled Vessels', Exp. Mech., 16, pp. 233-238.
12. Brechtel, C.E., Abou Sayed, A.S. & Jones, A.H. (1978), 'Fracture Containment Analysis Conducted on the Benson Pay Zone in Colombia Well 20538-T', in Proceedings of the Second Eastern Gas Shales Symposium, Morgantown, West Virginia, pp.264-272.
13. Atkinson, B.K. (1979), 'Fracture Toughness of Tennessee Sandstone and Carrara Marble using the Double Torsion Testing Method', Int. J. Rock Mech. Sci. & Geomech. Abstracts, 16, pp. 49-53.
14. Abou Sayed, A.S. (1977), 'Fracture Toughness of Triaxially Loaded Indiana Limestone', Proc. 18th U.S. Symposium on Rock Mechanics, Vol. 2, 2A3-1 to 2A3-7, Colorado School of Mines, Golden.
15. Brechtel et al. (1978), 'Measurements for Michell Energy Corporation, Cotton Valley Limestone', Reported in Western Gas Sands Project, Status Report.
16. Schmidt, R.A. (1976), 'Fracture Toughness Testing of Limestone', Expl. Mech., 16. pp. 161-167.
17. Schmidt, R.A. & Huddle, C.W. (1977), 'Effect of Confining Pressure on Fracture Toughness of Indiana Limestone', Int. J. Rock Mech. Min. Sci. and Geomech. Abstr., 14, pp. 289-293.
18. Abou Sayed, A.S. & Brechtel, C.E. (1978), 'In-situ Stress Determination by Hydro-fracturing: A Fracture Mechanics Approach', J. Geophys. Res., 83, pp. 2851-2862.
19. Cleary, M.P. (1978), 'Primary factors Governing Hydraulic Fractures in Heterogeneous Stratified Porous Formations', ASME Paper 78-Pet-47, Energy Technology Conference and Exhibition, Houston, Texas.
20. Daneshy, A.A. (1976), 'Hydraulic Fracture Propagation in Layered Formations', SPE Paper 6088, 51st Annual Fall Technical Conference and Exhibition, New Orleans.
21. Goodier, J.N. (1978), 'Mathematical Theory of Equilibrium Cracks', in 'Fracture, An Advances Treatise', Vol. 2, Mathematical Fundamentals, H. Liebowitz (Ed.), Academic Press, pp. 1-66 (Sections VIII and IX).
22. Kristianovitch, S.A. & Zheltov, Y.P (1955) 'Formation of Vertical Fractures by Highly Viscous Fluids', Proc. 4th World Pet. Cong., Vol. II, 579.
23. Biot, M.A. (1941), 'General Theory of Three-Dimensional Consolidation', J. Appl. Phys., 12, pp. 155-164.
24. Rice, J.R. & Cleary, M.P. (1976), 'Some Basic Stress-Diffusion Solutions for Fluid-Saturated Elastic Porous Media with Compressible Constituents', Rev. Geophys. Space Phys., 14, pp.227-241.
25. Rice, J.R. (1978), 'The Mechanic of Quasi-Static Crack Growth', Proc. 8th U.S. National Congress of Applied Mechanics, UCLA, June.
26. Simonson, E.R., Jones, A.H. & Abou Sayed, A.S. (1975), 'Experimental and Theoretical Considerations of Massive Hydraulic Fracturing', Terra Tek Report TR 75-39, Salt Lake City.
27. Schmidt, R., Northrop, D. & Warpinski, N. (1979), 'Hydraulic Fracturing Near an Interface: Observations and Calculations Regarding Geometry and Containment', Proc. 20th U.S. Symp. on Rock Mech., Vol. 2.
28. Warpinski, N.R., Schmidt, R.A. & Northrop, D.A. (1980), 'In-situ Stresses, the Predominant Influence on Hydraulic Fracture Containment', SPE Paper 8932, Proc. Unconventional Gas Recovery Symposium, Pittsburgh, pp. 83-94.
29. Hanson, M.E., Anderson, G.D. & Schaffer, R.J. (1978), 'Theoretical and Experimental Research on Hydraulic Fracturing', ASME Paper 78-Pet-49, Energy Technology Conference and Exhibition, Houston, Texas.
30. Clifton, R.J. & Abou Sayed, A.S. (1979), 'On the Computation of the Three-Dimensional Geometry of Hydraulic Fractures', SPE Paper 7943, SPE Symposium on Low Permeability Gas Reservoirs, Denver.
31. Cleary, M.P. (1979), 'Rate and Structure Sensitivity in Hydraulic Fracturing of Fluid-Saturated Porous Formations', Proc. 20th U.S. Symposium on Rock Mech., Austin, Texas, pp. 137-142.

32. Simonson, E.R., Abou Sayed, A.S. & Clifton, R.J. (1976), 'Containment of Massive Hydraulic Fractures', SPE Paper 6089, 51st Annual Fall Conference and Exhibition, New Orleans (SPE Journal, Feb. 1978).
33. Brechtel, C.E., Abou Sayed, A.S., Clifton, R.J. & Haimson, B.C. (1976), 'In-Situ Stress Determination in the Devonian Shales, (Ira McCoy 20402) Within the Rome Basin', Terra Tek Report TR 76-36, Salt Lake City.
34. Salz, L.B. (1977), 'Relationship between Fracture Propagation Pressure and Pore Pressure', SPE Paper 6870, 52nd Annual Fall Technical Conference and Exibition, Denver.

Society of Petroleum Engineers of AIME
6200 N. Central Expwy.
Dallas, Tex. 75206

PAPER
NUMBER SPE 6089

Containment of Massive Hydraulic Fractures

By

E. R. Simonson, Member SPE-AIME, A. S. Abou-Sayed and R. J. Clifton, Terra Tek, Inc.

ABSTRACT

Hydraulic fracture containment is discussed from the point of view of linear elastic fracture mechanics. Three cases are analyzed: a) Effect of different material properties for the pay zone and the barrier formation, b) Characteristic of fracture propagation into region of varying *in situ* stress and c) Effect of hydrostatic pressure gradients on fracture propagation into overlying or underlying barrier formations. The analysis shows the importance of the elastic properties, the *in situ* stresses and the pressure gradients on fracture containment.

INTRODUCTION

Application of massive hydraulic fracture (MHF) techniques to the Rocky Mountain gas fields have yielded results which vary from successful to extreme disappointing failures. The primary thrust of rock mechanics research in this area is to understand those factors which contribute to the success of MHF and those conditions which lead to failures. There are many possible reasons why MHF fail, including migration of the fracture into overlying or underlying barrier formations, degradation of permeability due to application of hydraulic fracture fluid, loss of frac fluid into pre-existing cracks or fissures or extreme errors in estimating the quantity of inplace gas. Additionally, a poor estimate of the *in situ* permeability can result in failures which may "appear" to be due to the hydraulic fracture process. Previous work showed that *in situ* permeabilities can be one order of magnitude, or more, lower than permeabilities measured at near atmospheric conditions.[1] Moreover, work has been done in studying the degradation in both fracture permeability and formation permeability due to the application of hydraulic fracture fluids.[2,3] Further discussion of this subject is beyond the scope of the present paper. This paper will deal mainly with the containment of hydraulic fractures to the pay zone.

In general, the lithology of the Rocky Mountain region consists of oil- and gas-bearing sandstone layers interspaced with shales as shown in Figure 1. However, some of these sandstone layers may be water aquifers and penetration of the hydraulic fracture into any of these aquifer layers is undesirable. Additionally the shale layers could be separating producible from nonproducible oil- and gas-bearing zones. The existence of the shale layers between the pay zone and these other zones could be vital in increasing the chances for successful

References and illustrations at end of paper

& 3C

stimulation. If the shale layers would act as barrier layers, the hydraulic fracture could be contained within the pay zones.

The *in situ* stresses and the stiffness moduli of the zones can also play a significant role in the containment of hydraulic fracture. These stresses result from loads acting within the earth's crust and constitute the compressive far field stresses which act to close the hydraulic fracture. Figure 2 shows a schematic representation of *in situ* stresses acting on a vertical hydraulic fracture. *In situ* stresses especially the horizontal component may vary from layer to layer as shown in Figure 2. For example, direct measurements of *in situ* stresses in shales has shown the stresses to be nearly hydrostatic and equal to the overburden stress.[4] On the other hand, in sandstones, the lateral tectonic stresses are generally less than the vertical or overburden stress.[5] With these differences in stress between shales and sandstones it becomes important to consider their effect on fracture containment.

Hydraulic fracture analysis is inherently a three-dimensional problem, the mathematical solutions of which are extremely complicated if not impossible in a great many cases. Three-dimensional solutions to some problems have been worked out using the finite element technique, however, these solutions usually appear to be very costly and extremely time consuming.[6] Two-dimensional analyses on the other hand are on much firmer ground and many solutions of two-dimensional crack problems have been worked out. Such simplified analyses provide a considerable insight into understanding those parameters and conditions which influence hydraulic fracture propagation. For the present work we will limit ourselves to treating two-dimensional cracks in linear elastic media. Furthermore, considerations are only given to symmetrically loaded cracks (mode I).

A two-dimensional representation of a hydraulic fracture embedded in a sand layer bounded by barrier formations is shown schematically in Figure 3. The fracture is assumed to be infinite in extent normal to the plane of the paper and that we are sufficiently removed from the well bore to neglect its effects. These assumptions are reasonable when we consider that most hydraulic fractures are assumed to have lengths many times their heights.

In linear elastic fracture mechanics for Mode-I cracks, the important parameters to consider are the stress-intensity factors K_I at the crack tip and the critical stress intensity factors (K_{Ic}) or fracture toughness of the material. The former is a mathematical quantity that uniquely characterizes the load sensed at the crack tip. It is given by the limit as $r \to 0$ of the expression for the normal stress component in the vicinity of the crack tip, i.e.,[7] (Figure 4)

$$K_I = \lim_{r \to 0} \frac{1}{\sqrt{2\pi r}} \sigma_{yy}(r,0) \qquad . \qquad (1)$$

On the other hand, K_{Ic} is a material property to be measured. Its importance stems from the fact that a crack will extend when the stress intensity K_I at its tip reaches the critical value K_{Ic}. The idea then is to measure the fracture toughness K_{Ic} for a material and then perform a stress analysis of the problem and deduce what applied loading will produce K_{Ic} at the crack tip. This loading will suffice to cause further cracking in the material. With this very brief review of fracture mechanics concepts, the following three cases of hydraulic fracturing will be considered.

i) Effect of different material properties for the pay zone and the barrier formation.

ii) Characteristics of fracture propagation into regions of varying *in situ* stress.

iii) Effect of hydrostatic pressure gradients on fracture propagation into overlying or underlying barrier formations.

CASE I. EFFECTS OF DIFFERING MATERIAL PROPERTIES

It is well known that there are differences in mechanical properties between the pay zone formation and the barrier formations. The question then arises as to what role does the mechanical properties play in the containment of the hydraulic fracture to the pay sand. The effect is best seen by looking at how the stress intensity at the crack tip nearest the interface $(K_I)_a$ varies as the fracture approaches the interface.[8] Figure 5 illustrates the variation in the intensity factors for two cases. These cases have been worked out for the following set of mechanical properties[9]

G_1 = 7.03 GPA (1.02 x 10^6 psi)

ν_1 = .14

G_2 = 13.38 GPa (1.94 x 10^6 psi)

ν_2 = .14

Case I is the one in which the stiffness of the barrier formation as measured by the shear modulus is less than the stiffness of the pay zone. For this case, the stress intensity factor $(K_I)_a \to \infty$ as $r/\ell \to 0$. Thus, the closer the fracture gets to the interface the easier it is to extend and will eventually pass through the interface. Case II however, is where the stiffness of the barrier layer is greater than the stiffness of the pay zone. For this case, the stress intensity factor $(K_I)_a \to 0$ as $r/\ell \to 0$. This situation provides a "blunting" effect and tends to arrest the crack at the interface. Therefore, if there is some choice as to which zone to perforate, it would seem better to choose those zones which have lower stiffness than the adjacent barrier formations.

CASE II. EFFECT OF *IN SITU* STRESS VARIATIONS

As pointed out earlier, there can be differences in *in situ* stress between shales and sandstones. Let us now consider the problem of a crack embedded in a homogeneous isotropic medium subjected to differing *in situ* stress loading. This problem may be thought of as one in which a hydraulic fracture, by some mechanism or other, has extended into adjacent layers where possibly different tectonic stresses may be acting. Figure 6 is a schematic representation of this case.

The stress intensity factor at each end of the crack is found by superposition of the two problems shown in Figure 7.

The stress intensity factor K_I is the sum of the contribution from loading A and B. The contribution from B is zero and the only contribution comes from A. The value of K_I can be computed directly from the following equation[10,11]

$$K_I = \frac{1}{\sqrt{\pi \ell}} \int_{-\ell}^{\ell} P(y) \sqrt{\frac{\ell + y}{\ell - y}}\, dy \qquad (2)$$

where

$$P(y) = \begin{cases} P - S_2 & h < y < \ell \\ P - S_1 & -h < y < h \\ P - S_2 & -h < y < -\ell \end{cases} \qquad (3)$$

Substituting Equation (3) into Equation (2) and performing the integration, one obtains the following expression for K_I

$$K_I = (S_2 - S_1)\sqrt{\frac{\ell}{\pi}}\left\{2 \sin^{-1}\left(\frac{h}{\ell}\right)\right\} + (P - S_2)\sqrt{\pi \ell} \qquad (4)$$

If we let $\ell = h(1 + \epsilon)$ where ϵ is the percentage of "h" that the crack has propagated into the high stress region, then by rearranging terms we get

$$\frac{\ell}{\ell + \epsilon} = \cos\left[\left(\frac{K_I - (P - S_1)\sqrt{\pi h(1+\epsilon)}}{2(S_2 - S_1)\sqrt{h(1+\epsilon)}}\sqrt{\pi}\right)\right] \qquad (5)$$

If P_o is the pressure required for crack extension when $\epsilon = 0$, then

$$K_{Ic} = (P_o - S_1)\sqrt{\pi h} \qquad (6)$$

Substitution of Equation (6) into Equation (5) gives a relation between $P - P_o$ and ϵ when $K_I = K_{Ic}$. The result is

$$P - P_o = \frac{K_{Ic}}{\sqrt{\pi h}}\left(\frac{1}{\sqrt{1+\epsilon}} - 1\right) + \frac{2(S_2 - S_1)}{\pi}\cos^{-1}\left(\frac{1}{1+\epsilon}\right) \qquad (7)$$

Figure 8 shows a plot of Equation (7) in terms of excess pressure $P - P_o$ versus ℓ, the distance the crack has advanced into the region of high stress. The curves in this figure are for a crack height of 61 m (200 feet), a fracture toughness of K_{Ic} = 1.1 MN/m$^{3/2}$(1000 lb-in$^{-3/2}$) and for parametric values of the *in situ* stress difference $S_2 - S_1$. Thus, if the stress difference $S_2 - S_1$ = 7.58 MPa (1100 psi), for example, an over pressure of 3.45 MPa (500 psi) would be expected if the fracture were to propagate into the region of higher *in situ* stress. This analysis although simplified does indicate an *increase* in fracture propagation pressure if the fracture extends into a barrier formation with higher *in situ* stress. If one had an accurate measure of the fracture propagation pressure, it might be possible to tell when the fracture was extending into the barrier zone provided, of course, there is a significant difference in *in situ* stress between the barrier layer and the pay zone.

As a last comment, if the *in situ* stress in the barrier layer (S_2) was less than the *in situ* stress in the pay zone (S_1) a situation would exist where it requires less pressure to propagate the fracture in the barrier layer than in the pay sand. Propagation into the barrier layer would be highly probable if $S_2 < S_1$.

CASE III. PRESSURE GRADIENT EFFECTS

Consider the problem shown in Figure 9. In this case we have a vertical plane strain crack in an infinite medium subjected to hydrostatic pressure loading. Due to gravitational effects, a linear pressure gradient which acts on the faces is developed with a gradient coefficient of β MPa/m. The externally applied loads are the tectonic stresses. The solution to this problem was arrived at independently by Terra Tek and Secor and Pollard[12] and its solution will be presented for completeness of this paper.

The magnitude of the tectonic stresses, of course, is a function of depth and may vary from formation to formation. There are many theories advanced as to how the tectonic stress varies with depth. One of these theories assumes there are no lateral displacements as a function of depth and hence uniaxial strain conditions prevail.[13] For uniaxial strain loading, the ratio of σ_1 (overburden stress) to lateral stress σ_3 (tectonic stress) for a linear isotropic homogeneous elastic material is given by

$$\frac{\sigma_1}{\sigma_3} = \frac{1-\nu}{\nu} \qquad (8)$$

where

ν = Poisson's ratio.

Equation (8) shows that the overburden stress σ_1 is linearly related to the lateral stress σ_3. At any rate, it seems plausible that the deeper you go the greater becomes the lateral stress and that a linear stress gradient is realistic. Exactly what is the value of the gradient is a topic of discussion and will likely never be resolved except by direct measurement.[14] For this problem, however, let us assume there is a linear variation in the applied or tectonic stress of α MPa/m as shown in Figure 9.

The solution for $(K_I)_1$ and $(K_I)_2$ for this problem is again found by the superposition of the following two loadings shown in Figure 10.

The contribution to K_I from loading (B) is zero and the only contribution comes from loading (A). The values for $(K_I)_2$ and $(K_I)_1$ are calculated as before from Equation (2) with

$$P(y) = (\beta-\alpha)y + \frac{1}{2}[P_u + P_b - S_u - S_b] \qquad (9)$$

Integration of Equation (2) with Equation (9) substituted for P(y) results in the following expression for the difference in stress intensity factors between the top and bottom of the crack, i.e.,

$$(K_I)_2 - (K_I)_1 = (\beta-\alpha)\ell\sqrt{\pi\ell} \qquad (10)$$

where

ℓ = half crack length.

From Equation (10) it can be seen that if $\beta > \alpha$ then $(K_I)_2 > (K_I)_1$ implying that the bottom of the fracture reaches the critical value K_{Ic} first and that downward migration is probable. Conversely, if $\alpha > \beta$ then $(K_I)_1 > (K_I)_2$ and upward migration is most probable. Thus, it is conceivable that vertical motion of the crack could be controlled by using hydraulic fracture fluids with various densities depending on whether upward ($\alpha>\beta$), downward ($\beta>\alpha$) or both upward and downward (equal probability, $\beta=\alpha$) motion is desired.

An additional interesting observation can be made by further examination of Equation (10). If the difference in stress intensity factors $(K_I)_2-(K_I)_1$, was equal to K_{Ic} then crack extension would be certain for $(K_I)_2 > (K_I)_1 > 0$. Thus the relationship between this difference and the difference in β and α is given by

$$\beta - \alpha = \frac{K_{Ic}}{\ell\sqrt{\pi\ell}} \qquad (11)$$

Figure 11 shows a plot of this equation for various values of the fracture toughness K_{Ic}. We consider two cases, both of which give the same value for $|\beta-\alpha| = .25$. Case one assumes the pressure gradient is due to water pressure on the crack face (β = 9.73 KPa/m (.43 psi/ft)) and case two assumes a 21.2 KN/m^3 (18 lb/gal) mud is pressurizing the crack (β = 15.4 KPa/m (.93 psi/ft)). For both cases, the tectonic stress variation was taken to be 15.4 KPa/m (.68 psi/ft). Case one would correspond to upward migration of the crack and Case two corresponds to downward migration. The crack length for which $|\beta-\alpha| = .25$ and K_{Ic} = 1.65 MN/m$^{3/2}$(1500 lb in$^{-3/2}$) is approximately 54.8 m (180 ft). For crack lengths less than this value ΔK_I is less than K_{Ic}. That is, $(K_I)_2$ is closer to $(K_I)_1$. When the crack reaches 54.8 m (180 ft) total vertical height, $\Delta K_I = K_{Ic}$ which implies $(K_I)_2 = K_{Ic}$, $(K_I)_1 = 0$ for $\beta-\alpha < 0$. For crack lengths exceeding 54.8 m (180 ft), $(K_I)_2 = K_{Ic}$ and $(K_I)_1 < 0$. Negative values for K_I implies the crack is closed and the crack length must be reduced to the point where $K_I = 0$. We, therefore, have the interesting result that the crack reaches a critical length at which point a crack of constant length propagates either upward or downward depending on the sign of $\beta-\alpha$. In the field case, this result cannot occur to any great extent since as the crack closes during upward or downward migration, the source of pressurization (perforation holes) would be "covered up" and crack pressurization would not be possible. It is conceivable, however, that as the crack extends away from the well bore that it would tend to propagate upward and downward at fixed height since near the well bore the propping agent might hold the crack open allowing fluid to flow out into the fracture. The important thing to note, however, is that preferred upward or downward crack migration is entirely possible and that by adjustment of the hydraulic fracture fluid density, chances can be maximized to have a horizontally propagating fracture. In order to do this, information as to the variation in *in situ* stress with depth must be determined.

CONCLUSIONS

Three cases of hydraulic fracture containment have been discussed from the point of view of linear elastic fracture mechanics. Analyses of fracture containment as a two dimensional problem has yielded several fundamental results which may be applied in general to the design of massive hydraulic fractures. The following conclusions were made.

1. Hydraulic fractures in a pay zone located between two adjacent barrier

layers will tend to be contained provided the stiffness of the pay zone is less than the stiffness of the barrier layers. Furthermore, if the opposite condition exists, barrier penetration is most likely.

2. Migration of a hydraulic fracture either upward or downward in an isotropic, homogeneous medium may be controlled by the density of the hydraulic fracture fluid. If the fluid density gradient is greater (less) than the *in situ* stress gradient downward (upward) migration is most probable.

3. If there exists a difference in *in situ* stress between the barrier layer and the pay zone with greater *in situ* stress in the barrier layer, then it may be possible to detect fracture propagation into the barrier formation. A sudden increase in pumping pressure will occur as the fracture crosses the interface and extends into the barrier layer. The increase in pressure is a function of the difference in *in situ* stress between the barrier and pay zone layers and the height of the pay zone.

From these results, it can be seen that the mechanical properties of the pay zone and the barrier formation as well as *in situ* stress information play a very important role in the prediction of hydraulic fracture containment.

REFERENCES

1. Simonson, E. R. and A. H. Jones, "Correlation of Log Data with Laboratory Determined Values of Elastic Moduli, Density, Porosity and Sonic Velocities," *Terra Tek Report* TR 76-37, August, 1976.

2. Simonson, E. R. and A. H. Jones, "Hydraulic Fracture Analysis of the Kinney #1 and #3 Wells, *Terra Tek Report* TR 76-25, May, 1976.

3. Cooke, C. E., "Effect of Fracturing Fluids on Fracture Conductivity," *J. of Petr. Tech.*, October, 1975.

4. Brechtel, C. E., A. S. Abou-Sayed, R. J. Clifton and B. C. Haimson, "*In Situ* Stress Determination in the Devonian Shales (Ira McCoy 20402) Within the Rome Basin," *Terra Tek Report* TR 76-36, July, 1976.

5. Haimson, B. C., "Earthquake Related Stresses at Rangely Colorado," in New Horizons in Rock Mechanics, Hardy, H. G. and Strefouks, R., editors; American Society of Civil Engineers, N. Y., pp. 689-708, 1973.

6. Advani, S. H., L. Z. Shuck, H. Y. Chang, and H. V. GangaRoa, "Analytical and Experimental Investigations on Induced Fracturing of Reservoir Rock," Preprint of a paper to be presented in the 1976 ASME meeting in Mexico City.

7. Irwin, G., "Analysis of Stresses and Strains Near the End of a Crack Transversing a Plate," *J. Appl. Mech.*, Vol. 24, p. 361, 1957.

8. Cooke, T. S. and F. Erdogan, "Stress in Bonded Materials with a Crack Perpendicular to the Interface," *Int. J. of Eng. Sci.*, Vol. 10, p. 677, 1972.

9. Simonson, E. R., A. H. Jones and A. S. Abou-Sayed, "Experimental and Theoretical Consideration of Massive Hydraulic Fracturing," *Terra Tek Report* TR 75-39, December, 1975.

10. Rice, J. R., "Mathematical Analysis in the Mechanics of Fracture," Chapter 3 of Treatise on Fracture - Volume II, edited by H. Liebowitz, Academic Press, New York, p. 191, 1968.

11. Erdogan, F., "On the Stress Distribution of Plates with Collinear Cuts under Arbitrary Loads," *Proceedings Fourth U. S. National Congress of Applied Mechanics*, p. 547, 1962.

12. Secor, D. T. J. and D. D. Pollard, "On the Stability of Open Hydraulic Fractures in the Earth's Crust," *Geophys. Res. Letters*, Vol. 2, November, 1975.

13. Jaeger, J. C. and N. G. W. Cook, Fundamentals of Rock Mechanics, Methuen and Co. Ltd., 1969.

14. Haimson, B. and C. Fairhurst, "Initiation and Extension of Hydraulic Fractures in Rocks," *Society of Petroleum Engineers Journal*, Vol. 7, p. 310, September, 1967.

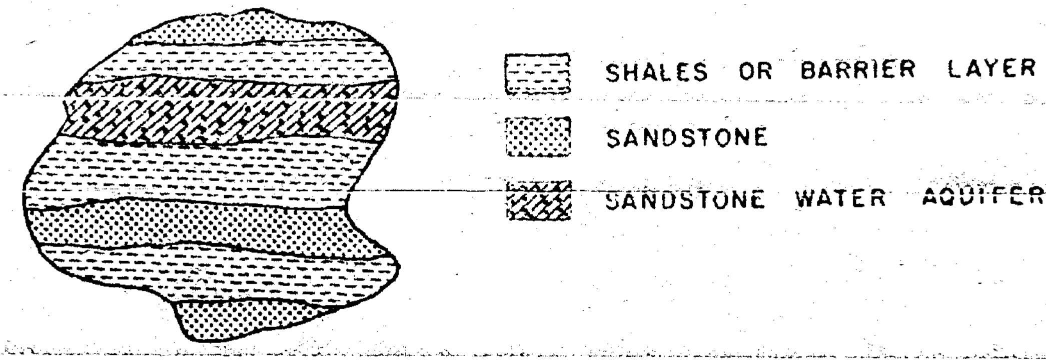

FIG. 1 - SCHEMATIC REPRESENTATION OF THE GAS BEARING FORMATION IN THE ROCKY MOUNTAIN REGION.

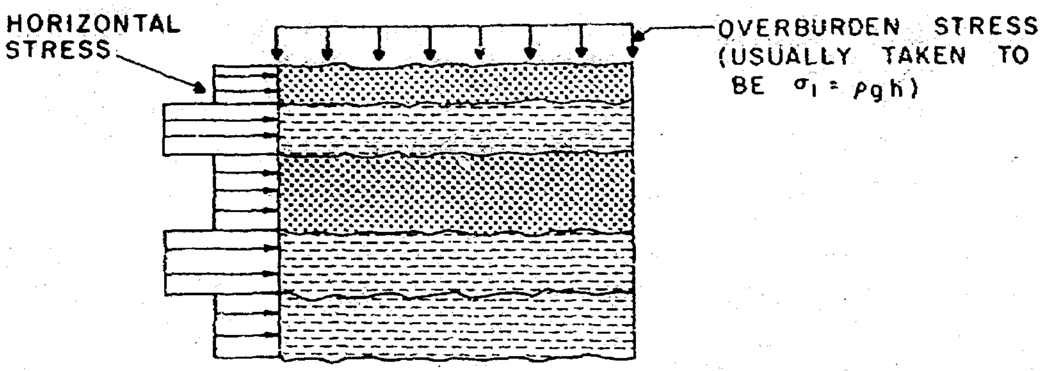

FIG. 2 - SCHEMATIC REPRESENTATION OF *IN SITU* STRESSES ACTING BENEATH THE EARTH'S SURFACE.

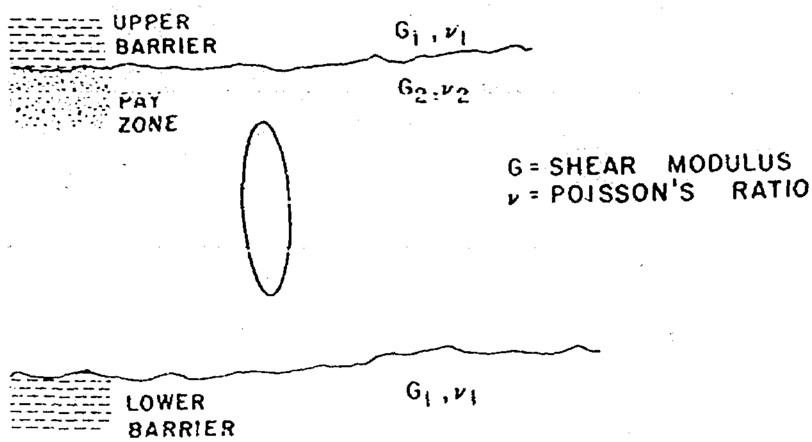

FIG. 3 - SCHEMATIC DRAWING OF A HYDRAULIC FRACTURE EMBEDDED IN A SAND LAYER BOUNDED BY UPPER AND LOWER BARRIER LAYERS.

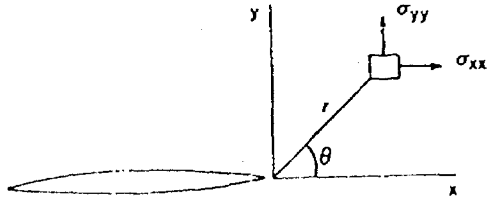

FIG. 4 - STRESS COMPONENTS NEAR THE TIP OF A SHARP CRACK.

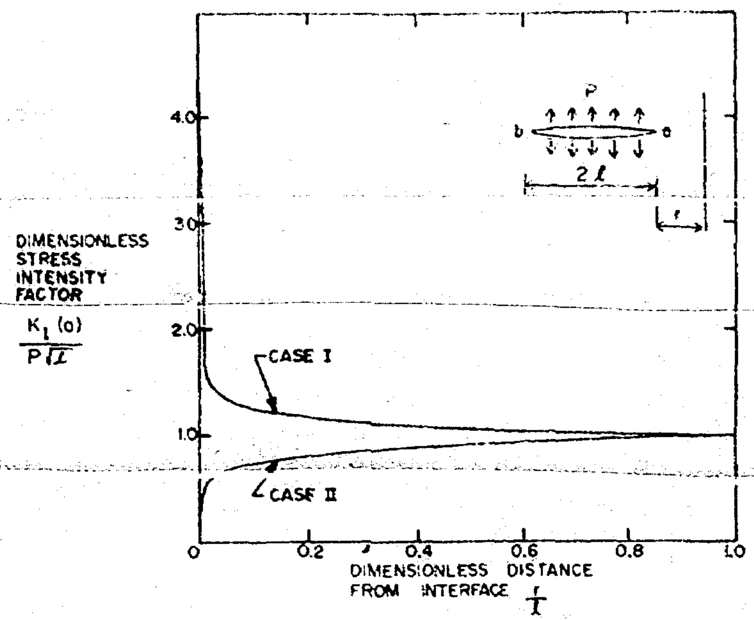

FIG. 5 - VARIATION IN THE STRESS INTENSITY FACTOR $(K_I)_A$ AS A FUNCTION OF DISTANCE (R/ℓ) TO THE INTERFACE.

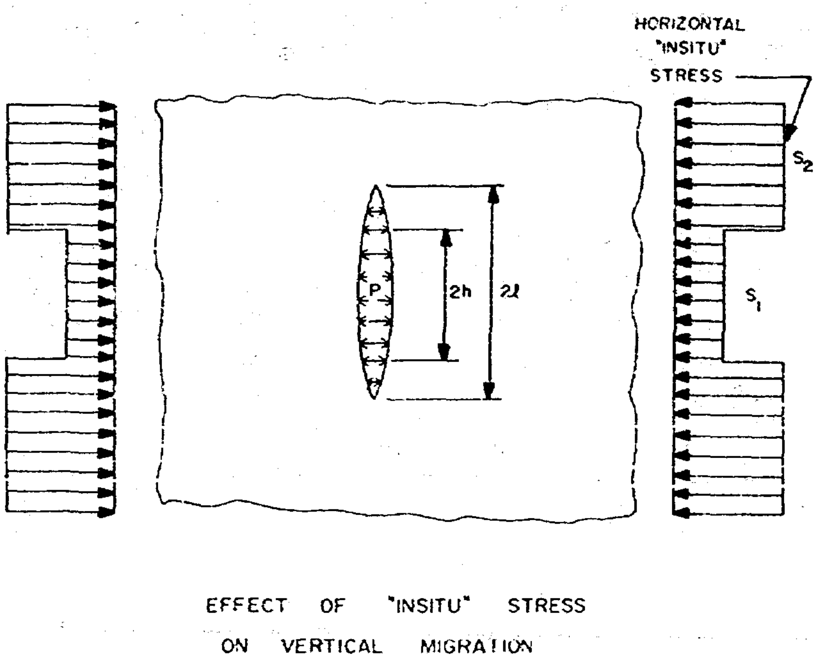

FIG. 6 - VERTICAL HYDRAULIC FRACTURE LOADED UNDER UNIFORM PRESSURE P WITH DIFFERING HORIZONTAL IN SITU STRESS.

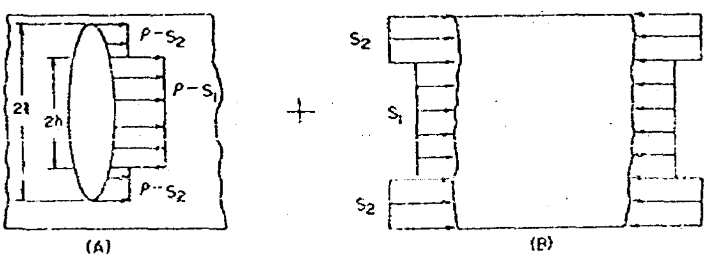

FIG. 7 - EQUIVALENT LOADING FOR THE PROBLEM SHOWN IN FIG. 6.

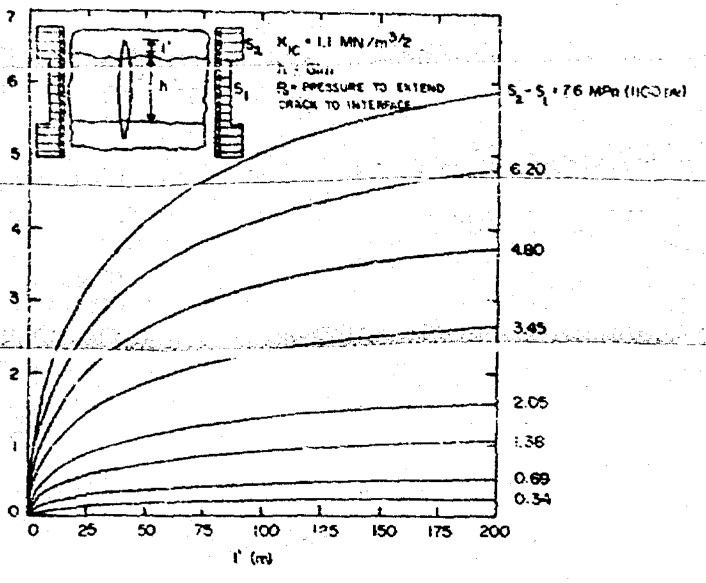

Fig. 8 - Plot of excess pressure P - P_0 versus distance advanced into the region of high stress. The in situ stress difference $S_2 - S_1$ is a parameter.

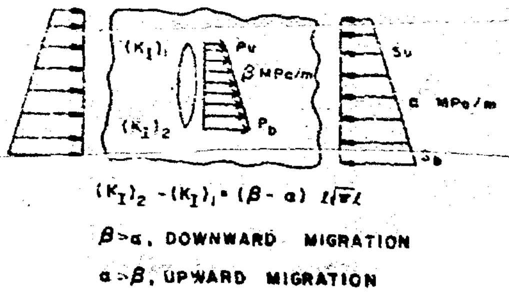

Fig. 9 - Plain strain idealization of a vertical hydraulic fracture in an infinite medium subjected to hydrostatic pressure loading with tectonic stress as far field loading; $(K_I)_1$ and $(K_I)_2$ are the stress intensity factors at the top and bottom of the fracture respectively.

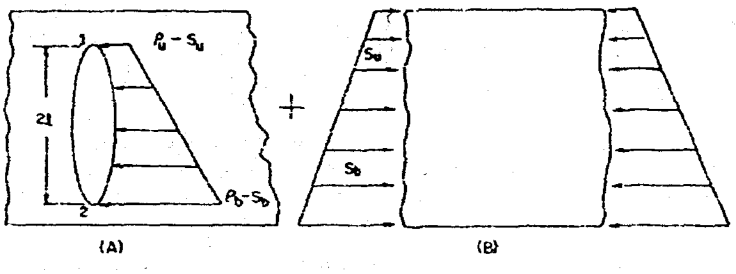

Fig. 10 - Equivalent loading for the problem shown in Fig. 9.

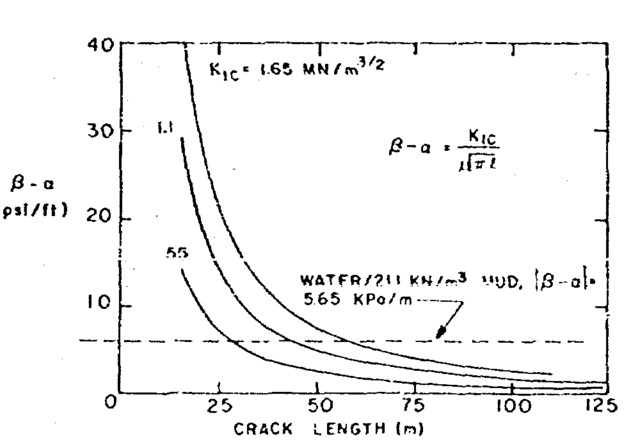

Fig. 11 - Plot of the difference in stress or pressure gradients coefficients versus crack length with fracture toughness K_{1c} as a parameter.

BLACKEYE MESAVERDE

(Oil)

T. 20 N., R. 9 W., NMPM

San Juan County, New Mexico

By: Bruce A. Black
Colorado Plateau Geological Services, Incorporated

GEOLOGY

Regional Setting: South flank of the San Juan Basin

Surface Formations: Cretaceous, Menefee Formation

Exploration Method Leading to Discovery: Follow up to oil show noted in Menefee while drilling offset well to Blackeye Dakota discovery

Type of Trap: Stratigraphic

Producing Formation: Cretaceous, Menefee Formation

Gross Thickness and Lithology of Reservoir Rocks: 12 feet of nonmarine channel sandstone

Geometry of Reservoir Rock: Lenticular channel sandstone

Other Significant Shows: None

Oldest Stratigraphic Horizon Penetrated: Cretaceous, Mancos Shale

DISCOVERY WELL

Name: Jaco, Inc. No. 55-4 Jaco Slaughter

Location: NW NW sec. 32, T. 20 N., R. 9 W.

Elevation (KB): 6,522 feet

Date of Completion: May 4, 1972

Total Depth: 2,737 feet

Production Casing: 4½" at 1,170 feet

Perforations: 1,048 feet to 1,056 feet

Stimulation: None; natural completion

Initial Potential: Pump 20 BOD

Bottom Hole Pressure: 454 psi

DRILLING AND COMPLETION PRACTICES

Wells are drilled with natural water base mud through the pay and perforated. Wells are acid washed and completed on pump.

RESERVOIR DATA

Productive Area:
- Proved (as determined geologically): 30 acres
- Unproved: 80 acres
- Approved Spacing: 10 acres
- No. of Producing Wells: 3
- No. of Abandoned Wells: 0
- No. of Dry Holes: 8

Average Net Pay: 10 feet

Porosity: 26 percent

Permeability: 400 millidarcies

Water Saturation: 40 percent

Initial Field Pressure: 454 psi

Type of Drive: Solution gas (?)

Gas Characteristics and Analysis: Small amounts of methane through pentane with methane predominating

Oil Characteristics and Analysis: Dark brown 32° API gravity crude

Associated Water Characteristics and Analysis: Fresh water

Original Gas, Oil and Water Contact Datums: Unknown

Estimated Primary Recovery: 20,000 BO

Type of Secondary Recovery: Probable waterflood

Estimated Ultimate Recovery: 40,000 BO

Present Daily Average Production: 10 BOD

Market Outlets: Oil is trucked to Farmington

FIELD COMMENTARY

The Blackeye Mesaverde pool is located in secs. 30 and 32 of T. 20 N., R. 9 W., NMPM. The pool was originally discovered in May of 1972 by the Jaco 55-4 Jaco Slaughter well. This well was drilled as an immediate offset to the Young and Walters Jaco No. 2 Dakota test which cut 12 feet of oil sandstone at 1,050 feet while attempting to offset the indicated new Dakota pool discovery found by the Blackeye No. 1 well in sec. 29. The Jaco 55-4 initialed for 20 barrels of 32° API gravity oil per day, with 10 barrels of water and very small amounts of associated gas. The accumulation appears to be localized in a small fluvial channel sandstone in the Menefee Formation. Additional drilling has yielded two additional oil wells and 8 dry holes in an attempt to follow this channel.

Another well, the Birdseye Federal 30-1, is also classified as part of the Blackeye Mesaverde pool. This well was drilled to test shows reported in the Beard Oil Company 8-30 Federal No. 1 in section 30, T. 20 N., R. 9 W. The Federal 30-1 was drilled on the same location pad and 50 feet north of the Beard well. The well was spuded on April 30, 1972 and cut 10 feet of saturated oil sandstone from 1,059 to 1,069 feet on May 3, 1972. The well was put on pump on May 8th and made an initial production of 12 barrels of oil and 30 barrels of water per day.

This well, also classified within the Blackeye Mesaverde pool, is undoubtably producing from a separate and distinct channel from the Jaco wells. Both the Jaco wells and the Federal 30-1 produce from non-marine channel sandstone at approximately 1,050 feet. The sandstones run approximately 26 percent porosity and 500 millidarcies permeability. Oil gravity in the Beard well, however, is 36° API gravity, while the oil gravity in the Jaco accumulation is 32° API gravity. Additional development work to follow up both of these channels is expected in the future.

REFERENCES

New Mexico Oil Conservation Commission Records
Personal and operators files
Files of H. S. Birdseye (deceased)

BEFORE EXAMINER STAMETS
OIL CONSERVATION DIVISION
EXHIBIT NO. 4a,b,c
CASE NO. 2459
Submitted by
Hearing Date 2/16/82

[Four Corners Geological Society

Ex 4A

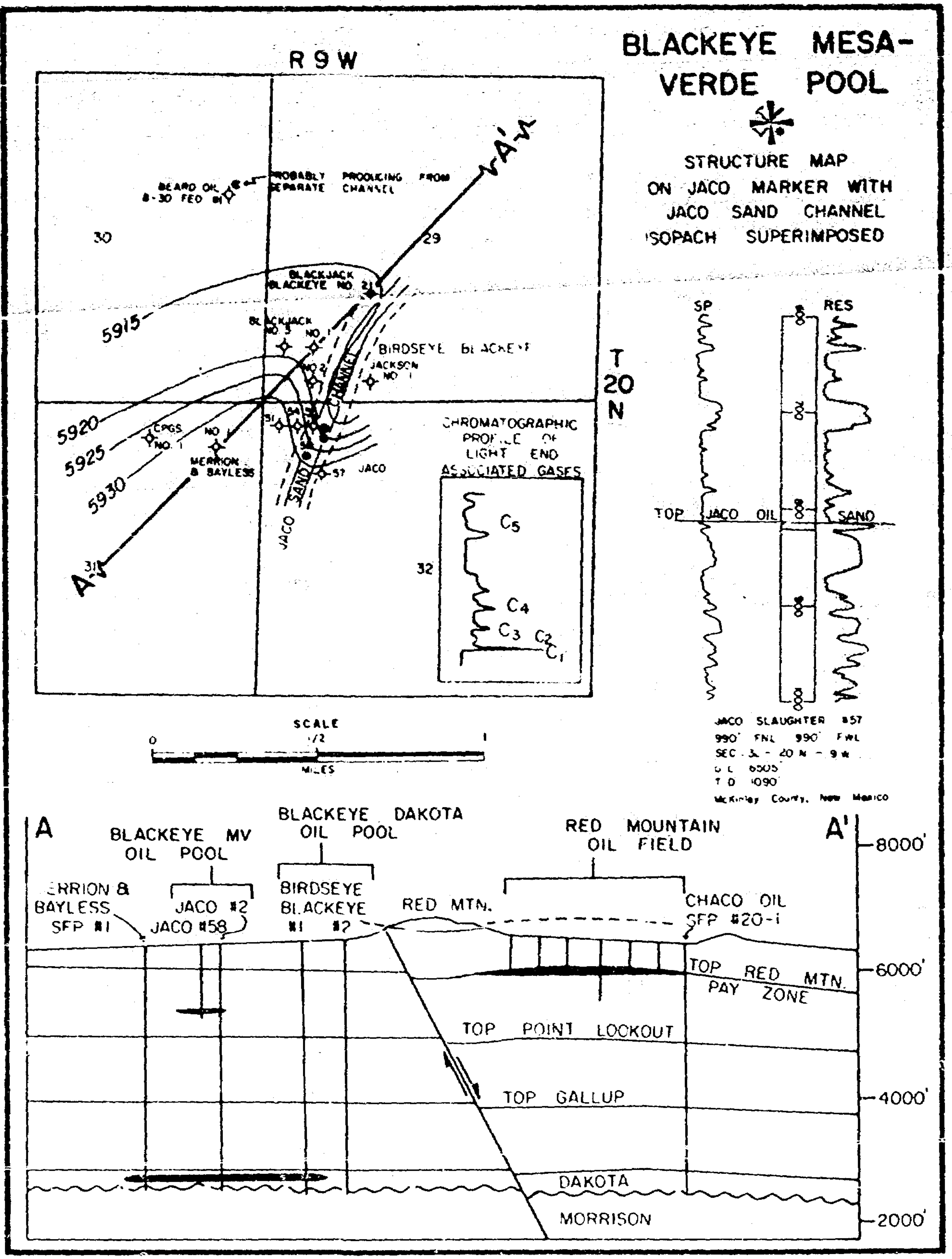
BLACKEYE MESA-VERDE POOL
STRUCTURE MAP ON JACO MARKER WITH JACO SAND CHANNEL ISOPACH SUPERIMPOSED
R 9 W
T 20 N
A
A'
30
29
31
32
5915
5920
5925
5930
BLACKJACK BLACKEYE NO. 21
BIRDSEYE BLACKEYE
JACKSON NO. 1
MERRION & BAYLESS
JACO
JACO SAND CHANNEL
CHROMATOGRAPHIC PROFILE OF LIGHT END ASSOCIATED GASES
C_5
C_4
C_3
C_2
C_1
SCALE
0
1/2
1
MILES
SP
RES
TOP JACO OIL SAND
JACO SLAUGHTER #57
BLACKEYE MV OIL POOL
BLACKEYE DAKOTA OIL POOL
RED MOUNTAIN OIL FIELD
BAYLESS SFP #1
JACO #2
JACO #58
BIRDSEYE BLACKEYE #1 #2
RED MTN.
CHACO OIL SFP #20-1
TOP RED MTN. PAY ZONE
TOP POINT LOOKOUT
TOP GALLUP
DAKOTA
MORRISON
8000'
6000'
4000'
2000'

CHACO WASH MESAVERDE
(Oil)
T. 20 N., R. 9 W., NMPM
McKinley County, New Mexico

By: Bruce A. Black
Colorado Plateau Geological Services

GEOLOGY

Regional Setting: South flank of the San Juan Basin

Surface Formations: Cretaceous, Menefee Formation

Exploration Method Leading to Discovery: Drilled on the projection of a surface anticlinal nose

Type of Trap: Structural-stratigraphic

Producing Formation: Cretaceous, Menefee Formation

Gross Thickness and Lithology of Reservoir Rocks: 10 feet of fluvial channel sandstone

Geometry of Reservoir Rocks: Lenticular channel

Other Significant Shows: None

Oldest Stratigraphic Horizon Penetrated: 1,583 feet, Menefee Formation (no shows)

DISCOVERY WELL

Name: Scanlon-Shepard No. 3 SFP (Oil was originally found in the pool in 1934, but available records do not show name of well or specific date.)

Location: SE SE sec. 21, T. 20 N., R. 9 W.

Elevation (KB): 6,423 feet

Date of Completion: September 18, 1961

Total Depth: 320 feet

Production Casing: 4½" at 314 feet

Perforations: None, completed open hole

Stimulation: 1 barrel mud acid

Initial Potential: Pump 17 BOD

Bottom Hole Pressure: 139 psi

DRILLING AND COMPLETION PRACTICES

Wells are drilled with natural water base mud through the pay zone; 4½" casing is set on top of the pay using a cement basket and the well is completed open-hole. Casing is cemented to surface. Rods, tubing and pump are installed. From spud to completion operations take three days. Wells are pumped with small pump jack.

RESERVOIR DATA

Productive Area:
- Proved (as determined geologically): 40 acres
- Unproved: 40 acres
- Approved Spacing: 5 acres
- No. of Producing Wells: 5
- No. of Abandoned Wells: 32
- No. of Dry Holes: 10

Average Net Pay: 10 feet

Porosity: 28 percent

Permeability: 344 millidarcies

Water Saturation: 50 percent

Initial Field Pressure: 140 psi

Type of Drive: Low pressure water drive

Gas Characteristics and Analysis: No methane or ethane, small amounts of propane, butane, and pentane with butane and pentane dominant

Oil Characteristics and Analysis: Oil is light brown, low sulfur, low paraffin, 46° API gravity

Associated Water Characteristics and Analysis: Fresh water

Original Gas, Oil, and Water Contact Datums: +6,075 feet

Estimated Primary Recovery: Recovery to date (January 1978) estimated at 5,000 bbls of oil

Type of Secondary Recovery: A pilot water flood was instigated in early 1974 with an invert 5 spot. The pilot demonstrated the feasibility of flooding and would be comparable with the Red Mountain flood. No flood has yet been instigated however.

Estimated Ultimate Recovery: In excess of 100,000 BO if properly flooded

Present Daily Average Production: 6 BOD

Market Outlets: Oil is trucked to Farmington by Plateau Corporation

FIELD COMMENTARY

The Chaco Wash Mesaverde oil pool is located in sections 21, 22, 27 and 28 of T. 20 N., R. 9 W., McKinley County, New Mexico. It is 50 miles north of Grants and 55 miles west of Cuba, New Mexico. The Chaco Wash oil pool was discovered in the late 1930's during the flurry of exploration drilling that followed discovery of the Red Mountain oil field a mile to the west. Forty-six degree API gravity oil was discovered at 340 feet in sandstones of the Menefee Formation. Early attempts to develop the Chaco Wash Pool were unsuccessful due primarily to lack of reservoir energy. Production from the field was very minor and sporadic until 1967 when the Santa Fe Pacific Railroad Company leased the area to Henry S. Birdseye.

Mr. Birdseye began orderly development of the pool in 1968 by drilling additional shallow holes to delineate the pay zone in preparation for instigating a water flood in the pool. The intended water injection well was spudded in February 1968 and encountered oil sandstone from 324 feet to 332 feet. The well was pump tested at 34 barrels of 43° API gravity oil per day and this and subsequent wells were put on primary production. The water flood plans were postponed indefinitely. Between 1968 and 1971, the field produced approximately 4,000 barrels of oil from an average of four wells with most of the oil being produced in the first two years. In June 1972, the operator was tragically killed in an aircraft crash, following which operations in the field were delegated to Colorado Plateau Geological Services, Inc. (CPGS) in 1973.

In May 1973, a single invert five-spot pilot water flood was initiated by CPGS, for the estate. This small pilot flood in-

Ex 4 B

creased production sixteen fold and demonstrated the floodability of the Chaco Wash sandstone in this area. In late 1975, CPGS obtained the leases from the Birdseye Estate.

Both the Red Mountain oil field and Chaco Wash oil pool lie along the same anticlinal axis on the Chaco Slope, on the south flank of the San Juan Basin. A major northeast-trending normal fault, downthrown to the west, probably crosses the saddle between the two areas and may have an important bearing on oil accumulations at Chaco Wash. No oil-water contact has yet been determined, and the producing area may expand to the east, north, and west.

The shallow oil pay at Chaco Wash is a lenticular sandstone of the Menefee Formation, Mesaverde Group, of Upper Cretaceous age, occurring at a depth of approximately 340 feet. The Menefee Formation is a series of sandstones, shales, and coal beds deposited in a nearshore lagoonal or swamp environment. In the Chaco Wash area, it extends to a depth of about 1,600 feet. The 340-foot pay at Chaco Wash is a fluvial channel sandstone, from 9 feet to 19 feet in thickness, draped over a structural nose.

The core analysis of 10 feet of net pay in the No. 10 well at Chaco Wash shows average porosity in excess of 28 percent, and permeability in excess of 340 millidarcies; a reservoir volume factor of 1.05 is assumed, and since the core was flushed considerably during coring, connate water saturation of 50 percent is assumed. Despite the relatively low oil saturations in the core, this well had an initial production of 34 barrels of oil per day, with no water. The reservoir factors at Chaco Wash are slightly better than those at Red Mountain, where water flooding has recovered more oil per acre than in any other flood in northwest New Mexico. Recovery from the 55-acre pilot flood at Red Mountain already exceeds 343 barrels per acre-foot, about half of the total original reserves, from an average pay thickness of 15 feet. At Chaco Wash, with an average pay thickness of 13 feet and original reserves of 701 barrels per acre-foot, a primary-plus-secondary recovery factor of 50 percent may eventually yield 4,500 barrels per acre from the 340-foot zone.

A source of artesian water from the massive Hospah-Gallup Sandstone, between 2,000 and 2,900 feet, supplies both the Red Mountain flood and the pilot flood at Chaco Wash.

REFERENCES

New Mexico Oil Conservations Commission Records.
Personal and operator's files.
Files of H. S. Birdseye (deceased).

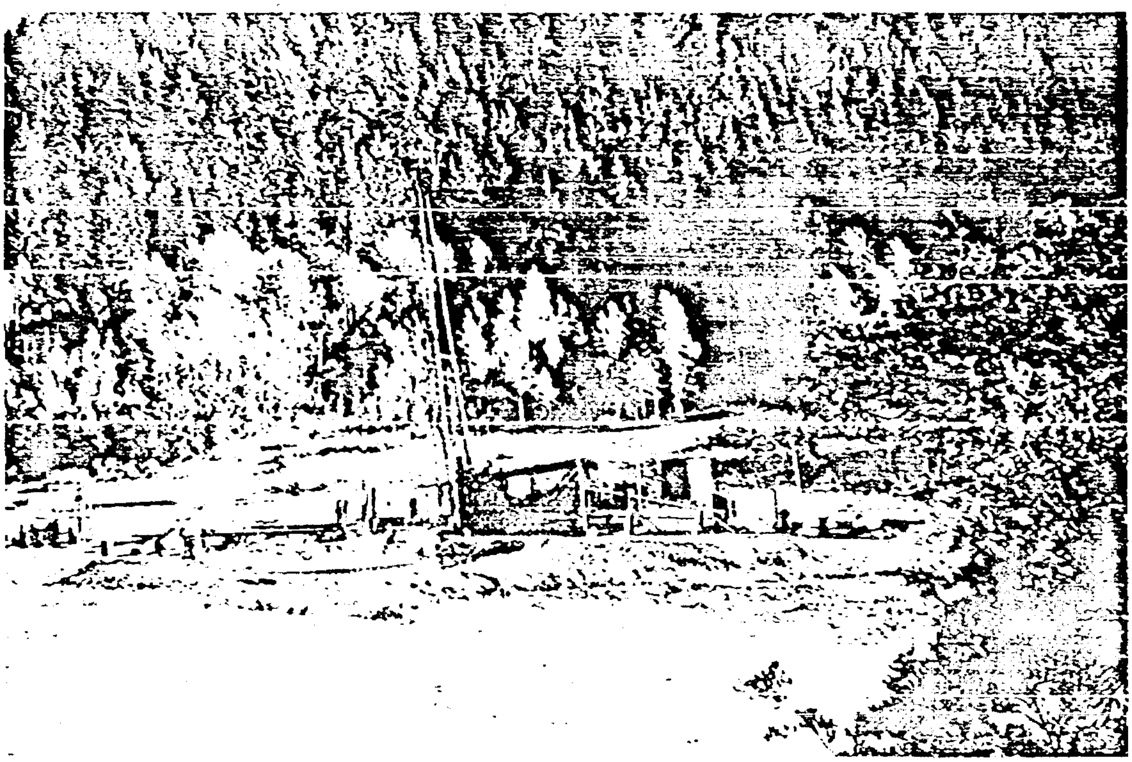

Butler No. 2 Crowley well drilling in the East Chromo Field, Colorado in 1951. The well bottomed in metamorphic boulders at 1,710 feet. (Photo from Walt Osterhoudt)

RED MOUNTAIN MESAVERDE
(Oil)
T. 20 N., R. 9 W., NMPM
McKinley County, New Mexico

By: Bruce A. Black
Colorado Plateau Geological Services

GEOLOGY

Regional Setting: South flank of the San Juan Basin

Surface Formations: Cretaceous, Menefee Formation

Exploration Method Leading to Discovery: Surface mapping

Type of Trap: Structural-stratigraphic

Producing Formation: Cretaceous, Menefee Formation

Gross Thickness and Lithology of Reservoir Rocks: 15 feet, fluvial channel sandstone

Geometry of Reservoir Rock: Lenticular channel sandstone which pinches out both east and west

Other Significant Shows: None

Oldest Stratigraphic Horizon Penetrated: Cretaceous, Menefee Formation (975 feet)

DISCOVERY WELL

Name: Stacy, Weber, et al. No. 1 SFP

Location: NE NE sec. 29, T. 20 N., R. 9 W.

Elevation (KB): 6,480 feet

Date of Completion: June, 1934

Total Depth: 495 feet

Production Casing: 478 feet of 4½"

Perforations: Completed open hole

Stimulation: None

Initial Potential: Pump 5 BOD

Bottom Hole Pressure: 195 psi

DRILLING AND COMPLETION PRACTICES

Wells are normally drilled with natural water-base mud through the pay zone. 4½" casing is set on top of the pay and cemented to surface. Rods, tubing and pump are installed. Wells are pumped with small pump jacks. From spud to completion, operation takes three days.

RESERVOIR DATA

Productive Area:
- Proved (as determined geologically): 40 acres
- Unproved: 20 acres
- Approved Spacing: 5 acres
- No. of Producing Wells: 4 (14 injectors)
- No. of Abandoned Wells: 25
- No. of Dry Holes: 10

Average Net Pay: 15 feet

Porosity: 28 percent

Permeability: 400 millidarcies

Water Saturation: 50 percent

Initial Field Pressure: 195 psi

Type of Drive: Low pressure water drive

Gas Characteristics and Analysis: Small amounts of methane, ethane, propane, butane, and pentane with butane and pentane dominant; gas is too small to measure

Oil Characteristics and Analysis: Oil is light brown, low sulfur, low paraffin 42° API gravity

Associated Water Characteristics and Analysis: Fresh water

Original Gas, Oil and Water Contact Datums: Oil-water contact approximately +6,025 feet

Estimated Primary Recovery: 173 BO per acre (15 percent estimated primary recovery factor). Prior to water flood, the field had produced 25,290 BO

Type of Secondary Recovery: Under water-flood the field produced an additional 225,000 BO from 40 acres (as of January, 1978)

Estimated Ultimate Recovery: Assuming no additional deeper pays, the ultimate is established at 300,000 bbls of oil

Present Daily Average Production: 4 BOD (January, 1978)

Market Outlets: Oil trucked to Farmington by Plateau Corporation. No gas production.

FIELD COMMENTARY

The Red Mountain oil field is located in sections 20 and 29, T. 20 N., R. 9 W., in northern McKinley County, New Mexico. The field is 55 miles north of Grants, 50 air miles west of Cuba, 57 air miles south-southeast of Farmington and 93 air miles northwest of Albuquerque. The Red Mountain structure is situated in a broad strike valley in shale members of the Mesaverde Group some two miles south of the escarpment known as Chacra Mesa, which is capped by the uppermost member of the Mesaverde Group, the Cliff House Sandstone. Topographic relief in this portion of the San Juan Basin is generally slight, interrupted by occasional buttes capped by erosion-resistant sandstone beds. In a regional sense, the Red Mountain field is on the Chaco Slope on the south flank of the San Juan Basin between the Zuni Uplift to the south and the deeper parts of the San Juan Basin to the north. Regional dip is to the northeast at an average of about 100 feet per mile.

The Red Mountain pay zone is a fluvial channel sandstone and is the only pay horizon in the field. It ranges from 5 to 25 feet in thickness with an average of 15 feet of net pay. Porosities average 28 percent in this channel sandstone. The channel sandstone and the Red Mountain anticline combine to form a combination stratigraphic-structural trap with a low pressure water drive.

Oil was originally discovered in the Menefee Formation at Red Mountain by the Stacey, Weber et al., No. 1 Santa Fe well in sec. 29, T. 20 N., R. 9 W., in June of 1934. The discovery well, completed near the crest of a small but obvious surface anticline, produced at a rate of 5 BOD from a depth of 478 to 495 feet. In the next three years, 25 additional wells were drilled on the structure. Seven of these wells were completed as producers. Sporadic shallow primary development con-

Ex 4C

tinued through the next two decades. Available state records indicate a cumulative production in excess of 22,000 barrels during this period of time.

However, since the field was discovered prior to the establishment of the Oil Conservation Commission, production and technical data now available are incomplete and unreliable. The productive area of the field, now covered by a lease from the Santa Fe Pacific Railroad Company, on the south half of section 20 and the north half of section 29, has changed hands intermittently since the field discovery. In 1937, this lease was assigned to Ben and Celia Sapir. In November of 1957, operation of this lease was assumed by Chaco Oil Company, a joint venture of Ben Sapir and Henry S. Birdseye. In November 1958, Chaco Oil Company assumed operations of the field. At this time, the field had four producers and was making approximately 300 barrels of oil per month. Chaco Oil Company drilled and logged an additional 10 shallow stratigraphic test holes to delineate the field boundaries and the structural configuration.

In July 1958, Chaco Oil Company drilled a Morrison test in the southeast quarter of section 20. This well bottomed at a total depth of 3,936 feet. The well was plugged and abandoned after encountering gas-cut salt water in the Dakota Sandstone. While this test did not find oil in the Dakota, oil and gas shows were logged in the samples and seen on the gas detector in the basal Menefee Formation, Point Lookout Sandstone, "Hospah" sandstone, "Gallup" sandstone, and Dakota Sandstone. Selected intervals in the "Hospah," "Gallup" and Dakota were drill-stem tested with negative hydrocarbon results. The well was plugged back to 900 feet and eventually completed as a water supply well in July of 1960 in preparation for flooding the north half of the Red Mountain field.

Chaco Oil Company began its first regular water injection into the Red Mountain field in January 1961. Between December of 1960 and March 1961, production was doubled to 1,080 barrels per month and by August of 1963, the field was making 5,440 barrels of oil per month. The water flood oil production peaked at 5,552 barrels per month in August 1963 and production gradually declined to its economic limit by September, 1969. Between 1960 and January 1971, the Red Mountain water flood had produced more than 241,156 barrels of 43° API gravity oil from approximately 55 acres of the field at an average depth of 450 feet, using a maximum of 15 injection and 10 producing wells. This is an average of approximately 293 barrels of oil recovered per net acre foot of reservoir flooded, or a cumulative oil recovery of 4,385 barrels per acre. Ninety percent of this oil was recovered in the six-year period from 1961 through 1966. This recovery is the highest flood recovery per acre in the San Juan Basin and is more than twice the per acre recovery of Gulf Oil's West Bisti Unit flood which is the next highest.

In December 1971, a partnership was formed to buy out the assets of the Chaco Oil Company. On June 20, 1972, and prior to beginning any additional water flood operations on the undeveloped and unflooded portions of the Red Mountain field, the general partner and operator were tragically killed in a small plane accident in southwestern New Mexico. The subsequent settlement of the general partners estate and resulting problems necessitated the termination of the partnership. Monback Associates acquired a 75 percent interest in the Red Mountain field in August 1973 and Colorado Plateau Geological Services, Inc. acquired the remaining 25 percent in 1975. A possible micellar flood is now being planned for the field in late 1979.

REFERENCES

Files of H. S. Birdseye (deceased).
New Mexico Oil Conservation Commission records.
Personal and operator's files.

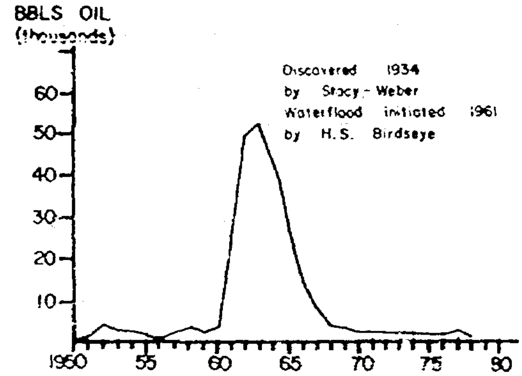

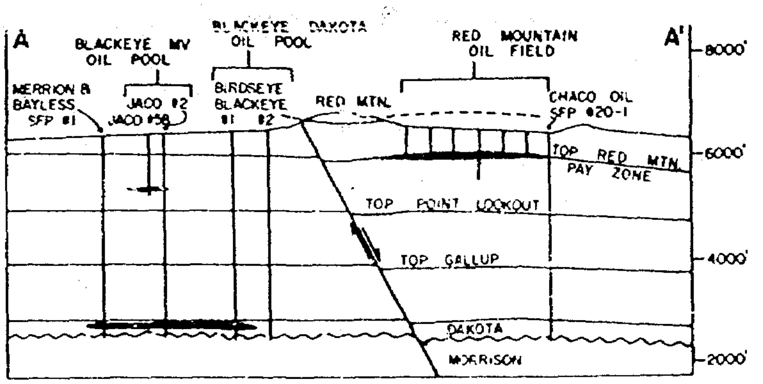

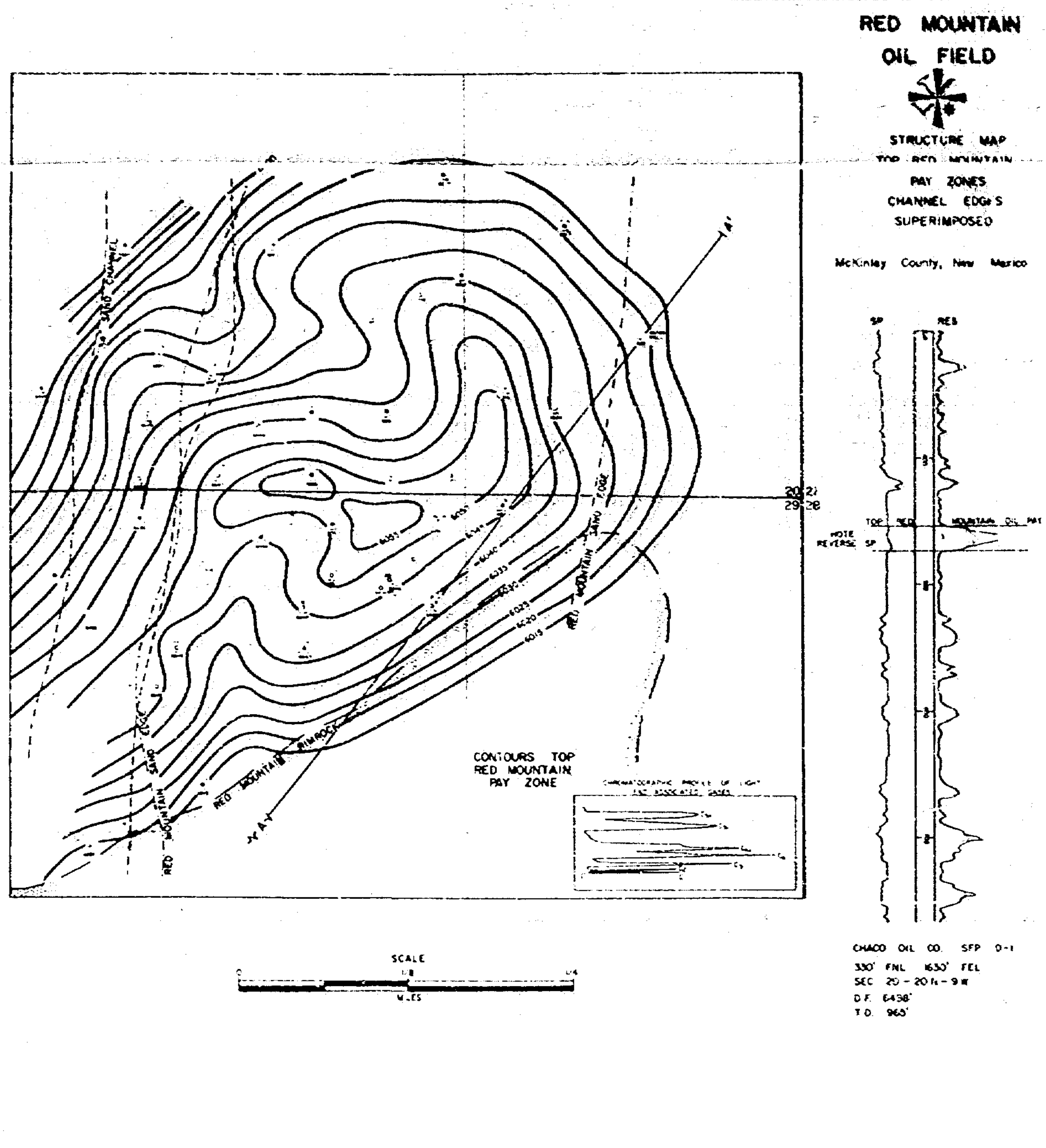

RED MOUNTAIN
OIL FIELD
STRUCTURE MAP
TOP RED MOUNTAIN
PAY ZONES
CHANNEL EDGES
SUPERIMPOSED
McKinley County, New Mexico
CONTOURS TOP
RED MOUNTAIN
PAY ZONE
RED MOUNTAIN RIMROCK
RED MOUNTAIN SAND EDGE
SAND CHANNEL
SCALE
MILES
SP
RES
TOP RED MOUNTAIN OIL PAY
NOTE REVERSE SP
CHACO OIL CO. SFP 0-1
330' FNL 1650' FEL
SEC 20 - 20 N - 9 W
D.F. 6438'
T.D. 965'

Dockets Nos. 9-82 and 10-82 are tentatively set for March 31, and April 14, 1982. Applications for hearing must be filed at least 22 days in advance of hearing date.

DOCKET: EXAMINER HEARING - TUESDAY - MARCH 16, 1982

9 A.M. - OIL CONSERVATION DIVISION CONFERENCE ROOM
STATE LAND OFFICE BUILDING, SANTA FE, NEW MEXICO

The following cases will be heard before Richard L. Stamets, Examiner, or Daniel S. Nutter, Alternate Examiner:

ALLOWABLE: (1) Consideration of the allowable production of gas for April, 1982, from fifteen prorated pools in Lea, Eddy, and Chaves Counties, New Mexico.

(2) Consideration of the allowable production of gas for April, 1982, from four prorated pools in San Juan, Rio Arriba, and Sandoval Counties, New Mexico.

CASE 7502: Application of Sun Oil Company for an unorthodox gas well location and non-standard gas proration unit, Lea County, New Mexico. Applicant, in the above-styled cause, seeks approval for the unorthodox location of a well to be drilled 760 feet from the South line and 960 feet from the East line of Section 6, Township 24 South, Range 37 East, Jalmat Gas Pool, and a 160-acre non-standard proration unit comprising the SE/4 of said Section 6.

CASE 7503: Application of Sun Oil Company for an unorthodox gas well location and non-standard gas proration unit, Lea County, New Mexico. Applicant, in the above-styled cause, seeks approval for the unorthodox location of a well to be drilled 1980 feet from the North line and 1400 feet from the East line of Section 22, Township 22 South, Range 36 East, Jalmat Gas Pool, and a 120-acre non-standard proration unit comprising the W/2 NE/4 and SE/4 NE/4 of said Section 22.

CASE 7504: Application of Cities Service Company for the extension of vertical limits of the Langlie Mattix Pool, Lea County, New Mexico. Applicant, in the above-styled cause, seeks the contraction of the vertical limits of the Jalmat Pool and the upward extension of the vertical limits of the Langlie Mattix Pool to a subsurface depth of 3416 feet underlying the NW/4 of Section 19, Township 24 South, Range 37 East.

CASE 7505: Application of BCO, Inc. for downhole commingling, Rio Arriba County, New Mexico. Applicant, in the above-styled cause, seeks approval for the downhole commingling of Lybrook-Gallup and Basin-Dakota production in the wellbores of wells drilled and to be drilled in Section 2, 3, 4, 9 and 10, Township 23 North, Range 7 West.

CASE 7506: Application of Getty Oil Company for salt water disposal, Lea County, New Mexico. Applicant, in the above-styled cause, seeks authority to dispose of salt water into the Abo formation in the perforated interval from 8900 feet to 9300 feet in its State "P" Well No. 1, located in Unit P, Section 32, Township 16 South, Range 37 East, Lovington-Abo Pool.

CASE 7507: Application of Sonny's Oilfield Service, Inc. for an oil treating plant permit, Lea County, New Mexico. Applicant, in the above-styled cause, seeks authority for the construction and operation of an oil treating plant for the purpose of treating and reclaiming sediment oil at a site in the NW/4 NE/4 of Section 29, Township 18 South, Range 38 East.

CASE 7508: Application of P & O Oilfield Services, Inc. for an oil treating plant permit, Lea County, New Maxico. Applicant, in the above-styled cause, seeks authority for the construction and operation of an oil treating plant for the purpose of treating and reclaiming sediment oil at a site in the SW/4 NE/4 of Section 10, Township 25 South, Range 36 East.

CASE 7459: (Continued from February 17, 1982, Examiner Hearing)

Application of Red Mountain Associates for the Amendment of Order No. R-6538, McKinley County, New Mexico. Applicant, in the above-styled cause, seeks the amendment of Order No. R-6538, which authorized applicant to conduct waterflood operations in the Chaco Wash-Mesa Verde Oil Pool. Applicant seeks approval for the injection of water through various other wells than those originally approved, seeks deletion of the requirement for packers in injection wells, and seeks an increase in the previously authorized 68-pound limitation on injection pressure.

CASE 7457: (Continued from February 17, 1982, Examiner Hearing)
(This Case will be continued to April 28, 1982)

Application of E. T. Ross for nine non-standard gas proration units, Harding County, New Mexico. Applicant, in the above-styled cause, seeks approval for nine 40-acre non-standard gas proration units in the Bravo Dome Carbon Dioxide Area. In Township 19 North, Range 30 East: Section 12, the NW/4 NW/4 and NE/4 NW/4; Section 14, the NW/4 NE/4, SW/4 NE/4, and SE/4 NE/4. In Township 20 North, Range 30 East: Section 11, the NE/4 SW/4, SW/4 SE/4, SE/4 SW/4, and NW/4 SE/4.

CASE 7509: Application of Supron Energy Corporation for a non-standard proration unit or compulsory pooling, San Juan County, New Mexico. Applicant, in the above-styled cause, seeks approval of a 160-acre non-standard proration unit for the Dakota and Mesaverde formations comprising the SW/4 of Section 2, Township 21 North, Range 8 West, or in the alternative, an order pooling all mineral interests from the surface down through the Dakota formation underlying the S/2 of said Section 2, to be dedicated to a well to be drilled at a standard location thereon. Also to be considered will be the cost of drilling and completing said well and the allocation of the cost thereof as well as actual operating costs and charges for supervision, designation of applicant as operator of the well, and a charge for risk involved in drilling said well.

CASE 7510: Application of Union Oil Company of California for compulsory pooling, Lea County, New Mexico. Applicant, in the above-styled cause, seeks an order pooling all mineral interests in the Wolfcamp and Penn formations underlying the N/2 of Section 10, Township 22 South, Range 32 East, to be dedicated to a well to be drilled at a standard location thereon. Also to be considered will be the cost of drilling and completing said well and the allocation of the cost thereof as well as actual operating costs and charges for supervision, designation of applicant as operator of the well, and a charge for risk involved in drilling said well.

CASE 7511: (This Case will be continued to March 31, 1982)
Application of Buffton Oil & Gas Inc. for compulsory pooling, Lea County, New Mexico. Applicant, in the above-styled cause, seeks an order pooling all mineral interests in the Wolfcamp through Devonian formations underlying the W/2 of Section 35, Township 16 South, Range 35 East, to be dedicated to a well to be drilled at a standard location thereon. Also to be considered will be the cost of drilling and completing said well and the allocation of the cost thereof as well as actual operating costs and charges for supervision, designation of applicant as operator of the well, and a charge for risk involved in drilling said well.

CASE 7496: (Continued from March 3, 1982, Examiner Hearing)

Application of Viking Petroleum, Inc. for an unorthodox location, Chaves County, New Mexico. Applicant, in the above-styled cause, seeks approval for the unorthodox location of an Abo gas well to be drilled 62 feet from the South line and 1984 feet from the East line of Section 29, Township 5 South, Range 24 East, the SE/4 of said Section to be dedicated to the well.

CASE 7512: Application of Viking Petroleum, Inc. for an unorthodox location, Lea County, New Mexico. Applicant, in the above-styled cause, seeks approval for the unorthodox location of a well located in Unit H of Section 31, Township 13 South, Range 34 East, Nonombre-Penn Pool, said well being a recompleted Morrow test and located in the SE/4 of the quarter section whereas the pool rules require wells to be located in the NE/4 or SW/4 of the quarter section.

CASE 7476: (Continued from March 3, 1982, Examiner Hearing)

Application of Jack J. Grynberg for compulsory pooling, Chaves County, New Mexico. Applicant, in the above-styled cause, seeks an order pooling all mineral interests down through and including the Abo formation, underlying two 160-acre gas spacing units, being the NE/4 and SE/4, respectively, of Section 12, Township 5 South, Range 24 East, each to be dedicated to a well to be drilled at a standard location thereon. Also to be considered will be the cost of drilling and completing said wells and the allocation of the cost thereof as well as actual operating costs and charges for supervision, designation of applicant as operator of the wells and a charge for risk involved in drilling said wells.

CASE 7513: Application of Mesa Petroleum Company for compulsory pooling, Chaves County, New Mexico. Applicant, in the above-styled cause, seeks an order pooling all mineral interests in the Abo formation underlying the SE/4 of Section 12, Township 5 South, Range 24 East, to be dedicated to a well to be drilled at a standard location thereon. Also to be considered will be the cost of drilling and completing said well and the allocation of the cost thereof as well as actual operating costs and charges for supervision, designation of applicant as operator of the well, and a charge for risk involved in drilling said well.

CASE 7514: Application of Santa Fe Exploration Co. for compulsory pooling, or in the alternative a non-standard proration unit, Eddy County, New Mexico. Applicant, in the above-styled cause, seeks an order pooling all mineral interests in the Permo-Penn, Strawn, Atoka and Morrow formations underlying the W/2 of Section 2, Township 20 South, Range 25 East to be dedicated to a well to be drilled at a standard location thereon. Also to be considered will be the cost of drilling and completing said well and the allocation of the cost thereof as well as actual operating costs and charges for supervision, designation of applicant as operator of the well, and a 200 percent charge for risk involved in drilling said well. In the event said 200 percent risk factor is not approved, applicant seeks a non-standard unit excluding the lands of owners not participating in the well.

EXAMINER HEARING - TUESDAY - MARCH 16, 1982

CASE 7515: Application of Four Corners Gas Producers Association for designation of a tight formation, San Juan County, New Mexico. Applicant, in the above-styled cause, seeks the designation of the Dakota formation underlying all or portions of Townships 26 and 27 North, Ranges 12, and 13 West, Township 29 North, Ranges 13 through 15 West, and Township 30 North, Ranges 14 and 15 West, containing 164,120 acres, more or less, as a tight formation pursuant to Section 107 of the Natural Gas Policy Act and 18 CFR Section 271. 701-705.

CASE 7445: (Continued from February 17, 1982, Examiner Hearing)
(This Case will be continued to April 28, 1982)

Application of Harvey E. Yates Company for an NGPA determination, Eddy County, New Mexico. Applicant, in theabove-styled cause, seeks a new onshore reservoir [illegible] formation for its Fulton Collier Well No. 1 in Unit G of Section 1, Township 16 South, Range 28 East.

CASE 7492: (Continued and Readvertised)

Application of Harvey E. Yates Company for a tight formation, Chaves County, New Mexico. Applicant, in the above-styled cause, seeks the designation of the Atoka-Morrow formation underlying all or portions of Townships 7, 8, and 9 South, Ranges 28, 29, 30 and 31 East, containing 161,280 acres, more or less, as a tight formation pursuant to Section 107 of the Natural Gas Policy Act and 18 CFR Section 271. 701-705.

CASE 7500: (Continued from March 3, 1982, Examiner Hearing)

Application of Read & Stevens, Inc. for an exception to the maximum allowable base price provisions of the New Mexico Natural Gas Pricing Act, Eddy County, New Mexico. Applicant, in the above-styled cause, seeks an order of the Division prescribing the price allowed for production enhancement gas under Section 107 of the Natural Gas Policy Act as the maximum allowable base price if production enhancement work which qualifies under the NGPA is performed on its Hackberry Hills Unit Well No. 4 located in Section 22, Township 22 South, Range 26 East, Eddy County, New Mexico.

Docket No. 6-82

Dockets Nos. 7-82 and 8-82 are tentatively set for March 3 and March 17, 1982. Applications for hearing must be filed at least 22 days in advance of hearing date.

DOCKET: EXAMINER HEARING - WEDNESDAY - FEBRUARY 17, 1982

9 A.M. - OIL CONSERVATION DIVISION CONFERENCE ROOM
STATE LAND OFFICE BUILDING, SANTA FE, NEW MEXICO

The following cases will be heard before Richard L. Stamets, Examiner, or Daniel S. Nutter, Alternate Examiner:

ALLOWABLE: (1) Consideration of the allowable production of gas for March, 1982, from fifteen prorated pools in Lea, Eddy, and Chaves Counties, New Mexico.

(2) Consideration of the allowable production of gas for March, 1982, from four prorated pools in San Juan, Rio Arriba, and Sandoval Counties, New Mexico.

(3) Consideration of purchaser's nominations for the one year period beginning April 1, 1982, for both of the above areas.

CASE 7445: (Continued from December 16, 1981, Examiner Hearing)
(THIS CASE WILL BE CONTINUED TO THE EXAMINER HEARING ON MARCH 17, 1982)

Application of Harvey E. Yates Company for an NGPA determination, Eddy County, New Mexico. Applicant, in the above-styled cause, seeks a new onshore reservoir determination in the San Andres formation for its Fulton Collier Well No. 1 in Unit G of Section 1, Township 18 South, Range 28 East.

CASE 7479: Application of Northwest Pipeline Corporation for amendment of Order No. R-2046, Rio Arriba County, New Mexico. Applicant, in the above-styled cause, seeks the Amendment of Division Order No. R-2046, which authorized approval of six non-standard proration units, Basin-Dakota Gas Pool.

The amendment sought is for the creation of the following non-standard proration units to be drilled at standard locations thereon: Township 31 North, Range 6 West, Section 25: N/2 (272.16 acres) and S/2 (273.3 acres); Section 36: N/2 (272.56 acres) and S/2 (272.88 acres); Township 30 North, Range 6 West; Section 1: N/2 (272.81 acres) and S/2 (273.49 acres).

CASE 7480: Application of Arco Oil & Gas Company for pool creation, Lea County, New Mexico. Applicant, in the above-styled cause, seeks the creation of a new Upper Devonian gas pool for its Custer Well No. 1 located 1810 feet from the North line and 2164 feet from the West line of Section 6, Township 25 South, Range 37 East, Custer Field.

CASE 7481: Application of Arco Oil & Gas Company for amendment of Order No. R-6792, Lea County, New Mexico. Applicant, in the above-styled cause, seeks the amendment of Division Order No. R-6792, which authorized the directional drilling of applicant's Custer Wells Well No. 1 to an unorthodox location in the Devonian and Ellenburger formations and imposed a penalty in the Devonian. By stipulation applicant and the offset operator have agreed that the subject well is not affecting the offsetting property and applicant herein seeks removal of the penalty imposed for so long as the well produces only from the present perforated interval in the Upper Devonian.

CASE 7459: (Continued from January 20, 1982, Examiner Hearing)

Application of Red Mountain Associates for the Amendment of Order No. R-6538, McKinley County, New Mexico. Applicant, in the above-styled cause, seeks the amendment of Order No. R-6538, which authorized applicant to conduct waterflood operations in the Chaco Wash-Mesa Verde Oil Pool. Applicant seeks approval for the injection of water through various other wells than those originally approved, seeks deletion of the requirement for packers in injection wells, and seeks an increase in the previously authorized 68-pound limitation on injection pressure.

CASE 7410: (Continued from January 20, 1982, Examiner Hearing)

Application of B.O.A. Oil & Gas Company for two unorthodox oil well locations, San Juan County, New Mexico. Applicant, in the above-styled cause, seeks approval for the unorthodox location of a well to be drilled 2035 feet from the South line and 2455 feet from the East line and one to be drilled 2455 feet from the North line and 1944 feet from the East line, both in Section 31, Township 31 North, Range 15 West, Verde-Gallup Oil Pool, the NW/4 SE/4 and SW/4 NE/4, respectively, of said Section 31 to be dedicated to said wells.

CASE 7457: (Continued from January 20, 1982, Examiner Hearing)

Application of E. T. Ross for nine non-standard gas proration units, Harding County, New Mexico. Applicant, in the above-styled cause, seeks approval for nine 40-acre non-standard gas proration units in the Bravo Dome Carbon Dioxide Area. In Township 19 North, Range 30 East: Section 12, the NW/4 NW/4 and NE/4 SW/4; Section 14, the NW/4 NE/4, SW/4 NE/4, and SE/4 NE/4. In Township 20 North, Range 30 East: Section 11, the NE/4 SW/4, SW/4 SE/4, SE/4 SW/4, and NW/4 SE/4.

CASE 7482: Application of Wiser Oil Company for an unorthodox oil well location, Lea County, New Mexico. Applicant, in the above-styled cause, seeks approval of an unorthodox location 1295 feet from the South line and 1345 feet from the West line of Section 32, Township 21 South, Range 37 East, Penrose-Skelly Pool.

CASE 7483: Application of Adams Exploration Company for salt water disposal, Chaves County, New Mexico. Applicant, in the above-styled cause, seeks authority to dispose of produced salt water into the San Andres formation in the perforated interval from 4176 feet to 4293 feet in its Griffin Well No. 4 located in Unit A, of Section 10, Township 8 South, Range 32 East, Chaveroo-San Andres Pool.

CASE 7462: (Continued from February 3, 1982, Examiner Hearing)

Application of Marathon Oil Company for downhole commingling, Lea County, New Mexico. Applicant, in the above-styled cause, seeks approval for the downhole commingling of the Drinkard and Blinebry production in the wellbore of its C. J. Saunders Well No. 3, located in Unit C of Section 1, Township 22 South, Range 36 East.

CASE 7474: (Continued from February 3, 1982, Examiner Hearing)

Application of Union Oil Company of California for compulsory pooling, Lea County, New Mexico. Applicant, in the above-styled cause, seeks an order pooling all mineral interests in the Strawn, Atoka and Morrow formations underlying the E/2 of Section 25, Township 19 South, Range 33 East, to be dedicated to a well to be drilled at a standard location thereon. Also to be considered will be the cost of drilling and completing said well and the allocation of the cost thereof as well as actual operating costs and charges for supervision, designation of applicant as operator of the well, and a charge for risk involved in drilling said well.

CASE 7484: Application of Anadarko Production Company for compulsory pooling, Eddy County, New Mexico. Applicant, in the above-styled cause, seeks an order pooling all mineral interests in the Atoka and Morrow formations underlying the E/2 of Section 1, Township 19 South, Range 25 East, to be dedicated to a well to be drilled at a standard location thereon. Also to be considered will be the cost of drilling and completing said well and the allocation of the cost thereof as well as actual operating costs and charges for supervision, designation of applicant as operator of the the well, and a charge for risk involved in drilling said well.

CASE 7485: Application of Berge Exploration for compulsory pooling, Chaves County, New Mexico. Applicant, in the above-styled cause, seeks an order pooling all mineral interests in the Abo formation underlying two 160-acre proration units, the first being the NW/4 and the second being the SW/4 of Section 27, Township 7 South, Range 26 East, each to be dedicated to a well to be drilled at a standard location thereon. Also to be considered will be the cost of drilling and completing said wells and the allocation of the cost thereof as well as actual operating costs and charges for supervision, designation of applicant as operator of the wells and a charge for risk involved in drilling said wells.

CASE 7486: Application of MGF Oil Corporation for compulsory pooling, Lea County, New Mexico. Applicant, in the above-styled cause, seeks an order pooling all mineral interests down through and including the Abo formation underlying the NE/4 NE/4 of Section 6, Township 20 South, Range 39 East, to be dedicated to a well to be drilled at a standard location thereon. Also to be considered will be the cost of drilling and completing said well and the allocation of the cost thereof as well as actual operating costs and charges for supervision, designation of applicant as operator of the well and a charge for risk involved in drilling said well.

CASE 7487: Application of MGF Oil Corporation for compulsory pooling, Lea County, New Mexico. Applicant, in the above-styled cause, seeks an order pooling all mineral interests down through and including the Abo formation underlying the SE/4 SE/4 of Section 31, Township 19 South, Range 39 East, to be dedicated to a well to be drilled at a standard location thereon. Also to be considered will be the cost of drilling and completing said well and the allocation of the cost thereof as well as actual operating costs and charges for supervision, designation of applicant as operator of the well and a charge for risk involved in drilling said well.

CASE 7488: Application of Burkhart Petroleum Company for compulsory pooling, Roosevelt County, New Mexico. Applicant, in the above-styled cause, seeks an order pooling all mineral interests in the San Andres formation underlying the SW/4 NW/4 of Section 13, Township 8 South, Range 37 East, to be dedicated to a well to be drilled at a standard location thereon. Also to be considered will be the cost of drilling and completing said well and the allocation of the cost thereof as well as actual operating costs and charges for supervision, designation of applicant as operator of the well and a charge for risk involved in drilling said well.

CASE 7073: (Reopened and Readvertised)

In the matter of Case 7073 being reopened pursuant to the provisions of Order No. R-6558, which order promulgated special rules for the South Elkins-Fusselman Pool in Chaves County including provisions for 80-acre spacing units and a limiting gas-oil ratio of 2000 to one. All interested parties may appear and show cause why said pool should not be developed on 40-acre spacing units with a limiting gas-oil ratio of 2000 to one.

CASE 7074: (Reopened and Readvertised)

In the matter of Case 7074 being reopened pursuant to the provisions of Orders Nos. R-6565 and R-6565-B, which created the South Elkins-Fusselman Gas Pool in Chaves County. All interested parties may appear and present evidence as to the exact nature of the reservoir, and more particularly, as to the proper rate of withdrawal from the reservoir if it is determined that said pool is producing from a retrograde gas condensate reservoir.

CASE 6373: (Reopened and Readvertised)

In the matter of Case 6373 being reopened pursuant to the provisions of Orders Nos. R-5875 and R-5875-A, which created the East High Hope - Abo Gas pool in Eddy County, and promulgated special rules therefor, including a provision for 320-acre spacing units. All interested parties may appear and show cause why said pool should not be developed on 160-acre spacing units.

CASE 7489: Application of Curtis J. Little for designation of a tight formation, Rio Arriba County, New Mexico. Applicant, in the above-styled cause, seeks the designation of the Chacra formation underlying portions of Township 25 North, Range 6 West, containing 6,720 acres, more or less, as a tight formation pursuant to Section 107 of the Natural Gas Policy Act and 18 CFR Section 271.701-705.

CASE 7490: Application of Harvey E. Yates Company for compulsory pooling, Chaves County, New Mexico. Applicant, in the above-styled cause, seeks an order pooling all mineral interests down through and including the Atoka-Morrow formation, underlying the N/2 of Section 19, Township 8 South, Range 30 East, to be dedicated to a well to be drilled at a standard location thereon. Also to be considered will be the cost of drilling and completing said well and the allocation of the cost thereof as well as actual operating costs and charges for supervision, designation of applicant as operator of the well and a charge for risk involved in drilling said well.

CASE 7491: Application of Harvey E. Yates Company for designation of a tight formation, Lea County, New Mexico. Applicant, in the above-styled cause, seeks the designation of the Atoka formation underlying portions of Townships 12, 13, and 14 South, Ranges 35 and 36 East, containing 46,720 acres, more or less, as a tight formation pursuant to Section 107 of the Natural Gas Policy Act and 18 CFR Section 271.701-705, said area being an eastward and westward extension of previously approved tight formation area.

CASE 7492: Application of Harvey E. Yates Company for designation of a tight formation, Chaves County, New Mexico. Applicant, in the above-styled cause, seeks the designation of the Atoka-Morrow formation underlying all or portions of Townships 7, 8, and 9 South, Ranges 29,30, and 31 East, containing 115,200 acres, more or less, as a tight formation pursuant to Section 107 of the Natural Gas Policy Act and 18 CFR Section 271.701-705.

CASE 7493: In the matter of the hearing called by the Oil Conservation Division on its own motion for an order creating and extending certain pools in Chaves, Eddy, Lea, and Roosevelt Counties, New Mexico.

(a) CREATE a new pool in Lea County, New Mexico, classified as a gas pool for Morrow production and designated as the East Bootleg Ridge-Morrow Gas Pool. The discovery well is Getty Oil Company Getty 15 Federal Well No. 1 located in Unit J of Section 15, Township 22 South, Range 33 East, NMPM. Said Pool would comprise:

TOWNSHIP 22 SOUTH, RANGE 33 EAST, NMPM
Section 15: S/2

(b) CREATE a new pool in Lea County, New Mexico, classified as an oil pool for Devonian production and designated as the North King-Devonian Pool. The discovery well is Samedan Oil Corporation Speight Well No. 1 located in Unit B of Section 3, Township 13 South, Range 37 East, NMPM. Said pool would comprise:

TOWNSHIP 13 SOUTH, RANGE 37 EAST, NMPM
Section 3: NE/4

(c) CREATE a new pool in Eddy County, New Mexico, classified as a gas pool for Atoka production and designated as the North Loving-Atoka Gas Pool. The discovery well is Gulf Oil Corporation Eddy GR State Well No. 1 located in Unit E of Section 16, Township 23 South, Range 28 East, NMPM. Said pool would comprise:

TOWNSHIP 23 SOUTH, RANGE 27 EAST, NMPM
Section 12: N/2

TOWNSHIP 23 SOUTH, RANGE 28 EAST, NMPM
Section 4: S/2
Section 7: All
Section 8: All
Section 9: All
Section 16: All
Section 17: All
Section 18: E/2

(d) CREATE a new pool in Lea County, New Mexico, classified as an oil pool for Drinkard production and designated as the Teague-Drinkard Pool. The discovery well is Alpha Twenty-One Production Company Lea Well No. 1 located in Unit B of Section 17, Township 23 South, Range 37 East, NMPM. Said pool would comprise:

TOWNSHIP 23 SOUTH, RANGE 37 EAST, NMPM
Section 17: NE/4

(e) EXTEND the West Atoka-Morrow Gas Pool in Eddy County, New Mexico, to include therein:

TOWNSHIP 18 SOUTH, RANGE 25 EAST, NMPM
Section 23: All
Section 24: W/2

(f) EXTEND the Atoka-Pennsylvanian Gas Pool in Eddy County, New Mexico, to include therein:

TOWNSHIP 18 SOUTH, RANGE 26 EAST, NMPM
Section 16: W/2

(g) EXTEND the Avalon-Morrow Gas Pool in Eddy County, New Mexico, to include therein:

TOWNSHIP 21 SOUTH, RANGE 26 EAST, NMPM
Section 2: Lots 1 through 8

(h) EXTEND the Brunson-Fusselman Pool in Lea County, New Mexico, to include therein:

TOWNSHIP 22 SOUTH, RANGE 37 EAST, NMPM
Section 5: SE/4

(i) EXTEND the Brushy Draw-Delaware Pool in Eddy County, New Mexico, to include therein:

TOWNSHIP 26 SOUTH, RANGE 29 EAST, NMPM
Section 26: E/2

(j) EXTEND the Buffalo Valley-Pennsylvanian Gas Pool in Chaves County, New Mexico, to include therein:

TOWNSHIP 15 SOUTH, RANGE 27 EAST, NMPM
Section 23: All
Section 26: All

(k) EXTEND the Cary-Montoya Pool in Lea County, New Mexico, to include therein:

TOWNSHIP 22 SOUTH, RANGE 37 EAST, NMPM
Section 4: W/2 SW/4
Section 5: SE/4
Section 9: W/2 W/2

(l) EXTEND the Crow Flats-Morrow Gas Pool in Eddy County, New Mexico to include therein:

TOWNSHIP 16 SOUTH, RANGE 27 EAST, NMPM
Section 35: E/2
Section 36: W/2

(m) EXTEND the South Culebra Bluff-Bone Spring Pool in Eddy County, New Mexico, to include therein:

TOWNSHIP 23 SOUTH, RANGE 28 EAST, NMPM
Section 25: S/2 SW/4
Section 27: SW/4

(n) EXTEND the Elkins-San Andres Pool in Chaves County, New Mexico, to include therein:

TOWNSHIP 7 SOUTH, RANGE 28 EAST, NMPM
Section 21: NE/4

(o) EXTEND the Empire-Abo Pool in Eddy County, New Mexico, to include therein:

TOWNSHIP 17 SOUTH, RANGE 29 EAST, NMPM
Section 19: S/2 SW/4

(p) EXTEND the Henshaw-Queen Grayburg-San Andres Pool in Eddy County, New Mexico, to include therein:

TOWNSHIP 16 SOUTH, RANGE 31 EAST, NMPM
Section 19: NE/4 NW/4

(q) EXTEND the Indian Flats-Morrow Gas Pool in Eddy County, New Mexico, to include therein:

TOWNSHIP 21 SOUTH, RANGE 28 EAST, NMPM
Section 26: W/2

(r) EXTEND the West Nadine-Blinebry Pool in Lea County, New Mexico, to include therein:

TOWNSHIP 20 SOUTH, RANGE 38 EAST, NMPM
Section 8: NW/4

(s) EXTEND the Peterson-Mississippian Pool in Roosevelt County, New Mexico, to include therein:

TOWNSHIP 4 SOUTH, RANGE 33 EAST, NMPM
Section 28: NW/4

(t) EXTEND the Race Track-San Andres Pool in Chaves County, New Mexico, to include therein:

TOWNSHIP 10 SOUTH, RANGE 28 EAST, NMPM
Section 7: S/2 SW/4
Section 18: NW/4 and N/2 SW/4 and SW/4 SW/4

(u) **EXTEND** the Railroad Mountain-San Andres Pool in Chaves County, New Mexico, to include therein:

> <u>TOWNSHIP 8 SOUTH, RANGE 29 EAST, NMPM</u>
> Section 2: NE/4 and E/2 NW/4

(v) **EXTEND** the Red Lake-Queen-Grayburg-San Andres Pool in Eddy County, New Mexico, to include therein:

> <u>TOWNSHIP 17 SOUTH, RANGE 28 EAST, NMPM</u>
> Section 7: S/2
> Section 8: SW/4
> Section 18: E/2 NW/4

(w) **EXTEND THE** West Sawyer-San Andres Pool in Lea County, New Mexico, to include therein:

> <u>TOWNSHIP 10 SOUTH, RANGE 37 EAST, NMPM</u>
> Section 5: SW/4

(x) **EXTEND** the Turkey Track-Atoka Gas Pool in Eddy County, New Mexico, to include therein:

> <u>TOWNSHIP 19 SOUTH, RANGE 29 EAST, NMPM</u>
> Section 15: All

(y) **EXTEND** the Twin Lakes-San Andres Associated Pool in Chaves County, New Mexico, to include therein:

> <u>TOWNSHIP 8 SOUTH, RANGE 28 EAST, NMPM</u>
> Section 13: SE/4
> Section 24: NE/4
>
> <u>TOWNSHIP 9 SOUTH, RANGE 28 EAST, NMPM</u>
> Section 12: S/2 NE/4
>
> <u>TOWNSHIP 9 SOUTH, RANGE 29 EAST, NMPM</u>
> Section 7: S/2
> Section 8: NW/4

Docket No. 3-82

Dockets Nos. 4-82 and 5-82 are tentatively set for February 3 and February 17, 1982. Applications for hearing must be filed at least 22 days in advance of hearing date.

DOCKET: EXAMINER HEARING - WEDNESDAY - JANUARY 20, 1982

9 A.M. - OIL CONSERVATION DIVISION CONFERENCE ROOM
STATE LAND OFFICE BUILDING, SANTA FE, NEW MEXICO

The following cases will be heard before Richard L. Stamets, Examiner, or Daniel S. Nutter, Alternate Examiner:

ALLOWABLE: (1) Consideration of the allowable production of gas for February, 1982, from fifteen prorated pools in Lea, Eddy, and Chaves Counties, New Mexico.

(2) Consideration of the allowable production of gas for February, 1982, from four prorated pools in San Juan, Rio Arriba, and Sandoval Counties, New Mexico.

CASE 7462: Application of Marathon Oil Company for downhole commingling, Lea County, New Mexico. Applicant, in the above-styled cause, seeks approval for the downhole commingling of the Drinkard and Blinebry production in the wellbore of its C. J. Saunders Well No. 3, located in Unit C of Section 1, Township 22 South, Range 36 East.

CASE 7463: Application of Texaco Inc. for a dual completion, Lea County, New Mexico. Applicant, in the above-styled cause, seeks approval for the dual completion of its C. H. Weir "A" Well No. 12 located in Unit G of Section 12, Township 20 South, Range 37 East, to produce oil from the Skaggs-Drinkard and an undesignated Abo pool.

CASE 7464: Application of Exxon Corporation for two unorthodox oil well locations, Lea County, New Mexico. Applicant, in the above-styled cause, seeks approval for two unorthodox oil well locations in Section 4, Township 19 South, Range 35 East, Scharb-Bone Spring Pool, as follows: State DD Well No. 1 to be drilled in the center of the SE/4 SW/4 and State DD Well No. 3 to be drilled in the center of the NW/4 NE/4. Pool rules require wells to be drilled in the NE/4 or SW/4 of a quarter section.

CASE 7465: Application of Superior Oil Company for an unorthodox gas well location, Eddy County, New Mexico. Applicant, in the above-styled cause, seeks approval for the unorthodox location of a well to be drilled 1980 feet from the South line and 660 feet from the East line of Section 26, Township 24 South, Range 29 East, Wolfcamp-Pennsylvanian formations, the S/2 of said Section 26 to be dedicated to the well.

CASE 7466: Application of Conoco Inc. for a waterflood project, Lea County, New Mexico. Applicant, in the above-styled cause, seeks authority for it and Southland Royalty Company to each institute a cooperative waterflood project in the Blinebry Oil and Gas Pool by the injection of water into the Blinebry formation through nine injection wells located on Conoco's Warren Unit and Hawk B-3 Leases and Southland's State Lease in Sections 33 and 34 of Township 20 South, Range 38 East, and Sections 2 and 3 of Township 21 South, Range 37 East.

CASE 7072: In the matter of Case No. 7072 being reopened on the motion of the Oil Conservation Division and pursuant to the provisions of Order No. R-6554 which order promulgated temporary special rules and regulations for the North Peterson-Pennsylvanian Pool in Roosevelt County, New Mexico, including a provision for 80-acre spacing units. Operators in said pool may appear and show cause why said pool should not be developed on 40-acre proration units.

CASE 7460: (Continued from January 6, 1982, Examiner Hearing)

Application of Northwest Pipeline Corporation for 13 non-standard gas proration units, San Juan County, New Mexico. Applicant, in the above-styled cause, seeks approval for 13 non-standard Pictured Cliffs gas proration units ranging in size from 142.39 acres to 176.77 acres and each comprised of various contiguous lots or tracts in Sections 4,5,6,7, and 18 of Township 31 North, Range 7 West. Said proration units result from corrections in the survey lines [illegible] the North and West sides of Township 31 North, Range 7 West and overlap seven non-standard [illegible] proration units previously approved by Order No. R-1066.

CASE 7467: Application of Inexco Oil Company for pool creation, special pool rules, and a discovery allowable, Lea County, New Mexico. Applicant, in the above-styled cause, seeks creation of a new Strawn oil pool for its Lottie York Well No. 1 located in Unit P of Section 14, Township 17 South, Range 37 East, and the promulgation of special rules therefor, including a provision for 80-acre spacing. Applicant further seeks the assignment of 57,150 barrels of oil discovery allowable to said well.

CASE 7459: (Continued from January 6, 1982, Examiner Hearing)

Application of Red Mountain Associates for the Amendment of Order No. R-6538, McKinley County, New Mexico. Applicant, in the above-styled cause, seeks the amendment of Order No. R-6538, which authorized applicant to conduct waterflood operations in the Chaco Wash-Mesa Verde Oil Pool. Applicant seeks approval for the injection of water through various other wells than those originally approved, seeks deletion of the requirement for packers in injection wells, and seeks an increase in the previously authorized 68-pound limitation on injection pressure.

CASE 7410: (Continued from January 6, 1982, Examiner Hearing)

Application of B.O.A. Oil & Gas Company for two unorthodox oil well locations, San Juan County, New Mexico. Applicant, in the above-styled cause, seeks approval for the unorthodox location of a well to be drilled 2035 feet from the South line and 2455 feet from the East line and one to be drilled 2455 feet from the North line and 1944 feet from the East line, both in Section 31, Township 31 North, Range 15 West, Verde-Gallup Oil Pool, the NW/4 SE/4 and SW/4 NE/4, respectively, of said Section 31 to be dedicated to said wells.

CASE 7451: (Continued from January 6, 1982, Examiner Hearing)

Application of Yates Petroleum Corporation for compulsory pooling, Chaves County, New Mexico. Applicant, in the above-styled cause, seeks an order pooling all mineral interests down through the Abo formation underlying the SE/4 of Section 11, Township 6 South, Range 25 East, to be dedicated to a well to be drilled at a standard location thereon. Also to be considered will be the cost of drilling and completing said well and the allocation of the cost thereof as well as actual operating costs and charges for supervision, designation of applicant as operator of the well and a charge for risk involved in drilling said well.

CASE 7453: (Continued from January 6, 1982, Examiner Hearing)

Application of T. D. Skelton for compulsory pooling, Lea County, New Mexico. Applicant, in the above-styled cause, seeks an order pooling all mineral interests in the Devonian and Mississippian formations underlying the NE/4 NW/4 of Section 7, Township 12 South, Range 38 East, to be dedicated to the re-entry of an old well at a standard location thereon. Also to be considered will be the cost of re-entering and completing said well and the allocation of the cost thereof as well as actual operating costs and charges for supervision, designation of applicant as operator of the well and a charge for risk involved in re-entry of said well.

CASE 7457: (Continued from January 6, 1982, Examiner Hearing)

Application of E. T. Ross for nine non-standard gas proration units, Harding County, New Mexico. Applicant, in the above-styled cause, seeks approval for nine 40-acre non-standard gas proration units in the Bravo Dome Carbon Dioxide Area. In Township 19 North, Range 30 East: Section 12, the NW/4 NW/4 and NE/4 NW/4; Section 14, the NW/4 NE/4, SW/4 NE/4, and SE/4 NE/4. In Township 20 North, Range 30 East: Section 11, the NE/4 SW/4, SW/4 SE/4, SE/4 SW/4, and NW/4 SE/4.

CASE 7468: In the matter of the hearing called by the Oil Conservation Division on its own motion for an order creating and extending certain pools in Chaves, Eddy, and Lea Counties, New Mexico.

(a) CREATE a new pool in Lea County, New Mexico, classified as an oil pool for Paddock production and designated as the East Monument-Paddock Pool. The discovery well is Morris R. Antweil State SX Well No. 1 located in Unit J of Section 36, Township 19 South, Range 37 East, NMPM. Said pool would comprise:

TOWNSHIP 19 SOUTH, RANGE 37 EAST, NMPM
Section 36: SE/4

(b) CREATE a new pool in Eddy County, New Mexico, classified as a gas pool for Morrow production and designated as the Ross Draw-Morrow Gas Pool. The discovery well is Florida Exploration Company Ross Draw Unit Well No. 10 located in Unit E of Section 27, Township 26 South, Range 30 East, NMPM. Said pool would comprise:

TOWNSHIP 26 SOUTH, RANGE 30 EAST, NMPM
Section 27: N/2

(c) CREATE a new Pool in Lea County, New Mexico, classified as an oil pool for Morrow production. and designated as the Sowell-Morrow Pool. The discovery well is Santa Fe Energy Company State NM2 Well No. 1 located in Unit M of Section 2, Township 15 South, Range 32 East, NMPM. Said pool would comprise:

TOWNSHIP 15 SOUTH, RANGE 32 EAST, NMPM
Section 2: SW/4

(d) EXTEND the Angell Ranch-Atoka-Morrow Gas Pool in Eddy County, New Mexico, to include therein:

TOWNSHIP 19 SOUTH, RANGE 27 EAST, NMPM
Section 12: All
Section 13: N/2

(e) EXTEND the Antelope Ridge-Atoka Gas Pool in Lea County, New Mexico, to include therein:

TOWNSHIP 23 SOUTH, RANGE 34 EAST, NMPM
Section 27: N/2
Section 28: E/2

(f) EXTEND the Atoka-Yeso Pool in Eddy County, New Mexico, to include therein:

TOWNSHIP 18 SOUTH, RANGE 26 EAST, NMPM
Section 23: S/2 S/2
Section 26: W/2 NW/4

(g) EXTEND the Bunker Hill-Penrose Pool in Eddy County, New Mexico, to include therein:

TOWNSHIP 16 SOUTH, RANGE 31 EAST, NMPM
Section 14: SW/4 SE/4

(h) EXTEND the Burton Flat-Morrow Gas Pool in Eddy County, New Mexico, to include therein:

TOWNSHIP 20 SOUTH, RANGE 27 EAST, NMPM
Section 25: W/2
Section 26: S/2

TOWNSHIP 20 SOUTH, RANGE 28 EAST, NMPM
Section 17: N/2

TOWNSHIP 21 SOUTH, RANGE 27 EAST, NMPM
Section 14: S/2
Section 23: W/2

(i) EXTEND the Cinta Roja-Morrow Gas Pool in Lea County, New Mexico, to include therein:

TOWNSHIP 24 SOUTH, RANGE 35 EAST, NMPM
Section 8: All

(j) EXTEND the South Culebra Bluff-Atoka Pool in Eddy County, New Mexico, to include therein:

TOWNSHIP 23 SOUTH, RANGE 28 EAST, NMPM
Section 36: W/2

(k) EXTEND the South Empire-Morrow Gas Pool in Eddy County, New Mexico, to include therein:

TOWNSHIP 17 SOUTH, RANGE 29 EAST, NMPM
Section 7: S/2

(l) EXTEND the Gem-Morrow Gas Pool in Lea County, New Mexico, to include therein:

TOWNSHIP 19 SOUTH, RANGE 33 EAST, NMPM
Section 30: E/2
Section 32: S/2

(m) EXTEND the Hat Mesa-Morrow Gas Pool in Lea County, New Mexico, to include therein:

TOWNSHIP 21 SOUTH, RANGE 32 EAST, NMPM
Section 13: E/2

TOWNSHIP 21 SOUTH, RANGE 33 EAST, NMPM
Section 7: W/2

(n) EXTEND the Herradura Bend-Delaware Pool in Eddy County, New Mexico, to include therein:

TOWNSHIP 22 SOUTH, RANGE 28 EAST, NMPM
Section 29: E/2 SE/4

(o) EXTEND the Southwest Indian Flats-Morrow Gas Pool in Eddy County, New Mexico, to include therein:

TOWNSHIP 22 SOUTH, RANGE 28 EAST, NMPM
Section 10: E/2

(p) EXTEND the Leo-Queen-Grayburg Pool in Eddy County, New Mexico, to include therein:

TOWNSHIP 18 SOUTH, RANGE 30 EAST, NMPM
Section 23: N/2 NE/4

(q) EXTEND the West Lynch-Morrow Gas Pool in Lea County, New Mexico, to include therein:

TOWNSHIP 20 SOUTH, RANGE 34 EAST, NMPM
Section 32: N/2
Section 33: NW/4

(r) EXTEND the North San Simon-Yates Pool in Lea County, New Mexico, to include therein:

TOWNSHIP 21 SOUTH, RANGE 35 EAST, NMPM
Section 33: E/2 NW/4

(s) EXTEND the South Saunders-Permo Pennsylvanian Pool in Lea County, New Mexico, to include therein:

TOWNSHIP 15 SOUTH, RANGE 32 EAST, NMPM
Section 25: N/2

(t) EXTEND the Scharb-Bone Spring Pool in Lea County, New Mexico, to include therein:

TOWNSHIP 19 SOUTH, RANGE 35 EAST, NMPM
Section 9: NW/4

(u) EXTEND the Tom-Tom-San Andres Pool in Chaves County, New Mexico, to include therein:

TOWNSHIP 8 SOUTH, RANGE 31 EAST, NMPM
Section 8: S/2 NW/4 and SW/4

(v) EXTEND the Winchester-Atoka Gas Pool in Eddy County, New Mexico, to include therein:

TOWNSHIP 20 SOUTH, RANGE 28 EAST, NMPM
Section 3: W/2

Dockets Nos. 3-82 and 4-82 are tentatively set for January 20 and February 3, 1982. Applications for hearing must be filed at least 22 days in advance of hearing date.

DOCKET: EXAMINER HEARING - WEDNESDAY - JANUARY 6, 1982

9 A.M. - OIL CONSERVATION DIVISION CONFERENCE ROOM
STATE LAND OFFICE BUILDING, SANTA FE, NEW MEXICO

The following cases will be heard before Daniel S. Nutter, Examiner, or Richard L. Stamets, Alternate Examiner:

CASE 7410: (Continued from December 16, 1981, Examiner Hearing)

Application of R.C.A. Oil & Gas Company for two unorthodox oil well locations, San Juan County, New Mexico. Applicant, in the above-styled cause, seeks approval for the unorthodox location of a well to be drilled 2035 feet from the South line and 2455 feet from the East line and one to be drilled 2455 feet from the North line and 1944 feet from the East line, both in Section 31, Township 31 North, Range 15 West, Verde-Gallup Oil Pool, the NW/4 SE/4 and SW/4 NE/4, respectively, of said Section 31 to be dedicated to said wells.

CASE 7448: (Continued and Readvertised)

Application of Energy Reserves Group Inc. for creation of a new gas pool and an unorthodox location, Roosevelt County, New Mexico. Applicant, in the above-styled cause, seeks the creation of a new gas pool for Cisco production comprising the S/2 of Section 12 and the N/2 of Section 13, Township 6 South, Range 33 East; applicant further seeks approval of the unorthodox location of its Miller Com Well No. 1-Y located 660 feet from the South and West lines of said Section 12.

CASE 7451: Application of Yates Petroleum Corporation for compulsory pooling, Chaves County, New Mexico. Applicant, in the above-styled cause, seeks an order pooling all mineral interests down through the Abo formation underlying the SE/4 of Section 11, Township 6 South, Range 25 East, to be dedicated to a well to be drilled at a standard location thereon. Also to be considered will be the cost of drilling and completing said well and the allocation of the cost thereof as well as actual operating costs and charges for supervision, designation of applicant as operator of the well and a charge for risk involved in drilling said well.

CASE 7452: Application of Superior Oil Company for an unorthodox well location, Lea County, New Mexico. Applicant, in the above-styled cause, seeks approval for the unorthodox location of a Wolfcamp-Penn well to be drilled 1980 feet from the South line and 2480 feet from the East line of Section 14, Township 23 South, Range 32 East, the S/2 of said Section 14, to be dedicated to the well.

CASE 7453: Application of T. D. Skelton for compulsory pooling, Lea County, New Mexico. Applicant, in the above-styled cause, seeks an order pooling all mineral interests in the Devonian and and Mississippian formations underlying the NE/4 NW/4 of Section 7, Township 12 South, Range 38 East, to be dedicated to the re-entry of an old well at a standard location thereon. Also to be considered will be the cost of re-entering and completing said well and the allocation of the cost thereof as well as actual operating costs and charges for supervision, designation of applicant as operator of the well and a charge for risk involved in re-entry of said well.

CASE 7454: Application of Uriah Exploration, Inc., for approval of an unorthdox gas well location, Eddy County, New Mexico. Applicant, in the above-styled cause, seeks approval for the unorthodox location of a well to be drilled 1090 feet from the North line and 560 feet from the East line of Section 30, Township 22 South, Range 25 East, Wolfcamp-Pennsylvanian formations, the N/2 of said Section to be dedicated to the well.

CASE 7455: Application of H. L. Brown, Jr. for compulsory pooling at an unorthodox location, Roosevelt County, New Mexico. Applicant, in the above-styled cause, seeks an order pooling all mineral interests from the top of the Wolfcamp formation to the base of the Granite Wash formation underlying the S/2 of Section 11, Township 6 South, Range 33 East, to be dedicated to a well to be drilled at an unorthodox location 1300 feet from the South line and 660 feet from the East line of said Section 11. Also to be considered will be the cost of drilling and completing said well and the allocation of the cost thereof as well as actual operating costs and charges for supervision, designation of applicant as operator of the well, and a charge for risk involved in drilling said well.

CASE 7456: Application of Colonial Production Company for gas well commingling, Rio Arriba County, New Mexico. Applicant, in the above-styled cause, seeks approval for the commingling of Ballard-Pictured Cliffs production from its Jicarilla Apache Wells Nos. 9 and 10, located in Units A and C of Section 15, Township 23 North, Range 4 West, prior to metering.

CASE 7457: Application of E. T. Ross for nine non-standard gas proration units, Harding County, New Mexico. Applicant, in the above-styled cause, seeks approval for nine 40-acre non-standard gas proration units in the Bravo Dome Carbon Dioxide Area. In Township 19 North, Range 30 East: Section 12, the NW/4 NW/4 and NE/4 NW/4; Section 14, the NW/4 NE/4, SW/4 NE/4, and SE/4 NE/4. In Township 20 North, Range 30 East: Section 11, the NE/4 SW/4, SW/4 SE/4, SE/4 SW/4, and NW/4 SE/4.

CASE 7458: Application of Marks & Garner Production Company for salt water disposal, Lea County, New Mexico. Applicant, in the above-styled cause, seeks authority to dispose of salt water into the Bough C formation in the perforated interval from 9596 feet to 9616 feet in its Betenbough Well No. 2, located in Unit M of Section 12, Township 9 South, Range 35 East.

CASE 7459: Application of Red Mountain Associates for the Amendment of Order No. R-6538, McKinley County, New Mexico. Applicant, in the above-styled cause, seeks the amendment of Order No. R-6538, which authorized applicant to conduct waterflood operations in the Chaco Wash-Mesa Verde Oil Pool. Applicant seeks approval for the injection of water through various other wells than those originally approved, seeks deletion of the requirement for packers in injection wells, and seeks an increase in the previously authorized 68-pound limitation on injection pressure.

CASE 7460: Application of Northwest Pipeline Corporation for 13 non-standard gas proration units, San Juan County, New Mexico. Applicant, in the above-styled cause, seeks approval for 13 non-standard Pictured Cliffs gas proration units ranging in size from 142.39 acres to 176.77 acres and each comprised of various contiguous lots or tracts in Sections 4,5,6,7, and 18 of Township 31 North, Range 7 West. Said proration units result from corrections in the survey lines on the North and West sides of Township 31 North, Range 7 West and overlap seven non-standard Mesaverde proration units previously approved by Order No. R-1066.

CASE 7461: Application of Wainoco Oil & Gas Company for an unorthodox location, Lea County, New Mexico. Applicant, in the above-styled cause, seeks approval for a well to be drilled at an unorthodox location 660 feet from the South and West lines of Section 18, Township 16 South, Range 37 East, Northeast Lovington Penn Pool, said location being 177.7 feet west of the center of Lot 4 whereas the pool rules specify that well be drilled within 150 feet of the center of the lot. Lots 3 and 4 of said Section 18 would be dedicated to the well.

CASE 7421: (Readvertised)

Application of Doyle Hartman for compulsory pooling, unorthodox well location and non-standard spacing unit, Lea County, New Mexico. Applicant, in the above-styled cause, seeks an order pooling all mineral interests in the Eumont Gas Pool underlying a 120-acre non-standard spacing unit consisting of the S/2 SW/4 and the NW/4 SW/4 of Section 3, Township 20 South, Range 37 East, to be dedicated to a well to be drilled at an unorthodox location 660 feet from the South line and 330 feet from the West line of Section 3. Also to be considered will be the cost of drilling and completing said well and the allocation of the cost thereof as well as actual operating costs and charges for supervision, designation of applicant as operator of the well and a charge for risk involved in drilling said well.

****

Docket No. 2-82

DOCKET: COMMISSION HEARING - MONDAY - JANUARY 11, 1982
9 A.M. - OIL CONSERVATION COMMISSION - ROOM 205
STATE LAND OFFICE BUILDING, SANTA FE, NEW MEXICO

CASE 7393: (DE NOVO)

Application of Uriah Exploration Incorporated for compulsory pooling, Eddy County, New Mexico. Applicant, in the above-styled cause, seeks an order pooling all mineral interests in the Cisco, Canyon and Morrow formations underlying the W/2 of Section 13, Township 22 South, Range 24 East, to be dedicated to a well to be drilled at a standard location thereon. Also to be considered will be the cost of drilling and completing said well and the allocation of the cost thereof as well as actual operating costs and charges for supervision, designation of applicant as operator of the well, and a charge for risk involved in drilling said well.

Upon application of Supron Energy Corporation, this case will be heard De Novo pursuant to the provisions of Rule 1220.

CASE 7394: (DE NOVO)

Application of Supron Energy Corporation for an unorthodox gas well location, Eddy County, New Mexico. Applicant, in the above-styled cause, seeks approval for the unorthodox location of a Pennsylvanian well to be drilled 467 feet from the North line and 1650 feet from the West line of Section 13, Township 22 South, Range 24 East, the N/2 of said Section 13 to be dedicated to the well.

Upon application of Supron Energy Corporation, this case will be heard De Novo pursuant to the provisions of Rule 1220.

MAR 17 1982
OIL CONSERVATION DIVISION
SANTA FE

STATE OF NEW MEXICO

ENERGY AND MINERALS DEPARTMENT

OIL CONSERVATION DIVISION

IN THE MA TER OF THE HEARING
CALLED BY THE OIL CONSERVATION
DIVISION FOR THE PURPOSE OF
CONSIDERING:

CASE NO. 7459

APPLICATION OF RED MOUNTAIN ASSOCIATES

ENTRY OF APPEARANCE

COMES NOW Alex J. Armijo, Commissioner of Public Lands for the State of New Mexico, by and through the undersigned counsel, and requests of the Oil Conservation Division that he be allowed to enter this Appearance as a party of record in the aforesaid proceeding.

The Commissioner states further that oil and gas lands owned by the State of New Mexico are involved in this proceeding that may or may not be adversely affected by the order or decision of the Division in this matter.

Respectfully submitted,

J. SCOTT HALL
Attorney for Alex J. Armijo
Commissioner of Public Lands
for the State of New Mexico
P.O. Box 1148
Santa Fe, New Mexico 87501
505/827-2743

CERTIFICATE

I hereby certify that a true and correct copy of the foregoing pleading was mailed to opposing counsel of record this 17th day of March, 1982.

RED MOUNTAIN ASSOCIATES
1517 REISTERSTOWN ROAD, SUITE 205
BALTIMORE, MARYLAND 21208
(301) 653-3060

Case 7459

Florene - Pls send copy of Jan 20 docket to and to

January 3, 1982

Mr. Dan Nutter
New Mexico Oil Conservation Commission
P. O. Box 2088
Santa Fe, New Mexico 87501

Dear Mr. Nutter:

We have just been advised by our petroleum engineer, Mr. Mohamed Zenati that he has requested a delayed date for the hearing originally scheduled for January 6, 1982. The reason for the postponement is that conflicting schedules preclude his attendance at the hearing on behalf of Red Mountain Associates.

It is my understanding that the hearing before the Commission will take place on January 20, 1982, two weeks after the original date of January 6, 1982. We would appreciate your confirming the new date of January 20 as soon as practicable. May I remain,

Sincerely,

RED MOUNTAIN ASSOCIATES

By: Lloyd L. Temple Jr.
Lloyd L. Temple, Jr.
General Partner

cc: Mr. Mohamed Zenati/2626 Holly Street/Denver, Colorado 80207
303 333-8143

RED MOUNTAIN ASSOCIATES
7847 REISTERSTOWN ROAD, SUITE 205
BALTIMORE, MARYLAND 21208
(301) 653-3080

Case 7459

November 30, 1981

Def for Hrg Jan 6

Mr. Dan Nutter
c/o The Oil Conservation Division
P.O. Box 2088
Santa Fe, New Mexico 87501

Dear Dan:

As you requested during our conversation several days ago, I would appreciate our partnership being put on the docket for hearing at your earliest convenience in January, 1982. We have made several adjustments to our water flood operation and wish to change several of the existing producing wells to injectors and vice versa. Additionally, I know you have talked to Mohamed Zenati concerning an increase in pressure on a graduated scale from the existing, approved 68 pounds up to such a pressure that will provide us with a satisfactory injection and resultant production. Mohamed has also mentioned to you, I know, that there are many reasons why we feel that production packers are not necessary on this particular field, and the added expense, coupled with the overall operational problems are posing a financial burden on the overall program.

I know the above matters have been discussed in some detail with you and that you and the Commissioner are in need of further detailed information which we certainly are prepared to provide at the hearing.

Everyone concerned with this project is most appreciative of your kind cooperation and that of Mr. Frank Chavez and Jeff Edmister and Aztec, without whose cooperation would make our mission most difficult.

Very truly yours,

Stephen F. Meszaros

SFM:dh

cc: Mohamed Zenati

R-6538
12/17/80

Called in 9/8/80
by Mr. Donati 303 825-2222

Red Mountain & Associates
Waterflood Project

Menefee formation
Chaco Wash Sand
Section 28 Sand

~~15~~ 8 wells
Sections ~~21, 22, 27~~, and 28
T20N, R9W

McKinley County

Application of Red Mountain Associates for the amendment of Order No. R-6538, McKinley County, New Mexico

Applicant, in the above styled cause, seeks the amendment of Order No. R-6538, which authorized applicant to conduct waterflood operations in the Chaco Wash-Mesaverde Oil Pool. Applicant seeks approval for the injection of water thru various other wells than those originally approved, seeks deletion of the requirement for packers in injection wells, and seeks ~~and~~ an increase in the previously authorized 68-pound limitation on injection pressure.

ROUGH

STATE OF NEW MEXICO
ENERGY AND MINERALS DEPARTMENT
OIL CONSERVATION DIVISION

IN THE MATTER OF THE HEARING
CALLED BY THE OIL CONSERVATION
DIVISION FOR THE PURPOSE OF
CONSIDERING:

CASE NO. 7459

Order No. R-~~10~~ 6538-A

Application of Red Mountain Associates for the Amendment of Order No. R-6538, McKinley County, New Mexico.

M.S.

ORDER OF THE DIVISION

BY THE DIVISION:

This cause came on for hearing at 9 a.m. on February 17 and March 16 1982, at Santa Fe, New Mexico, before Examiner RLS.

NOW, on this ______ day of ____________, 19_____, the Division Director, having considered the testimony, the record, and the recommendations of the Examiner, and being fully advised in the premises,

FINDS:

(1) That due public notice having been given as required by law, the Division has jurisdiction of this cause and the subject matter thereof.

(2) That the applicant, Red Mountain Associates, seeks the amendment of Order No. R-6538, which authorized applicant to conduct waterflood operations in the Chaco Wash-Mesa Verde Oil Pool. Applicant seeks approval for the injection of water through various other wells than those originally approved, seeks deletion of the requirement for packers in injection wells, and seeks an increase in the previously authorized 68-pound limitation on injection pressure.

(3) That the applicant failed to present any substantial evidence in this case upon which the proposed amendments to said Order No R-6538 could be based.

(4) That the application should be denied.

IT IS THEREFORE ORDERED:

(1) That the application of Red Mountain Associates for amendment of Division Order No R-6538 is hereby denied.

2 Jurisdiction

TION FOR 13 NON-STANDARD GAS PRORATION tion
UNITS, SAN JUAN COUNTY, NEW MEXICO

Cont to
1/20

12/28/81
1/8/82